

Amphiphilic Polymers as Enhanced Drug Delivery Systems



Noorjahan Aibani (M. Pharm)

Faculty of Life and Health Sciences

Ulster University

A thesis submitted in fulfilment of the requirements for the degree of

Doctor of Philosophy

May 2018

I confirm that the word count of this thesis is less than 100,000 words.

Declaration

I hereby declare that with effect from the date on which the thesis is deposited in the library of Ulster University, I permit,

1. The librarian of the university to allow the thesis to be copied in whole or in part without reference to me on the understanding that such authority applies to the provision of single copies made for study purposes or for inclusion within the stock of another library.
2. The thesis to be made available through the Ulster institutional repository and/or EthOS under the terms of the Ulster eTheses deposit agreement which I have signed.

This thesis is the sole work of the author and has not been submitted for any previous application for a higher degree.

Noorjahan Aibani

Acknowledgements

I would like to take this opportunity to thank my supervisor Dr. Bridgeen Callan for her unwavering support. Dr. Callan made me feel right at home from the very first day and has been the same until the last. I couldn't have asked for a better supervisor and as I always say- You are the best! Thanks to Dr. Susan Fetherston, who left me in such capable hands.

To my second supervisor, Prof. Anthony McHale, for the *in-vivo* studies- I can't imagine going through them without his guidance and support and his honest appreciation of my work makes me fill up with pride.

Special note of thanks to my third supervisor, Prof. John Callan for all the dinners and summer trips! And for his direct and indirect support towards the successful completion of my research work.

Thanks to Dr. Sukanta Kamila and Dr. Colin Fowley for teaching me the basic techniques that helped shape the early days of my PhD and who I always look up to.

To all my colleagues and friends who have endured my happy chirpy days and my demotivated days- Dean, Conor, David, Jordan, Scarlett, Fernanda, Chloe, Jason, Kieran, Nino, Ivana, Heather, Federica, Siman, Bernie and particularly Varun- you all deserve a special accolade. Thank you so much.

Thanks to Ulster University Vice Chancellor Research Scholarship for giving me this unique opportunity of pursuing a fully funded PhD in an international environment. I am grateful for the kind and supportive nature of all the people of Northern Ireland who made me feel accepted in this foreign place away from home.

Lastly, I would like to extend a heartfelt thank you to my lifeline- my little brother, Tausif- who has stood by me like a pillar at all times since childhood and throughout my PhD journey. He is my pride and joy and he deserves the best in life.

Summary

This thesis involves the application of different amphiphilic copolymers as self-assembling nanoparticulate drug delivery systems such as micelles and polymersomes. The first chapter starts with the introduction to nanoparticulate drug delivery systems and the significance of liposomes to nanoparticulate drug delivery research. It describes the advantages of polymeric systems as future contenders in the preparation of nanoparticles. Later, different types of self-assembling copolymers and the methods of preparation of different nanoparticles are discussed. The chapter concludes with the recent applications of polymeric micelles and polymersomes in several areas of drug delivery and diagnostics.

The second chapter presents the comparison of liposomes made from egg phosphatidylcholine, cholesterol and PEG conjugates (Mn 500 and Mn 2000) with polymersomes made from random copolymers having the same composition to that of the liposomes. The polymersomes were neutral in charge due to the absence of zwitterionic choline head groups as compared to liposomes. They were found to be smaller in size than liposomes when prepared by the reverse phase evaporation method. The comparison of polymersomes to liposomes revealed enhanced cellular uptake and good stability upon storage for the polymersome preparations.

The third chapter of this research thesis focuses on the application of polymeric micelles for triggered drug delivery combined with real time monitoring of drug release using FRET. The micelles were prepared from amphiphilic random copolymers comprising of a decyl chain group and PEG (Mn 500) and encapsulated a FRET pair of bodipy and spiropyran compounds. The spiropyran moiety is capable of ring transformation to its merocyanine counterpart upon triggering by UV light. This transformation leads to the release of some of the micellar contents to the surrounding media while concomitantly displaying a molecular communication with the bodipy moiety remaining within the micelle. The *in-vitro* release of merocyanine and FRET efficiency between bodipy and

merocyanine in HeLa cells was confirmed. Validation of real time quantification of spiropyran conjugated API release through bodipy fluorescence was also demonstrated.

Finally, the fourth chapter establishes the application of amphiphilic copolymer polymersomes for enhanced anticancer therapy. Three anticancer drugs namely, Dox, 5-FU and Leucovorin calcium were encapsulated into polymersomes and observed for *in-vivo* anti-tumour effects in pancreatic BxPC-3 ectopic xenograft mouse model after intratumoral and intravenous injections. Polymersomes encapsulated with the anticancer agents displayed an enhanced tumour reduction and less peripheral toxicity as compared to combination free drug solution at the same concentration.

In conclusion, the work presented within this thesis highlights the important role of amphiphilic polymers within drug delivery.

Table of Contents

Chapter 1	Introduction	20
1.1	Introduction to drug delivery	21
1.2	Nanoparticulate drug delivery	22
1.2.1	Need for nanoparticulate DDSs	25
1.3	Liposomes- Reigning nanoparticulate systems for drug delivery	25
1.4	Polymeric systems for drug delivery	29
1.5	Amphiphilic copolymer vesicles- Next generation nanoparticulate drug delivery systems.....	30
1.6	Introduction to amphiphilic copolymers.....	33
1.6.1	Block copolymers	35
1.6.2	Random copolymers	36
1.6.3	Graft copolymers	37
1.6.4	Self-assembling polymers based on PEG	39
1.7	Self-assembling micelles of amphiphilic copolymers.....	45
1.7.1	Methods for the preparation of micelles	46
1.8	Self-assembling polymersomes of amphiphilic polymers.....	48
1.8.1	Methods of preparation of polymersomes	50
1.9	Applications of self-assembling amphiphilic copolymers	51
1.9.1	Drug solubilizing agents	52
1.9.2	Stability improvement	53
1.9.3	Sustained release	54
1.9.4	Triggered release	54
1.9.5	Imaging applications	58
1.9.6	Multifunctional nanocarriers	59
1.9.7	Passive targeting	61
1.9.8	Active targeting.....	62
1.9.9	Simultaneous drug delivery	63
1.10	Aims and Objectives	64
1.10.1	Chapter 2: Design of self-assembling random copolymer based polymersomes and their comparison to pegylated liposomes.....	64

1.10.2	Chapter 3: The integration of triggered drug delivery with real time quantification using FRET; creating a super 'smart' drug delivery system.	64
1.10.3	Chapter 4: Multi drug loaded polymersomes for increased efficacy of cancer therapy	65
Chapter 2	Design of self-assembling random copolymer based polymersomes and their comparison to pegylated liposomes	66
2.1	Introduction to bilayer drug delivery systems	67
2.2	Composition of liposomes	68
2.3	Polymersomes synthesized with amphiphilic random copolymers	69
2.4	Aims of Chapter	70
2.5	Results and discussion	72
2.5.1	Synthesis of monomers and polymers	72
2.5.2	Preparation and characterisation of liposomes and polymersomes	82
2.5.3	Cellular uptake of FCD and anthracene loaded polymersomes and liposomes	87
2.5.4	Fluorescence microscopy	88
2.5.5	Mechanism of uptake by chemical inhibition of endocytosis	90
2.5.6	Cell viability using MTT assay	91
2.5.7	<i>In-vitro</i> release studies	92
2.5.8	Physical stability studies	94
2.6	Conclusion	96
Chapter 3	The integration of triggered drug delivery with real time quantification using FRET; creating a super 'smart' drug delivery system	98
3.1	Introduction	99
3.1.1	Fluorescence resonance energy transfer (FRET)	100
3.1.2	Photochromic compounds	101
3.1.3	The FRET pair	102
3.1.4	Chapter overview	104
3.1.5	Aims of chapter	105
3.2	Results and Discussion	106
3.2.1	Preparation and characterization of micelles	106
3.2.2	Quantification of photo physical transformation of 32a to 32b	109
3.2.3	FRET efficiency between 31 and 32b	111

3.2.4	<i>In-vitro</i> triggered release	113
3.2.5	Observation of FRET in HeLa cells.....	114
3.2.6	Application of the delivery system	117
3.2.7	Real time quantification of encapsulated cargo	120
3.3	Conclusion	121
Chapter 4	Multi drug loaded polymersomes for increased efficacy of cancer therapy	123
4.1	Introduction to cancer chemotherapy	124
4.2	Different classes of anticancer agents	125
4.2.1	Anthracycline based antitumour antibiotics	125
4.2.2	Antimetabolites	126
4.2.3	Alkylating agents	127
4.2.4	Microtubule disruptors	128
4.2.5	Nontoxic compounds included within chemotherapeutic regimens	129
4.3	Multidrug combinations for anticancer therapy.....	130
4.4	Nanoparticulate drug delivery for cancer therapy	131
4.5	Liposomes in multi-drug anticancer therapy	132
4.6	Polymersomes in multidrug anticancer therapy.....	133
4.7	Aims of Chapter.....	134
4.8	Results and Discussion	135
4.8.1	Preparation and characterisation of polymersomes	135
4.8.2	Cell viability studies.....	139
4.8.3	<i>In-vivo</i> pharmacokinetics of polymersomes.....	141
4.8.4	<i>In-vivo</i> toxicity after Intratumoral injection	144
4.8.5	<i>In-vivo</i> toxicity after Intravenous injection	148
4.9	Conclusion	152
Chapter 5	Overall conclusion.....	154
5.1	Conclusion	155
5.2	Challenges and future perspectives	160
Chapter 6	Materials and methods.....	161
6.1	Materials	162
6.2	General methods.....	162

6.2.1	Column Chromatography.....	162
6.2.2	Thin layer chromatography (TLC)	163
6.2.3	Mass spectroscopy (MS)	163
6.2.4	Nuclear magnetic resonance (NMR) spectroscopy	163
6.2.5	Dynamic light scattering (DLS) measurements.....	163
6.2.6	Zeta potential measurements.....	163
6.2.7	Scanning Electron Microscopy (SEM)	164
6.2.8	Ultraviolet and Fluorescence spectroscopy.....	164
6.2.9	Percentage encapsulation efficiency (% EE)	164
6.2.10	<i>In-vitro</i> release studies.....	165
6.2.11	Maintenance of Cell lines.....	165
6.2.12	MTT assay for cell viability	166
6.2.13	Statistical analysis	166
6.3	Specific methods for Chapter 2.....	166
6.3.1	Synthesis of Cholesteryl methacrylate (21)	166
6.3.2	Synthesis of Oleic methacrylate (24)	167
6.3.3	Synthesis of Octadecyl methacrylate (26)	167
6.3.4	Synthesis of Polymers (28)	168
6.3.5	Synthesis of CH-mPEG 2000 (30) and CH-mPEG 550 (30) for pegylated liposomes.....	168
6.3.6	Measurement of fixed aqueous layer thickness (FALT).....	168
6.3.7	Preparation of liposomes and polymersomes by reverse phase evaporation method.....	169
6.3.8	Preparation of liposomes and polymersomes by emulsion evaporation method (EM-EV).....	169
6.3.9	Preparation of liposomes and polymersomes by thin film hydration method (TFH).....	169
6.3.10	Characterisation of nanoparticles.....	170
6.3.11	<i>In-vitro</i> release studies.....	170
6.3.12	Cellular uptake	170
6.3.13	Mechanism of cell uptake by inhibition of endocytosis	170
6.3.14	Observation of cells by Fluorescence microscopy.....	171

6.3.15	Stability studies	171
6.4	Specific methods for Chapter 3	171
6.4.1	Preparation and characterisation of micelles	171
6.4.2	Evaluation of phototransformation 32a to 32b	171
6.4.3	FRET efficiency	172
6.4.4	<i>In-vitro</i> triggered release using Franz Diffusion cells.....	172
6.4.5	Observation of FRET in HeLa cells.....	172
6.4.6	Comparative release study to quantify triggered release by FRET	173
6.5	Specific methods for chapter 4	173
6.5.1	Preparation and characterisation of polymersomes	173
6.5.2	Cell viability studies.....	173
6.5.3	<i>In-vivo</i> studies on ectopic xenograft mouse model.....	174
6.5.4	Observation of pharmacokinetics of polymersomes.....	174
6.5.5	<i>In-vivo</i> toxicity of polymersomes loaded with combination drugs	175
Chapter 7	References	176
Appendix 1	213
Appendix 2	218
Appendix 3	228

List of abbreviations

5-FU	5-Fluorouracil
AICN	1,1'-Azobis(cyclohexanecarbonitrile)
API	Active pharmaceutical ingredient
CHO	Chinese hamster ovarian
DCC	N,N'-Dicyclohexylcarbodiimide
DDS	Drug delivery system
DLS	Dynamic light scattering
DMAP	4-Dimethylaminopyridine
DMF	Dimethyl formamide
DOX	Doxorubicin hydrochloride
EE	Encapsulation efficiency
Em	Emission wavelength
EM-EV	Emulsion evaporation
EPR	Enhanced permeation and retention
ESI	Electrospray ionization
Ex	Excitation wavelength
FBS	Foetal bovine serum
FCD	FITC-CM-Dextran
F-D	FITC-Dextran
FDA	Food and Drug Administration
FDD	FITC-DEAE-Dextran
FITC-CM-Dextran	Fluorescein isothiocyanate carboxymethyl dextran
FITC-DEAE-Dextran	Fluorescein isothiocyanate Diethylaminoethyl Dextran
FITC-Dextran	Fluorescein isothiocyanate Dextran
FRET	Förster resonance energy transfer
ICG	Indocyanine green
IV	Intravenous
IVIS	<i>In-vivo</i> imaging systems

LC/MS	Liquid chromatography mass spectroscopy
LV	Leucovorin calcium
MDR	Multi drug resistance
MTT	(3-(4,5-Dimethylthiazol-2-yl)-2,5-Diphenyltetrazolium Bromide)
N	Number of replicates
NEAA	Non-essential amino acids
NIR	Near infrared
NMR	Nuclear magnetic resonance
NOD-SCID	Non-obese diabetic/severe combined immunodeficiency
NP	Nanoparticles
PBS	Phosphate buffered saline
PDI	Polydispersity index
PEG	Polyethylene glycol
Penstrep	Penicillin Streptomycin
PS	Polymersomes
RES	Reticulo-endothelial system
RPE	Reverse phase evaporation
SD	Standard deviation
SEM	Standard error of mean
SEM	Scanning electron microscopy
TFH	Thin film hydration
UV	Ultraviolet

List of figures

Figure 1-1 Illustration of the different types of NPs and their size range ²³	23
Figure 1-2 Types of amphiphilic copolymers	34
Figure 1-3 Schematic representation of different arrangements of block and graft copolymers	36
Figure 1-4 Schematic representation of A. micelles and B. polymersomes	47
Figure 1-5 Role of <i>f</i> value and molecular weight in the formation of vesicles and thickness of bilayer	49
Figure 1-6 Schematic representation of multifunctional nanocarriers	60
Figure 1-7 Mechanism of passive and active targeting in tumour tissues	62
Figure 2-1 : Schematic representation of comparison and design of chemical structure of polymers to lipid	71
Figure 2-2 Mass spectrum of cholesteryl ethylene diamine conjugate (19)	73
Figure 2-3 Mass spectrum of cholesteryl methacrylate (21)	74
Figure 2-4 ¹ H NMR spectrum of cholesteryl methacrylate (21)	74
Figure 2-5 Mass spectrum of oleic ethylene diamine conjugate (23)	75
Figure 2-6 Mass spectrum of oleic methacrylate (24)	76
Figure 2-7 ¹ H NMR spectrum of oleic methacrylate (24)	76
Figure 2-8 Mass spectrum of octadecyl methacrylate (26)	77
Figure 2-9 ¹ H NMR spectrum of octadecyl methacrylate (26)	78
Figure 2-10 Stacked ¹ H NMR spectra of polymers (28) P500 and P2000	80

Figure 2-11 Stacked ^1H NMR spectra of (30) cholesteryl-mPEG 550 and 2000	81
Figure 2-12 (a) Representative size distribution graph of polymersomes showing formation of bilayer polymersomes of size approx. 150nm and a small number of micelles formed in the process. (b) SEM image of P2000 polymersomes.	87
Figure 2-13 Cellular uptake of FCD and anthracene in liposomes and polymersomes. N=3, represented as average \pm SEM, * indicates p value <0.1.	88
Figure 2-14 Fluorescence microscopic observation of FCD and anthracene loaded liposomes and polymersomes.....	89
Figure 2-15 Effect of inhibition of endocytosis using chlorpromazine HCl incubation of 30 minutes before treatment of cells with FCD loaded liposomes and polymersomes. N=3, represented as average \pm SEM, * indicates p value <0.1.	90
Figure 2-16 Cytotoxicity of blank P2000 and L2000 at 0.25mg/ml in 3 cell lines after overnight incubation. N=3, represented as average \pm SEM, * indicates p value <0.1.	91
Figure 2-17 Cytotoxicity of blank P2000 and L2000 at 0.5mg/ml in 3 cell lines. N=3, represented as average \pm SEM, ** indicates p value <0.01, *** indicates p value <0.001.	92
Figure 2-18 <i>In-vitro</i> release of L2000 and P2000 loaded with FCD and anthracene in PBS and Ethanol:PBS 1:1 respectively at 37°C for 24 hours. N=3, represented as average \pm SEM.	93
Figure 2-19 <i>In-vitro</i> release studies in PBS at 37°C of L2000 and P2000 loaded with FDD and F-D to evaluate effect of charged compounds on release. N=3, represented as average \pm SEM.	94
Figure 2-20 Effect of storage time and temperature on encapsulation efficiency of L2000 and P2000 loaded with FCD and anthracene. N=2, represented as average \pm SEM, * indicates p value <0.1, ** indicates p value <0.01.	95
Figure 2-21 Effect of storage time and temperature on size of L2000 and P2000 loaded with FCD and anthracene. N=2, represented as average \pm SEM, * indicates p value <0.1.	95

Figure 2-22 Physical stability studies of L2000 and P2000 loaded with FDD and F-D at refrigerated and 25°C for 8 weeks. (a) Effect of storage time and temperature on encapsulation efficiency (b) Effect of storage time and temperature on size. N=2, represented as average±SEM, * indicates p value <0.1, ** indicates p value <0.01.	96
Figure 3-1 Illustration of FRET energy transfer between a donor and acceptor FRET pair.	100
Figure 3-2 Illustration of the phototransformation of spiropyran to merocyanine and transformation back under visible irradiation	102
Figure 3-3 Schematic representation of the UV triggered release caused by the photoisomerism of spiropyran to the zwitterionic merocyanine transcending the amphiphilic micelle and concomitant quantification using FRET with a bodipy donor moiety.	105
Figure 3-4 A. Dynamic light scattering displaying the hydrodynamic radius of micelles. B. SEM image of micelles	108
Figure 3-5 Absorbance spectra of 32a and following photoconversion to 32b with the emission spectra of 31 with Ex 525 nm.	109
Figure 3-6 Absorbance spectra of 32b in DMF after photo-conversion of 32a by UV exposure at 365nm for specific time intervals at increments of 2 minutes.....	110
Figure 3-7 Absorbance spectra of 32b at λ_{max} 550nm increasing with increasing exposure to UV light of 365nm encapsulated in micelles in PBS. Spectra displayed following exposure to 0, 0.5, 1.0, 1.5, 2, 2.5, 3, 3.5, 4, 4.5, 5, 5.5, 6 and 6.5 mins UV light at 465 nm from a fixed distance. .	111
Figure 3-8 Fluorescence emission of 31 following exposure to varying molar ratios of 32 after photoconversion to 32b . a: no UV exposure and b-h: solutions were exposed to 5 mins UV light at 365 nm from a fixed distance and molar ratios of compounds bodipy 31 : merocyanine 32b b-1:0.5; c-1:1, d-1:2, e-1:4, f-1:6, g-1:8 and h-1:10 consecutively.	112

Figure 3-9 FRET efficiency of **31** and **32b** following exposure to 5 mins UV light at 365 nm from a fixed distance. Concentration of **31** remains constant at 3.64 μ M. Percentage efficiency was determined by the relation depletion in the emission of **31** at 545 nm. 113

Figure 3-10 *In-vitro* triggered release of **32b** from micelles after continuous activation with UV light for 12 minutes and no UV activation. N=3, represented as average \pm SEM, ** indicates $p < 0.005$ 114

Figure 3-11 Bar chart: Fluorescence emission of **31** in HeLa cells incubated overnight with micelles loaded with **31** and **32a** and following cycles of UV exposure (365 nm, 5 mins) leading to conversion of **32a** to **32b** and subsequent resting time in visible light conditions permitting reversion of **32b** back to **32a**. Line graph: control using micelles containing **31** only. Insert: % quenching of **31** following UV irradiation. N=3 represented as average \pm SEM, ** indicates $p < 0.01$, * indicates $p < 0.05$ 115

Figure 3-13 Fluorescence emission of **31** in HeLa cells incubated overnight with micelles loaded with **31** and **32a** and following cycles of UV exposure (365 nm, 5 mins) leading to conversion of **32a** to **32b** and subsequent resting time in dark conditions permitting reversion of **32b** back to **32a**. N=3 represented as average \pm SEM. 116

Figure 3-12 Confocal microscopic images of HeLa cells incubated with micelles loaded with **31** and **32a** showing (a) Clear field (b) Fluorescence emission of **31** (Ex 514nm, Em 520-590nm) before UV exposure (c) Fluorescence emission of **31** after UV exposure (365nm, 5 mins)..... 116

Figure 3-14 Bar chart: Fluorescence emission of **31** within micelles loaded with **35a** following cycles of UV exposure (365 nm, 5 mins) leading to conversion of **35a** to **35b** and subsequent resting time in dark conditions permitting reversion of **35b** back to **35a**. Line graph: control with micelles containing only **31**. Insert: % quenching of **31** following UV irradiation. N=3 represented as average \pm SEM. * indicates $p < 0.05$, ** indicates $p < 0.005$ 118

Figure 3-15 Bar chart: Fluorescence emission of **31** within micelles loaded with **35a** following cycles of UV exposure (365 nm, 5 mins) leading to conversion of **35a** to **35b** and subsequent

resting time in light conditions permitting reversion of **35b** back to **35a**. Line graph: control with micelles containing only **31**. Insert: % quenching of **31** following UV irradiation. N=3 represented as average \pm SEM. * indicates $p<0.05$ 119

Figure 3-16 (a) In-vitro release of **35a** from micelles with and without UV trigger and subsequent resting time in dark and visible light conditions measured by decrease in UV absorbance at 345 nm. **(b)** Observation of % increase in fluorescence emission of **31** at Ex 503 Em 514 nm measured concomitantly with release of **35a**. N=3 represented as average \pm SEM, ** indicates $p<0.005$, *** indicates $p<0.0005$ 121

Figure 4-1 Schematic representation of multi drug loaded polymersomes and in-vivo mouse model 134

Figure 4-2 Schematic diagram of amphiphilic copolymer **41** 136

Figure 4-3 *In-vitro* release profiles of Dox, 5-FU and LV in multi drug loaded polymersomes at 37°C in PBS. N=3 represented as average \pm SEM..... 138

Figure 4-4 Viability of BxPC-3 cells after treatment for 22 hours with 5-FU (4mM), LV (0.25mM), Dox (0.1mM) individual and combination solutions and combination polymersomes at same concentration showing synergistic action. N=3 represented as average \pm SEM. ** indicates $p<0.01$ 140

Figure 4-5 Cell viability after treatment with 5-FU (4mM), LV (0.25mM), Dox (0.2mM) combination free solution and polymersomes loaded drugs and individual Dox solution (0.2mM) showing enhanced cytotoxicity. N=3 represented as average \pm SEM. *** indicates $p<0.001$ 141

Figure 4-6 *In-vivo* kinetics of ICG loaded polymersomes at various time intervals showing preferential accumulation in tumour. 142

Figure 4-7 Plot of tumour fluorescence with respect to peripheral tissue fluorescence, N=2 represented as average \pm SEM. 142

Figure 4-8 Observation of fluorescence in organs obtained from sacrificing the mice after 22 hours pharmacokinetic study. N=2 represented as average \pm SEM.....	143
Figure 4-9 Faeces of mouse with fluorescence emission pre injection and 22 hours following injection with polymersome containing 12	144
Figure 4-10 Graph of percentage increase in tumour growth after intratumoral injection of combination drugs loaded polymersomes and combination free drugs. N=3 represented as average \pm SEM, * indicates $p<0.1$, *** indicates $p<0.001$	145
Figure 4-11 Graph showing percentage body weight change after intratumoral injection for each of the four groups over the 13 days duration of experiment.	146
Figure 4-12 Photograph of one mouse from each group before tumour excision with the actual excised tumour below.	147
Figure 4-13 (A) Percentage increase in tumour weight after the study. (B) Estimated tumour doubling of different groups after intratumoral injection. N=3 represented as average \pm SEM, * indicates $p<0.1$	148
Figure 4-14 Percentage tumour growth of combination drug loaded polymersomes and combination free solution after intravenous injection. N=3 represented as average \pm SEM, * indicates $p<0.1$	149
Figure 4-15 Graph showing percentage body weight change after intravenous injection for each of the three groups over the 7 days duration of experiment. N=3 represented as average \pm SEM, * indicates $p<0.1$, ** indicates $p<0.01$	149
Figure 4-16 Photograph of one mouse from each group before tumour excision with the actual excised tumour below.	150

Figure 4-17 (A) Percentage increase in tumour weight after intravenous study. (B) Estimated tumour doubling time of combination polymersomes and combination free drug solutions. N=3 represented as average \pm SEM.	151
Figure 4-18 Average heart weight of each mouse in the three groups. N=3 represented as average \pm SEM.	152
Figure 8-1 Standard Calibration curve of FITC-CM-Dextran (FCD) by fluorescence spectroscopy at Ex 490nm Em 517nm.	214
Figure 8-2 Standard Calibration curve of FITC-DEAE-Dextran (FDD) by fluorescence spectroscopy at Ex 490nm Em 517nm.	214
Figure 8-3 Standard Calibration curve of FITC-Dextran (F-D) by fluorescence spectroscopy at Ex 490nm Em 517nm.	215
Figure 8-4 Standard calibration curve of anthracene by fluorescence spectroscopy at Ex 355nm Em 400nm	215
Figure 8-5 Standard Calibration curve of merocyanine using fluorescence spectroscopy at Ex 360nm Em 637 nm.	216
Figure 8-6 Standard Calibration curve of Dox by fluorescence spectroscopy at Ex 485nm Em 580nm	216
Figure 8-7 Standard Calibration curve of 5- fluorouracil by UV spectroscopy at absorbance maximum 265nm	217
Figure 8-8 Standard Calibration curve of LV by UV spectroscopy at absorbance maximum 285nm	217

Chapter 1

Introduction

1.1 Introduction to drug delivery

Drug delivery systems (DDS) lie at the interface between chemistry and pharmacology and provide an effective way to deliver drugs to ensure maximum therapeutic effect and high patient compliance. Before 1950, all drugs were manufactured as pills and capsules which immediately released the drug upon contact with water^{1, 2}. The first sustained release dosage form was manufactured by SmithKlein Beecham in 1952, which provided a 12-hour release profile known as 'Spansule technology'. During the next three decades various oral and transdermal dosage forms with controlled release profile were produced. These were based on different release mechanisms, such as dissolution and diffusion controlled systems utilizing a polymer pump or matrix, some of which are available in the market even today³. Oral drug delivery still remains the most attractive route of administration due to the cost of manufacture as well as the ease of dose regulation and patient compliance. Controlled release systems offer several advantages over immediate release, such as; maintaining therapeutic plasma levels, reduction of harmful side effects by allowing local administration and improvement of the half-life of drugs⁴. The second generation drug delivery systems developed after 1980 focused on different routes of drug delivery, such as; long term intramuscular or subcutaneous depot formulations and pulmonary delivery of insulin to overcome the various drawbacks of conventional oral dosage forms^{5, 6}. Around 1990s, research involved the use of hydrogels and mucoadhesion techniques and the use of smart polymers responsive to temperature and pH⁷. In the late 1980's and early 1990's various controlled release oral formulations such as Procardia XL[®] and Ditropan XL[®], based on osmotic push pull controlled delivery systems, were developed. The advent of biopharmaceuticals such as proteins, peptides and gene delivery further introduced the need for controlled delivery systems which can mimic the physiological pattern⁸. The last decade of the 20th century, saw a boost in research for cancer chemotherapy combined with surgery using nanoparticulate delivery⁹. In 1986, Maeda *et al.* observed that nanoparticles (NPs) accumulated better in tumour vasculature than normal blood vessels owing to enhanced permeation and retention (EPR) effects due to their nanometre size^{10, 11}. This observation led to a shift in

focus on improving delivery vehicles for enhanced therapeutic effect rather than inventing new therapeutic molecules.

1.2 Nanoparticulate drug delivery

The industrial revolution sparked a dramatic interest in nanotechnology based systems with Richard Zsigmondy, a 1925 Nobel Laureate in chemistry, coining the term “nanometer” for the size of gold colloids that he measured under an ultramicroscope¹². However, modern nanotechnology is credited to Richard Feynman, a Nobel Laureate in Physics, who, in 1965, presented a lecture at Caltech (the California Institute of Technology), at an APS (American Physical Society) meeting titled “There’s plenty of room at the bottom” where he introduced the notion of manipulating matter at atomic level. At around the same time in 1965, Bangham introduced lipid based bilayers for encapsulating small molecules and slightly later, in 1974, Nario Taniguchi, a Japanese scientist coined the term “Nanotechnology” for semiconductor processes at nanometer level. Towards the end of the 1980’s, Eric Drexler of MIT (Massachusetts Institute of Technology) published a book entitled “Engines of Creation: The Coming Era of Nanotechnology” in 1986 utilizing the ideas from Richard Feynman and Taniguchi’s term of nanotechnology, generating further interest in the field^{13, 14}. Today, nanotechnology based drug delivery systems have become the driving force for advancements in the field of drug delivery. Nanotechnology has helped bridge the gap between conventional therapies and the need for novel targeted drug delivery systems for new age diseases such as cancer. It has provided a tremendous boost in the field of drug delivery specifically in the delivery of new chemical entities, targeted drug delivery, co-delivery of multiple drugs, controlled release of drugs, tissue engineering, theranostics and also micro-/nanoelectromechanical device-based drug delivery systems¹⁵ utilizing both biodegradable and non-biodegradable materials for a variety of applications. A brief overview of different nanoparticulate systems is depicted in Table 1-1.

The use of nanotechnology has helped in the design of therapies of the future by lowering doses required for therapeutic efficacy as well as increasing the therapeutic index and improving safety profiles of new therapeutic molecules. Current nanoparticulate DDS utilizing biodegradable materials being investigated include liposomes¹⁶, micelles¹⁷, nanospheres¹⁸, nanocapsules¹⁹, niosomes²⁰ and polymersomes^{21, 22} among others. Nanotechnology based delivery systems are in the nanometre sized particles generally in the size range of 50 - 500nm containing encapsulated, conjugated, dispersed or adsorbed therapeutic or imaging agents. A schematic representation of the different types of NPs and their size range is illustrated in Figure 1-1²³.

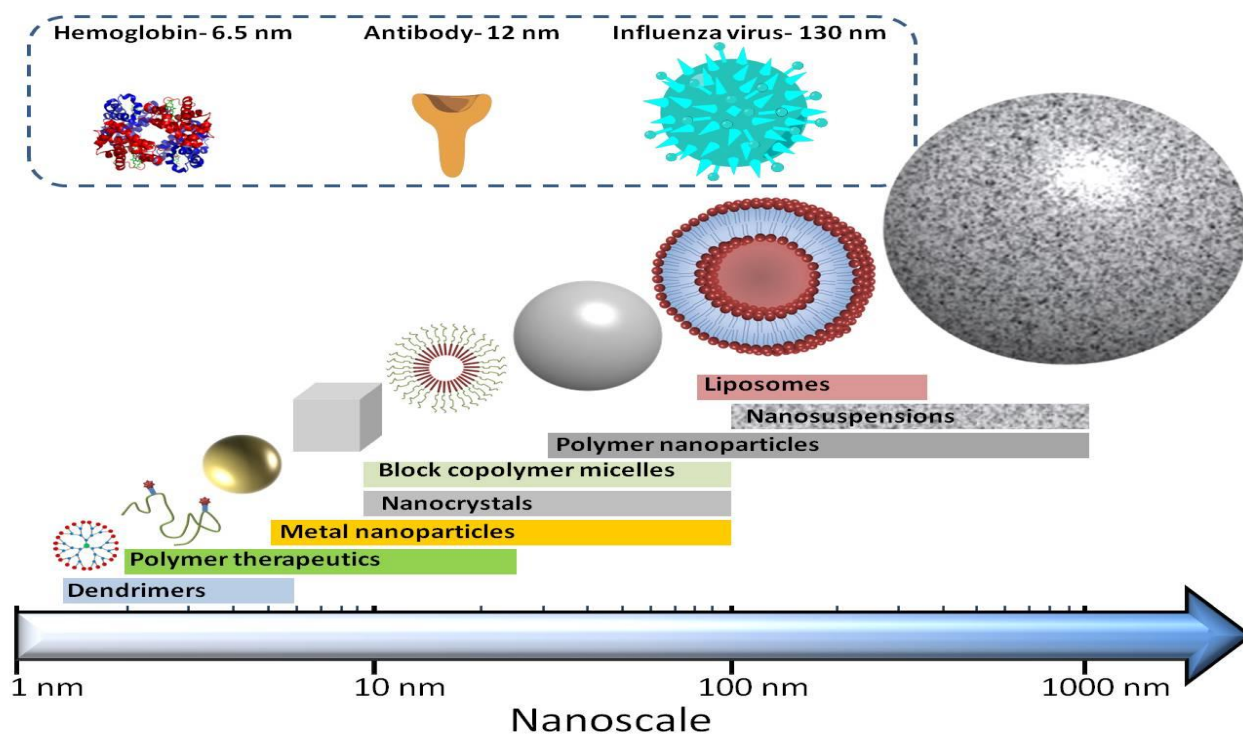


Figure 1-1 Illustration of the different types of NPs and their size range²³.

Table 1-1 Different types of NPs in drug delivery

Type	Composition	Size (nm)	Applications in drug delivery	Ref.
Carbon nanotubes	Seamless cylinders of one or more layers of graphene	0.8 - 2 or 5 - 20 depending on number of layers	Biosensors and medical devices, compatibility with DNA and proteins. Used for fluorescent and photoacoustic imaging, cell internalization for transport of anticancer drugs	²⁴
Metallic NPs	Colloids of gold and silver, iron oxide NPs, nanoshells and nanocages made of silica-gold shell	1 - 100	Biomedical imaging such as Ultrasound, Magnetic resonance imaging (MRI), Computerized tomography (CT), optical imaging, Positron emission tomography (PET) and Surface enhanced raman spectroscopy (SERS).	²⁵
Quantum Dots nanocrystal	Semiconductor NPs made of CdS, CuBr, CdSe, PbS, ZnS, Zn ₃ P ₂ , Cd ₃ P ₂ synthesized in silicate glass and colloidal solutions	10 - 100nm	Bioimaging with/replacing organic fluorescent dyes	^{26, 27}
Liposome	Bilayered nanovesicles made of natural and synthetic phospholipids	Less than 500	Various areas of drug delivery especially anticancer therapy such as active and passive targeting, triggered delivery, controlled release, diagnostics etc.	²⁸
Polymeric NPs	Micelles, dendrimers, polymersomes made of amphiphilic copolymers	Less than 500	Various areas of drug delivery	²⁹

1.2.1 Need for nanoparticulate DDSs

The discovery of new therapeutics to target specific diseases has led to many formulation challenges associated with the method of delivery. In particular, in cases where parenteral delivery is the inevitable mode of administration. The problems associated include poor retention of the pharmaceutical at the site of action, short circulation half-life and infinite dilution of the therapeutic agent leading to injection of high concentrations or increased dosing frequencies. The administration of drugs with the help of delivery vehicles allows the therapeutic agent to be encapsulated within the DDS and subsequent release in a controlled fashion over a period of time, or on occasion the DDS can be adapted to ensure the local delivery of the drug at the site of action³⁰. This nanometre size range allows them to be injected without obstructing needles and proves advantageous for certain disorders such as cancer and inflammation due to the pathophysiology of these conditions³¹.

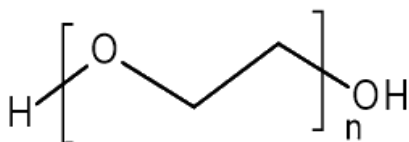
NP DDSs have provided a tremendous boost to enhance the parenteral delivery of therapeutic agents which typically have to be administered parenterally due to limited water solubility, low oral bioavailability and/or very short half-lives. For example, hydrophobic molecules such as anticancer drugs, hormones, anti-inflammatory drugs and drugs for pain relief such as morphine can be encapsulated into the hydrophobic interiors of the delivery vehicle and transported to the site of action to improve their efficacy³⁰. Non-specific anticancer drugs such as Doxorubicin hydrochloride (Dox) are best encapsulated into a delivery vehicle to reduce its adverse side effects and help target the specific tumour sites. Many biopharmaceutical protein and peptide drugs, such as insulin and hormones, have a short shelf life due to limited structural stability on storage, benefit from encapsulation within a DDS to help improve their stability and efficacy³⁰.

1.3 Liposomes- Reigning nanoparticulate systems for drug delivery

The therapeutic use of siRNAs, proteins and enzymes has allowed for a revolution in healthcare regimes³². In order to reach its full potential, it is essential that such therapeutics can be delivered to their required site of action. The size and hydrophilic

nature of these compounds, combined with the fact they are often highly charged, presents a significant challenge from a formulation perspective. One successful method of delivering these types of compounds to their target cells is through the use of liposomes. Since the late nineteenth/early twentieth century scientists have appreciated that the cellular membrane consists of a lipid bilayer³³ and as such, most nonpolar compounds can readily pass through this membrane to the interior of the cell. The translation of this mechanism for drug delivery purposes occurred in 1965 when Bangham³⁴ coined the term 'liposomes' with a description of self-forming lipid vehicles capable of encapsulating compounds for cellular transport. By mimicking the lipid bilayer, these vehicles, together with their content, could transcend the structurally similar cell membrane and enter the interior of the cell. Liposomes are composed of phospholipids with concentric lipid layers having an aqueous core. The presence of the hydrophobic bilayer allows the entrapment of hydrophobic drug molecules while hydrophilic molecules can be encapsulated into the aqueous core. This unique property allows them to deliver a large variety of drugs across the cell membrane³⁵⁻³⁸. Liposomes offer several advantages such as biocompatibility, ability of surface modification to enable active targeting and encapsulation of large amounts of payload³⁵⁻³⁸.

First generation liposomes had no surface modifications leading to limited performance in terms of circulation half-life and protection against serum proteins but could be adapted for desired sizes and rigidities³⁹⁻⁴². These properties lead to the first commercialized liposomes loaded with Amphotericin B for the treatment of Leishmaniasis^{43, 44}. The limitations of conventional liposomes lead to the development of various surface modification strategies such as, coating the liposome surface with polyethylene glycol (PEG) **(1)** which proved successful for liposome stabilization and increasing circulation times giving rise to second generation of surface modified liposomes also called as Stealth liposomes⁴⁵⁻⁴⁸.



(1)

Several commercially available liposomes and those in clinical development consist of surface modification with PEG. Various first and second generation liposomes approved for clinical use and in different stages of clinical trials are depicted in Table 1-2^{49, 50}.

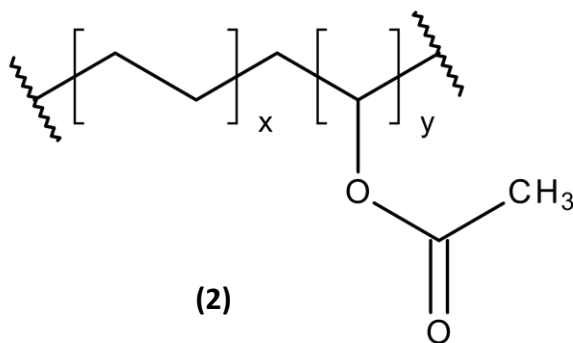
Table 1-2 Various liposomal formulations in clinical use and different stages of clinical trials^{49, 50}

Tradename®	Drug encapsulated	Indication	Current status
AmBisome	Amphotericin B	Fungal infections Leishmaniasis	Approved
Doxil/Caelyx	Doxorubicin	Kaposi's sarcoma, Breast cancer, Ovarian cancer	Approved
DaunoXome	Daunorubicin	Kaposi's sarcoma	Approved
Myocet	Doxorubicin	Breast cancer	
Amphotec, Abelcet	Amphotericin B	Aspergillosis	Approved
DepoDur	Morphine sulfate	Post-surgical pain	Approved
Diprivan	Propofol	Anesthesia	Approved
Lipo-Dox	Doxorubicin	Kaposi's sarcoma, Breast cancer, Ovarian cancer	Approved
SPI-077	Cisplatin	Solid tumours	Phase II
CPX-351	Cytarabine:daunorubicin	Acute myeloid leukemia	Phase I
CPX-1	Irinotecan HCl:floxuridine	Colorectal cancer	Phase II
MM-302	ErbB2/ErbB3-targeted doxorubicin	ErbB2-positive breast cancer	Phase I
MBP-436	Transferrin-targeted oxaliplatin	Gastric and gastro-esophageal junction cancer	Phase II
Lipoplatin	cisplatin	Non-small cell lung cancer	Phase III
ThermoDox	Thermosensitive doxorubicin	Primary hepatocellular carcinoma	Phase III

Since their development liposomes have been utilized for numerous applications ranging from biomiaging to gene and vaccine delivery, treatments of infections and inflammation, lung diseases and most importantly anticancer therapy⁴⁹. Liposomes have proved to be useful in reducing the side effects of encapsulated drugs and passively accumulate in areas of high vasculature when the particle size is below 200nm, an example of which is the clinically approved formulation with Dox. Dox has irreversible cardiotoxicity when injected as a free solution which is significantly reduced when encapsulated in liposomes and is commercially available as Doxil^{®51, 52}. Active targeting strategies of liposomes have garnered a lot of attention recently. For example, Gabizon *et al.* and Yamada *et al.* found increased cellular uptake within tumour cells of folate conjugated to PEG linkers coated on the liposome surface^{53, 54}. Another area of research for liposome development is the use of internal and external triggers for the controlled release of encapsulated drugs. Many intrinsic triggers such as enzyme triggered release, pH and redox triggered, and temperature sensitive liposomes⁵⁵⁻⁵⁷ as well as various remote triggers such as ultrasound, light and magnetic field⁵⁸⁻⁶¹ have been developed recently. Even with the triggered drug release capabilities of liposomes and the problems of quick elimination by the RES in the first generation of liposomes being overcome by surface coating with PEG, they still possess several problems; such as physical and chemical instability due to their biological nature and drug leakage over time^{62, 63}. They also lack control over the rate of drug release, have difficulty in overriding barriers such as the blood brain barrier, and insufficient loading of drugs⁶⁴. These limitations have led to an exploration towards more synthetic polymer analogues of lipids, which possess similar properties of assembling into monolayer and bilayer NPs and can provide more stability than liposomes.

1.4 Polymeric systems for drug delivery

During the latter part of the 20th century polymers had been utilized and marketed for a variety of functions. These included development of 1974 sustained release Pilocarpine by Alza Corp., Ocuserts[®] for the treatment of glaucoma⁶⁵ as well as the 1976 FDA approved Progestasert[®], an intrauterine device for sustained release of progesterone⁶⁶ by the same company. In 1990, Wyeth-Ayerst Laboratories developed the contraceptive subcutaneous implants Norplant[®] for sustained release levonorgestrel⁶⁷. Poly (ethylene-co-vinyl acetate) **(2)** was commonly used drug release rate controlling polymer for the above mentioned devices⁶⁸. With advancements in nanotechnology during this time, polymers have been increasingly used in various micro and nanoparticulate systems with various micro-sized systems based on zero order kinetics having more sustained release profiles⁶⁹. Polymers used in drug delivery systems can be divided into two categories- **Nonbiodegradable**-mainly used as implants for diffusion controlled systems and **Biodegradable**-used for chemically controlled and triggered release systems as micro and NPs⁷⁰.



Various polymer based drug delivery systems can be summarized as follows;

Implants: Implantable polymers can be biodegradable or nonbiodegradable depending on their application. Examples of such implants include those for ocular drug delivery such as non- biodegradable Vitasert[®] controlled release ganciclovir for the treatment of cytomegalovirus retinitis, Retisert[®] containing fluocinolone acetonide for non-infectious

uveitis and biodegradable Ozurdex® intravitreal implant for sustained release dexamethasone for treatment of macular oedema^{71, 72}. Polymers mostly used for non-biodegradable implants include silicone, polyvinyl acetate (PVA) and ethylene vinyl acetate (EVA) whereas those used for biodegradable implants generally consist of natural polymers such as albumin, collagen and gelatin. The major disadvantage of implantable drug delivery systems is the need for surgery to introduce it into the body and the potential need for removing it from the body after use⁷³.

Hydrogel systems: Hydrogels are three-dimensional crosslinked polymer networks which swell rapidly in the presence of water. Hydrogels can be made of water soluble polymers which have the ability to absorb large amounts of water and can be formulated into various forms such as microparticles, NPs, films and coatings for a large range of applications^{74, 75}. Despite various advantages, hydrogels have certain limitations such as rapid release of drugs due to fast swelling of polymer and fast degradation of polymer. Several strategies have been developed to overcome these drawbacks such as covalent bonding of the drug to the polymer, however their use is still limited in controlled drug delivery⁷⁶.

Microspheres: Microspheres can be defined as spherical particles in a size range of 10-1000 microns. In these systems, the drug is either encapsulated inside the porous microspheres or dispersed into the polymer matrix. Polymer based microspheres have the potential to release their load either by the leaching of drug from polymer or by degradation of the polymer matrix. They can be manufactured by several methods such as emulsion-solvent evaporation, spray-drying, suspension polymerization, ultrasonication and phase separation⁷⁷. However their large size limits their application for cancer therapy.

1.5 Amphiphilic copolymer vesicles- Next generation nanoparticulate drug delivery systems

Supramolecular self-assembling DDS expanded from lipids to include both natural and synthetic polymers with the only prerequisite for successful formation being the presence

of both hydrophobic and hydrophilic units. The use of biopharmaceuticals has not replaced traditional small molecule drugs, when prescribed together they often display a synergistic benefit to the patient. The advances in such combination therapies has led to the requirement of drug delivery systems to expand so that both hydrophobic and hydrophilic drugs can be delivered in the same vehicle simultaneously⁷⁸. This can present a significant challenge as the physicochemical properties of these two classes of compounds are quite literally 'polar opposites'. The development of drug delivery systems formed from amphiphilic building blocks has obvious benefits when considering the delivery of compounds with distinctly different physical properties. These amphiphiles can self-assemble in solution to form entities with both hydrophilic and hydrophobic regions that are capable of delivering a wide range of both polar and nonpolar compounds⁷⁹. Often these particles have diameters in the nanometre range and provide improved stability for their cargo, have good biocompatibility with tissues and cells and due to their subcellular size display a relatively high intracellular uptake⁸⁰. It has been established that nanocarriers can become concentrated preferentially in tumours, inflammatory sites and at antigen sampling sites by virtue of the EPR effect of the vasculature. Once accumulated at the site, these NPs can act as a drug depot, providing a source of active pharmaceutical ingredient (API) to be released as and when required. This leads to enhanced bioavailability, a more sustained/controlled release and reduced toxicity that can be caused by a 'burst release' of the API. Central to the development of these delivery systems is the flexibility offered by using polymers as the building block. In particular, amphiphilic co-polymers⁸¹, formed from covalently linked polymer chains in blocks of two or more⁸², have demonstrated significant potential for the delivery of both large highly charged biological compounds as well as the more conventional small molecule and typically hydrophobic drug compounds. Several polymeric NPs, especially micelles, in various stages of clinical development for anticancer therapy are depicted in Table 1-3^{83, 84}.

Table 1-3 : Different polymeric NPs for cancer therapy in different stages of clinical development.

Formulation	Indication	Clinical phase
PEG–polyglutamate micelle loaded with 7-ethyl, 10-hydroxy camptothecin	Breast cancer	Phase II
PEG–polyaspartate micelles loaded with paclitaxel	Advanced gastric cancer	Phase II
Pluronic® L61 and F127 micelles loaded with doxorubicin	Adenocarcinoma of gastrointestinal tract	Phase III
PEG–poly(d,l-lactide) micelles loaded with paclitaxel	Non small-cell lung, bladder, pancreatic, and ovarian cancer	Phase II
PEG–poly(γ-benzyl-L-glutamate) loaded with cisplatin	Solid tumours	Phase I/II
PEG–polyaspartate micelles loaded with doxorubicin	Various types of cancers	Phase II
Cyclodextrin–PEG micelles loaded with camptothecin	Lung & ovarian cancer	Phase II
PSMA targeted PEG-PLGA or PLA-PEG NPs with docetaxel	Various types of cancers	Phase II
Polymeric micelles loaded with Paclitaxel	Head and neck or breast cancer	Phase II
Poly amino acids with PEG conjugated with cisplatin as micellar systems	Lungs, pancreatic, biliary or bladder advanced solid tumours	Phase III
Poly amino acid with PEG, conjugated with Oxaliplatin as micelles	lymphomas and advanced solid tumours	Phase I
Silica-gold nano-shells coated with PEG for NIR light mediated thermal ablation	Thermal ablation of lung and solid primary metastatic tumours	N/A
Silica NPs coated with PEG loaded with a NIR fluorophore and ¹²⁴ I radiolabeled cRGDY targeting peptide	<i>In-vivo</i> imaging of melanoma and brain tumours	N/A

1.6 Introduction to amphiphilic copolymers

Amphiphilic systems capable of self-assembling provide unique opportunities in the design of advanced materials for applications in nanoparticulate drug delivery. The ability to self-assemble into ordered morphologies is mainly dependant on the thermodynamic incompatibility of the hydrophilic and hydrophobic blocks. This leads to their spatial organisation whereby blocks of similar nature align themselves in the nanoscale region. Furthermore, the reversible non-covalent interactions allow dynamic switching of the conformations into various other morphologies and functions in response to external stimuli, further providing a platform for designing smart amphiphilic supramolecules for nanobased drug delivery⁸⁵. Amphiphilic polymers are capable of self-assembling into a wide variety of structures such as spherical micelles, cylindrical micelles, bilayered vesicles, nanofibers, nanotubes, lamellae and bi-continuous structures. These supramolecular moieties mimic the assembly of biological molecules such as proteins and lipids allowing them to integrate into the body and perform specific cellular functions. The recent advancements in polymerisation techniques has facilitated the facile synthesis of amphiphilic copolymers with defined compositions, molecular weights and elaborate structural design⁸⁶.

Many examples can be found in the literature where amphiphilic polymers have been used for drug delivery applications⁸⁷. Such polymers have the ability to form a variety of assemblies depending on the nature of the two blocks hydrophilic and hydrophobic, the number of monomers used in the polymer synthesis and the particular polymerization process chosen for their assembly^{87, 88}. The most common number of monomers used for the preparation of amphiphilic polymers is two, hence the term co-polymer⁸⁸, three monomers polymerized are known as terpolymers⁸⁹, while one amphiphilic monomer can also create an amphiphilic homopolymer⁹⁰. The blocks can align themselves in the aqueous phase into various shapes depending on the hydrophilic lipophilic balance which affects their ability to form spherical structures. Diblock copolymers with hydrophilic fractions (f value) less than 20% have a stronger tendency towards forming solid particles. Whereas increasing the f value between 20-40% generally form loose fluid-like bilayer

The diagram illustrates six types of copolymers, each represented by a specific arrangement of 'A' and 'B' monomers:

- Random Copolymers:** A single horizontal chain with a random sequence of 'A' and 'B' monomers: $-A-A-B-A-B-A-A-A-B-A-B-B-A-B-B-A-A-A-B-$.
- Alternating Copolymers:** A single horizontal chain with 'A' and 'B' monomers alternating regularly: $-B-A-B-A-B-A-B-A-B-A-B-A-B-A-B-A-B-$.
- Block Copolymers:** A single horizontal chain with distinct blocks of 'A' and 'B' monomers: $-A-A-A-A-B-B-B-B-B-B-B-B-A-A-A-A-$.
- Graft Copolymers:** A main horizontal chain of 'B' monomers with three vertical chains of 'A' monomers grafted at different points: $-B-B-B-B-B-B-B-B-B-B-B-B-B-B-B-B-$ with $A-A-A-A-A-A-A-$, $A-A-A-A-A-A-A-$, and $A-A-A-A-A-A-A-$ branches.
- Brush Copolymers:** A single horizontal chain of 'B' monomers with ten vertical chains of 'A' monomers grafted at regular intervals: $-B-B-B-B-B-B-B-B-B-B-B-$ with ten $A-A-A-A-A-$ branches.
- Star Copolymers:** A central 'B' monomer with four arms of 'A' monomers radiating outwards: $-A-A-A-B-A-A-A-$ with four $A-A-A-A-$ arms.

34

1.6.1 Block copolymers

Block copolymers consist of two or more blocks of copolymers covalently attached to each other sequentially. Linear block copolymers consist of the copolymers attached in a linear fashion whereas star block copolymers are composed of three or more blocks attached at a common point although they can also be viewed as graft polymers⁹¹. Simple block copolymers composed of a single segment of A and B monomers are called A-B block polymers, whereas when monomer B is connected on both sides with monomer A, it is termed as ABA type block copolymer. In the third type, A and B segments are connected multiple times and are termed as multiblock copolymers¹⁰⁰ as depicted in Figure 1-3. Block polymers consisting of two different monomer units have been termed as diblock polymers whereas those with three different monomer units have been termed as triblock polymers¹⁰¹. Novel synthetic strategies using ionic and radical polymerisation permit the synthesis of advanced tailor-made block copolymers capable of a multitude of functions. It is possible to combine the properties of incompatible materials, for example hydrophilic and hydrophobic monomers to generate amphiphilic block copolymers which are capable of demonstrating various interfacial properties in different solvents making them attractive for numerous applications. The synthesis of block copolymers has to be controlled precisely by sequential addition of monomers leading to effective control of molar mass distribution and thus the chemical heterogeneity which influence the final properties of the block copolymer¹⁰². Even though block copolymers exhibit excellent self-assembling behaviour, their synthesis can be tedious and time consuming due to controlled synthesis and prolonged post polymerisation procedures such as grafting, hydrolysis, substitution and click chemistries. Amphiphilic block copolymers having different compositions and by various methods of preparation can produce different types of nanostructures such as micelles, core-shell NPs, nanospheres, nanocapsules and polymersomes.

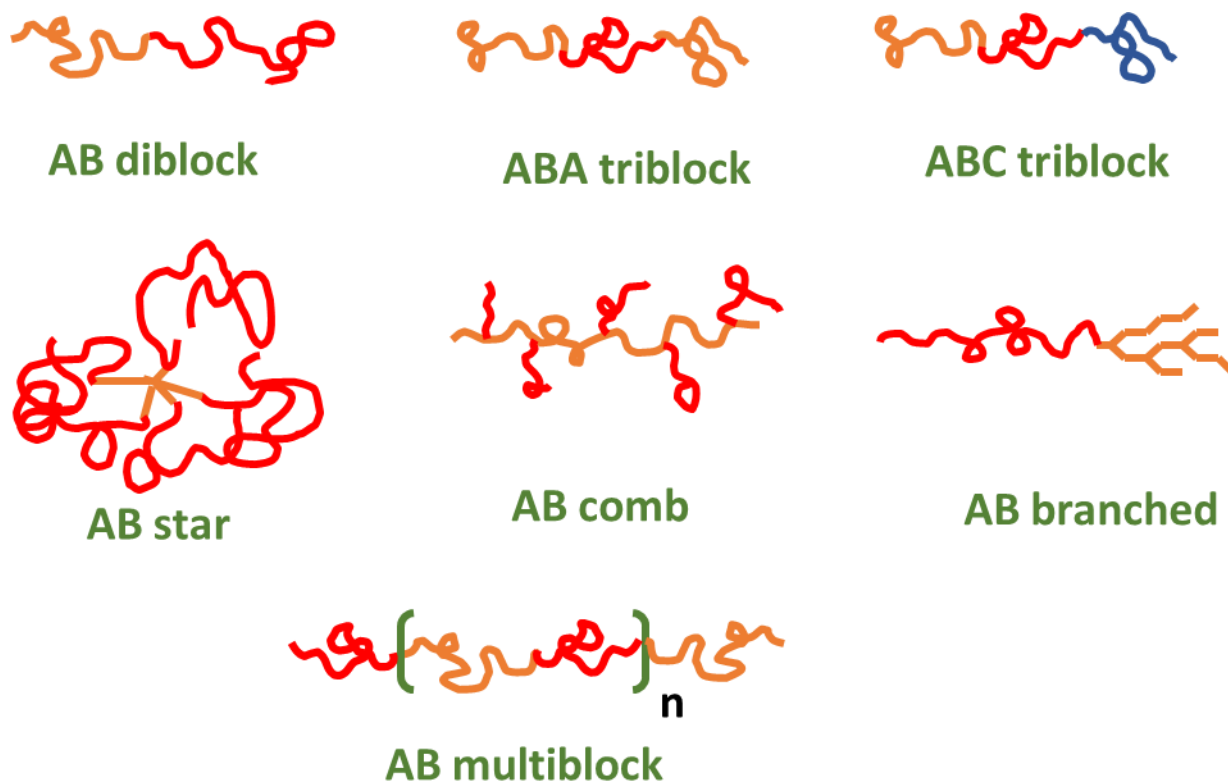


Figure 1-3 Schematic representation of different arrangements of block and graft copolymers

1.6.2 Random copolymers

Also referred to as ‘statistical polymers’ random copolymers are a type of copolymer in which different monomers are arranged randomly and the likelihood of finding a monomer at any given point in the polymer is independent of the adjacent units. The synthesis of random copolymers is typically achieved by one step polymerisation of one or more monomers also called a “one pot” synthesis. The self-assembling properties of random copolymers is largely dependent on the hydrophilic/lipophilic balance of the monomers and affects the assembling morphologies of the copolymers. The assemblies can be easily tuned by controlling the ratio of the two monomer blocks. The resulting size of the polymer depends on the hydrophobic chains and the nature of the solvent used. Random copolymers have been employed for different applications not only due to their

advantage over block copolymers for ease of preparation but also their ability to form different types of nanostructures similar to block copolymers¹⁰³.

Yukari Oda *et al.* compared the structure activity relationship of block versus random copolymers as antibacterial and haemolytic agents¹⁰⁴. They utilised random and block copolymers having poly (vinyl ether) based derivatives with both copolymers having a similar composition of monomers prepared by the living cationic polymerisation technique and demonstrated their activity against E Coli. They found that both copolymers had similar activity against E Coli however block copolymers had lesser haemolytic activity when compared to random copolymers. Thus, suggesting that copolymer assembly is not a determining factor for antimicrobial activity and the different single chain conformations of both the copolymers plays an important role¹⁰⁴. In another example Matsumoto *et al.* created PEG and urea based random, block and graft copolymers having different monomer sequences, chain length, composition and functional groups by ruthenium-catalysed living radical polymerisation and observed their self-folding properties in water and chloroform¹⁰⁵. They observed that PEGMA/BPUMA (PEG methyl ether methacrylate/urea-bearing methacrylate) based random copolymers having 30-40 % urea units efficiently assembled in water to form globular unimer micelles which were dynamic and reversible by the addition of methanol to the system and had good reproducibility. Thus, these polymers provide on demand controlling of assembly into micelles by temperature, solvents and presence of acidic compounds in the system, opening new applications in various areas of drug delivery¹⁰⁵. Random copolymers have also been utilised as supramolecular assemblies which response to pH, temperature and light making them suitable for stimuli responsive drug delivery systems¹⁰⁶⁻¹⁰⁸ and those responsive to multiple stimuli¹⁰⁹.

1.6.3 Graft copolymers

Graft copolymers are segmented copolymers composing of a linear backbone with random branches of another homopolymer or copolymer attached, the branches of which

are structurally different from the main chain. These copolymers are capable of self-assembling into unique nanostructures such as wormlike conformations possessing tight molecular dimensions and distinguished chain end arrangements as compared to linear block copolymers¹¹⁰. Graft copolymers can be formulated into a variety of shapes and conformations such as branched copolymers, cross linked polymers, comb like structures, star shaped configurations and dendritic systems (Figure 1-3) as well as many other recent complex topological systems. The growing attention to the synthetic strategies of well-defined polymers has led to the development of three different methods for synthesizing graft polymers which allow diversity, functionality and flexibility to these polymers and allow precise control over the micro environment, topology and composition to these graft polymers. These methods of polymerisation include:

Grafting-onto method: based on attaching pre-formed side chains to a pre-synthesized backbone by coupling them together. Both the polymer chains are synthesized separately allowing easy control on their pathways of synthesis and nature of the parent and attaching chains¹¹¹.

Grafting-from method: involves pre-synthesis of a polymer backbone which functions as micro-initiator for the growth of side chains onto its multifunctional sites. Living radical polymerization technique is commonly used for this type of synthesis. Low concentration of free radical propagating species allows better control over the coupling and termination of the polymerization chain reaction and also limits the steric hindrances which are unavoidable in the grafting-onto method forming polymers with narrow weight distribution and high grafting density. Tedious post processing and purification of the polymers can also be avoided by this method because of the absence of unreacted initiator after the completion of polymerization¹¹².

Grafting-through method: employs the use of surface attached self-assembled monolayer macromolecules having polymerizable groups. Thus the polymer generation is initiated in solution and the growing chains can be integrated into the surface bound polymer chains allowing its direct anchoring onto the monolayer polymer backbone,

however the chains can continue to grow allowing the integration of free or surface bound chains to the growing polymer chains. Thus the grafting through methodology is a combination of both grafting onto and grafting from methods ¹¹³.

Examples of graft copolymers are reported in literature emphasizing their use in different drug delivery applications. Hoskins *et al.* have presented a comprehensive review on Comb shaped graft copolymers highlighting the different homopolymer backbones used and various hydrophilic and hydrophobic side chains attached to the backbone¹¹⁴. Comb shaped copolymers have been used for various site- specific delivery applications, stimuli responsive NPs, anticancer drug delivery and have potential for oral delivery of proteins and peptides¹¹⁴. Fan *et al.* reviewed the formation of unimolecular micelles using various graft polymers such as amphiphilic dendrimers and dendritic polymers, hyperbranched polymers, star shaped polymers, cyclic and brush copolymers. They concluded that unimolecular micelles present various advantages over multimolecular micelles because of their non-reliance on self-assembly hence imparting better stability to environmental changes such as pH, temperature, dilution and ionic strength ¹¹⁵.

1.6.4 Self-assembling polymers based on PEG

Polyethylene Glycol (PEG) (**1**) is the most commonly used hydrophilic monomer for the synthesis of different types of amphiphilic copolymers. PEG is a non-ionic water-soluble polyether having good biocompatibility and poor immunogenicity. Additionally, it provides stealth properties to the NPs by reducing the adhesion of opsonins present in the blood serum thereby avoiding their recognition by the reticuloendothelial system (RES) and being invisible to the phagocytic cells allowing them longer circulation time in the blood. The most likely and acceptable mechanism for this property of PEG is the extendable conformations of PEG on the surface of the NPs which create steric hindrances and repulsive forces for the opsonins thus effectively blocking interactions with the NPs. PEG, with a molecular weight less than 30kDa, are eliminated from the body by renal clearance. The circulation half-life and accumulation in tumour of PEG based NPs

is largely dependent on the molecular weight, chain density and molecular conformation^{116, 117}. PEG has been derivatized and conjugated to a number of bioactive molecules. It not only offers the advantage of a hydrophilic polymer backbone having low molecular weight dispersity which is inert and soluble in most organic solvents but also provides reactive terminating end groups, generally an alcohol. These favourable reactive properties allow PEG to be employed as a building block in many areas of biomaterials synthesis and pharmaceutical preparations¹¹⁸.

Polymer NPs self-assemble using PEG as the hydrophilic polymer and can be synthesized using a variety of hydrophobic polymers, for example, in micelles the hydrophobic part of the polymer chain is generally composed of poly (lactic acid) (PLA), poly (aspartic acid) (PAsp), poly (ε-caprolactone) (PCL), poly (propylene oxide) (PPO), poly (lactic-co-glycolic acid) (PLGA) and poly (sebacic acid) (PSA). These block copolymer conjugates have been utilised for the encapsulation of a variety of drugs. The most common conjugates are PEG-*b*-PAAs (poly amino acids), PEG-*b*-Polyesters and PEG-*b*-PLGA. PEG based amphiphilic polymers are capable of forming micelles and polymersomes depending on the type of application. Self-assembling copolymers of PEG-*b*-PAA have shown promising results in anticancer drug delivery. The presence of poly amino acids provides good biocompatibility, are biodegradable and have significantly lower toxicity when compared to free drug solutions. Furthermore, PAAs have a wide range of highly reactive functional groups on their surface such as amino, hydroxyl, carboxyl and thiol groups which can be utilised to design site specific delivery vehicles with improved drug loading. The most common amino acids used to synthesize these block copolymers are PAsp and PGlu (Poly (Glutamic acid))¹¹⁶. PEG-*b*-Polyesters such as PEG-PCL are synthesized by the ring opening polymerisation of ε-caprolactone with the help of stannous octoate as a catalyst and the reaction is initiated by PEG. These block copolymers have been widely used for the encapsulation of a number of anticancer drugs and conjugated with different targeting ligands¹¹⁹. These copolymers can exhibit a variety of shapes by simply adjusting the salt concentration of the micellar solutions. The different shapes can have varying degrees of cellular uptake and antitumour activity. The hydrophilic/hydrophobic ratios of the two

monomers affect the drug loading, size and trigger responsiveness of these self-assembled NPs. Hence PEG-PCL copolymers can be easily tuned to a variety of desired functionalities. PEG-PLA are another widely investigated block copolymer for drug delivery and are synthesized in a manner similar to PEG-PCL. The self-assembling properties of PEG-PLA can be adjusted by varying the hydrophilic-hydrophobic ratio which also affects its size and drug loading capacity¹¹⁹. Other examples of amphiphilic copolymers having PEG as the amphiphilic block are depicted in Table 1-4.

Table 1-4 Recent examples of different types of amphiphilic copolymers with PEG as the hydrophilic block

<i>Type of Polymer</i>	<i>Hydrophobic block</i>	<i>Type of drug encapsulated</i>	<i>Type of NP</i>	<i>Disorders</i>	<i>Ref.</i>
Block copolymers	PLGA-b-PEG-b-PLGA triblock	Paclitaxel encapsulation with surface modification with protamine	Not specified	Liver cancer	120
	PEG–GATGE dendritic block copolymers, based on a gallic acid (GA) core and triethylene glycol (TG) butanoate arms	SiRNA complexation	Dendriplex NPs	Nucleic acid delivery	121
	PEG–polypeptide copolymers with pH responsive pendant amine chains	Doxorubicin	Nanovesicles	Breast cancer	122
Random copolymers	Poly (dodecyl methacrylate-co-polyethylene glycol methyl ether methacrylate), poly[DMAx-co-mPEGy]	(S)-(+)-camptothecin (CPT)	Micelles	Anticancer activity	123
	Poly(lactide-co-glycolide)-d-a-tocopheryl polyethylene glycol 1000 succinate	Docetaxel	Not specified	Cancer chemotherapy	124
	Poly [(2-hydroxyethyl methacrylate-3,3'-dithiodipropanoic acid) _x -co-(poly(ethylene glycol) methyl ether methacrylate) _y], poly[(HEMA-DTDPA) _x -co-mPEG _y], redox and pH	Hydrophilic and hydrophobic dyes	Polymersomes	Cancer chemotherapy	125

sensitive copolymers					
	I-cys-graft-poly[GMA-co-mPEG300]	Hydrophilic and hydrophobic dyes	Polymersomes	Drug delivery	126
	Decyl chain	Hydrophilic FITC-CM-Dextran	Polymersomes	Drug delivery	127
	Decyl chain with Cholesterol	Hydrophilic FITC-CM-Dextran and Doxorubicin	Polymersomes	Drug Delivery	128
Random & Block	Oligo (ethylene glycol) and cholic acid pendant groups	Paclitaxel	Micelles	Ovarian cancer	129
Star-shaped copolymers	Poly (ethylene glycol) methyl ether methacrylate macromonomer (PEGMA), 2-(dimethylamino)ethyl methacrylate (DMAEMA) and a disulfide dimethacrylate (cross-linker, SS)	SiRNA complexation	Not specified	Nucleic acid delivery	130
	Poly(PEG-b-L-lysine) arm poly(Lcystine) core stars with outer PEG coronas decorated with folic acid targeting moieties	Tagged fluorescent dye	Not specified	Targeted drug delivery	131

Graft copolymers	Poly(dimethylsiloxane-g-ethyleneoxide) grafted copolymers (PDMS-g-PEO)	Coated fibrinogen	Microparticles	Blood contacting	132
	g 2-(ω-methoxy)PEGyl-1,3-dioxan-5-ylamine with poly(N-(acryloyloxy)succinimide-co-butyl methacrylate) by an acid-labile diamine cross-linker bearing two symmetrical cyclic orthoesters	Paclitaxel encapsulation	Crosslinked micelles	Cancer chemotherapy	133
	Poly(D,L-lactide-co-2-methyl-2-carboxytrimethylenecarbonate)-g-poly(ethylene glycol) (P(LA-co-TMCC)-g-PEG)	docetaxel	Micelles	Cancer chemotherapy	134
	Poly(ethylene glycol) methacrylate with Methyl methacrylate P(PEGMA-co-MMA)	Indomethacin	Micelles	Anti-inflammatory therapy	135

1.7 Self-assembling micelles of amphiphilic copolymers

Amphiphilic molecules such as surfactants assemble at the boundary of two immiscible phases or in aqueous solutions they tend to orientate themselves such that the hydrophobic blocks get removed from contact with the aqueous surface to achieve minimum free energy. At a specific narrow concentration range called the critical micellar concentration (CMC) these molecules tend to self-assemble themselves into definite colloidal particles termed as micelles which have an inner hydrophobic core and an outer hydrophilic shell thus minimizing the interaction of the hydrophobic blocks with the aqueous phase. At concentrations higher than the CMC, the micelles are thermodynamically stable whereas at lower concentrations they tend to disassemble, thus effectively breaking the micellar structure. Micelles made of amphiphilic copolymers have a distinct advantage over conventional surfactants as they typically have lower CMCs and resist dissociation upon dilution due to the interactions among the polymer chains⁸¹. Polymeric micelles are generally made of amphiphilic AB type block copolymers however micelles made from other types of polymers have also been explored for drug delivery applications. They are typically in the size range of 10-100nm and can be used for various triggered drug delivery applications. Moreover, unique functional moieties can be added onto the block polymer backbone enabling them to be tuned for desired applications such as cell targeting¹³⁶. Different parts of a micelle serve different purposes, for example the core of the micelle is responsible for encapsulating the drug and protecting it from degradation by the surrounding environment (Figure 1-4A). The outer shell provides stealth properties to the micelles protecting them from phagocytosis by the RES leading to prolonged blood circulation thus enhancing drug efficiency. The corona also determines the hydrophilicity, surface functionality and charge of the micelles along with the stability, biocompatibility and pharmacokinetic behaviour of the encapsulated drugs¹³⁷. The core of the micelles can be modified to obtain high encapsulation efficiency leading to good therapeutic drug levels. The miscibility of the polymer and drug along with hydrophobic interactions between the micelle core and the drug plays an important role. The length of the hydrophobic chain and types of

substituents also affect the encapsulation of certain drugs. Insoluble drugs can be encapsulated by physical encapsulation methods such as dialysis and emulsification¹³⁸.

1.7.1 Methods for the preparation of micelles

There are various methods documented for the formulation of polymeric micelles, a number of which have been described below:

Direct dissolution method: Commonly used for preparing micelles of block copolymers with low molecular weights and short hydrophobic blocks, this method has the polymer directly dispersed in an appropriate solvent. When dispersed in the solvent, which should be a good solvent for one block but a non-solvent for the other block, the polymer forms micelles through association of insoluble segments. This association can be aided by stirring, heat and sonication leading to formation of uniform spherical micelles at optimum conditions. Improper processing conditions can lead to aggregation and uncontrolled growth and attachment of structures which eventually aggregate¹³⁹.

Addition of a precipitating solvent: In this method, the polymer is first dissolved in a non-solvent to which a selective solvent for one of the blocks is added leading to the formation of micelles at the interface of the two phases. This non-solvent can also be a change in physical conditions such as temperature, pH and ionic compositions such as the addition of salts¹⁴⁰.

Dialysis method: Unsuitable for large scale production, the dialysis method involves solubilisation of the copolymer and drug in water-miscible organic solvent and dialyzing it against water. The slow replacement of organic solvent with water leads to the association of the block copolymer with the drug encapsulated into spherical micelles. The use of a semi permeable membrane allows separation of the micelles from the unencapsulated drug which gets dialyzed outside in the surrounding water. However, a drawback of this method is the incomplete removal of the free drug¹⁴¹.

Oil-in-water emulsion method: In this method, the drug and block copolymer are dissolved in an organic solvent which is not miscible in water, such as chloroform, an

emulsion is formed in water by vigorous stirring. The organic solvent is then evaporated to instantly form micelles¹⁴².

Solvent evaporation/Thin film hydration method: This method can be employed for encapsulation of both hydrophilic and hydrophobic drugs in which the former is dissolved in the aqueous medium. In this method, the drug and polymer are dissolved in an organic solvent such as chloroform and evaporated to form a thin film in a round bottom flask. This thin film is then hydrated with the aqueous phase by rotation for a specific period, or vigorous shaking or sonication to aid self-assembly into micelles. This method has the advantage of large scale production however can only be utilized for block polymers having a high hydrophilic lipophilic balance which aids in easy dispersion of the film in the aqueous medium¹⁴³.

Freeze-drying: This method involves the use of a freeze dryable solvent such as tert-butanol in which the drug and polymer are dissolved and freeze dried. The freeze-dried powder is later reconstituted in isotonic solution such as phosphate buffered saline. Even though this method is feasible for large scale production it has the limitation of limited solvents available for freeze drying^{142, 144}.

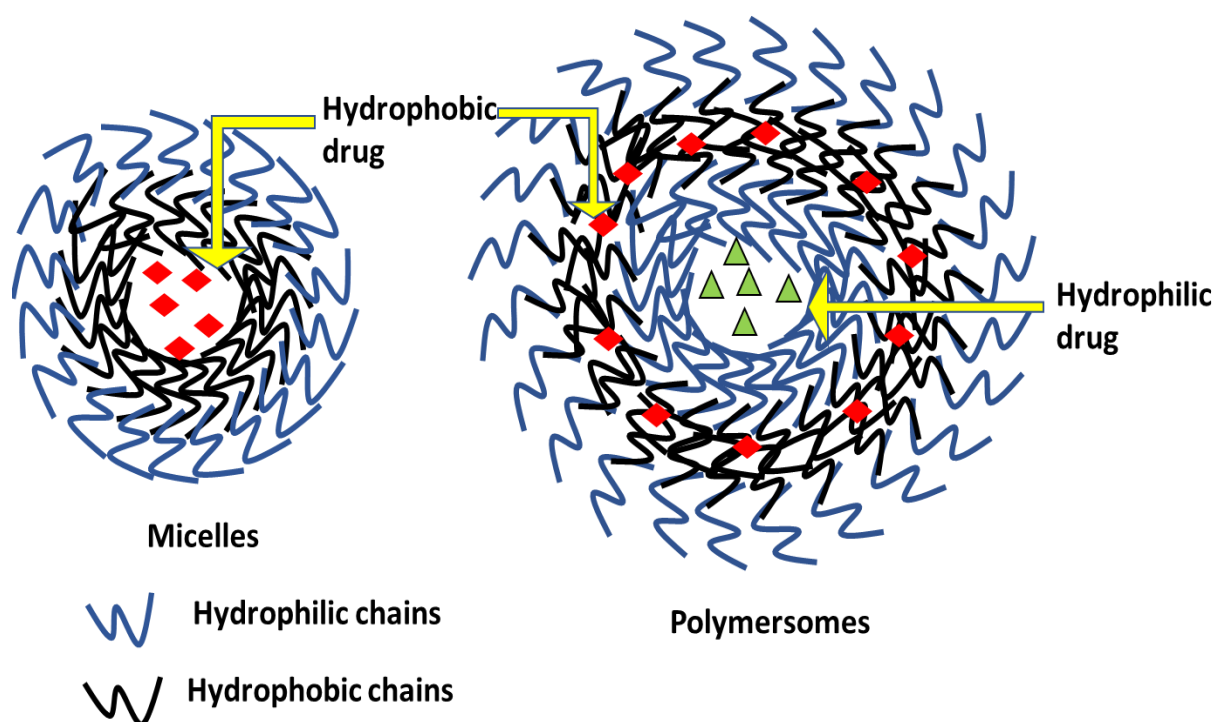


Figure 1-4 Schematic representation of A. micelles and B. polymersomes

The functionality of micelles can be further enhanced by surface and core modifications such as shell crosslinked micelles, surface crosslinked micelles and surface functionalized micelles¹⁴⁵. The addition of crosslinks reinforces the multimolecular micelle structure thus making micelles as a single molecule with crosslinked arms imparting better stability upon dilution and environmental changes along with maintaining their size and morphology. Unimolecular micelles consisting of a single polymer molecule have also been explored. They can be made with polymers having star-shaped or dendritic architecture. These are generally made up of graft copolymers and require controlled synthetic procedures as discussed in section 1.6.3¹⁴⁶. Micelles having different polymer compositions and architecture have been used recently for a variety of applications especially for cancer drug delivery. Micelles have been designed with built in drug interactive cores to enhance the encapsulation of drug and its delivery to the tumour sites and PEG-drug conjugates as dual function carriers for cancer drug delivery¹⁴⁷. Various types of polymeric micelles for active and passive targeting including functional micelles which respond to various external triggers such as pH, temperature and light have also been designed¹⁴⁸. The various applications of micelles will be reviewed in the next sections.

1.8 Self-assembling polymersomes of amphiphilic polymers

In addition to the unilayered micellar systems, amphiphilic block copolymers can also self-assemble into bilayered vesicles called polymersomes composed of a hydrophilic core and a hydrophobic bilayer (Figure 1-4B). They are analogous to liposomes which are made up of lipids however polymersomes are solely made up of amphiphilic copolymers. The mechanism of formation of these bilayered vesicles is similar to those of micelles such that the hydrophobic blocks of the copolymer associate with each other to minimize interactions with the outer aqueous environment whereas the hydrophilic blocks face the inner aqueous core and the outer aqueous environment. Polymersomes can prove advantageous over liposomes because of the better control over the bilayer composition which can be engineered to make much thicker than those of liposomes making them more stable on physical storage and better able to encapsulate hydrophobic drugs¹⁴⁹. The ability of amphiphilic copolymers to self-assemble into bilayered polymersomes largely depends on the

hydrophilic/hydrophobic balance. Discher *et al.* reported that block copolymers having a hydrophilic fraction (f) of $35\% \pm 10\%$ by weight of the total polymers generally tend to self-assemble into polymersomes, whereas polymers with $f > 45\%$ tend to form micelles and those with $f < 25\%$ form inverted microstructures¹⁵⁰ as shown in Figure 1-5. Polymersomes are a distinct class of drug delivery vehicle as their molecular weight is often very large compared to lipid based vesicles and other small molecule surfactants. Asymmetric block copolymers are capable of assembling into various types of structures, the ability of which is dependent on the core-chain and inter-coronal interactions and the interfacial energy in equilibrium with the surrounding media which depends on the composition of the various blocks. Block copolymers with long chain blocks have shown more stability due to a higher bending modulus when compared to short chain block copolymers. The reason for this is that the vesicular phase is more favoured than the lamellar phase, as the molecular weight of the polymer increases increasing the bending modulus. The hydrophobic bilayer of lipids generally lies between 3-5nm whereas that of polymersomes bilayers are bigger and can be designed from 3nm to up to 30nm by choosing the appropriate block compositions (Figure 1-5)^{151, 152}. Apart from the composition of the building blocks, several other factors affect the size and dispersity of the polymersomes such as the presence of ionizable groups on the polymer chain, hydrogen bonding, electrostatic interactions and also several processing factors such as solvent, temperature, additives and preparation method¹⁵³.

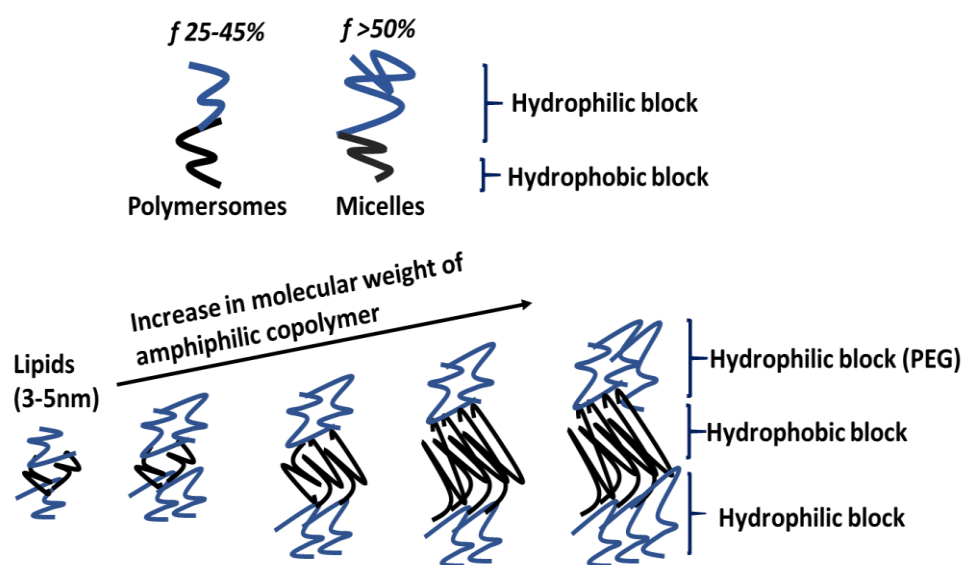


Figure 1-5 Role of f value and molecular weight in the formation of vesicles and thickness of bilayer

Polymersomes can be prepared using the same methods as that of liposomes and can be further fractionated and made uniform in size by extrusion, vortexing, sonication or freeze thawing methods similar to liposomes.

1.8.1 Methods of preparation of polymersomes

Several methods for preparation of polymersomes are reported, they can generally be divided into two major categories: solvent free techniques and solvent displacement techniques.

Solvent free techniques: In these techniques, the polymer is directly brought into contact with the aqueous phase in a dry state, thus eliminating the use of organic solvent. Several methods use this technique such as¹⁵⁴:

Thin film hydration: In this method, the block copolymer is first dissolved in an organic solvent with or without the drug in a round bottom flask which is then evaporated under reduced pressure to form a thin film around the internal wall of the flask. This film is then rehydrated with aqueous medium to form vesicles¹⁵⁵.

Direct hydration: Some block copolymers are capable of self-assembling into polymersomes directly upon dissolving in the aqueous phase without the aid of other solvents¹⁵⁶.

Electroformation: This method is similar to thin film hydration method and is very suitable to produce homogeneous unilamellar polymersomes which are very large in size up to one micrometer. In the method, instead of preparing a film on a solid surface, it is spread out on a pair of electrodes such as indium-tin-oxide glass plates or gold or platinum wires. After the addition of buffer to the system, an electric current is applied which causes vesicles to form by reducing the membrane tension and electrostatic effects¹⁵⁷.

Solvent displacement techniques: These techniques involve dissolving the polymer in an organic solvent and then mixing it with the aqueous phase, the organic solvent is subsequently evaporated using various methods¹⁵⁴.

Solvent displacement/Solvent injection: In this technique, the polymer is dissolved in an organic solvent and added dropwise to the aqueous phase with vigorous stirring. The organic solvent is then removed by dialysis. This method can be used for large scale production of polymers but it has certain drawbacks namely, the organic solvent is retained inside the polymersomes and in the surrounding aqueous phase which can lead to the collapse of the polymersome architecture and faster aggregation rates. The size and dispersity of polymersomes depends largely on the type of solvent, rate of injection and polymer concentration¹⁵⁸.

Solvent evaporation/reverse phase evaporation method: In this method, the amphiphilic polymer in the form of a film is redissolved in a water immiscible organic solvent or a solution of the polymer in the organic solvent is mixed with water to form a two-phase emulsion system. The organic solvent is then removed from the system by evaporation under vacuum. This is an easy and fast technique resulting in small unilamellar vesicles¹²⁷.

Double emulsion: This method involves the formation of water-oil-water (w/o/w) double emulsion and then evaporating the organic solvent to form polymersomes at the concentric interface of the double emulsion¹⁵⁹.

Different methods of preparation can yield different types of vesicles along with polymersomes such as micelles, nanovesicles or tubes. The presence of residual organic solvent can affect biological applications^{154, 160}.

1.9 Applications of self-assembling amphiphilic copolymers

The ability to encapsulate a wide variety of drug including hydrophilic, hydrophobic and amphiphilic molecules renders polymersomes compatible with *in-vivo* applications with their thick outer membrane providing stability to these vesicles. Since most polymersome preparations have PEG as the amphiphilic block they have stealth properties and enhanced circulation times. These advantages of polymersomes have led to numerous applications in various areas of drug delivery such as anticancer therapy, quantum dots, gene and protein delivery and many more¹⁶¹. The combination

of polymersomes with triggered drug delivery has led to several applications especially in cancer therapy. This has been achieved by designing polymers responsive to various stimuli such as temperature, pH and light or the incorporation of dynamic molecules into the core or the hydrophobic bilayers of polymersomes¹⁶². Furthermore, crosslinking these polymersomes can make them structurally “locked” which provides better stability to these nanovesicles and allows controlled release of encapsulated cargo for the desired period of time⁹⁰. The ability to tune surface properties of polymersomes has provided unique opportunities for bioconjugation of various protein, lipids and antibodies allowing more functional diversity to these vesicles being fully derived from synthetic materials¹⁶³.

Some recent applications of amphiphilic polymers are described in the following sections.

1.9.1 Drug solubilizing agents

More than 70% of new chemical entities (NCEs) are poorly water soluble with approximately 40% of oral immediate drug release formulations on the market considered practically water insoluble leading to various issues. Low solubility affects drug dissolution leading to low bioavailability and hence necessitating increase in therapeutic dose causing additional side effects. This further causes decreased patient compliance and increased manufacturing costs¹⁶⁴. The utilization of micelles made of amphiphilic block copolymers has been researched extensively for anticancer drugs which have poor aqueous solubility. The solubilisation ability of micelles largely depends on the nature of the hydrophobic core of the amphiphilic block copolymer. Kim *et al.* describe an increase in the solubility of paclitaxel, a poorly water soluble anticancer drug (5.6mg/L), to up to 38.9mg/ml by the use of N, N-diethylnicotinamide and N-picolyl nicotinamide which proved to be good hydrotropic agents for Paclitaxel¹⁶⁵. Another study utilizing PEG-DSPE/TPGS micelles enhanced the solubilization of Paclitaxel from 0.3µg/ml to 5mg/ml increasing the solubility up to 5000 times¹⁶⁶. Additionally, the solubility of tamoxifen, another poorly soluble anticancer drug, increased from 0.24ug/ml to 0.12mg/ml indicating a 500-fold increase. This was achieved by encapsulating tamoxifen into amphiphilic copolymer

micelles made of PEG 2000 and Palmitic acid with polyaspartylhydrazide (PAHy) graft copolymers¹⁶⁷⁻¹⁶⁹. Camptothecin, a topoisomerase I enzyme inhibitor is utilized for treatment of several cancers, with an aqueous solubility of approximately 1.3 µg/ml when loaded into micelles composed of PEG-Pluronic copolymers conjugated with poly (acrylic acid) a 3-4 fold enhancement in solubility in aqueous medium was recorded^{170, 171}.

1.9.2 Stability improvement

The presence of PEG in amphiphilic copolymers allows the encapsulated drug to be shielded from interactions with opsonins and phagocytosis leading to better circulation times and stability of the drug molecule by inhibiting drug degradation *in-vivo*. The encapsulation of Camptothecin in N-phthaloylchitosan-grafted PEG methyl ether (PLC-g-MPEG) micelles increased the *in-vivo* circulation time by up to 96 hours and also protected the lactone block of the molecule from being hydrolyzed which is crucial for its activity and prevent systemic toxicity as compared to unencapsulated Camptothecin¹⁷². Nagano *et al.* demonstrated that the encapsulation of Dox in PEG-poly(beta-benzyl-L-aspartate) (PEG-PBLA) amphiphilic block copolymer micelles caused 77.5% of drug to be cleared from circulation as compared to free Dox which was 100% cleared, leading to better concentration in tumour site and reducing unwanted side effects¹⁷³. These stabilization and protection properties apply not only to micelles but also polymersomes made of amphiphilic copolymers. Lee *et al.* demonstrated the stability of proteins encapsulated into polymersomes of PEG diblock copolymers. They found that polymersomes readily entrapped these large proteins and also protected them from plasma degradation. The polymersomes were inert to white blood cells and were thermally stable¹⁵⁶. Furthermore, Photos *et al.* have shown the effect of varying molecular weight on the circulation half-life of amphiphilic block copolymers. They state that it is difficult to incorporate high molecular weight PEG into lipids because of the preference to form micelles by very large molecular weight PEG however, polymersomes are mainly composed of PEG-based copolymers which provide additional advantages towards stability and stealth properties. They found that the *in-vivo* circulation time of PEG based polymersomes was up to two fold longer (20h-30h) than that of PEGylated liposomes. The blood clearance of these PEGylated

polymersomes was by opsonization by plasma protein and elimination through liver and spleen ¹⁷⁴.

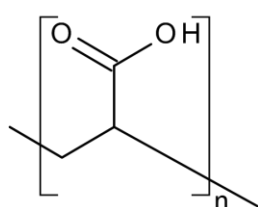
1.9.3 Sustained release

The release of entrapped drug molecules from polymersomes is directly dependent on the thickness of the polymersomes membrane¹⁷⁵. By reducing interactions with plasma proteins, however it improves the uptake by cells and release of drugs by proteases present in the cellular environment. This uptake is favoured by the functionalization of the outer corona with negative charge and addition of more site-specific moieties⁸⁷. Controlled release of drugs plays a very important role when designing scaffolds for tissue engineering. In a recent study by Saito *et al.*, the incorporation of recombinant human bone morphogenetic protein-2 (rhBMP-2) which is an osteoinductive growth factor, into PEG-PLA micelles, supported better ectopic bone formation when implanted in dorsal muscles of mice than micelles with just PLA homopolymers. This effect is attributed to the sustained release of the growth factor rather than a burst release at the site of action and is attributed to the lower degradation rate of micelles ¹⁷⁶.

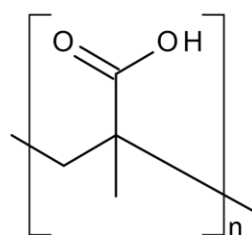
1.9.4 Triggered release

Stimuli sensitive amphiphilic copolymers form a special class of polymers which undergo structural changes in response to various internal or external stimuli leading to the disintegration, isomerization, destabilization or polymerization of the self-assembled nanostructures. Tumour microenvironment can have various intrinsic properties such as elevated temperature, redox potential, lowered pH and overexpressed enzymes. External stimuli constitute temperature, light, magnetic fields, ultrasound or their combinations. Various external and internal stimuli have been exploited to trigger the stabilization of polymeric micelles or vesicles to release their content in specific microenvironments to reduce side effects in other parts of the body¹⁷⁷. Amphiphilic copolymers composed of an ionic block are mainly pH sensitive which enables their destabilization at the low pH of the tumour microenvironment. Most commonly used pH sensitive ionic blocks are poly (acrylic acid) (**3**) and poly (methacrylic acid) (**4**) which have acid labile carboxylic groups which are unionised at

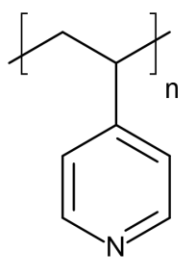
lower pH leading to disruption of the vesicular structure. Cationic polymers having tertiary amino group such as poly (vinyl pyridine) **(5)** and poly (histidine) **(6)** are non-ionic at physiological pH but become protonated at low pH are other examples of pH sensitive polymers¹⁷⁸.



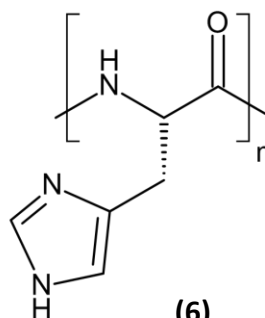
(3)



(4)



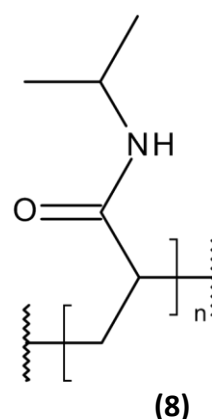
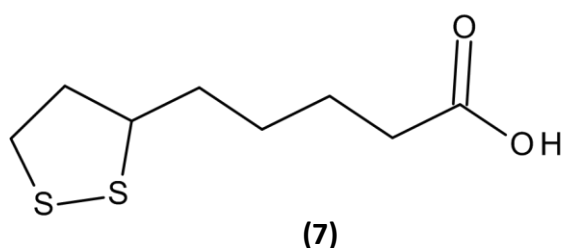
(5)



(6)

The elevated levels of glutathione present in cancer cells has been exploited to trigger release of drugs in the intra-tumoral environment. Amphiphilic copolymers having a sulfide bond are stable at room temperature but the disulfide bond is reduced in the presence of glutathione tripeptide (GSH) and instantly release the encapsulated drug at the target site¹⁷⁹. Disulfide crosslinks (-S-S- linkages) are generally introduced at the interface of the hydrophilic and hydrophobic blocks. Fan *et al.* synthesized micelles having amphiphilic copolymers using thioctic acid **(7)** based disulfide linkages and loaded them with paclitaxel. Resultant micelles demonstrated ~3-5 fold greater plasma concentration than non-crosslinked amphiphilic copolymer micelles and improved kinetic and thermodynamic stability with instant release of drug in high GSH tumour environment¹⁸⁰.

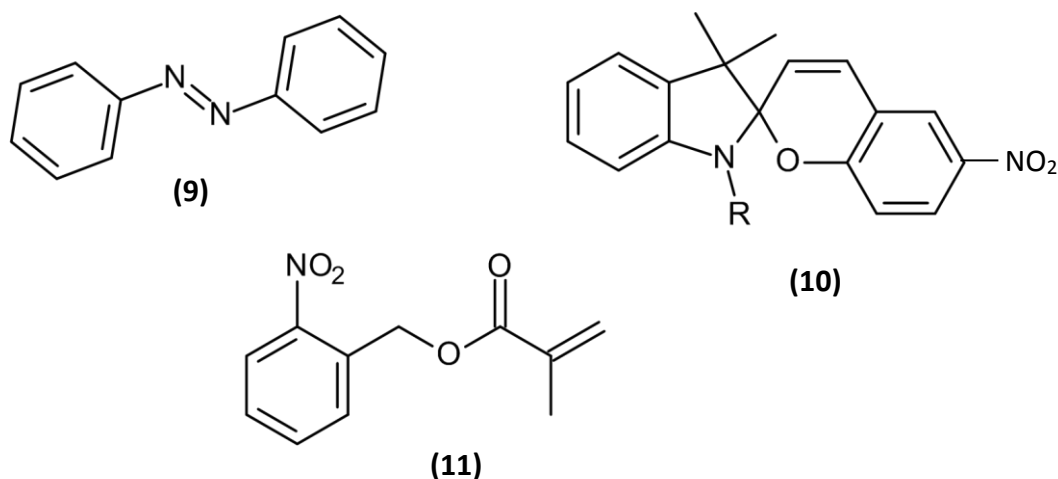
Temperature responsive polymers rely on the thermo-responsive properties of the amphiphilic block copolymers which are completely soluble below a certain temperature but at slightly elevated temperatures undergo a sharp change in their solubility due to breakage of hydrogen bonds, leading to destabilization of the nanostructures, thus releasing the drug in the surrounding environment.



A common example of a thermo-responsive polymer is poly (N-isopropyl acrylamide) **(8)** which is a hydrophilic coil-like structure at room temperature but above 32°C undergoes a phase change leading to a hydrophobic globule state which precipitates out of solution triggering drug release¹⁸¹.

Apart from the above intrinsic triggers, many external stimuli such as light, magnetic field and ultrasound can be employed to enable the release of drugs from within the nanosphere environment. Light has been used extensively as a trigger because of its ease of use and the ability to control drug release with spatial and temporal accuracy^{182, 183}. Light can work in two ways as a stimulus, first by photoinduced structural changes such as reversible isomerization, crosslinking and/or changes in hydrophilicity/lipophilicity. Secondly, light can induce degradation or cleavage of the polymer at specific junctions leading to breakage of the nanoassembly. Most widely used photoresponsive materials are azobenzenes **(9)**, spiropyrans **(10)**, O-nitrobenzyls **(11)**, 2-diazo-1,2-naphthoquinones and coumarin derivatives. For example, spiropyrans **(10)** undergo reversible photoisomerization in UV light from the closed

ring hydrophobic spiropyran to a hydrophilic open ring merocyanine and reverses in the presence of visible light. Liu *et al.* reported the synthesis of PEG-b-PSPA block copolymer with spiropyran using carbamate linkages and formed polymersomes with a reversible bilayer permeability alternating UV and visible light¹⁸⁴. In another example, O-Nitrobenzyl (ONB) (**11**) has been utilized as a photocleavable photochromic moiety which can be integrated in copolymer blocks during synthesis. As reported by Meier *et al.*, amphiphilic block copolymers having ONB linkers were synthesized and loaded with low molecular weight dyes into the vesicles. Upon exposure to UV radiation, the vesicles disintegrated into smaller micellar structures releasing the payload in the process which was controllable by varying intensity of UV light^{185, 186}.

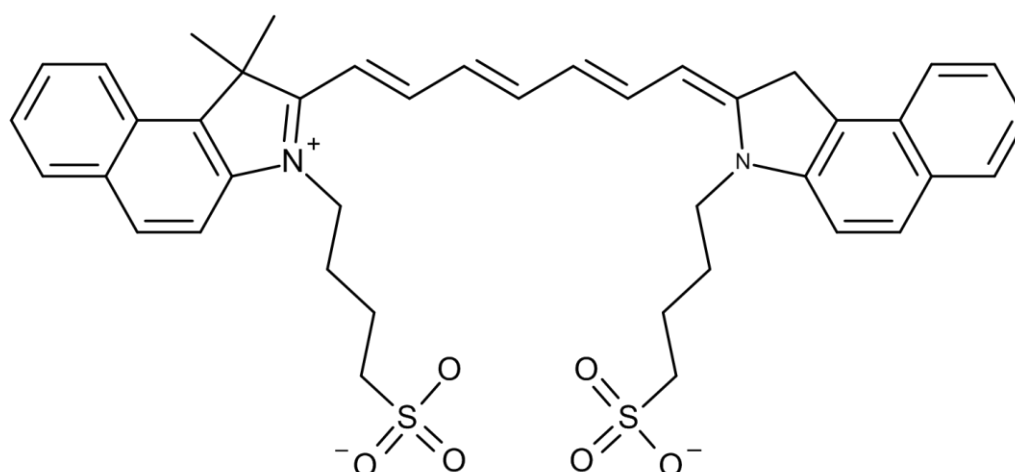


Furthermore, a magnetic field has been employed as an external stimulus by encapsulating ferromagnetic molecules, such as ferric oxide, along with the drug inside the nanovesicles. The application of an extracorporeal magnetic field at the biological site causes high accumulation of the nanocarrier at the target site leading to increased drug concentration and thus better efficacy¹⁸⁷. Ultrasound is another external stimulus which employs the use of ultrasound waves to trigger destabilization by cavitation phenomenon¹⁸⁸ of micelles, polymersomes, liposomes and microbubbles. Examples of ultrasound mediated delivery include PEG-PCL nanobubbles loaded with perfluorocarbon and curcumin, mPEG-PLGA micelles loaded

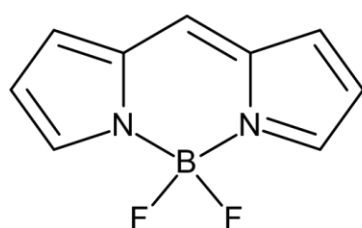
with Dox and perfluorocarbon and paclitaxel loaded mPEG-poly (D, L-lactide) micelles to achieve high accumulation in prostate cancer cells¹⁸⁹⁻¹⁹¹.

1.9.5 Imaging applications

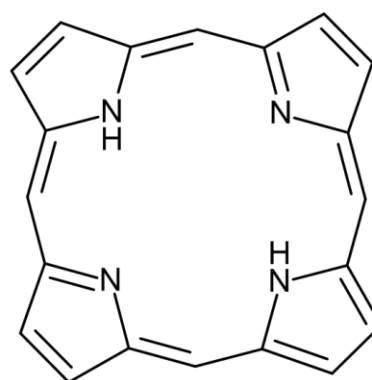
In-vivo imaging can play a major role in determining the kinetics of drug molecules further influencing its therapeutic efficiency. Non-invasive techniques to study biodistribution of amphiphilic molecules can help greatly in the development of delivery vehicles without the need to sacrifice animals. Infrared and near-infrared light are more commonly used for deep tissue imaging than visible light because of their better penetration ability. Hence dyes which fluoresce/luminesce in the presence of near infrared light can be encapsulated or conjugated to a polymer and monitored *in-vivo* to observe the effects of the amphiphilic copolymers in real time^{22, 192}. Amphiphilic copolymer micelles have been extensively used for different areas of purely diagnostic imaging or imaging with drug delivery for visual control of kinetics¹⁹³. Encapsulation of contrasting agents for imaging into NPs provides many advantages, such as longer circulation time and targeting of delivery vehicle to the desired site of imaging to reduce signal to noise ratio. In addition, multiple molecules of the contrast agent can be encapsulated into a single NP along with cancer targeting ligands allowing better contrast specificity and tuneable biodistribution¹⁹⁴. Paramagnetic materials such as iron oxide, gadolinium (Gd), Manganese (Mn) are a few examples of contrast agents commonly used for bioimaging. Apart from contrast agents, many fluorescence based dyes that excite in the near infrared region are also utilized for bioimaging. These dyes have advantages of minimal interference from biological fluids, good tissue penetration and reduced light scattering. NIR dyes commonly used for biological applications are cyanines such as indocyanines (**12**), porphyrins such as photoporphyrins (**14**) and BODIPY (**13**) analogs¹⁹⁵.



(12)



(13)



(14)

1.9.6 Multifunctional nanocarriers

Recent challenges in the development of advanced drug delivery systems have led to the development of multifunctional carriers which combine the therapeutic purpose of the nanovehicles with a diagnostic/imaging property to provide unique theranostic systems. Multiple modes of treatment such as triggered release, tumour targeting using ligands, photodynamic therapy, chemotherapy etc. can be combined with imaging techniques such as MRI, fluorescent dyes as markers for imaging or FRET, nuclear imaging methods such as CTs, PETs to facilitate real time or retrospective imaging of the drug delivery system which can provide insights into the pharmacokinetics, pathways and efficacy of the delivery system^{196, 197}. Schematic representation of different attachments to obtain multifunctional nanocarriers is depicted in Figure 1-6.

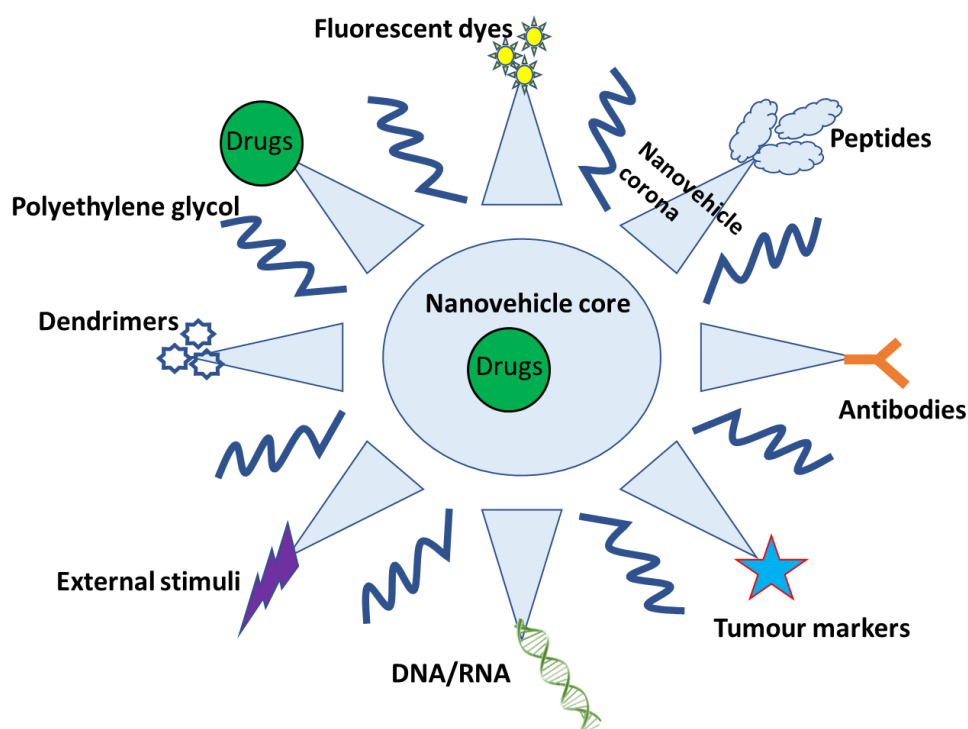


Figure 1-6 Schematic representation of multifunctional nanocarriers

In a recent example by Gong *et al.*, they developed pH responsive amphiphilic copolymer vesicles using heterofunctional triblock polymers loaded with superparamagnetic iron oxide NPs (SPIONs) into the inner core and Dox conjugated to the PGlu segment of the polymer via hydrazine linkages. This dual property of the NPs allowed excellent stability with pH controlled release of Dox and MRI contrast imaging of the NPs at the tumour site¹⁹⁸. Furthermore, multifunctional NPs can be used to combine different targeting strategies into one nanocarrier to achieve selectivity or enhanced therapeutic efficacy of the delivery system. For example, Huang *et al.* synthesized complex NPs into which SPIONs were loaded in the inner core and cisplatin was coordinated in the hydrophilic shell. These NPs showed increased anticancer activity with the combined effects of cisplatin and SPION induced hyperthermia¹⁹⁹. Kataoka *et al.* developed cancer specific folate bound ligands on the micelle surface and Dox linked to the hydrophilic block via acid cleavable bonds, the folate leads the micelles to the tumour tissue and were endocytosed via receptor mediated endocytosis²⁰⁰. The folate bound micelles displayed significant cell growth inhibition and higher cellular uptake when analysed by MTT and flow cytometry respectively.

1.9.7 Passive targeting

NPs can passively retain in tumours for longer duration of time due to the enhanced EPR effect even if there are no targeting ligands present on the delivery vehicle²⁰¹. Generally, solid tumours possess high vasculature, incomplete vascular profile, increased extravasation due to presence of vascular permeability factors and immature lymphatic network (Figure 1-7). These properties make them vulnerable to macromolecules which are not easily drained due to improper lymphatic drainage leading to retention of these molecules in tumours for prolonged periods of time^{46, 202}. To achieve good passive targeting by the EPR effect, many obstacles such as glomerular excretion, elimination by the RES, interaction by plasma proteins and phagocytosis have to be overcome. The addition of PEG to the amphiphilic copolymer provides stealth properties which help overcome some of the above mentioned problems. Particle size is also a key factor in passive targeting since a lot physiological elimination processes such as hepatic filtration, renal excretion, tissue diffusion and extravasation are dependent on particle size²⁰³. The optimum particle size to avoid phagocytosis and hepatic clearance is less than 200nm²⁰⁴ and upto 40kDa mass to avoid renal filtration. The leaky vasculature of tumour blood vessels means they contain intercellular gaps which do not require energy dependent material movement. Jain *et al.* determined that liposomes up to 400nm in diameter were permeable into tumour tissue suggesting tumour penetration cut off size of 400-600nm²⁰⁵. The shape of NPs is also favoured to achieve good passive diffusion. Inert worm-shaped micelles have shown to have longer circulation times than spherical micelles with short worm-like micelles more preferred than longer worms^{206, 207}. Although passive diffusion helps to concentrate NPs, various factors such as tumour heterogeneity, types and location of tumour limit this approach of drug delivery²⁰⁸.

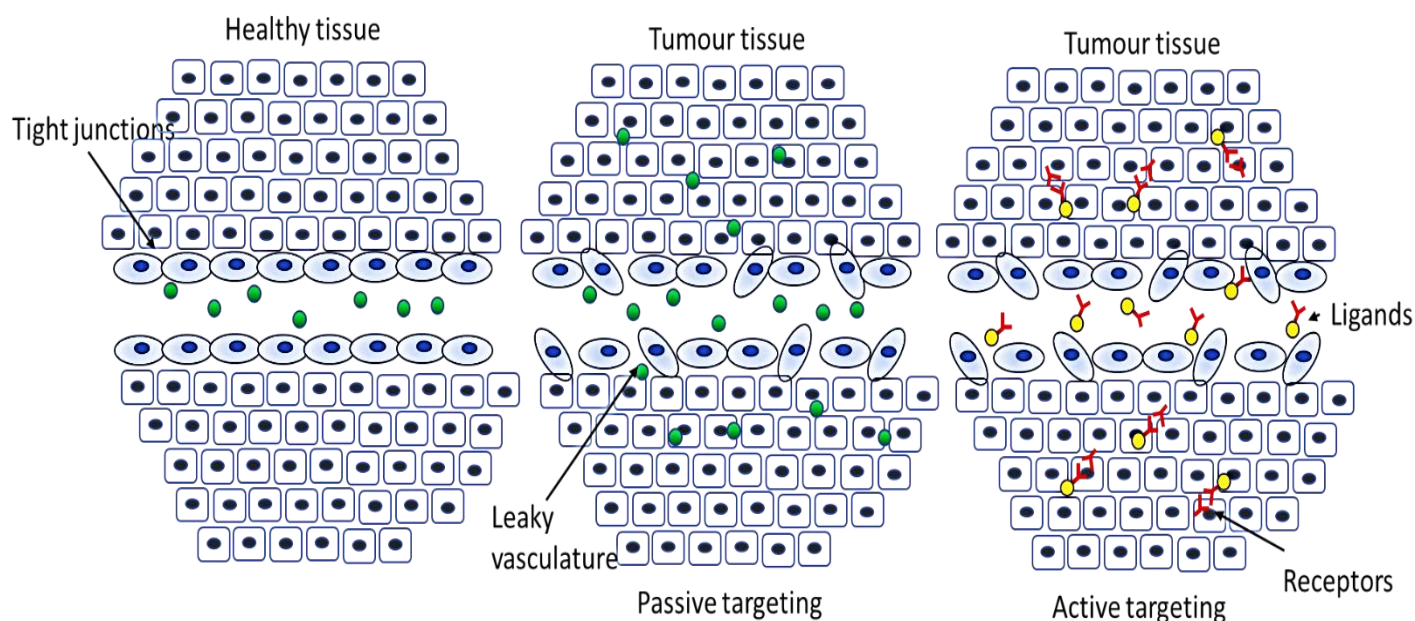


Figure 1-7 Mechanism of passive and active targeting in tumour tissues

1.9.8 Active targeting

Diseases such as cancer and inflammation have overexpressed epitopes and receptors which can be used as targets to enhance accumulation of NPs at the desired tumour site. Ligands coupled to the NP surface which bind specifically to the target receptors can be used for active targeting of therapeutics for enhanced activity^{209, 210} (Figure 1-7). Ligands can be coupled to the surface of the amphiphilic copolymer by various methods such as covalent and noncovalent binding. Common binding methods include disulfide bonds, crosslinking, acid base reactions and aldehyde-amine reactions. However, these methods can be rigorous and destructive for the binding ligand. Non-covalent bindings also have associated problems such as weak binding, low concentrations and poor control of binding reactions²¹¹. Active targeting by binding ligands to polymer NPs has several advantages, such as a high encapsulation ability, avoidance of drug modification by binding ligand to drugs leading to efficient therapeutic activity of drug, possibility of large number of ligands attachment at various sites on the surface of the polymer and small size of the ligand-polymer conjugate leads to higher extravasation into the tumour site without affecting any

binding sites on healthy tissues³¹. Various targeting receptors that are overexpressed in tumours are: carbohydrate based targeting, mAb based targeting, folate based targeting, protein/peptide based targeting and aptamer based targeting¹³⁷. Another active targeting approach is to take advantage of locally applied signals such as ultrasound and magnetic field to mediate the transport of the nanocarriers to the site of action¹³⁷.

1.9.9 Simultaneous drug delivery

The advances in combination therapies has led to the requirement of drug delivery systems to expand so that both hydrophobic and hydrophilic drugs can be delivered in the same vehicle simultaneously⁷⁸. Several examples of amphiphilic copolymer micelles for simultaneous delivery of both hydrophobic and hydrophilic drugs are reported¹⁷⁹. The most common approach is where the nonpolar core is used to encapsulate the hydrophobic drug while a charged outer corona (usually positively charged) is used to electrostatically interact with the biological component. Both Qian *et al.* and Bian *et al.* have successfully encapsulated Dox in the core of the micelle and conjugated micro-RNA and green fluorescence labeled DNA^{212, 213} to the corona. Qian *et al.* used amphiphilic star branched copolymers using polylactic acid (PLA) and polydimethylaminoethyl methacrylate (PDMAEMA) while Bian *et al.* used poly(ethylethylene phosphate)-blockpoly(e-caprolactone)-block-poly[2-(dimethylamino) ethyl methacrylate (PEEP-b-PCL-b-PDMAEMA). The PLA and PCL chains formed the hydrophobic core whereas the PDMAEMA forms the positively charged outer corona to which the RNA/DNA was attached by electrostatic interactions. There are a few examples where these same drugs have been combined within a polymersome²¹⁴. Iatrou *et al.*²¹⁵ have investigated two different polymersomes for the independent delivery of Dox and PTX, comparing a tri block co-polymer with a terpolymer. They concluded that both forms of polymer were capable of encapsulating both drugs, but did not allude to whether the possibility of simultaneous delivery was to be investigated in the future but did anticipate the incorporation of genes with either of the anticancer drugs.

1.10 Aims and Objectives

The main aim of the work carried out in this thesis was to evaluate different amphiphilic copolymers for their ability to self-assemble into micelles and polymersomes and to evaluate their efficiency for encapsulating different types of dyes and anticancer drug *in-vitro* and *in-vivo*. Although the primary focus of this research work is the preparation and evaluation of polymersomes (Chapters 2 &4), chapter 3 evaluates the preparation of micelles using amphiphilic copolymers and a novel application approach. The specific aims of each chapter are as follows,

1.10.1 Chapter 2: Design of self-assembling random copolymer based polymersomes and their comparison to pegylated liposomes

The aim of this research work was to prepare amphiphilic random copolymers using free radical polymerization having structural similarities to liposomes. Accordingly amphiphilic random copolymers having composition consisting of an octadecyl chain and oleic acid, cholesterol and two chain lengths of PEG (P500 and P2000) were synthesized and confirmed using Mass spectroscopy and ^1H NMR spectroscopy. These polymers were evaluated for their ability to form bilayer polymersomes using dynamic light scattering and zeta potential. They were then compared to liposomes for cell toxicity, cellular uptake and stability over time.

1.10.2 Chapter 3: The integration of triggered drug delivery with real time quantification using FRET; creating a super 'smart' drug delivery system.

The aim of the work undertaken in this chapter involves the encapsulation of photodynamic spiropyran (**32**) within micelles of an amphiphilic copolymer. The application of UV light allowed hydrophobic spiropyran to convert to hydrophilic merocyanine allowing it to transcend across the micelle into the surrounding environment. This release affected the FRET relationship between a bodipy compound (**31**) and merocyanine, allowing real time quantification of merocyanine release from the micelles.

1.10.3 Chapter 4: Multi drug loaded polymersomes for increased efficacy of cancer therapy

This chapter involves the simultaneous encapsulation of multiple anticancer drugs into polymersomes and evaluation of their encapsulation efficiency and particle size. The polymersomes were evaluated for their pharmacokinetics in-vivo by imaging with Indocyanine green (ICG) loaded polymersomes. The tumour reduction ability of Doxorubicin hydrochloride (Dox), 5-Fluorouracil (5-FU) and Leucovorin calcium (LV) loaded polymersomes was observed after intratumoral and intravenous injection in mice and measurement of tumour volume over time.

Chapter 2

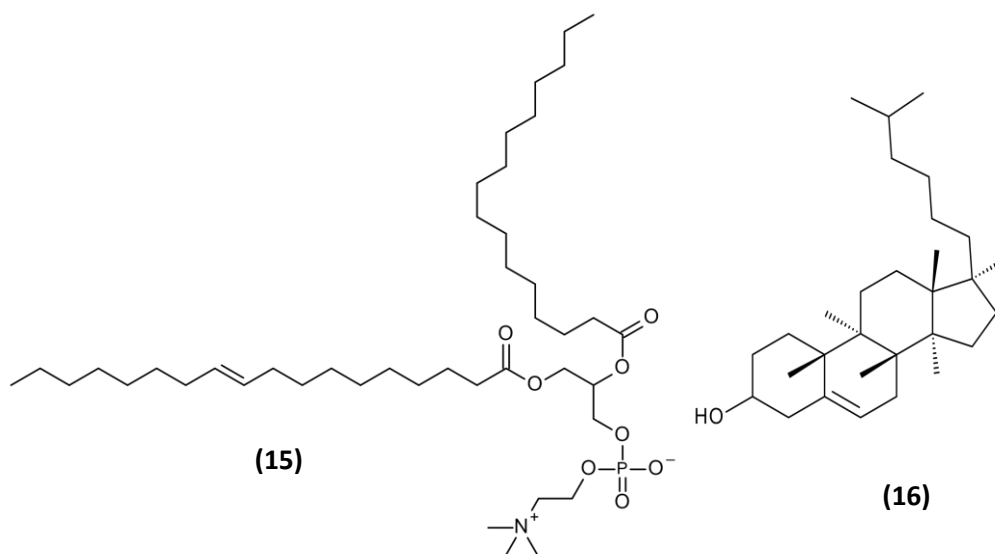
Design of self-assembling random copolymer based polymersomes and their comparison to pegylated liposomes

2.1 Introduction to bilayer drug delivery systems

Single layer drug delivery systems such as polymeric micelles made of amphiphilic copolymers have shown success as drug delivery vehicles for hydrophobic drugs having poor solubility and low bioavailability²¹⁶. Micelles have been employed as drug delivery systems not only for cancer chemotherapy²¹⁷⁻²²⁰ but also for other areas of therapeutic drug delivery such as Herpes Simplex Virus HSV infection²²¹, gene delivery²²² and inflammation²²³. Polymeric micelles are single layer supramolecular assemblies which have a hydrophobic core to accommodate hydrophobic drugs and hydrophilic shell which makes them easily water dispersible, thus allowing the delivery of these drugs²²⁴. However the presence of a single layer means that they can deliver only hydrophobic drugs making them less advantageous than bilayer systems such as liposomes and polymersomes. Liposomes are nanovesicular structures that are typically made of lipids whereas polymersomes are fully synthetic polymeric analogues of liposomes²²⁵. These bilayer structures are biphasic and consist of a hydrophilic core for encapsulation of hydrophilic drug and a hydrophobic bilayer which can accommodate hydrophobic drugs. They have a hydrophilic outer corona which allows them to disperse in aqueous medium^{226, 227}. Due to the amphiphilic nature of the lipids and polymer blocks, these molecules can spontaneously assemble into bilayer nanovesicles determined by the hydrophilic lipophilic balance. Based on the type of lipid and polymers, these systems can be tailored according to the nature of application²²⁸. Liposomes and polymersomes based bilayer systems offer several advantages such as the ability to encapsulate a larger variety of drugs and better multifunctionalisation than single layer micellar systems. Further, these systems can be utilized to co-encapsulate both hydrophilic and hydrophobic drugs simultaneously, further increasing their advantages over the single layer systems²²⁹. Liposome and polymersome based systems have been employed for a wide range of drug delivery systems such as theranostics involving both therapeutic and diagnostic delivery^{230, 231}, large molecules such as proteins and gene delivery^{232, 233} and stimuli responsive drug delivery²³⁴.

2.2 Composition of liposomes

Phosphatidylcholines extracted from egg or soybean are commonly used lipids for making liposomes because they are a major component of the cell membrane²³⁵. Phosphatidylcholine **(15)** typically consists of a choline head group with a saturated fatty acid such as palmitic or hexadecanoic acid and an unsaturated fatty acid such as oleic acid **(15)**²³⁶. Liposomes also consist of cholesterol **(16)** which helps achieve rigidity of the bilayer membrane and a PEG **(1)** outer layer which gives stealth properties to liposomes.



Nguyen *et al.* encapsulated paclitaxel in soy phosphatidylcholine and cholesterol liposomes and observed their *in-vitro* properties. They found that the liposomes were less than 200nm in size and demonstrated more than 90% encapsulation of paclitaxel²³⁷. Tao Yang *et al.* demonstrated increased solubility of paclitaxel encapsulated in egg phosphatidylcholine and cholesterol liposomes (molar ratio 90:10) and compared their cytotoxicity in MDA-MB-231 human breast cancer cell line against marketed formulation Taxol²³⁸.

Physical properties of liposomes depend on lipid composition, size, surface charge and method of preparation. For example phospholipids exhibit more permeable and unstable bilayers. Cationic surface charge on liposomes leads to rapid clearance from

the body but demonstrates better cell internalisation²³⁹. Even though liposomes are identical to biomembranes, they are still foreign objects to the body and are rapidly cleared by the mononuclear phagocytic system (MPS) on contact with plasma proteins. This problem is solved by coating liposomes with polyethylene glycol (PEG). PEG reduces uptake by macrophages and prolongs circulation time²⁴⁰. Surface modification of liposomes using PEG improves their circulation time thus providing better uptake into target cells and avoids elimination via RES^{241, 242}. Many liposomal formulations are currently in the market and many more are in different phases of clinical trials^{50, 243} for treatment of various cancers however they are still considered to be disadvantageous because of their low stability and membrane leakage²⁴⁴.

2.3 Polymersomes synthesized with amphiphilic random copolymers

Polymersomes as nanoparticulate drug delivery systems have gained a lot of attention recently for having several advantages over liposomes such as higher stability, better control over membrane properties and ability to encapsulate large variety of drugs²⁴⁵. Polymersomes are next generation nanovesicles facilitating to overcome the shortcomings of liposomes and provide advanced therapeutic care especially for cancer therapy. An insight into recent research demonstrates the ability of polymersomes used for targeted delivery, stimuli responsive drug delivery such as redox responsive¹²⁵, pH sensitive^{126, 246}, temperature sensitive²⁴⁷, hypoxia responsive²⁴⁸, delivery of genes²⁴⁹ and combined anticancer therapy²⁵⁰. Polymersomes have a vesicular structure similar to liposomes with a hydrophilic core and a hydrophobic bilayer allowing encapsulation of both hydrophilic and hydrophobic drugs with a hydrophilic corona. Polymersomes are mainly made of block polymers capable of self-assembling into nanoscale vesicles with PEG as the hydrophilic block²⁵¹. These high molecular weight polymers possess similar amphiphilic properties as lipids but are comprised of polymer chains covalently linked as successions of two or more blocks offering a membrane which is more compact providing rigidity and better stability to these vesicles²⁵². It is important for polymersomes to be biodegradable or to be at least biocompatible, most block polymers used for making polymersomes typically have PEG as the hydrophilic block attached to a hydrophobic block such as

poly-ε-caprolactone (PCL), poly(lactide), poly-(N-(2-hydroxypropyl) methacrylamide) (pHPMA), poly(ethylene-imine) (PEI), poly(vinylpyrrolidone) (PVP)^{245, 253} The main disadvantage of using block copolymers is their method of preparation. Synthesis of block copolymers requires controlled polymerisation and post processing such as substitution, hydrolysis and click chemistries making the process multi step and time consuming requiring specific equipment and additional resources^{254, 255}. Hence random copolymers have been explored for their ability to self-assemble and their ease of preparation and adaptability. Synthesis of random copolymers is an easy one-step process also referred to as 'one pot synthesis' proving attractive to synthetic chemists for use as self-assembling amphiphilic polymers¹⁰³. Recent research investigations using random copolymers have demonstrated self-assembly into different shapes such as nanovesicles, spheres and honeycomb films depending on the hydrophilic/lipophilic balance²⁵⁶. Dey *et al.* demonstrated the ability of amphiphilic random copolymer scaffolds to form vesicles and induce myotube formation from C2C12 cells which had the ability of differentiate in the presence of growth media allowing them to be used for muscle cell regeneration²⁵⁷. Hirai *et al.* demonstrated the ability of amphiphilic random copolymers to be able to form nanovesicles in an aqueous environment. These polymers were composed of PEG as the hydrophilic component and hydrophobic dodecyl chains which were polymerised using both metal catalysed living radical polymerisation and conventional free radical polymerisation. The tendency of those polymers to self-assemble into intramolecular and intermolecular nanovesicles could be controlled by increasing or decreasing the hydrophobic moiety and degree of polymerisation which also affected size of the particles²⁵⁸.

2.4 Aims of Chapter

The overall aim of this chapter was to create a polymersomal system to mimic a liposomal system closely then compare the two NP's in terms of stability, encapsulation and release as well as size and surface charge. The individual components of the liposomes and polymersomes were compared allowing the

creation of NP's of similar composition. Figure 2-1 displays the components with each DDS.

In this research chapter we investigate the ability of long chain polymers having octadecyl side chains with cholesterol and high molecular weight PEG to form polymersomes encapsulating both hydrophilic and hydrophobic dyes and compare their cellular uptake to liposomes having a similar composition. The hydrophilic dyes used were negatively charged FITC-CM-Dextran (FCD), positive charged FITC-DEAE-Dextran (FDD) and neutral FITC-Dextran(F-D) having average MW 4000 Da freely soluble in water and PBS. FITC-Carboxymethyl-Dextran has an anionic charge due to the presence of negatively charged carboxyl groups. FITC-Diethylaminoethyl-Dextran have a net positive charge due to the presence of tertiary amino groups. F-D is neutral due to the low level of substitution leading to minimal charges on the dextran moiety. The hydrophobic dye employed was anthracene, a polycyclic aromatic hydrocarbon which gives a blue fluorescence and is soluble in chloroform, alcohols and hexane.

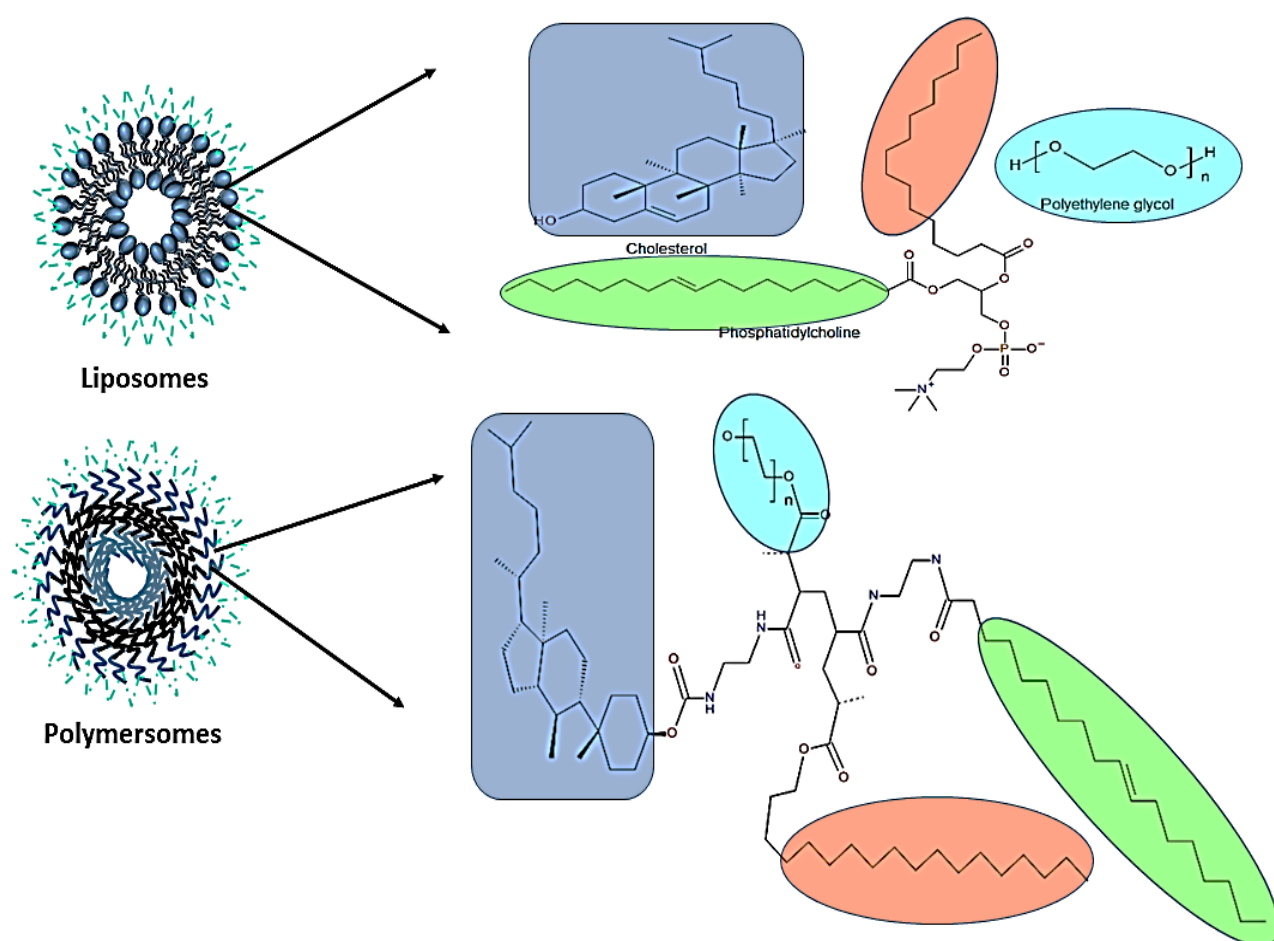


Figure 2-1 : Schematic representation of comparison and design of chemical structure of polymers to lipid

The aim of this research work was to prepare amphiphilic random copolymers using free radical polymerisation having composition analogous to liposomes, Figure 2-1.

The specific aims of the chapter were,

1. Synthesis of amphiphilic copolymers composed of an octadecyl chain and oleic acid, cholesterol and two chain lengths of PEG (P500 and P2000).
2. Preparation of polymersomes and liposomes by three methods of preparation-thin film hydration (TFH), emulsion evaporation (EMEV), reverse phase evaporation (RPE). Evaluation of size, PDI, zeta potential and % encapsulation efficiency of FCD, FDD, F-D and anthracene in liposomes and polymersomes.
3. Observation of cellular uptake of FCD and anthracene encapsulated polymersomes and liposomes in HeLa cells.
4. Observation of cellular uptake pathways of polymersomes and liposomes loaded with FCD by chemical inhibition of endocytosis using chlorpromazine in HeLa cells.
5. Fluorescence observation of cellular uptake of FCD and anthracene loaded liposomes and polymersomes.
6. Evaluation of cell cytotoxicity of polymersomes compared to liposomes having PEG 2000 in three cell lines-HeLa cells, BxPC-3 cells and CHO cells.
7. *In-vitro* release studies of liposomes and Polymersomes of PEG 2000 for both hydrophilic and hydrophobic dyes.
8. Physical stability studies of PEG 2000 liposomes and polymersomes loaded with hydrophilic and hydrophobic dyes under refrigerated conditions and 25°C for observation of changes in size and encapsulation efficiency.

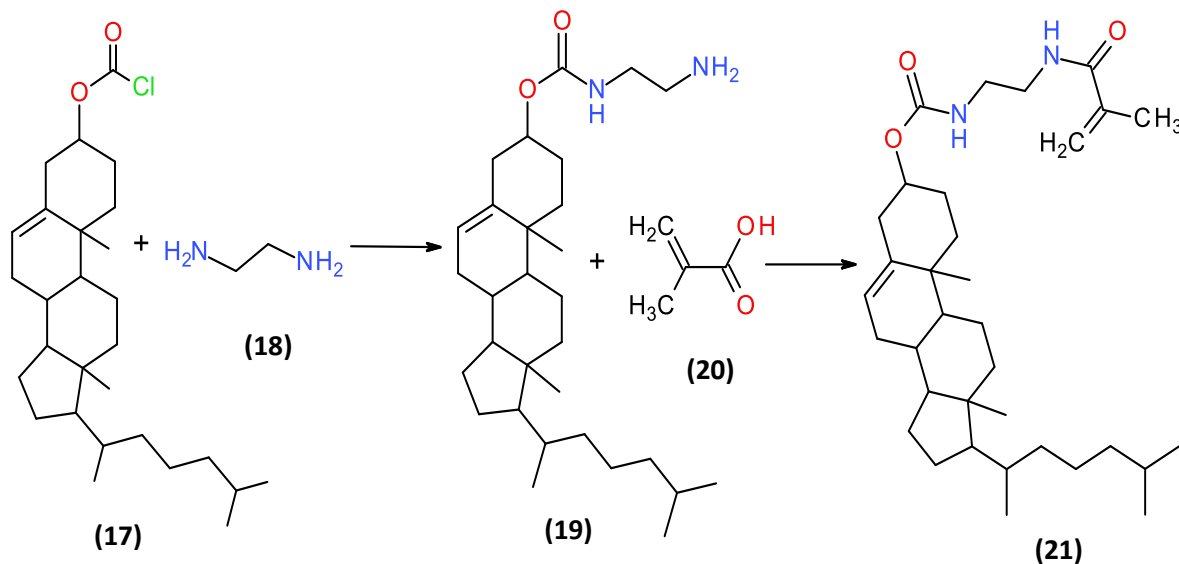
2.5 Results and discussion

2.5.1 Synthesis of monomers and polymers

Three monomers namely cholesteryl methacrylate, octadecyl methacrylate and oleic methacrylate were synthesized as discussed in below sections,

2.5.1.1 Synthesis of cholesteryl methacrylate (21)

Synthesis of **21** was a two-step process with an intermediate of cholesteryl ethylene diamine (19). The reaction scheme for synthesis of **21** is depicted in Scheme 2-1.



Scheme 2-1 Synthesis of cholesteryl methacrylate (21)

The compound **19** was synthesized according to the procedure described by Martin et al.¹²⁸ discussed in detail in section 6.3.1. and confirmed by mass spectroscopy. Figure 2-2 displays the LC/MS (ESI) m/z : $[M + H]^+$ positive mode for **19** with the expected parent ion of 474.7 confirming the conjugation of ethylene diamine (18) with cholesteryl chloroformate (17).

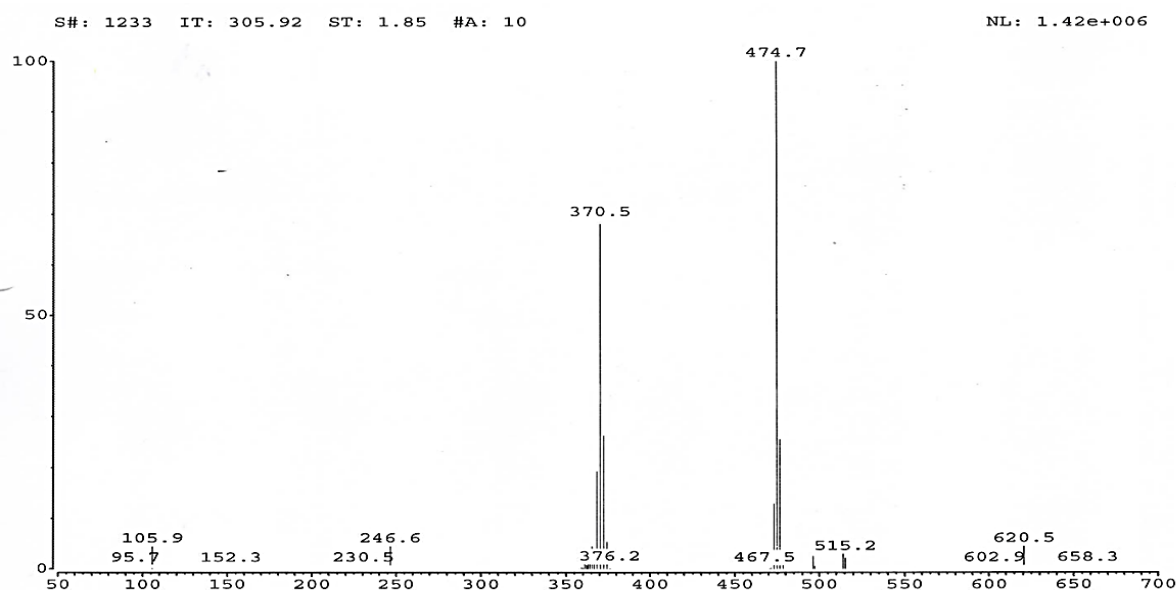


Figure 2-2 Mass spectrum of cholesteryl ethylene diamine conjugate (19)

The second step involved in the synthesis of **21** as depicted in reaction Scheme 2-1 and involves the formation of an amide bond. Successful synthesis of **21** was confirmed by Mass and ^1H NMR spectroscopy. The LC/MS (ESI) m/z : $[\text{M} + \text{H}]^+$ calculated for **21** was found at 541.0 accounting for the +1 peak (Figure 2-3).

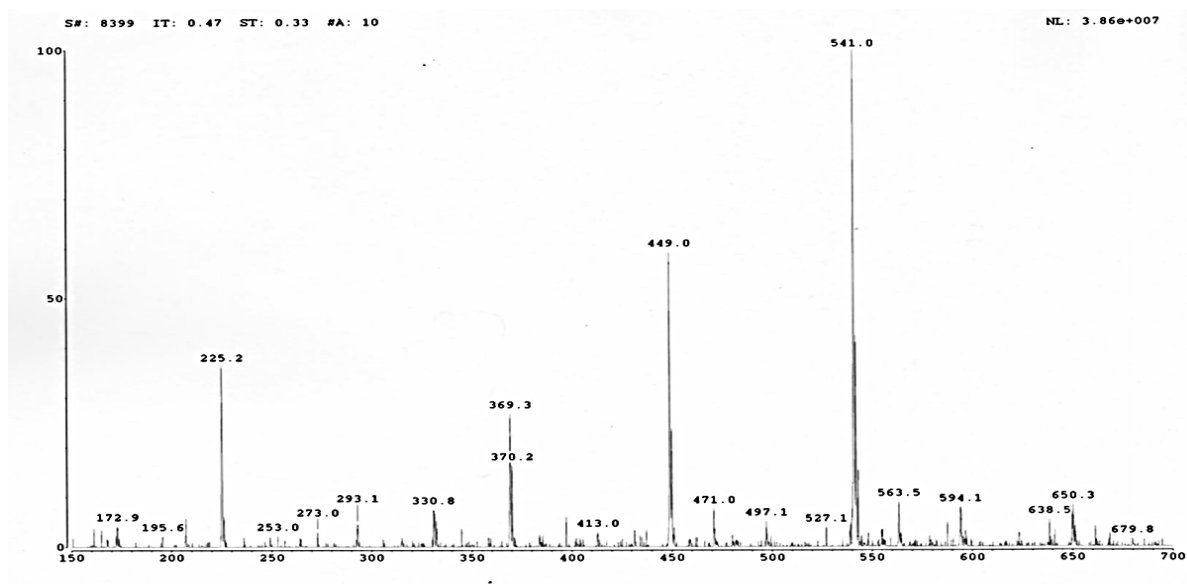


Figure 2-3 Mass spectrum of cholesteryl methacrylate (**21**)

Synthesis of **21** was further confirmed by ^1H NMR spectroscopy (Figure 2-4). The spectral shifts were assigned to their corresponding protons as illustrated in the structure insert.

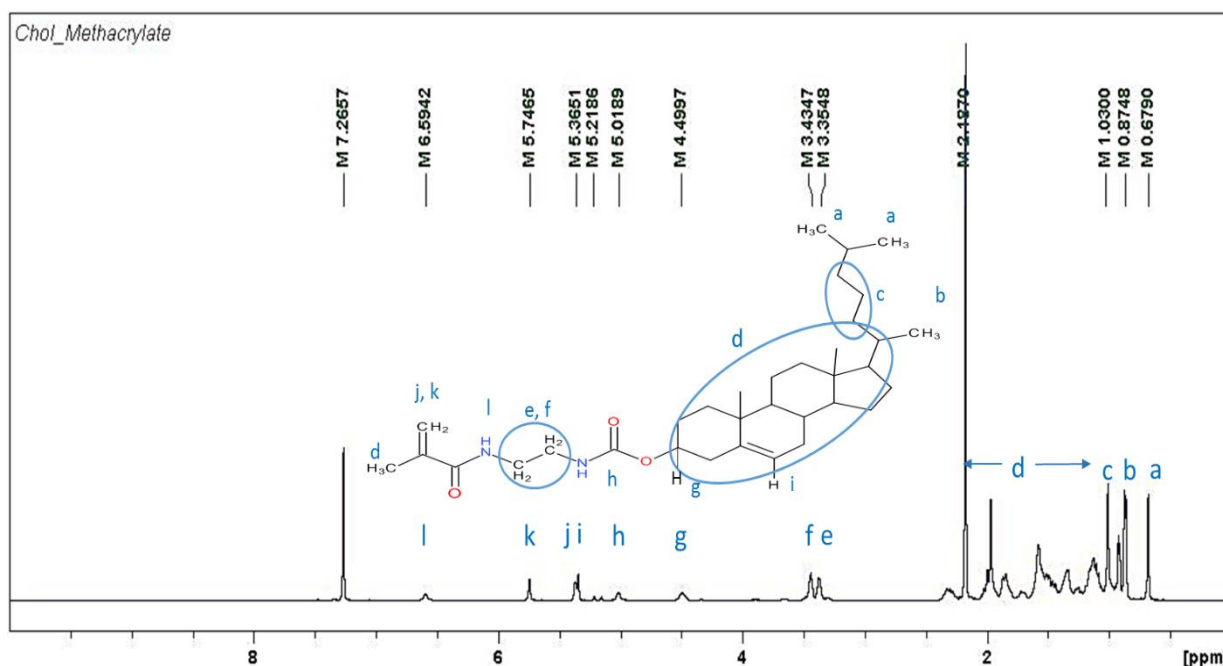
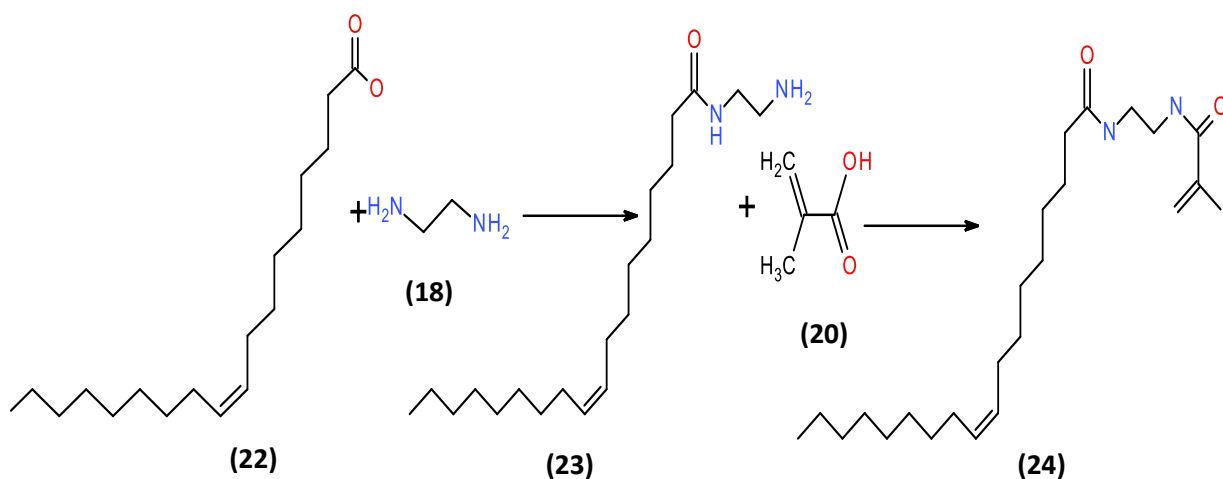


Figure 2-4 ^1H NMR spectrum of cholesteryl methacrylate (**21**)

2.5.1.2 Synthesis of oleic methacrylate (**24**)

Synthesis of **24** was a two-step process with the formation of the intermediate oleic ethylene diamine (**23**). The reaction scheme for the synthesis of **24** is illustrated in Scheme 2-2. The detailed procedure for synthesis is discussed in section 6.3.2.



*Scheme 2-2 Synthesis of oleic methacrylate (**24**)*

The first step involved the synthesis of **23** which was confirmed by Mass spectroscopy. LC/MS (ESI) m/z: [M + H]⁺ calculated for **23** was, 324.54; and found to be 325.2 as seen in Figure 2-5 confirming successful synthesis.

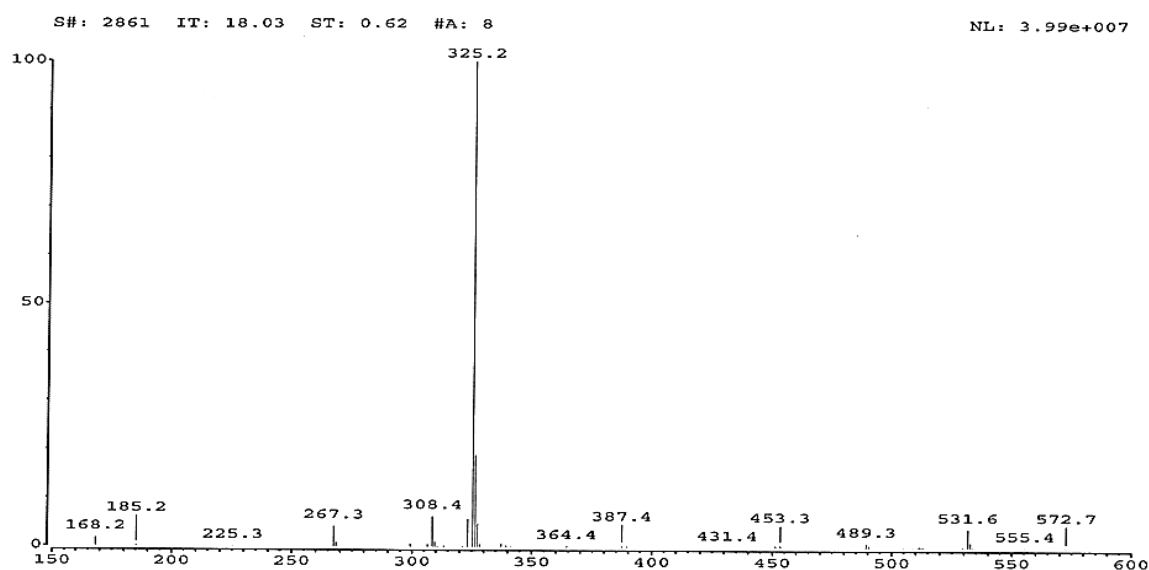


*Figure 2-5 Mass spectrum of oleic ethylene diamine conjugate (**23**)*

The second step involved the coupling of the methacrylic acid (**20**) to the primary amine of **23** to form **24**. LC/MS (ESI) m/z: [M + H]⁺ calculated for **24** C₂₄H₄₄N₂O₂, 392.3402; was found, 393.3 (Figure 2-6), confirming successful outcome.

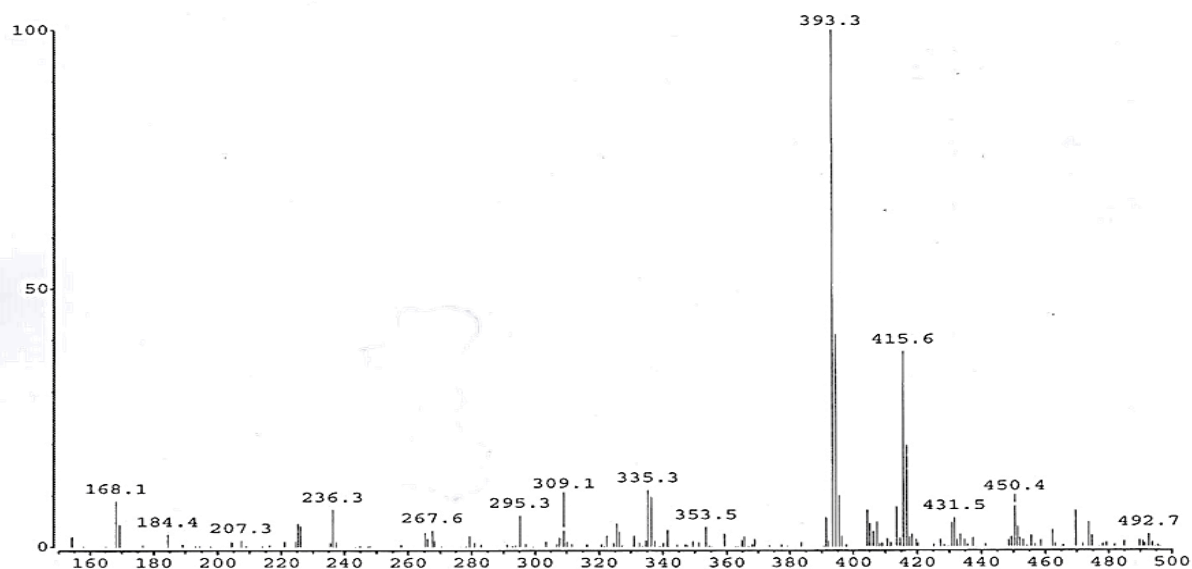


Figure 2-6 Mass spectrum of oleic methacrylate (**24**)

Synthesis of **24** was further confirmed by ¹H NMR spectroscopy (Figure 2-7). The spectral shifts were assigned to their corresponding protons as illustrated in the structure insert.

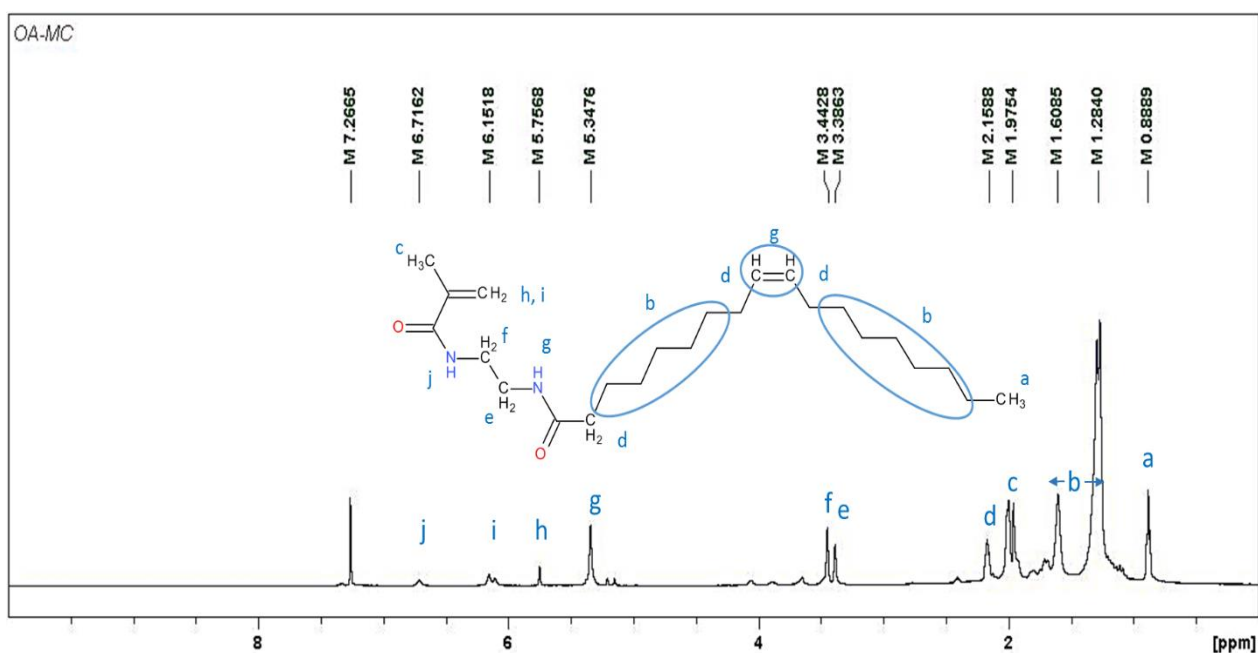
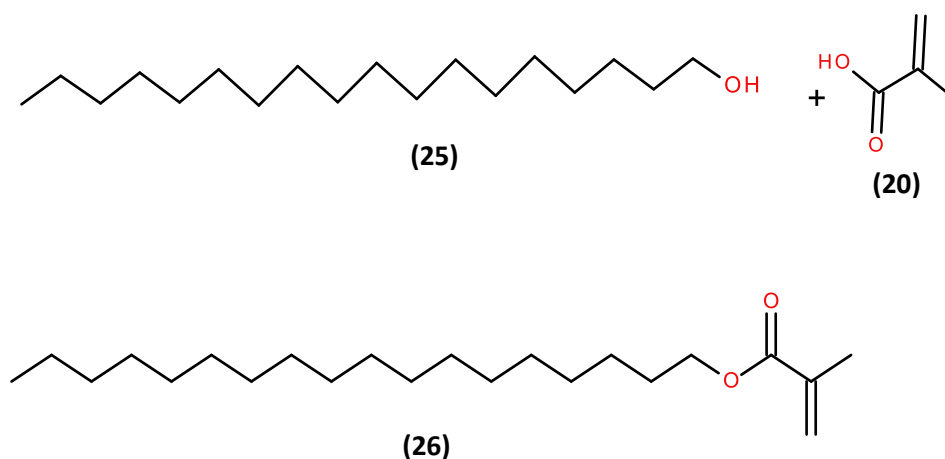


Figure 2-7 ¹H NMR spectrum of oleic methacrylate (**24**)

2.5.1.3 Synthesis of octadecyl methacrylate (26)

The synthesis of **26** was a one step process with the direct coupling of the carboxylic acid of the methacrylate moiety to the alcohol group of 1-octadecanol to create a new ether bond. The schematic diagram of the synthesis step is represented in Scheme 2-3 with the procedure detailed in section 6.3.3.



Scheme 2-3 Synthesis of octadecyl methacrylate (26)

The successful synthesis of **26** was confirmed by Mass and ^1H NMR spectroscopy. The LC/MS (ESI) m/z : $[\text{M} + \text{H}]^+$ calculated for **26** $\text{C}_{22}\text{H}_{42}\text{O}_2$, was 338.3 and found to be, 339.4, displayed in Figure 2-8, confirming successful synthesis.

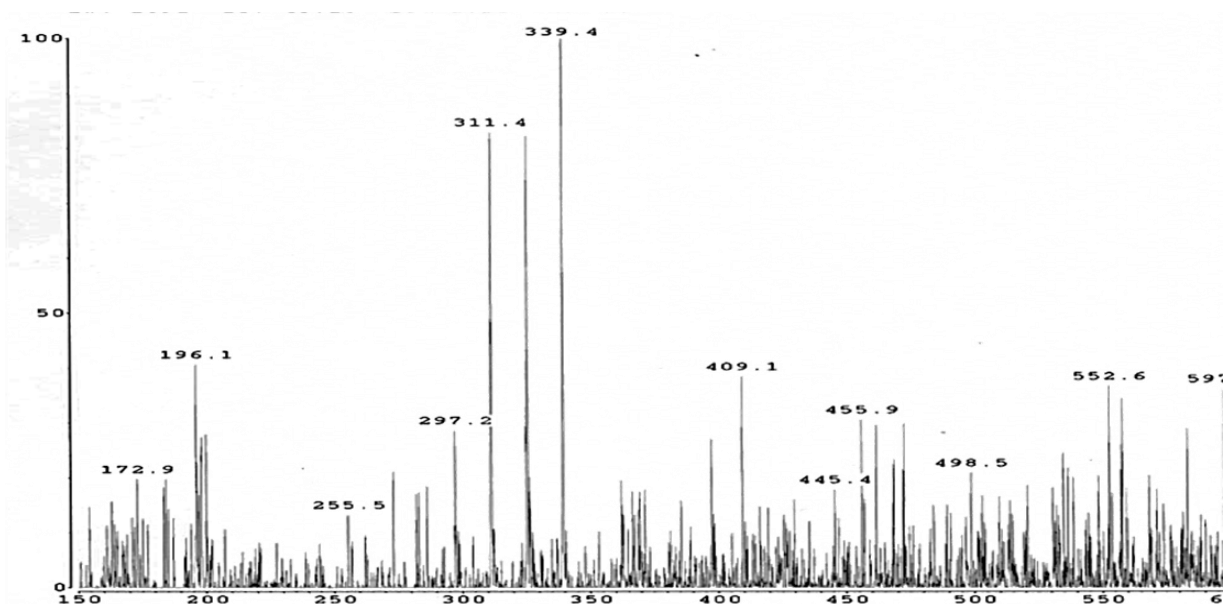


Figure 2-8 Mass spectrum of octadecyl methacrylate (26)

The ^1H NMR spectrum of **26** is shown in Figure 2-9. The addition of a new peak at 1.95 ppm, interpreting for three protons is indicative of the methyl group of the methacrylate. The two ethylene protons can be seen at 5.5 and 6.0 ppm, each interpreting for one proton.

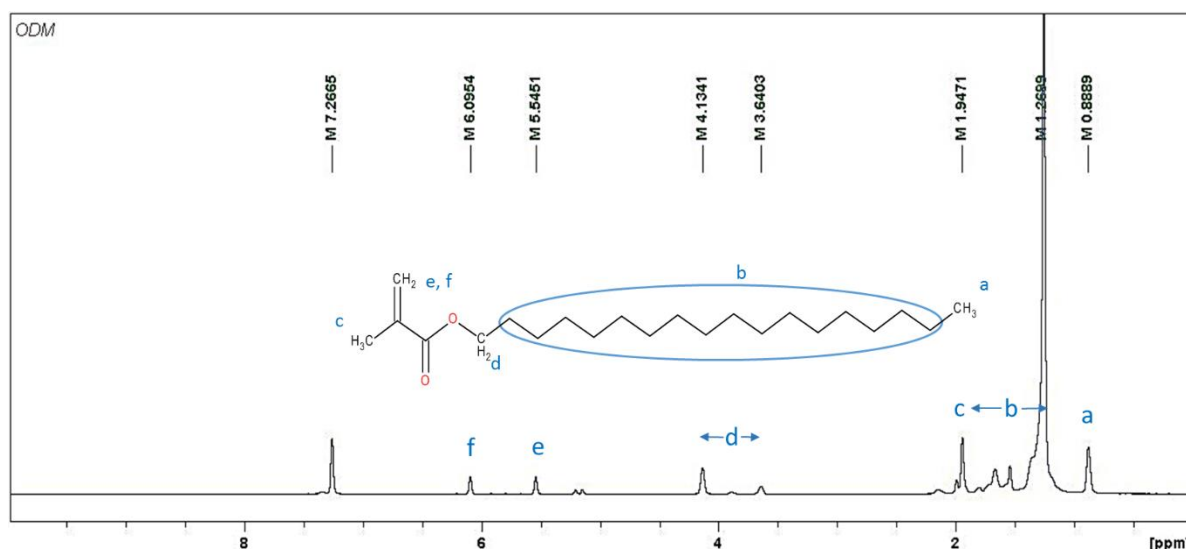


Figure 2-9 ^1H NMR spectrum of octadecyl methacrylate (26)

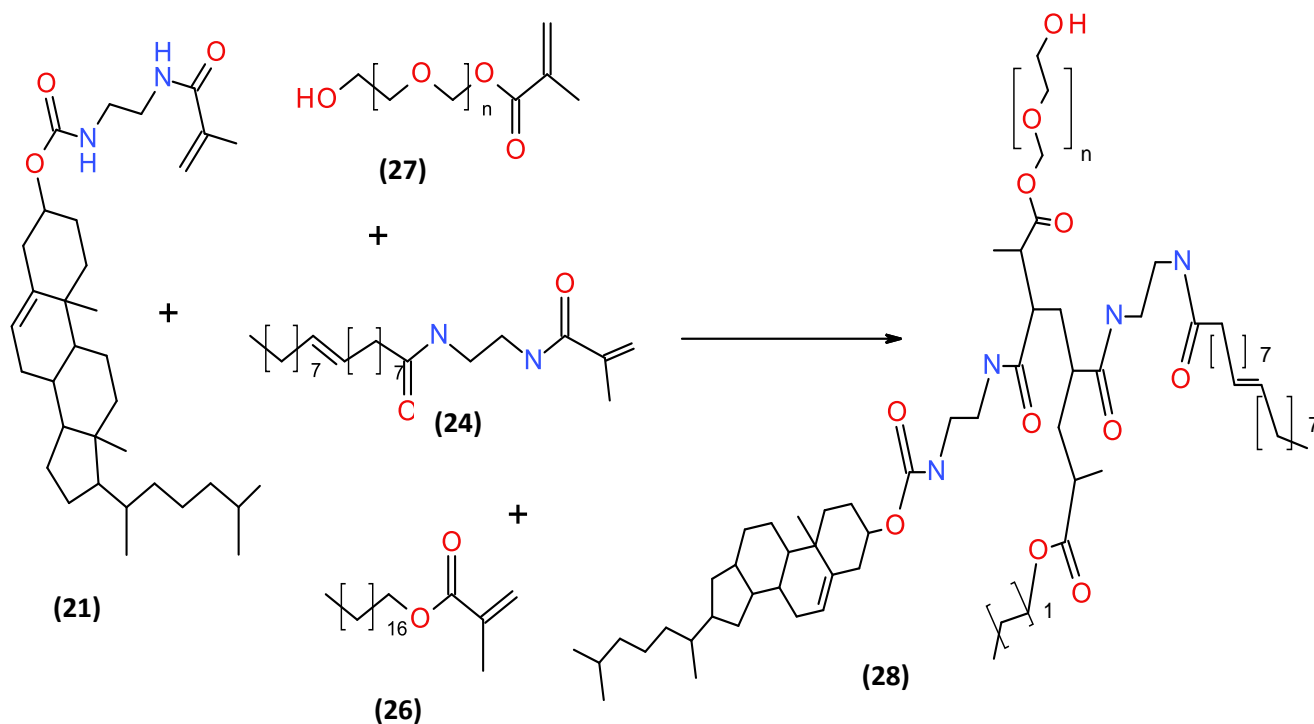
2.5.1.4 Synthesis of Polymers

The polymers were designed to mimic the composition of liposomes. Scheme 2-4 displays the different monomers used for the polymerisation reaction. An octadecyl side chain in the designed polymer was used in place of palmitic chain in liposomes, whereas oleic acid was incorporated as the unsaturated side chain. Cholesterol and PEG were added to the polymer to complete the final composition and ensure similarity to liposomes. The main difference between the polymersome and liposome is that of surface charge. The choline head group in liposomes imparts the typical zwitterionic charge to them whereas the synthetic polymers are neutral in charge. After the successful synthesis of monomers, they were combined together for the synthesis of polymers in specific molar ratios (detailed in Table 2-1) by Freeze-thaw method discussed in detail in section 6.3.4. Two different polymers were created by varying the size of the PEG moiety. PEG-methacrylate (Mn 500) and PEG-methyl ether methacrylate (Mn 2000) were purchased and added to final polymer to create one

polymer with low molecular weight PEG and the other with high molecular weight PEG. The reaction scheme for synthesis of polymers is represented in Scheme 2-4.

Table 2-1 Ratios of different monomers for synthesis of polymer (28)

	Moles	Mass (g)	Molecular weight
(21)	0.001	0.54	540.81
(26)	0.001	0.33	338.57
(24)	0.001	0.39	392.34
(27)	0.001/	0.5/	500/
MW 500/2000	0.00025	0.5	2000



Scheme 2-4 Synthesis of polymers (28)

Monomers were polymerised with either PEG 500 methacrylate or PEG 2000 methacrylate in the desired ratio using free radical polymerisation and AICN as the initiator. Monomers join together at the methacrylate end to form random copolymers P500 or P2000 depending on PEG chain length in a Michael addition reaction.

Polymers **28** were confirmed by ^1H NMR spectroscopy as seen in the stacked ^1H NMR (Figure 2-10) which shows the disappearance of the methacrylate proton peaks.

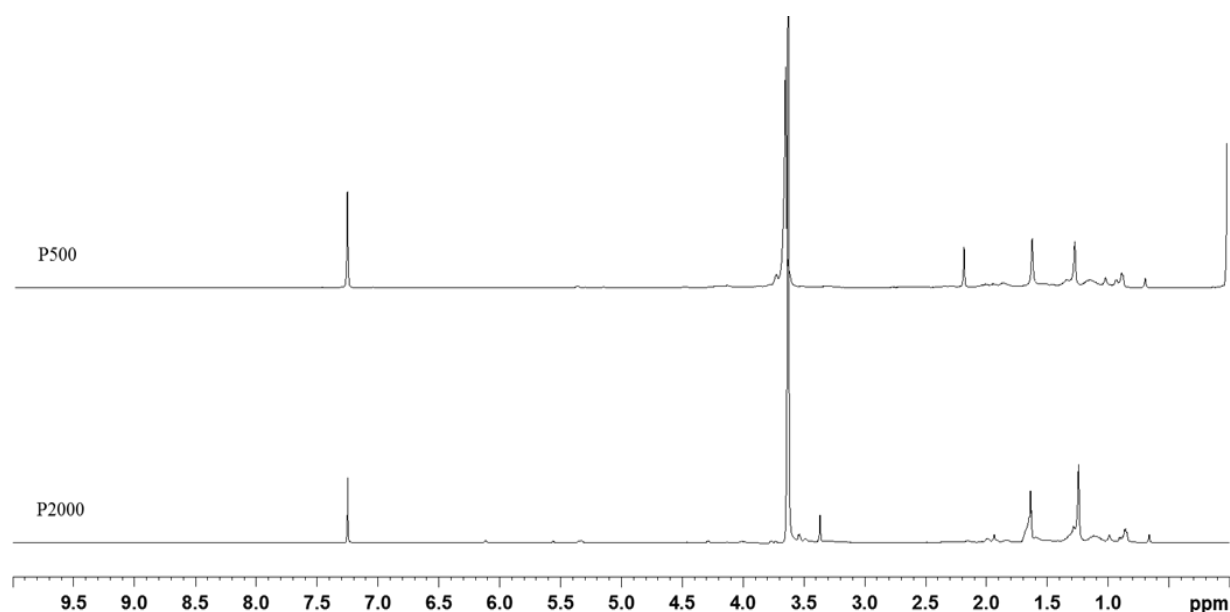
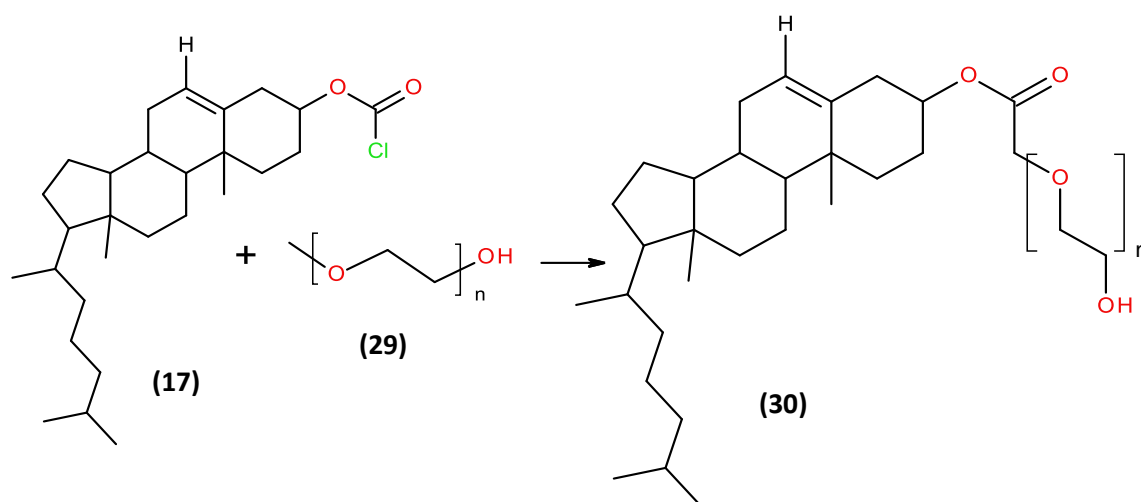


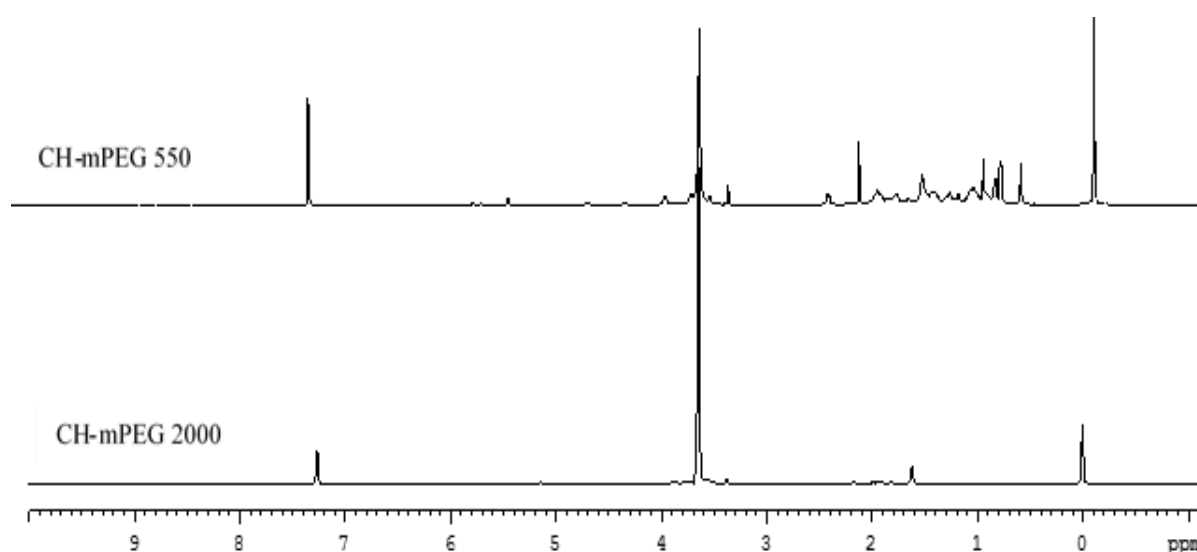
Figure 2-10 Stacked ^1H NMR spectra of polymers (28) P500 and P2000

The hydrophilic block fraction also called as the f value is the amount of hydrophilic volume with respect to overall polymer especially in PEG based polymers. According to Guan *et al.* and Christian *et al.*, it is calculated by the formula $f = H_p / H_p + H_n$ where H_p is the volume of PEG and H_n is the overall volume of polymer fraction. The f value should be 25 % < f < 40 % to obtain spherical uni-lamellar vesicles^{82, 259}. The f value of P500 was 25% (1:4 molar ratio) and P2000 was 30% (1:3.25 molar ratio) indicating that both the polymers are capable of forming bi-layered spherical polymersomes.

Methoxy PEGs (**29**) Mn 550 and 2000 were attached to cholesteryl chloroformate (**17**) to form cholesteryl-mPEG conjugates (CH-mPEG) (**30**). These conjugates were used for the preparation of pegylated liposomes to obtain chemical composition similar to polymersomes. The reaction scheme for the synthesis of **30** is depicted in Scheme 2-5 and the detailed synthesis procedure is discussed in section 6.3.5.



The successful synthesis of **30** was confirmed by ^1H NMR spectroscopy (Figure 2-11). The ^1H NMR shifts of both conjugates confirmed synthesis with the PEG protons in CH-mPEG 2000 integrating for significantly more than CH-mPEG 550.



81

2.5.1.6 Calculation of fixed aqueous layer thickness

Hydrophilic layer of PEG called the fixed aqueous layer surrounding NPs prevents their interaction with serum protein. Fixed aqueous layer thickness (FALT) can be measured by evaluating zeta potential of the nanoparticles in different concentrations of NaCl and gives an idea of the extent of PEG layer surrounding the NPs²⁶⁰. FALT of liposomes and polymersomes with PEG 500 (L500 and P500 respectively) and PEG 2000 (L2000 and P2000 respectively) are specified in Table 2-2 and proves that the extent of surrounding PEG layer of both polymersomes was comparable to that of liposomes.

Table 2-2 Fixed Aqueous Layer Thickness (nm) of different PEG chain lengths. N=3, represented as average \pm SD.

L500	P500	L2000	P2000
0.78 \pm 0.12	0.63 \pm 0.46	1.40 \pm 0.46	1.71 \pm 0.20

2.5.2 Preparation and characterisation of liposomes and polymersomes

Polymersomes were prepared using the polymers created above, with PEG 500, creating polymersome 500 (P500) or PEG 2000, creating polymersome 2000 (P2000). Liposomes were made using **15** from egg yolk and **30** with either PEG 550 (L500) or PEG 2000 (L2000) as discussed in detail in section **6.3.7**. There are a number of different methods available within the literature regarding the preparation of such NPs. The two most commonly used methods for preparation of liposomes are thin film hydration and reverse phase evaporation method. Thin film hydration method involves hydration of the thin polymer/lipid film formed after vacuum evaporation in a round bottom flask using an aqueous medium such as PBS²⁸. The emulsion evaporation method which is also referred to as the reverse phase evaporation method is less conventional and involves formation of an emulsion of the organic phase such as chloroform dissolving the lipid/polymer and the aqueous phase^{261, 262}. In this method, the liposomes/polymersomes are formed by evaporation of the organic phase from the emulsion under reduced pressure. The reverse phase evaporation method is a combination of both thin film hydration and emulsion evaporation method and involves formation of a lipid/polymer film followed by evaporation of a

drug layer on top of the film to ensure close contact between the lipid/polymer and drug. This is followed by emulsification of the drug and lipid/polymer layer and further evaporation of the organic layer which forms the NPs²⁶³.

As seen in Table 2-3, FCD loaded liposomes L500 and L2000 had a particle size of approximately 250nm and increased to 300nm for anthracene loaded liposomes. It is a general consideration that liposomes increase in size when encapsulating hydrophobic drugs because of the intercalation between the bilayers. However, polymersomes had a particle size of approx. 160 nm and managed to retain their low particle size even after loading anthracene with P500 having size of 180 nm and P2000 at upto 260nm. Even though polymers are considered to have a higher molecular weight than lipids, the polymersomes were significantly smaller in size than liposomes as seen in Table 2-3. Thus proving that the rigid dense membrane of polymersomes can help retain molecules without significantly affecting the particle size. The particle size of both liposomes and polymersomes was lowest for reverse phase evaporation method. The observation of bigger particle size of thin film evaporation method as compared to emulsion evaporation method (Table 2-3) can be attributed to the emulsion formation step in the latter method which aids in easier formation of particles whereas thin film hydration method requires hydration of film over a long period of time and may require an additional step of probe sonication to convert multilamellar particles to unilamellar and help reduce size.

L500 and L2000 had a PDI of 0.5-0.6 but P500 had very high PDI of approx. 0.7-0.9 whereas P2000 had PDI of less than 0.5. Similar to observations of size, reverse phase evaporation method had lowest PDI for liposomes and polymersomes with PEG 2000 when compared to other methods of preparation. Evaluation of zeta potential indicated that P500 and P2000 loaded FCD and anthracene were almost neutral having charge up to 1-4mV than liposomes which had a net negative charge from 3-16mV. L2000 and P2000 were more positively charged than L500 and P500 respectively owing to the dense PEG chain on them. Anthracene loaded liposomes and polymersomes were slightly more positive than FCD NPs. The method of preparation did not have any effect on the zeta potentials of the both types of NPs. Hence, from the observations of size and PDI, it can be concluded that the reverse

phase evaporation method provides smaller sized homogenous NPs as compared to the other two methods of preparation.

Table 2-3 Characterisation of liposomes (L500/2000) and polymersomes (P500/2000) loaded with FCD and anthracene prepared by three methods-Thin film hydration (TFH), Emulsion Evaporation (EMEV) & Reverse phase evaporation (RPE). N=3 represented as average \pm SD.

FCD		L500	P500	L2000	P2000
Size (nm)	TFH	394.3 \pm 74.7	160.3 \pm 47.5	444.3 \pm 75.1	188.1 \pm 66.7
	EMEV	305.9 \pm 14.6	174.2 \pm 45.4	318.5 \pm 84.6	223.4 \pm 50.3
	RPE	266.1 \pm 31.2	163.4 \pm 66.8	239.2 \pm 55.4	162.9 \pm 20.1
PDI					
TFH	TFH	0.5 \pm 0.1	1 \pm 0	0.3 \pm 0.01	0.3 \pm 0.05
	EMEV	0.5 \pm 0.1	0.8 \pm 0.1	0.4 \pm 0.07	0.4 \pm 0.1
	RPE	0.5 \pm 0.09	0.7 \pm 0.2	0.4 \pm 0.1	0.3 \pm 0.05
Zeta (mV)					
TFH	TFH	-16.4 \pm 2.9	0.9 \pm 2.1	-11.3 \pm 4.3	2.2 \pm 1.4
	EMEV	-10.2 \pm 4.09	1.8 \pm 1.2	-10.05 \pm 1.8	2.2 \pm 1.6
	RPE	-8.1 \pm 2.1	1.6 \pm 1.7	-10.8 \pm 1.8	0.9 \pm 1.5
Anthracene		L500	P500	L2000	P2000
Size (nm)	TFH	660 \pm 53.7	404.7 \pm 46.1	493.1 \pm 80.4	294.9 \pm 22.4
	EMEV	174.6 \pm 5.6	316.2 \pm 76.0	442.9 \pm 48.1	419.4 \pm 69.7
	RPE	348.2 \pm 18.5	184.8 \pm 23.5	300.2 \pm 71.0	261.9 \pm 82.6
PDI					
TFH	TFH	0.3 \pm 0.1	0.9 \pm 0.1	0.7 \pm 0.1	0.4 \pm 0.06
	EMEV	0.3 \pm 0.09	1 \pm 0	0.4 \pm 0.03	0.4 \pm 0.03
	RPE	0.4 \pm 0.05	0.9 \pm 0.1	0.4 \pm 0.09	0.5 \pm 0.1
Zeta (mV)					
TFH	TFH	-6.5 \pm 0.3	3.7 \pm 0.1	-4.3 \pm 0.8	4.3 \pm 0.9
	EMEV	-11.9 \pm 0.7	3.5 \pm 1.0	-2.6 \pm 1.3	4.8 \pm 0.1
	RPE	-9.8 \pm 1.8	3.1 \pm 0.3	-3.6 \pm 0.7	4.5 \pm 0.2

Table 2-4 represents the characterisation of L500, L2000 and P500, P2000 loaded with FCD and anthracene prepared by three methods for percentage encapsulation efficiency. There was almost no variation in encapsulation efficiency of FCD liposomes and polymersomes with PEG 500 and 2000 for all three methods of preparation. Reverse phase evaporation method indicated that the encapsulation efficiency of FCD in both liposomes and polymersomes was quiet high (up to approximately 75%). This relates to the findings of Sardan *et al.* who have shown that up to 75% encapsulation efficiency of a hydrophilic drug such as Dox in liposomes can be achieved when prepared by reverse phase evaporation method²⁶⁴. In other cases there has been up to 40% encapsulation of highly water soluble proteins such as Drosophila AChE and hydrophilic potassium chromate in liposomes prepared by thin film hydration method^{265, 266}. A slightly less encapsulation efficiency of FCD (upto 60%) was observed in liposomes L500 having smaller PEG chain length but there was good encapsulation efficiency in polymersomes for both P500 and P2000. Hence polymersomes having both smaller and larger PEG chain lengths can be used to achieve high encapsulation efficiency. Similarly there was high encapsulation of hydrophobic anthracene in both L2000 and P2000 and slightly less in L500 and P500 considering the more dense nature of PEG 2000 chain allows better entrapment of molecules.

Table 2-4 Comparison of liposomes and polymersomes loaded with FITC-CM-Dextran (FCD) and anthracene for % Encapsulation efficiency by three methods of preparation. N=3 represented as average \pm SD.

FCD	L500	P500	L2000	P2000
TFH	72.5 \pm 1.6	72.6 \pm 2.9	71.9 \pm 1.8	77.4 \pm 1.5
EMEV	65.4 \pm 5.8	72.8 \pm 5.3	71.2 \pm 5.9	76.7 \pm 0.9
RPE	58.3 \pm 10.6	75.9 \pm 4.4	75.1 \pm 6.9	75.9 \pm 1.9

Anthracene	L500	P500	L2000	P2000
TFH	78.6 \pm 7.3	82.7 \pm 10.0	78.5 \pm 9.0	88.5 \pm 9.3
EMEV	77.7 \pm 10.4	57.9 \pm 0.2	72.3 \pm 3.9	89.7 \pm 6.3
RPE	72.2 \pm 7.5	71.6 \pm 1.8	77.0 \pm 11.3	80.0 \pm 1.4

To study the effect of charged molecules on the polymersomes, L2000 and P2000 encapsulating FDD (positive charge) and F-D (Neutral) were prepared by reverse phase evaporation method and evaluated for particle characteristics (

Table 2-5). There was higher encapsulation of negatively charged FDD than neutral F-D. The particle size and PDI of L2000 and P2000 was not affected by charge of encapsulating moiety. There was no significant difference in zeta potential of polymersomes because of the presence of charged compounds. P2000 were significantly smaller in size and had a slightly higher encapsulation efficiency than L2000. Both L2000 and P2000 had PDI less than 0.5 and P2000 were more positive charged than L2000, thus leading to the conclusion that charge did not have any effect on the encapsulation and size of liposomes and polymersomes, this can again be attributed to the dense PEG layer coating the surface of liposomes and polymersomes.

FDD (FDD)	L2000	P2000
EE (%)	80.8±1.7	86.5±2.0
Size (nm)	285.6±21.8	154.3±14.1
PDI	0.4±0.07	0.2±0.01
Zeta (mV)	-0.9±1.9	4.0±0.8
F-D (F-D)	L2000	P2000
EE (%)	68.1±2.0	72.4±18.9
Size (nm)	241.9±39.7	147.±45.8
PDI	0.3±0.05	0.3±0.09
Zeta (mV)	-7.1±1.1	2. 1±1.3

Table 2-5 Characterisation of L2000 and P2000 loaded with FITC-DEAE-Dextran (FDD) (Positive) and FITC-Dextran (F-D) (Neutral) prepared by reverse phase evaporation method to enable evaluation of effect of charge. N=3 represented as average±SD.

Representative size distribution curve of polymersomes is shown in Figure 2-12a. Scanning Electron microscopic images Figure 2-12b of P2000 shows spherical particles which are uniform in size.

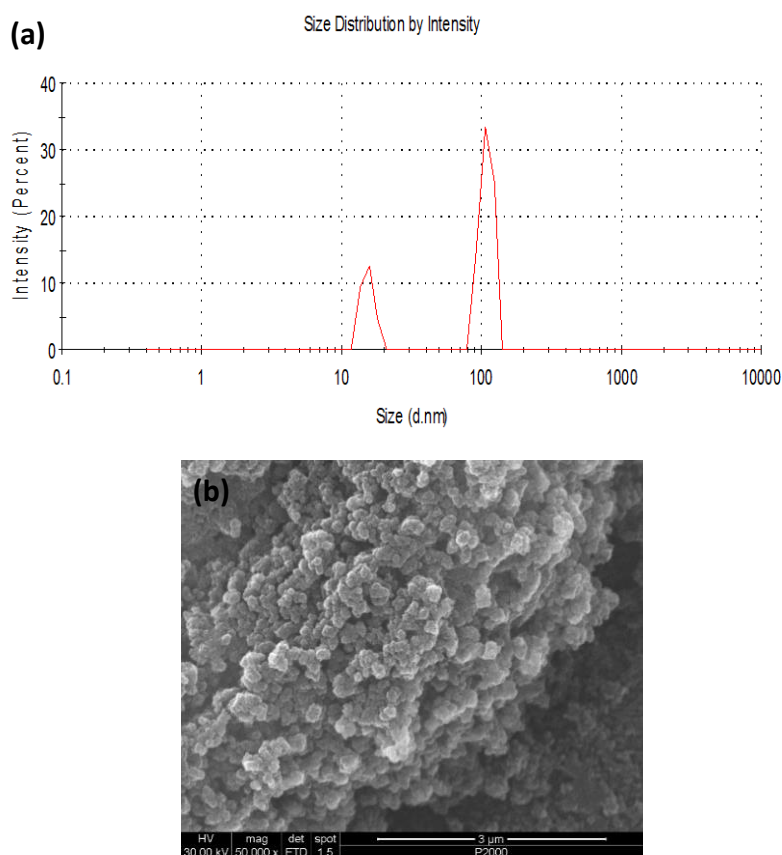


Figure 2-12 (a) Representative size distribution graph of polymersomes showing formation of bilayer polymersomes of size approx. 150nm and a small number of micelles formed in the process. (b) SEM image of P2000 polymersomes.

2.5.3 Cellular uptake of FCD and anthracene loaded polymersomes and liposomes

In an attempt to establish the cellular uptake of the 4 NP's, each DDS was loaded with a hydrophilic dye (FCD) or a hydrophobic dye (anthracene) and both were incubated with HeLa cells for 4 hours at 37°C at concentrations of 250μg mL⁻¹ FCD and 50μg mL⁻¹ anthracene.

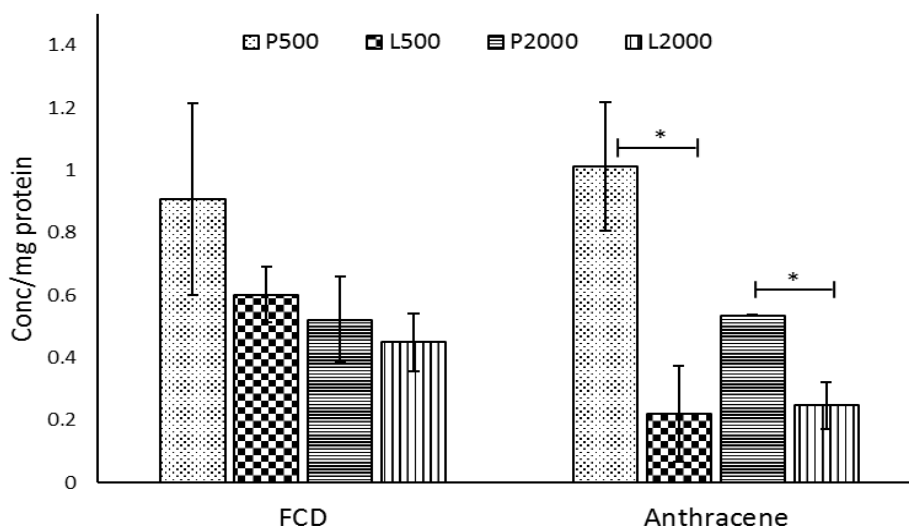


Figure 2-13 Cellular uptake of FCD and anthracene in liposomes and polymersomes. N=3, represented as average±SEM, * indicates p value <0.1.

As seen in Figure 2-13, P500 had an average higher uptake of FCD up to $0.9 \pm 0.3 \mu\text{g}/\text{mg}$ protein as compared to P2000 (0.6 ± 0.08) and L500 (0.5 ± 0.1) and L2000 (0.4 ± 0.09). The uptake of anthracene in polymersomes P500 and P2000 at 1.01 ± 0.2 and 0.5 ± 0.002 was significantly higher than liposomes. Due to the negative charge character of the plasma membrane, small sized positively charged and neutral particles are better absorbed and endocytosed than negatively charged particles especially through clathrin mediated endocytosis^{267, 268}. Due to their smaller size and neutral charge, polymersomes can prove advantageous for rapid uptake into cells. Hence it can be concluded that polymersomes have shown to have better uptake for both FCD and anthracene than liposomes. Random copolymers having cholesterol with PEG 500 and decyl side chains have been reported to have high uptake of FCD in polymersomes as compared to free FCD solution in HeLa cells¹²⁸. Even though there was a significant reduction of cellular uptake of L500, there was no significant change in the uptake of liposomes with L2000.

2.5.4 Fluorescence microscopy

Following the demonstration that our synthesized polymersomes have better cellular uptake than liposomes, especially for hydrophobic dyes, we visualised them in cells to see their effect on live cells by fluorescence microscopy. Evaluation of cellular uptake

enabled us to see the uptake of hydrophobic and hydrophilic compounds separately, however to go one step further, FCD and anthracene were encapsulated simultaneously in liposomes and polymersomes and incubated with Hela cells. Cells were then observed under microscope for simultaneous uptake of both dyes. Figure 2-14, showing merged images of P500 and P2000 demonstrate good overlap indicating clear uptake of both dyes. However merged images of liposomes did not show blue fluorescence of anthracene associated with green fluorescence of FCD indicating that anthracene was outside the cell rather than on the inside thus proving the lesser cellular uptake of anthracene. Hence P500 and P2000 have a better ability for simultaneous encapsulation and uptake of both FCD and anthracene which can prove advantageous in multiple drug delivery.

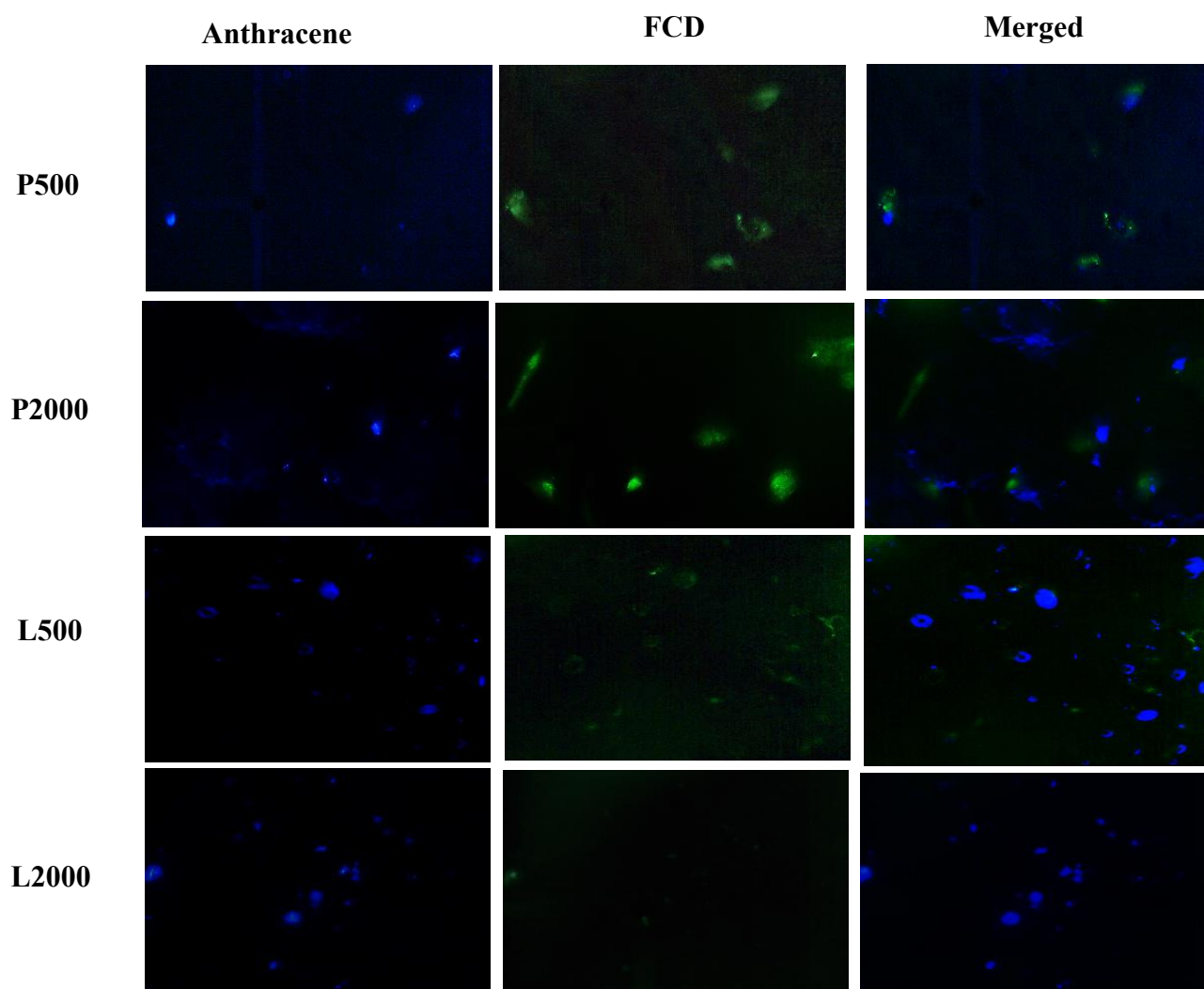


Figure 2-14 Fluorescence microscopic observation of FCD and anthracene loaded liposomes and polymersomes.

2.5.5 Mechanism of uptake by chemical inhibition of endocytosis

The mechanism of cellular uptake was evaluated by chemical inhibition of endocytosis using chlorpromazine HCl. Chlorpromazine inhibits clathrin coated pit formation by reversible displacement of clathrin and its adapter proteins from cell membrane to intracellular vesicles thereby inhibiting endocytosis by this pathway^{269, 270}. The results of which are displayed in Figure 2-15.

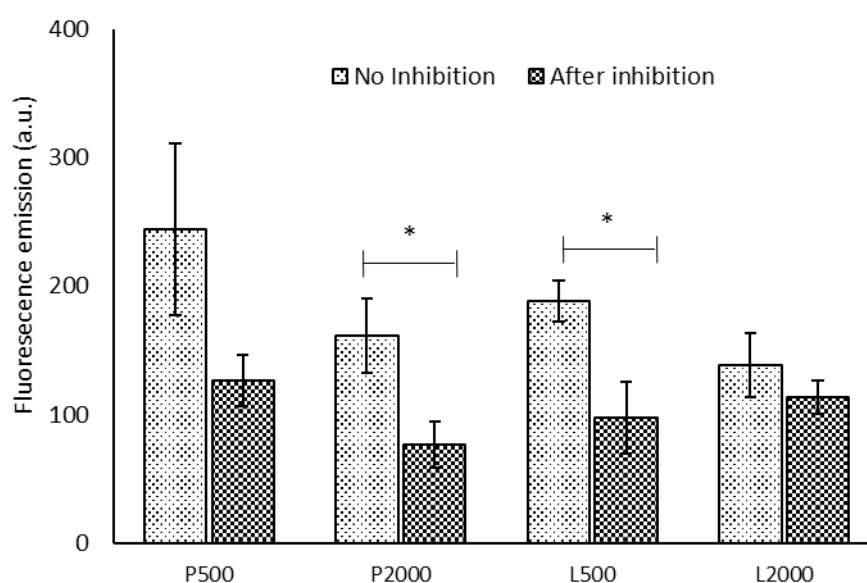


Figure 2-15 Effect of inhibition of endocytosis using chlorpromazine HCl incubation of 30 minutes before treatment of cells with FCD loaded liposomes and polymersomes. N=3, represented as average \pm SEM, * indicates p value <0.1.

Cellular uptake of P500 and P2000 decreased significantly by $37.6\pm 19.7\%$ and $46.3\pm 21.0\%$ respectively on inhibition of endocytosis thus indicating that uptake of polymersomes is predominantly by clathrin-mediated endocytosis as seen in Figure 2-15. Longer PEG chain lengths such as MW 2000 and 5000 have been associated with increased circulation time in blood when compared to liposomes modified with shorter PEG chain lengths such as PEG 500 and 750, even though smaller molecular weight PEG has shown to have higher cellular uptake in both liposomes and polymer NPs²⁷¹⁻²⁷⁴. Miller *et al.* have shown that sterically stabilised liposomes with PEG 2000 undergo significantly less endocytosis than conventional non pegylated liposomes and it is possible that they are taken up by other mechanisms. Thus proving our

observation of liposomes with PEG 2000 have only $10.2 \pm 22.5\%$ change in cellular uptake indicating cellular uptake via other pathways whereas liposomes with PEG 500 demonstrated $47.5 \pm 16.3\%$ decrease in uptake²⁷⁵.

2.5.6 Cell viability using MTT assay

Following the research described in section 2.5.3, it was established that polymersomes with PEG 500 have better cellular uptake of both FCD and anthracene. However, when this information was considered alongside the high PDI values they were not taken for further evaluation. Liposomes made with PEG 2000 have been extensively used in research for anticancer therapy for their stealth properties and providing effective masking from serum proteins²⁷⁶⁻²⁷⁸. Therefore only the two NP's using the higher weight PEG were analysed further within this study. Cell toxicity studies of blank liposomes and polymersomes at different concentrations in three cell lines after overnight incubation were observed using MTT assay. Figure 2-16 shows the percent cell viability of polymersomes and liposomes at 0.25 mg ml^{-1} in HeLa cells, CHO cells and BxPC-3 cells. There was no statistically significant difference in the cell toxicities of blank liposomes and polymersomes in HeLa and BxPC-3 cells with viabilities of $85.5 \pm 4.6\%$ and $87.2 \pm 9.4\%$ for liposomes in HeLa and BxPC-3 cells and $73.0 \pm 3.9\%$ and $86.8 \pm 6.2\%$ for polymersomes in HeLa and BxPC-3 cells respectively. Polymersomes were statistically slightly more toxic to CHO cells at 0.25 mg/ml demonstrating cell viability of $77.3 \pm 2.6\%$ viability as compared to liposomes having $88.0 \pm 1.4\%$ viability.

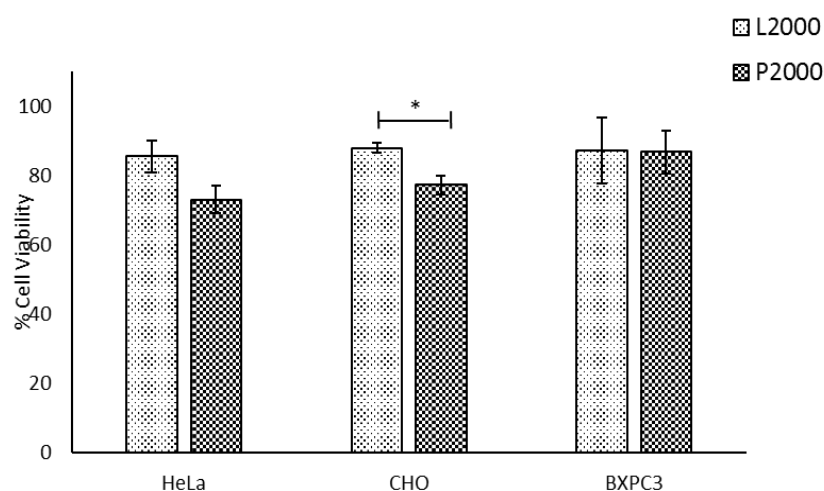


Figure 2-16 Cytotoxicity of blank P2000 and L2000 at 0.25 mg/ml in 3 cell lines after overnight incubation. $N=3$, represented as average \pm SEM, * indicates p value < 0.1 .

When compared to cell toxicity at 0.5mg/ml concentration (Figure 2-17), it was found that polymersomes were significantly more toxic to cells at higher concentration. There was 55.4±1.7% cell viability of HeLa cells when treated with polymersomes and 71.5±2.5% cells were viable in CHO cells whereas 83.6±8.2% cells were viable in BxPC-3 cell line as compared to liposomes having 81.7±4.4, 91.0±0.8 and 98.5±5.9% viability in HeLa, CHO and BxPC-3 cells respectively.

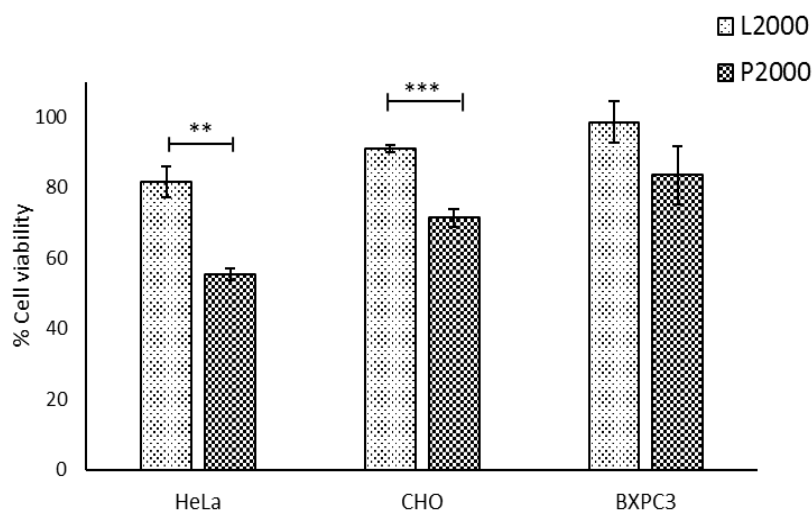


Figure 2-17 Cytotoxicity of blank P2000 and L2000 at 0.5mg/ml in 3 cell lines. N=3, represented as average±SEM, ** indicates p value <0.01, * indicates p value <0.001.**

Nevertheless 0.5mg/ml concentration is quiet high to work with and hence it is safe to conclude that our polymers are safe to use at concentrations up to 0.25mg/ml. On the contrary, toxicity of these polymers at higher concentrations can prove advantageous in cancer treatment where when combined with anticancer drugs can have the possibility of synergistic effect thus providing effective cell cytotoxicity at lower anticancer drug concentrations and reduce other unwanted side effects.

2.5.7 *In-vitro* release studies

Figure 2-18 shows the *in-vitro* release profile of P2000 and L2000 for FCD and anthracene conducted over a period of 24 hours. The results indicated that polymersomes were slightly faster at releasing their cargo than liposomes. There was a gradual release of FCD and 86.0±2.9 and 94.3±2.8% was released by 24 hours from

liposomes and polymersomes respectively. P2000 and L2000 with anthracene were slower in release with $44.3 \pm 4.4\%$ releasing after 24 hours from liposomes and P2000 showing slightly greater release of $60.0 \pm 9.2\%$ than liposomes but there was no statistically significant difference between the two release profiles.

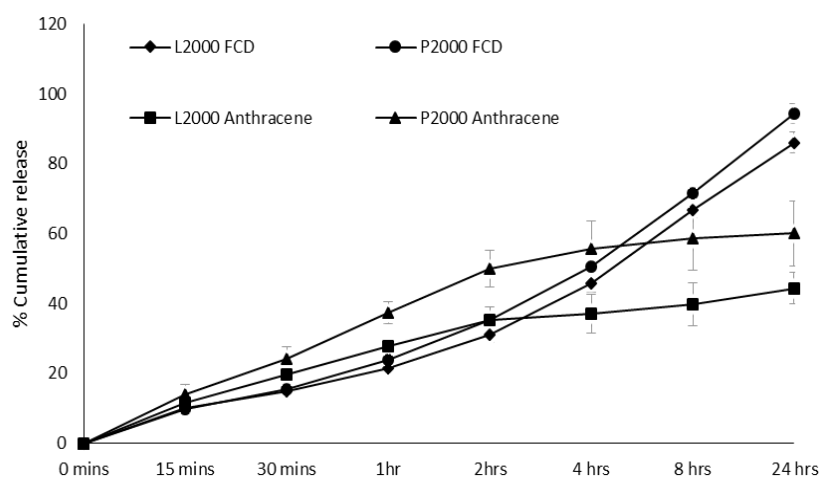


Figure 2-18 In-vitro release of L2000 and P2000 loaded with FCD and anthracene in PBS and Ethanol:PBS 1:1 respectively at 37°C for 24 hours. N=3, represented as average \pm SEM.

Polymersomes have been reported to be slower in release than liposomes which is considered as disadvantageous, however considering the above results we can say that our polymersomes have a release profile similar to liposomes^{279, 280}.

Release studies of L2000 and P2000 loaded with FDD (Figure 2-19) have shown release of $34.2 \pm 0.7\%$ and $38.3 \pm 2.9\%$ after 24 hours for L2000 and P2000, respectively but liposomes L2000 with FITC dextran were faster in releasing the dye at $87.0 \pm 7.9\%$ after 24 hours than polymersomes which released only $54.8 \pm 6.4\%$ of the dye after the same period leading to the conclusion that polymersomes are slower in releasing cationic and neutral molecules.

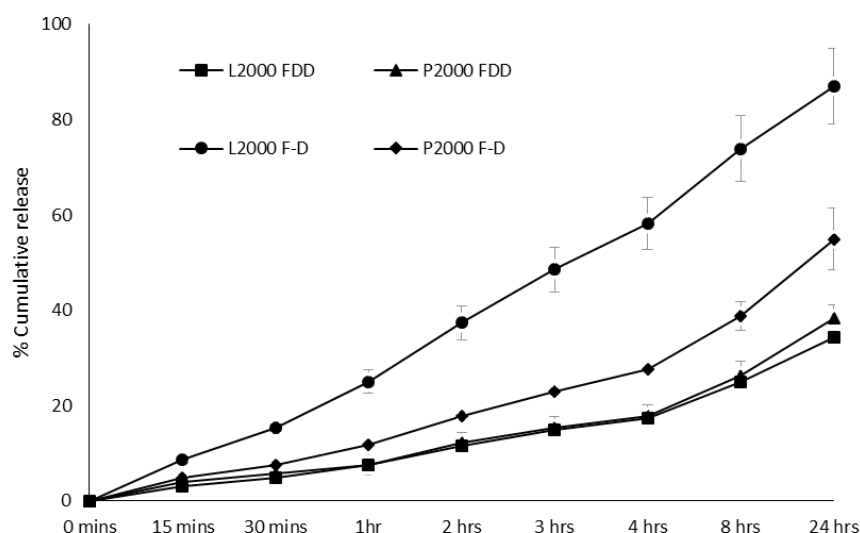


Figure 2-19 In-vitro release studies in PBS at 37°C of L2000 and P2000 loaded with FDD and F-D to evaluate effect of charged compounds on release. N=3, represented as average±SEM.

2.5.8 Physical stability studies

Physical stability of liposomes has always been a matter of concern especially for practical purposes of storage and handling. Thompson *et al.* have extensively studied the stability of liposomes made with soya phospholipids at various conditions such as pH, temperature and storage time²⁶⁶. They have found that there was substantial increase in particle size of liposomes after 10 days of storage at 20-30°C. In another study, liposomes loaded with vancomycin have shown an increase in particle size and reduction in encapsulation efficiency after 2 months storage at 25°C with fungal growth considering the biological nature of lipids²⁸¹. We compared the stability studies of P2000 to L2000 loaded with FCD and anthracene under refrigerated conditions and 25°C for 8 weeks and evaluated them for size and encapsulation efficiency. As seen in Figure 2-20, encapsulation efficiency of L2000 and P2000 of FCD and anthracene was not significantly affected at refrigerated conditions, however as the encapsulation efficiency decreased slightly at 25°C for FCD in liposomes and polymersomes, there was drastic decrease in encapsulation efficiency of anthracene liposomes.

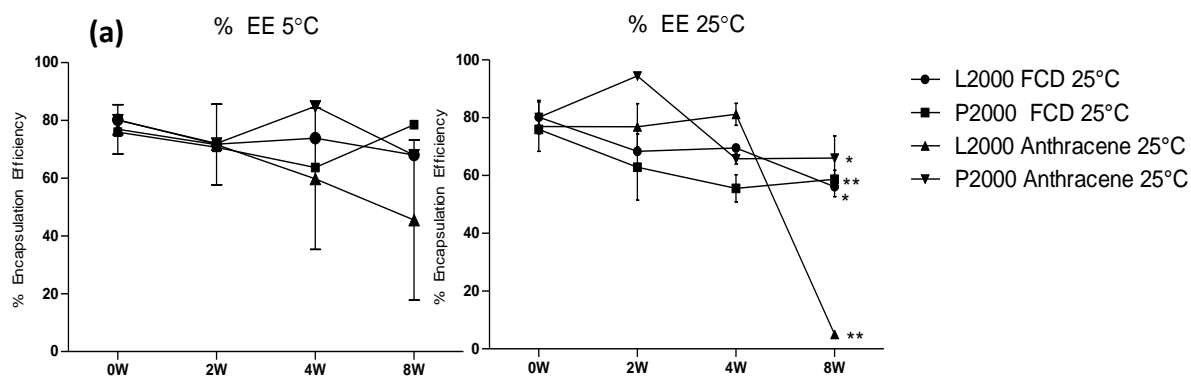


Figure 2-20 Effect of storage time and temperature on encapsulation efficiency of L2000 and P2000 loaded with FCD and anthracene. N=2, represented as average \pm SEM, * indicates p value <0.1, ** indicates p value <0.01.

This decrease in encapsulation is reflected in the increase in size of liposomes after 8 weeks (Figure 2-21). Encapsulation of anthracene in P2000 was not affected as much as L2000 and also size of P2000 was more stable after 8 weeks at 25°C than L2000 for both FCD and anthracene. There was a slight increase in size of polymersomes with FCD after 8 weeks at 5°C. Size of anthracene liposomes were not affected at 5°C. Hence our studies conclude that liposomes are more stable under refrigerated condition but they can be unstable when stored at room temperature which proves previous observations in literature, whereas the size and encapsulation efficiency of P2000 of both FCD and anthracene was stable at 25°C hence concluding that polymersomes were more stable than liposomes giving them an advantage over liposomes.

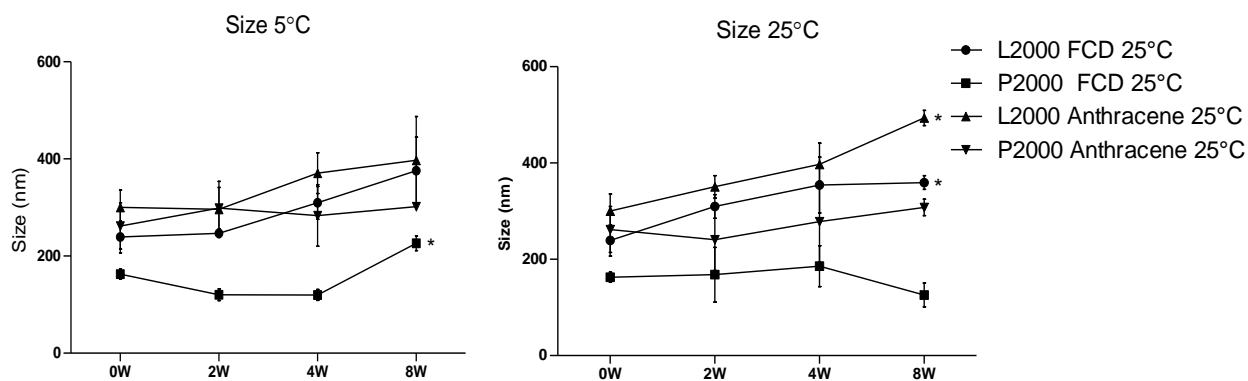


Figure 2-21 Effect of storage time and temperature on size of L2000 and P2000 loaded with FCD and anthracene. N=2, represented as average \pm SEM, * indicates p value <0.1.

Similarly the stability studies of L2000 and P2000 loaded with FDD and F-D were also conducted to study the effect of charge on stability however it was found that there was no significant difference in the encapsulation efficiency and size of polymersomes and liposomes over time Figure 2-22.

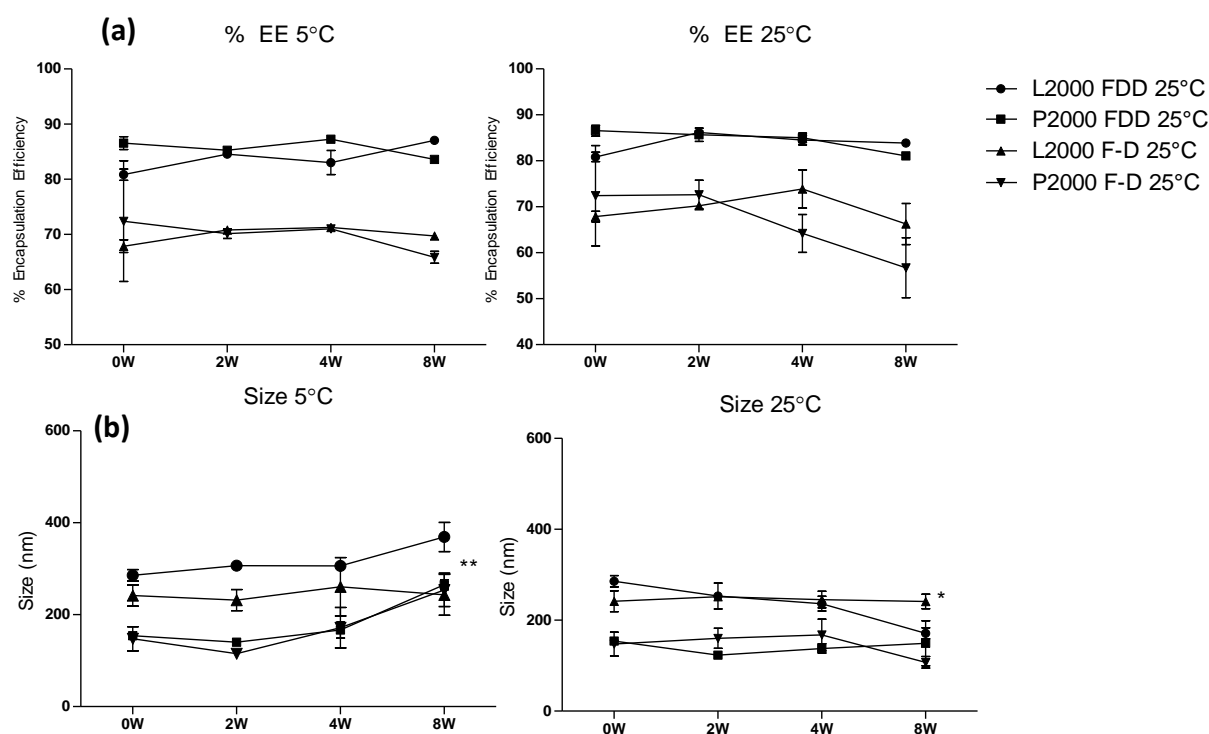


Figure 2-22 Physical stability studies of L2000 and P2000 loaded with FDD and F-D at refrigerated and 25°C for 8 weeks. (a) Effect of storage time and temperature on encapsulation efficiency (b) Effect of storage time and temperature on size. N=2, represented as average \pm SEM, * indicates p value < 0.1 , ** indicates p value < 0.01 .

2.6 Conclusion

Polymersomes are multipurpose polymeric nanoparticle carriers which can be adapted for numerous applications in nanomedicine. Polymersomes made with random copolymers can prove advantageous over block copolymers because of their ease of preparation. In this study we have synthesized random copolymers using octadecanol, oleic acid, cholesterol and PEG 500 (P500) or PEG2000 (P2000) to obtain a chemical composition similar to liposomes (L500 and L2000). These polymers were capable of self-assembling to form bilayer polymersomes when prepared by reverse phase evaporation method and compared to liposomes. The polymersomes had good

encapsulation efficiency of both hydrophilic (FCD) and hydrophobic anthracene dyes. The hydrodynamic radius of the polymersomes was smaller than their liposome counterpart and had better cellular uptake of FCD and anthracene than liposomes. Polymers were non-toxic to cells at 0.25mg/ml concentration and had a fast release of their cargo with 100% releasing within 24 hours. Physical stability of polymersomes was better than liposomes when stored at 25°C for 8 weeks. Thus, we have successfully synthesized biomimetic, versatile, biocompatible and stable polymersomes imitating liposomes encapsulating different types of compounds and having good cellular uptake. Polymersomes are versatile and capable of encapsulating different types of drugs. Even though liposomes are considered as good nanoparticulate delivery systems especially for cancer therapy, polymersomes have shown great promise and it will be interesting to see their use as multifunctional therapy systems in future.

Chapter 3

The integration of triggered drug delivery with real time quantification using FRET; creating a super 'smart' drug delivery system.

3.1 Introduction

In the past few decades, smart drug delivery systems (DDS) have evolved to deliver an appropriate dose to meet the individual patients' needs²⁸². Delivering the drug at a controlled rate, triggered drug release and targeted drug delivery are some methods that have been extensively investigated. Some examples of such systems include the development of biopharmaceutical systems capable of interacting with intracellular components that respond as a direct result to environmental stimuli²⁸³ and NPs that specifically bind to tumour cells using receptor targeted systems^{284, 285}. Among these, triggered release plays a substantial role in controlling timing and location of drug release, since it can be induced by several external stimuli acting on the intracellular vehicles response²⁸⁶. Examples of stimuli used to facilitate drug release are temperature²⁸⁷, pH²⁸⁸, magnetic field²⁸⁹, electric field²⁹⁰, ultrasound²⁹¹, enzymatic activity²⁹² and light²⁹³.

With increasing focus towards nanotechnology based drug delivery, many complex drug delivery systems such as liposomes, micelles polymersomes, nanofibers, dendrimers have been developed to treat a variety of disease. However, no compendial or regulatory standards exist for release testing from NPs²⁹⁴. There is an urgent need for a sensitive, robust, reliable and reproducible method for analysis of drug release from a nanoparticulate system. Forster Resonance Energy Transfer (FRET) is one such method which has been explored recently to allow real time observation drug release.

The ability to quantitatively monitor the amount of drug release, from a DDS in real time using a simple but effective approach is an essential companion in the advance towards second-generation health care. To this end, there have been a number of examples where mesoporous silica NPs (MSN) have been used as a cage for drug delivery with the drug co-incorporated alongside a photochromic compound²⁹⁵, an oligonucleotide containing a recognition element²⁹⁶ or a redox active FRET pair²⁹⁷ so that the system operates like a molecular valve. In each case, the drug was prevented from exiting the pores of the NP due to the large bulky groups surrounding the MSN. On application of external stimuli, the outer layer (valve) was disrupted and the inner

cargo released from the MSN. In addition to the triggered release, a FRET mechanism was utilized to enable real time monitoring of drug release.

3.1.1 Fluorescence resonance energy transfer (FRET)

FRET is non-radiative energy transference phenomenon in which quantum energy is carried from an excited fluorophore donor molecule to an acceptor molecule placed within close proximity to each other. The process does not consist of emission and reabsorption of photons, but involves energy transfer by inter-molecular dipole-dipole coupling, hence it is called “resonance energy transfer” (Figure 3-1). The principle of FRET is that a donor molecule absorbs light at a definite frequency that temporarily places it into a higher energy state. Before it decays down to its ground state, the close presence of another molecule results in non-radiative transfer of energy by dipole-induced dipole interaction²⁹⁸. The emission wavelength of the donor molecule must coincide with the absorption wavelength of the acceptor molecule, which is not necessarily fluorescent²⁹⁹.

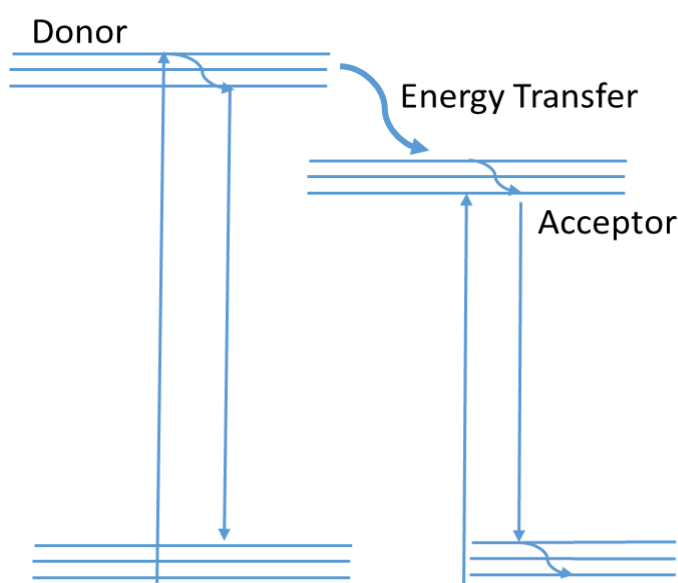


Figure 3-1 Illustration of FRET energy transfer between a donor and acceptor FRET pair.

For FRET to successfully occur between two molecules there are two essential criteria that must be met: The acceptor and donor moieties should have favourable dipole alignment and the emission spectrum of the donor molecule should overlap with the

excitation spectrum of the acceptor molecule. If there is no sufficient overlap in the spectra, then the dipole coupling between the donor and acceptor molecules will not occur and hence FRET will not take place between them³⁰⁰. FRET is sensitive to distance between the donor and acceptor as the two molecules should be separated by a distance typically 20–60 Å and the transfer efficiency falls inversely as the separation distance between the two molecules increases.

Due to its extreme sensitivity to molecular distances, FRET phenomenon can be utilized as an indicator for close proximity between the molecules as well as a communicator for very small fluctuations in proximity leading to FRET being referred as a “spectroscopic ruler”. Hence FRET is suitable for biomedical applications as the range at which FRET occurs matches with the dimensions of many biological molecules, such as proteins, cell membranes and polymeric NPs such as micelles. When encapsulated within a micellar system the FRET pair are in close proximity within the nanoscale region which favours efficient FRET between the molecules. The limited intra-micellar space can be exploited by the FRET mechanism allowing micellar delivery systems to incorporate FRET within the design producing self-communicating delivery systems. Another advantage of FRET is that it can be applied under physiological conditions in biological systems particularly in real time²⁹⁹.

3.1.2 Photochromic compounds

Light responsive drug release is an attractive mechanism because of its ease of production, non-invasiveness, controllable intensity and the ability to control the spatial and temporal triggering of the release process³⁰¹. Triggered release using light has been used in many applications for smart targeted drug delivery systems. The response to light of substrates can be irreversible or reversible depending on their nature of the substrates for example; photocleavable polymers have an irreversible response to light leading to cleavage of unstable bonds to polar stable states with the help of photons, whereas photochromic materials have a reversible reactions to light such as photo-oxidation, double bond rotation, and cleavage which undergo reformation or reisomerization after removing the light source. Furthermore, different types of light can be used like ultraviolet light with (100–400nm), visible light (400–750nm), and near-infrared (750–2000nm)³⁰². Numerous examples of

photochromic materials capable of transforming under the influence of activating radiation have been explored over recent years³⁰³. However, the photo activating ability of spiropyran compounds was recognised as early as the 1920's³⁰⁴.

Spiropyran is a dynamic molecule consisting of a chromene and indolene moiety bound together via a spiro junction and oriented perpendicular to each other. When exposed to UV light ($\lambda = 365\text{nm}$), spiropyran can undergo a reversible response to light and chemical stimulations. The closed ring stable state of spiropyran (**10a**) can be converted to its open form, merocyanine (**10b**), when irradiated with UV light, which is converted back into its original state when irradiated with visible light (Figure 3-2).

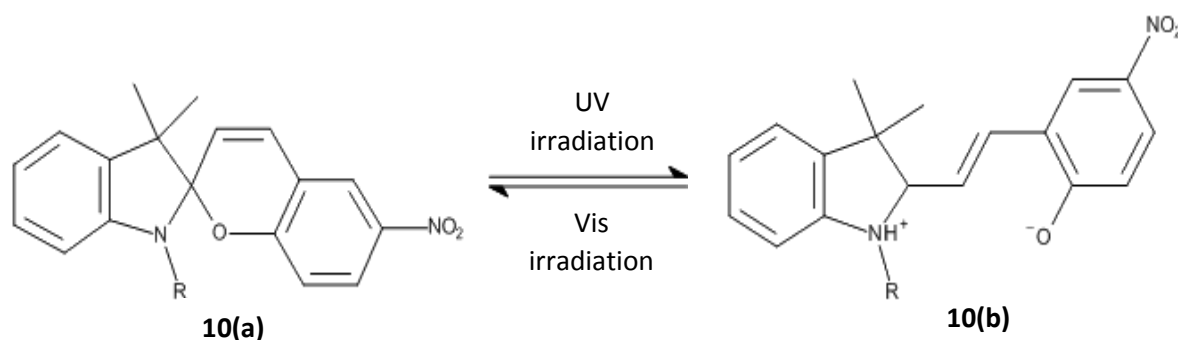


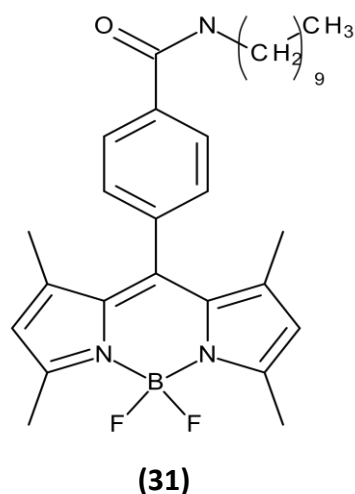
Figure 3-2 Illustration of the phototransformation of spiropyran to merocyanine and transformation back under visible irradiation

The property that makes spiropyrans unique is that both its isomers have very different properties. The spiropyran form, is a hydrophobic four-ring system and preferentially favours a non-polar environment whereas its open ring zwitterionic merocyanine counterpart prefers a more hydrophilic environment. In this chapter, we exploit differences in the hydrophobic/hydrophilic balance between the two isomers to mediate drug release from a micellar based delivery system. This simple photochromic transformation has found many applications ranging from molecular sensors³⁰⁵ to DNA-based logic operations³⁰⁶ and bioimaging⁹³.

3.1.3 The FRET pair

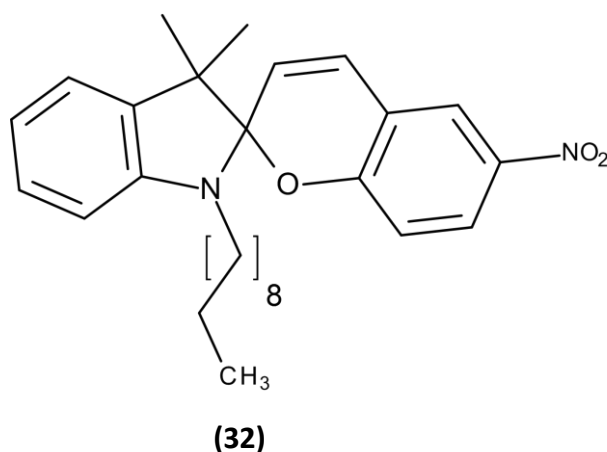
Boron-dipyrromethene (BODIPY) (**13**) belongs to the class of fluorescent dyes which have proved ideal as fluorescent probes for FRET analysis due to their high fluorescent

quantum yield, low molecular weight and small stokes shift³⁰⁷. The bodipy derivative **31** having an aliphatic decyl chain was synthesized in the laboratory and its structure was confirmed by ¹H NMR and mass spectroscopy and used without further modification.



The emission spectrum of bodipy overlaps with the absorption wavelength of merocyanine which renders it as a suitable donor chromophore in the FRET relationship. The phototransformation of spiropyran to merocyanine acts as photochromic switch to the fluorescence emission of bodipy. The presence of merocyanine in the system allows the transfer of excitation energy from bodipy to merocyanine resulting in quenching of bodipy fluorescence. Whereas the removal of light source, allows the reversion of merocyanine back to spiropyran causing increase of bodipy fluorescence. This process is termed as photochromic FRET and utilizes a dynamic photochromic compound to switch ON and OFF the fluorescence of the donor compound and can be repeated until fatigue resistance of the donor compound occurs³⁰⁸.

Hydrophobic spiropyran **(32)** was synthesized in the laboratory by attaching a decyl chain to it which enables sufficient hydrophobicity to spiropyran whereas its light induced isomer merocyanine is more hydrophilic which allows its transport across the micellar membrane. Its successful synthesis and structure were further confirmed by ¹H NMR and Mass spectroscopy.



The attachment of a decyl chain to the spiropyran molecule enabled it to achieve sufficient hydrophobicity to reside in the hydrophobic depths of the micellar core along with bodipy without affecting its photochromic isomerization properties. Thus allowing it to convert to merocyanine on irradiation with UV light.

3.1.4 Chapter overview

In this chapter, a micellar system capable of delivering hydrophobic drugs was combined with both a triggered drug release mechanism and FRET communication to allow for the real time quantitative analysis through molecular communication as well as triggered drug release of lipophilic compounds. This was achieved using a FRET mechanism whereby a hydrophobic FRET pair were contained within the interior of a self-forming amphiphilic micelle. Upon application of an external UV light trigger, one of the FRET pair, a spiropyran moiety, underwent the photo transformation described in Figure 3-3, to the more hydrophilic merocyanine isomer and subsequently transcended the micellar membrane into the aqueous external environment. The other half of the FRET pair, a hydrophobic bodipy fluorochrome, remained within the non-polar environment of the micelle. Thus, release of the merocyanine isomer from the micelle modulates the donor-acceptor energy transfer process enabling the release process to be followed by fluorescence spectroscopy, illustrated in Figure 3-3.

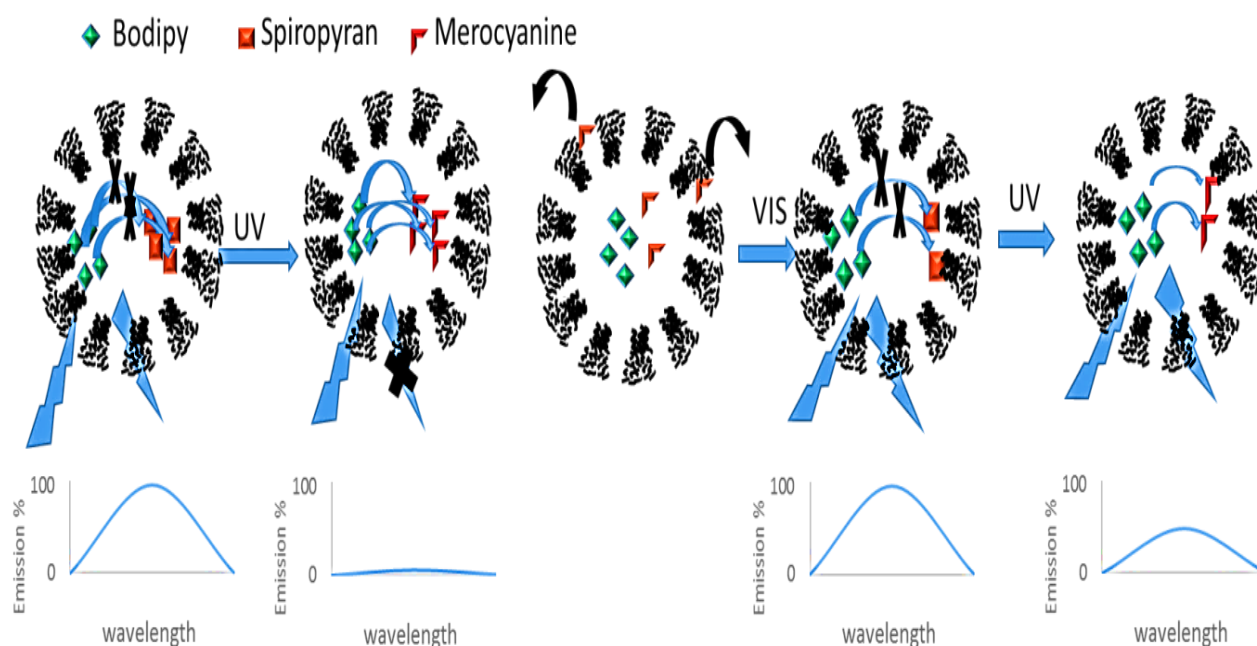


Figure 3-3 Schematic representation of the UV triggered release caused by the photoisomerism of spiropyran to the zwitterionic merocyanine transcending the amphiphilic micelle and concomitant quantification using FRET with a bodipy donor moiety.

The scope of this approach was further extended by conjugating an Active Pharmaceutical Ingredient (API) onto the spiropyran isomer enabling its release to be controlled and monitored in real time. To illustrate this, we have also attached ibuprofen to spiropyran using an ester linkage and determined its release from the micelle upon UV light irradiation and compare these results with unmodified spiropyran.

3.1.5 Aims of chapter

The creation of a micellar drug delivery system capable of triggered drug delivery and subsequent communication using a FRET mechanism to establish real time drug release from the micelle.

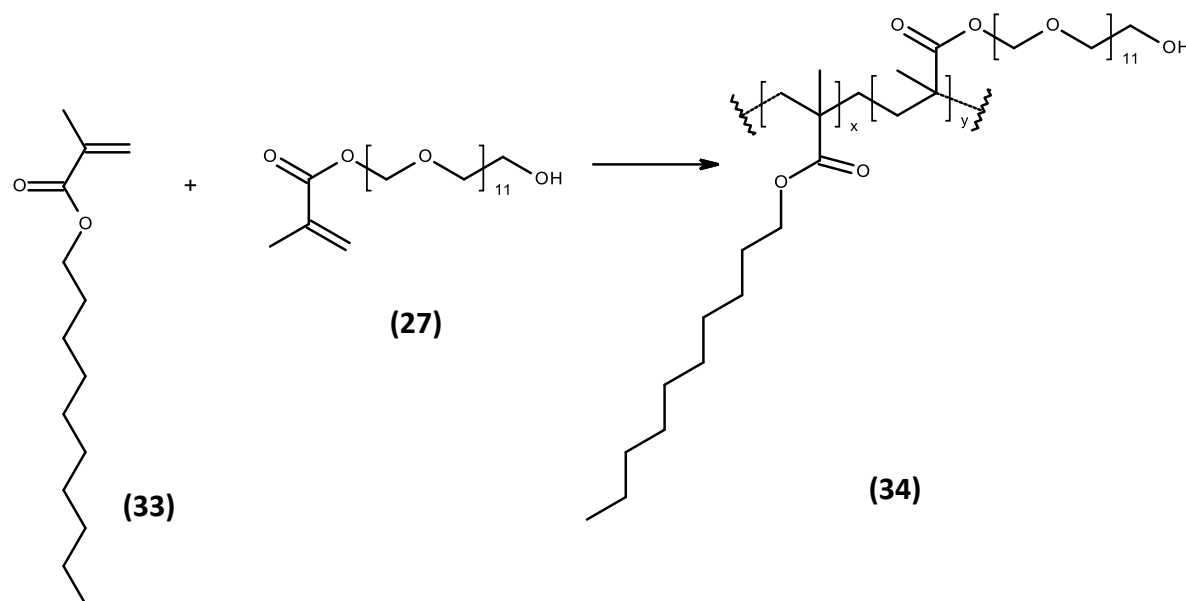
Specific aims:

1. Preparation of and characterization of micelles with the capacity to encapsulate FRET communicating compounds. Characterization will be achieved using particle size and PDI, zeta potential and encapsulation efficiency.
2. Establishment of the physical parameters required for the photo-transformation of spiropyran to merocyanine. In particular, the time required for complete conversion of spiropyran to merocyanine in both DMF and in aqueous medium (encapsulated within a micelle) will be determined.
3. Optimization of bodipy and merocyanine FRET relationship, by establishing the optimal molar ratio of bodipy to spiropyran at which optimal FRET efficiency occurs.
4. *In-vitro* triggered release of merocyanine from micelles using Franz diffusion cells.
5. Observation of FRET through changes in bodipy fluorescence in Hela cells following merocyanine release
6. Application of the delivery system demonstration release of encapsulated cargo attached to an API indirectly communicated by bodipy fluorescence following UV light trigger in visible and dark conditions.
7. Observation of real time release of spiropyran-ibuprofen complex and its correlation to quenching of bodipy fluorescence.

3.2 Results and Discussion

3.2.1 Preparation and characterization of micelles

Micelles made of amphiphilic polymers have been used extensively in recent years. Micelles made with polyethylene glycol have the ability to easily form micelles which are supramolecular structures having a hydrophobic core and a hydrophilic exterior. The amphiphilic polymer **(34)** used for the preparation of micelles was composed of a Decanyl chain **(33)** polymerized with PEG Mn 500 **(27)** in 3:5 ratio by free radical polymerization using AICN as the free radical initiator as seen in Scheme 3-1



Scheme 3-1 Synthesis of amphiphilic copolymer 34

Micelles are able to carry hydrophobic compounds in their interior whereas the hydrophilic exterior allows them to be suspended in aqueous medium. The encapsulation of a FRET pair inside the micelles offers several advantages which enhance their potential as self-communicating drug delivery systems. Firstly, bodipy and spiropyran are hydrophobic in nature which allows them to reside in the hydrophobic core of the micelles thus increasing their solubility in aqueous medium. The decyl chain attached to bodipy and ibuprofen moiety attached to spiropyran ensures that both compounds reside in the hydrophobic core of the micelles. Secondly, the presence of the FRET pair within the close proximity of a micelle core in the nanoscale region enhances their FRET relationship.

Micelles were prepared using the thin film evaporation method according to the procedure described in section **6.4.1**. Micelles encapsulating compounds **31** and **32** or **35** were prepared by hydrating polymer film with specified quantities of compounds after forming a film of mixture of polymer and compounds solution in chloroform in a round bottom flask and evaporating it to dryness. DLS measurements of micelles loaded with **31** and **32** indicate an average particle size of 27.5 ± 0.98 nm with PDI 0.416 ± 0.009 and surface charge of -1.67 ± 0.73 as determined by zeta potential

measurements (Table 3-1). These observations were in agreement with those observed previously by Yildiz *et al.* using the same polymeric micelle with encapsulated cargo⁹³. However, when **32** was replaced by **35**, the micelle size increased to 45.93 ± 2.72 nm and PDI was 0.346 ± 0.04 with -2.05 ± 0.61 zeta potential. This slight increase in micelle size may be attributed to the greater rigidity of **35** causing a larger hydrophobic internal core within the micelle. There was no major change in the PDI and zeta potential values for micelles following encapsulation with regards to content indicating successful incorporation of **35** inside the micelle. As indicated in table 3.1, the encapsulation efficiency of compound **32** in micelles was found to be $82.4 \pm 3.7\%$ whereas the encapsulation efficiency of compound **35** was $94 \pm 3.1\%$. Figure 3-4A shows a representative particle size distribution graph for micelles loaded with **31** and **32**, while a scanning electron microscopic image of micelles loaded with **31** and **35** (Figure 3-4B) shows well-formed particles with spherical morphology.

Table 3-1 Characterization of micelles. N=3 represented as average \pm SD.

	% EE of 32 & 35	Size (nm)	PDI	Zeta Potential (mV)
Micelles loaded with 31 & 32	82.4 ± 3.7	27.5 ± 0.9	0.4 ± 0.009	-1.6 ± 0.7
Micelles loaded with 31 & 35	94.0 ± 3.1	45.9 ± 2.7	0.3 ± 0.04	-2.05 ± 0.6

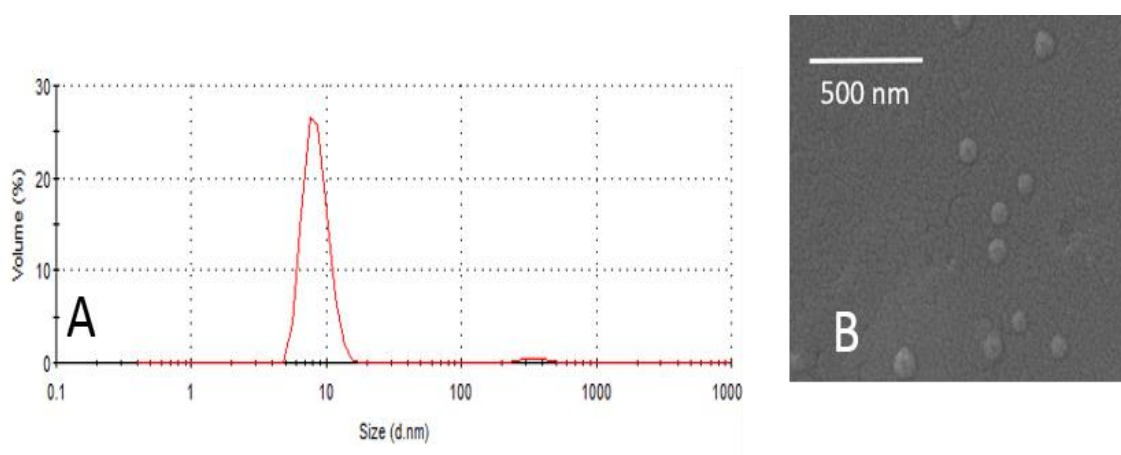


Figure 3-4 A. Dynamic light scattering displaying the hydrodynamic radius of micelles. B. SEM image of micelles

3.2.2 Quantification of photo physical transformation of 32a to 32b

For efficient FRET to occur between a donor-acceptor pair, two main criteria must be met. First, the donor and acceptor molecules must be in close proximity to each other and secondly, the emission spectrum of the donor must overlap effectively with the absorption spectrum of the acceptor. In the context of the micellar delivery system described above, as both the donor and acceptor are originally confined within the central hydrophobic core of the micelle, a nanoscale distance between the two molecules can be guaranteed²⁹⁹. In terms of spectral overlap, the absorbance spectrum of **32a** encapsulated within the micelle was determined to have a maximum absorbance centred at 360nm (Figure 3-5). Upon activation by UV light, **32a** undergoes a ring opening of the spiro carbon to its corresponding merocyanine, **32b** (Figure 3-2). The merocyanine is zwitterionic, and therefore more hydrophilic. It has also an extended area of conjugation and therefore induces a significant bathochromic shift to a new absorbance maximum at 550nm. The absorbance spectrum of merocyanine coincides with the emission wavelength of **31** (Figure 3-5) therefore providing an excellent spectral overlap from the donor moiety (**31**) to the acceptor moiety (**32b**). No such FRET relationship occurs between compound **31** and the spiropyran version of **32** (**32a**).

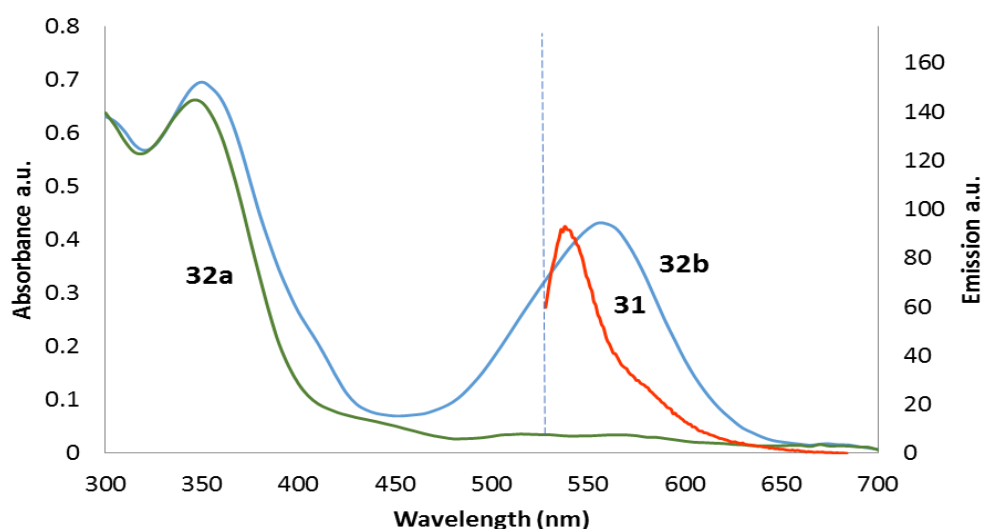


Figure 3-5 Absorbance spectra of 32a and following photoconversion to 32b with the emission spectra of 31 with Ex 525 nm.

This spectral cohesion of absorbance and emission of **32b** and **31** is imperative for energy transfer from **31** (the fluorescent donor) and **32b** (the photochromic acceptor). Nevertheless, the time required for conversion of **32a** to **32b** can significantly affect the energy transfer from **31** to **32b**.

In an attempt to understand the photoconversion of **32a** to **32b**, compound **32** was exposed to varying time intervals of UV light and the absorbance spectra collected at each point. As the compound was hydrophobic, this analysis was first carried out in DMF with the results shown in Figure 3-6.

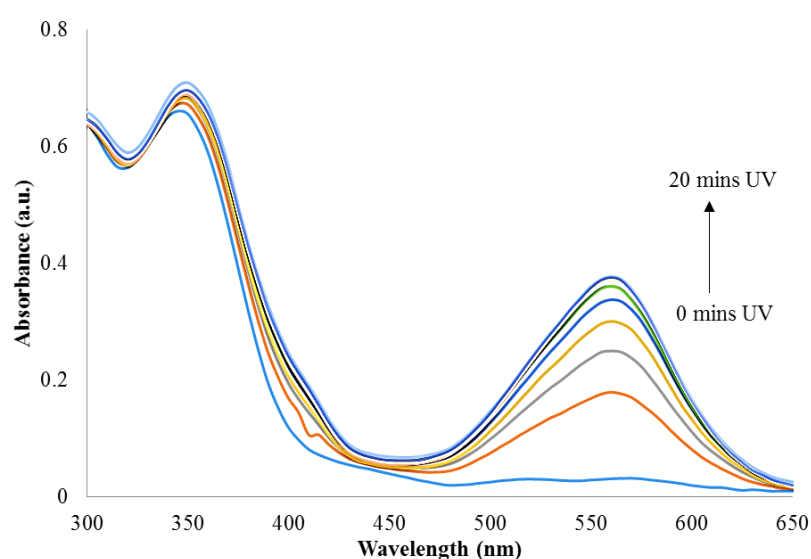


Figure 3-6 Absorbance spectra of 32b in DMF after photo-conversion of 32a by UV exposure at 365nm for specific time intervals at increments of 2 minutes

It can be seen from Figure 3-6, that complete conversion of **32a** to **32b** was achieved after 12 minutes exposure to UV light. A similar experiment was then conducted in the aqueous solution using the micelle drug delivery system to ensure solubility of the compounds. Figure 3-7 displays the results achieved from this experiment.

From Figure 3-7 it can be seen that it required 5 minutes irradiation for complete conversion from **32a** to **32b** loaded within a micelle. When considering the aqueous environment in the photoconversion, after 5 minutes, the absorption reached a plateau beyond which there was no increase in the absorption intensity. However complete conversion of **32a** to **32b** took 12 minutes in DMF medium (Figure 3-6). This can be explained by the increased polar nature of **32b** when compared to its **32a** counterpart, therefore favouring a faster conversion to the zwitterionic **32b** in the more polar aqueous medium. The polar nature of **32b** is fundamental to encourage its release from within the micelle to the surrounding polar aqueous environment, enabling a triggered release of micellar content.

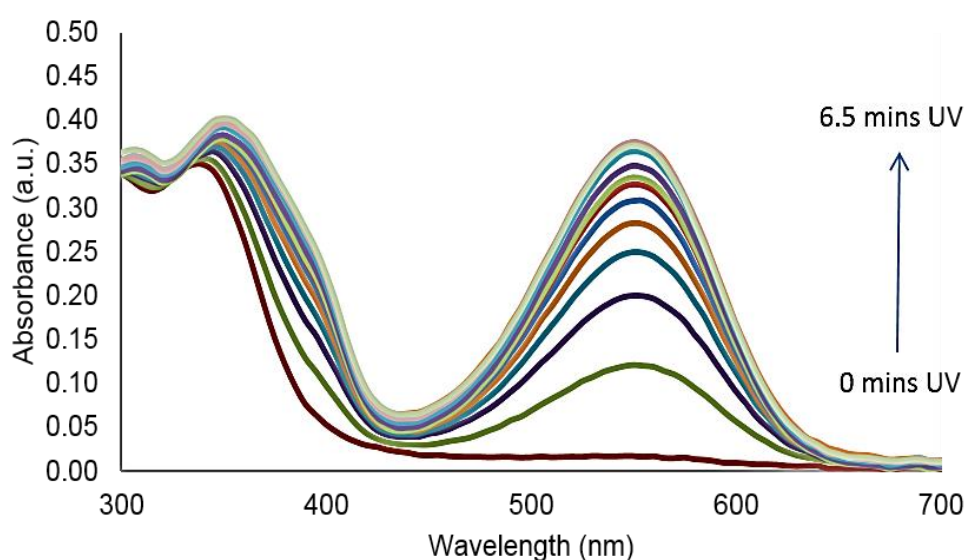


Figure 3-7 Absorbance spectra of 32b at λ_{max} 550nm increasing with increasing exposure to UV light of 365nm encapsulated in micelles in PBS. Spectra displayed following exposure to 0, 0.5, 1.0, 1.5, 2, 2.5, 3, 3.5, 4, 4.5, 5, 5.5, 6 and 6.5 mins UV light at 465 nm from a fixed distance.

3.2.3 FRET efficiency between **31** and **32b**

In order to identify the optimal ratio of **31** to **32b** which allows linearity between energy transfer and concentration between the fluorophore and photochrome, the two compounds were encapsulated into the micelles at different molar ratios and the decrease in fluorescence emission of **31** was recorded. From Figure 3-7, we deduced that 5 minutes irradiation with UV light was sufficient in aqueous media to facilitate complete conversion of **32a** to **32b**. Figure 3-8 shows the emission profile of **31** at

varying ratios of **32b**. As expected, the emission of **31** was highest when there was no **32b** present in the micelle (spectrum a). As the concentration of **32a** in the micelles increased, more **32a** was converted to **32b** upon irradiation with UV light and quenched the emission of **31** at 540nm proportionately (spectra b-h). In addition, emission from **32b** (merocyanine emission at 637nm) was observed as a broad bathochromic shifted peak upon increasing the concentration of compound **32** indicating an excess of **32b**. The plot of percentage depletion in fluorescence emission of **31** (Figure 3-9) shows that the relationship between **31** and **32b** is only linear until a certain concentration when a plateau was reached after a ratio 1:6 of **31:32**. In order for this system to be capable of self-quantifying it is essential that a linear relationship exists between donor and acceptor moieties. A molar ratio above that of 1:6 of **31:32** suggests a saturation concentration was reached with no more **31** available for energy transfer. Therefore it can be concluded that the optimal FRET molar ratio between donor and acceptor to allow for quantitative analysis is 1:6. This is reflective of the difference in extinction coefficient between our donor and acceptor moieties. This was the ratio chosen for all subsequent studies.

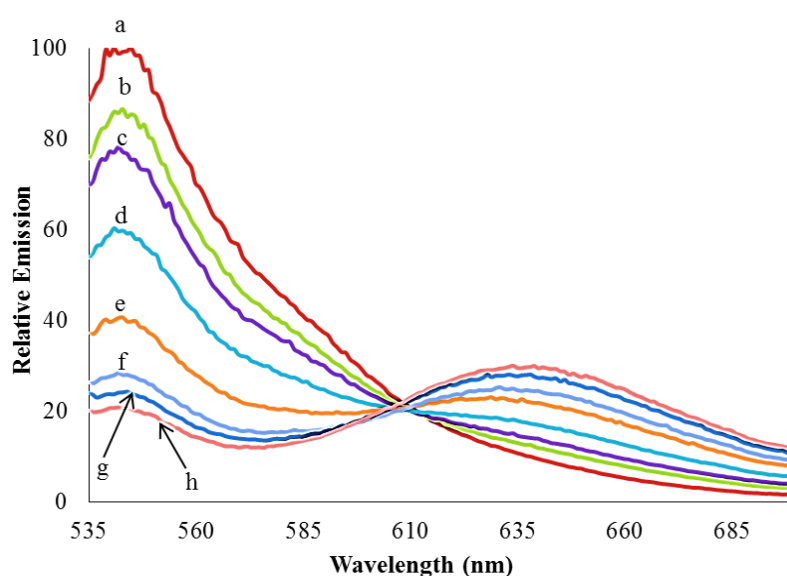


Figure 3-8 Fluorescence emission of 31 following exposure to varying molar ratios of 32 after photoconversion to 32b. a: no UV exposure and b-h: solutions were exposed to 5 mins UV light at 365 nm from a fixed distance and molar ratios of compounds bodipy 31 : merocyanine 32b b-1:0.5; c-1:1, d-1:2, e-1:4, f-1:6, g-1:8 and h-1:10 consecutively.

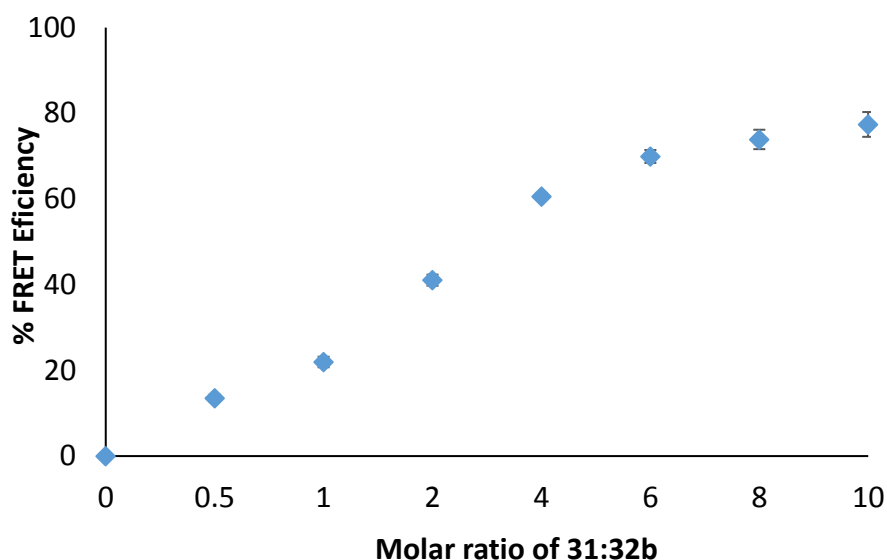


Figure 3-9 FRET efficiency of 31 and 32b following exposure to 5 mins UV light at 365 nm from a fixed distance. Concentration of 31 remains constant at 3.64 μ M. Percentage efficiency was determined by the relation depletion in the emission of 31 at 545 nm.

3.2.4 *In-vitro* triggered release

The ability of the micellar system to encapsulate the hydrophobic guests (**31** and **32**) was established by the encapsulation efficiency (results displayed in Table 3-1). Perhaps of more importance, is the ability of these delivery systems to release cargo under particular conditions. UV light acts as a trigger for the photoinduced transformation of **32a**, which is hydrophobic with a closed ring system, to an open ring **32b** which is polar in nature with higher solubility in aqueous medium. The dynamic property of micelles would suggest that **32b** can easily come out of the micellar system permitting release of encapsulated cargo. In an attempt to establish this relationship, we subjected the micelles containing compound **32** to continuous photoactivation and using a Franz diffusion cell loaded with a semi permeable membrane monitored the amount of **32b** released to the outside of the micellar environment through the semipermeable membrane into the wider aqueous environment. The results, displayed in Figure 3-10, show the release of **32b** from within the micelle with and without photoactivation using UV light. It can be seen that with UV activation the amount of **32b** released into the surrounding environment within 12 minutes was 24% which was significantly higher than the 5% release in the

absence of photoactivation. In order to ensure that no **32a** was being released from the DDS, all samples were subjected to further UV light just prior to the analysis of merocyanine.

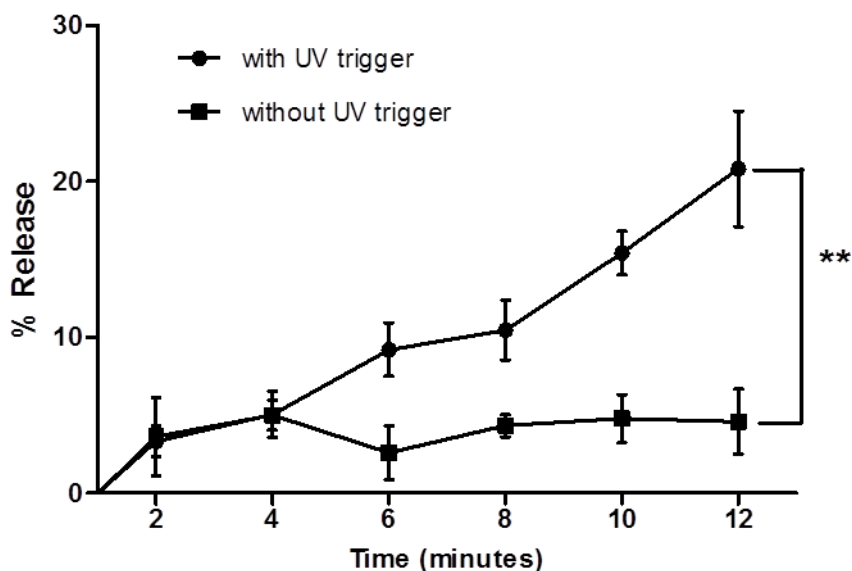


Figure 3-10 In-vitro triggered release of 32b from micelles after continuous activation with UV light for 12 minutes and no UV activation. N=3, represented as average \pm SEM, ** indicates $p < 0.005$.

This design of a triggered fast release system is essential for successful release of drugs attached to **32** for therapeutic applications. The results displayed above, suggest that the photoconversion of compound **32**, is indeed both fast enough with a sufficient change in polarity to drive the triggered release from the hydrophobic micellar environment.

3.2.5 Observation of FRET in HeLa cells

Encapsulation of cargo within micelles enables them to be transported across the cell membrane leading to better cellular uptake owing to their biocompatibility and size. In order to determine the feasibility of communication and triggered release from within the micelles, we incubated HeLa cells with micelles loaded with **31** and **32a** and enabled the photoconversion of **32a** to **32b** present within the cells to confirm FRET communication between **31** and **32b**. As seen in Figure 3-11, fluorescence emission of **31** fluctuated drastically according to status of **32b** present within the cells, as a direct result of molecular communication between them. The ability of **32b** to switch back to

32a in the presence of visible light broke the communication between **31** and **32b** allowing the emission of **31** to be observed. These results in HeLa cells support our previous observations *in-vitro* conditions in section 3.2.6. It can be seen that immediately following 5 minutes UV irradiation there is an 82.5% quench in the fluorescence emission of **31**, attributed to the energy transfer to the acceptor moiety, **32b**. Upon subsequent photoactivation cycles of **32b** there was significantly less quenching of the emission from our donor compound **31** (75.3% and 64.2% respectively). This can be attributed to the more polar **32b** form leaving the micelle DDS (24.7% and 35.8 % released after 10 and 15 minutes irradiation).

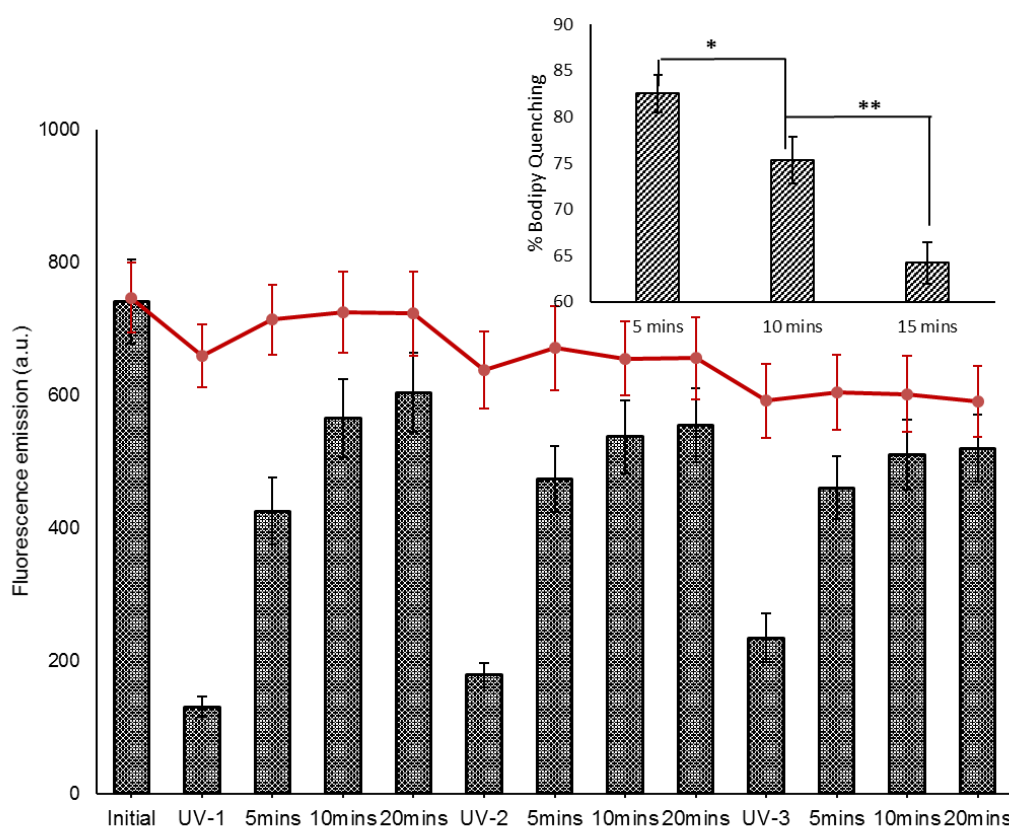


Figure 3-11 Bar chart: Fluorescence emission of 31 in HeLa cells incubated overnight with micelles loaded with 31 and 32a and following cycles of UV exposure (365 nm, 5 mins) leading to conversion of 32a to 32b and subsequent resting time in visible light conditions permitting reversion of 32b back to 32a. Line graph: control using micelles containing 31 only. Insert: % quenching of 31 following UV irradiation. N=3 represented as average \pm SEM, ** indicates $p<0.01$, * indicates $p<0.05$.

As expected the emission of **31** lapsed back faster in visible light conditions compared with dark conditions (Figure 3-12), further confirming that the photoconversion of **32b** to **32a** is faster in the presence of visible light and is indirectly communicated in the form of higher emission of **31**. Additionally, the quenching effect after subsequent UV irradiation cycles in the dark was similar to that seen in light conditions. Similarly, observations of cells by confocal microscopy indicated significant reduction in fluorescence emission of **31** on photoactivation of **32b** confirming its presence within cells (Figure 3-13).

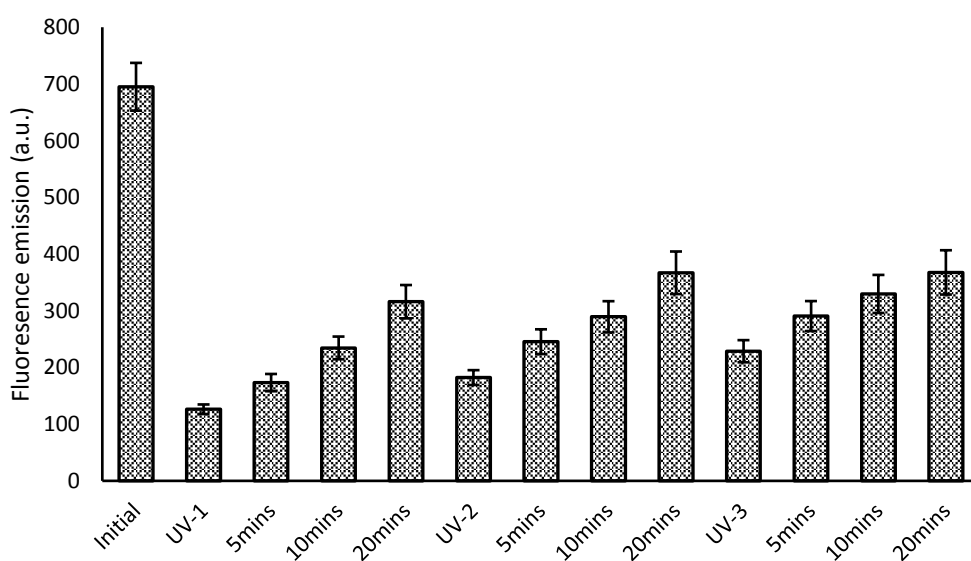


Figure 3-12 Fluorescence emission of **31** in HeLa cells incubated overnight with micelles loaded with **31** and **32a** and following cycles of UV exposure (365 nm, 5 mins) leading to conversion of **32a** to **32b** and subsequent resting time in dark conditions permitting reversion of **32b** back to **32a**. N=3 represented as average \pm SEM.

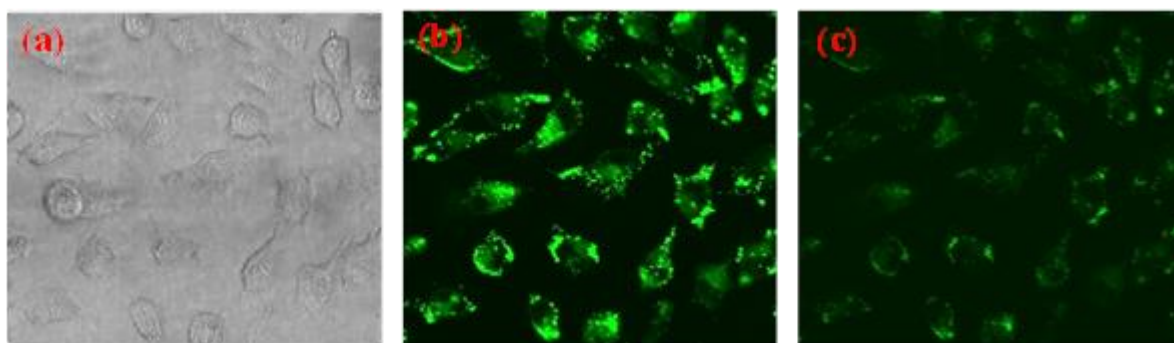
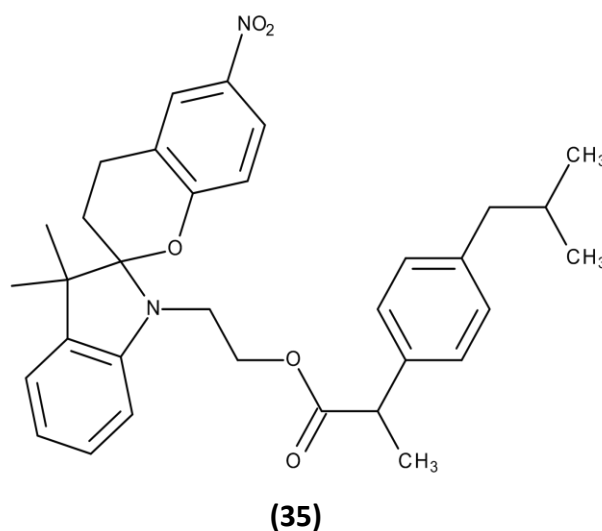


Figure 3-13 Confocal microscopic images of HeLa cells incubated with micelles loaded with **31** and **32a** showing (a) Clear field (b) Fluorescence emission of **31** (Ex 514nm, Em 520-590nm) before UV exposure (c) Fluorescence emission of **31** after UV exposure (365nm, 5 mins).

3.2.6 Application of the delivery system

Having established the FRET relationship between the bodipy (**31**) and spiropyran (**32**) moieties, the ability to extend upon these particular compounds, by the generation of conjugates was a paramount importance for the translation of this novel DDS into a more general delivery system. To this end, ibuprofen conjugated spiropyran (Compound **35**), was synthesized in the laboratory by an esterification reaction between spiropyran and ibuprofen. Compound **35** can be considered as a novel prodrug of ibuprofen conjugated via an ester bond to spiropyran. The spiropyran section of the compound is still capable of isomerization in the presence of UV and therefore would be expected to change the polarity of compound **35** sufficiently to allow the compound to transcend the micelle environment thus demonstrating the ease with which this triggered DDS can be applied to regular therapeutic drugs. Compound **35** was created as a prodrug, to contain an API (Ibuprofen) covalently linked to the photochromic spiropyran moiety.



Once released from the internal core of the micelle after phototransformation by a UV trigger, it is anticipated that compound **35** would be subjected to hydrolysis via esterase's enzymes and hence release the API. The micelles containing both compounds **31** and **35** were subjected to various cycles of UV exposure both in light and dark conditions. Figure 3-14 shows the *in-vitro* fluorescence emission of **31** in the presence of **35**, the subsequent photochromic switching between the spiropyran form (**35a**) to its merocyanine counterpart (**35b**) is visualized by the quenching of emission

from **31**. The UV exposure cycle was repeated three times with the results displayed in Figure 3-14 indicating the reproducibility of the system.

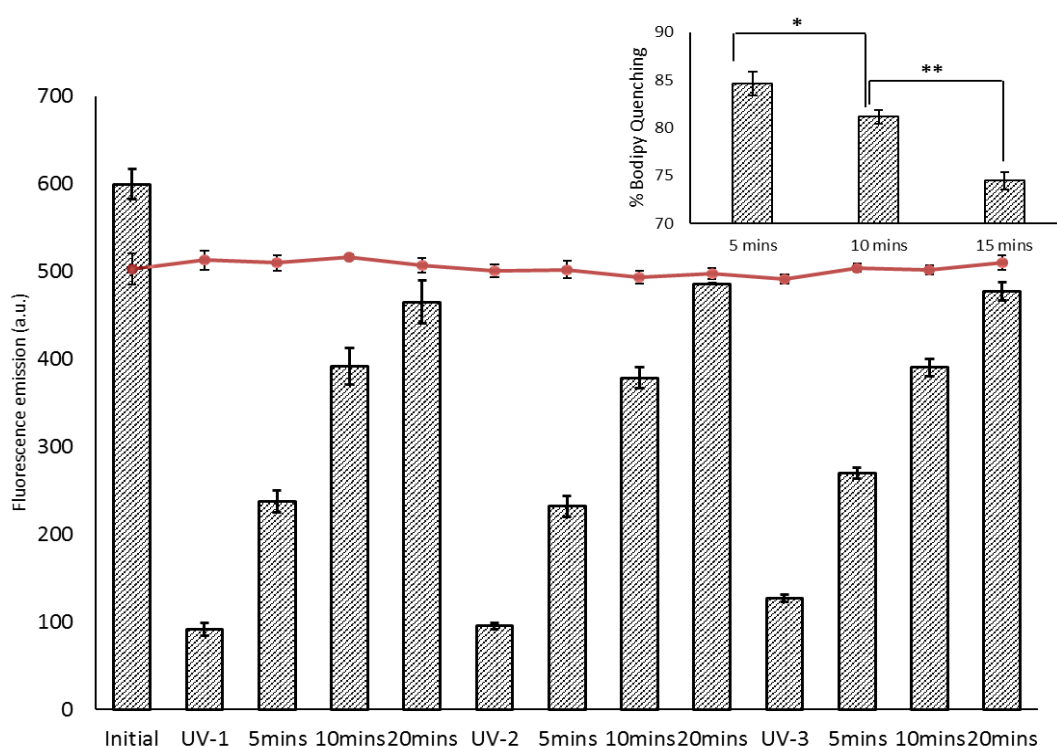


Figure 3-14 Bar chart: Fluorescence emission of 31 within micelles loaded with 35a following cycles of UV exposure (365 nm, 5 mins) leading to conversion of 35a to 35b and subsequent resting time in dark conditions permitting reversion of 35b back to 35a. Line graph: control with micelles containing only 31. Insert: % quenching of 31 following UV irradiation. N=3 represented as average \pm SEM. * indicates $p < 0.05$, ** indicates $p < 0.005$.

When there was no **35b** present in the system (in the absence of UV light), there was a significantly high emission of **31**. This emission was quenched upon photoactivation of **35a** to **35b** as the absorption signature of **35b** overlaps with emission signature of **31**. As **35b** slowly reverted back to **35a** owing to its reversibility in heat and visible light conditions, the emission of **31** slowly increased. The hydrophilic nature of **35b** encourages it to transcend the hydrophobic internal core of the micellar system into the wider aqueous environment. Although the system was kept in the dark, there were three cycles of 5 minutes irradiation, allowing for significant movement outside the micelle. This movement was observed as a decrease in the quenching efficiency of **31** upon subsequent photoactivation cycles (Figure 3-14 insert) as less **35b** was

present within nanoscale distance for FRET to successfully take place between the two molecules in each subsequent excitation. This decrease in the quenching of emission of **31** is of similar magnitude to the % release of internalized compound **32**, observed in Figure 3-10, with 19% release after 10 minutes of **35** when compared to the 15 % release of **32** after 10 minutes displayed in Figure 3-10. The increase in release is attributed to the time lapse between UV stimulation and subsequent photoconversion allowing for more hydrophobic **35b** to leave the micelle.

It is seen from Figure 3-14 inset that a further fluorescence quenching of 74.4 % is recorded after 15 mins UV irradiation and would suggest that 25.6 % of **35** has been released. A similar effect was seen in light conditions, but the % of quenching of **31** was slightly less, due to the faster photoconversion back to the original more hydrophobic spiropyran moiety (**35a**), ensuring that less compound was released and hence more available for the subsequent energy transfer to the donor (Figure 3-15). Micelles loaded with only **31** did not show any changes in fluorescence emission after photoactivation and after subsequent resting periods, in addition there was limited photobleaching of **31** after UV irradiation.

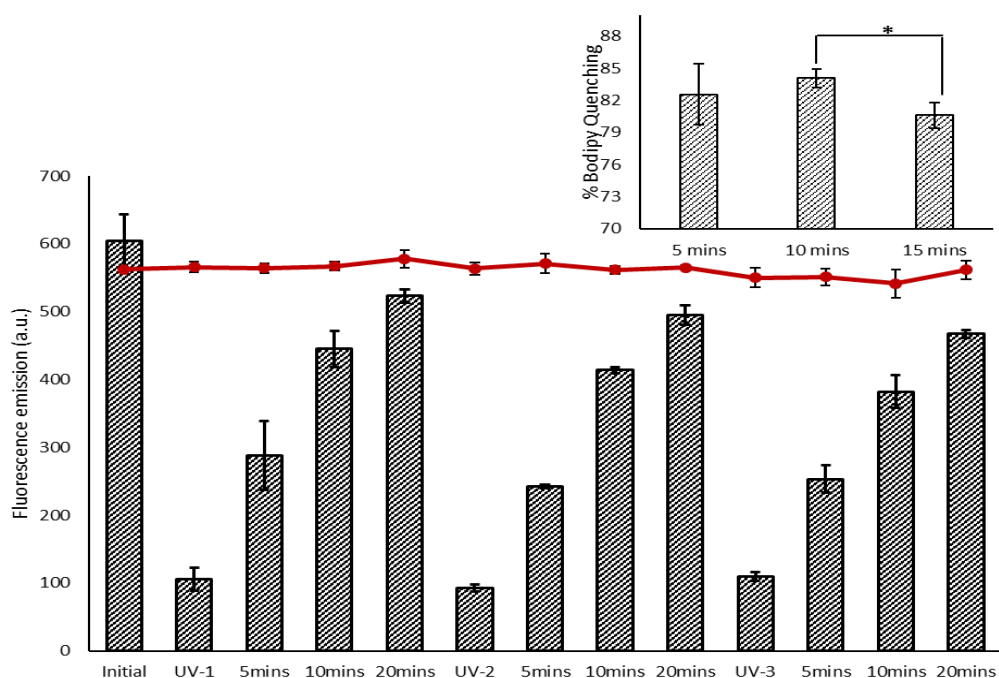


Figure 3-15 Bar chart: Fluorescence emission of 31 within micelles loaded with 35a following cycles of UV exposure (365 nm, 5 mins) leading to conversion of 35a to 35b and subsequent resting time in light conditions permitting reversion of 35b back to 35a. Line graph: control with micelles containing only 31. Insert: % quenching of 31 following UV irradiation. N=3 represented as average \pm SEM. * indicates $p < 0.05$.

3.2.7 Real time quantification of encapsulated cargo

The photoswitchable nature of **35** and its molecular communication with **31** can prove beneficial in real time quantification of release of encapsulated materials from within the micellar environment. To quantify this occurrence, micelles loaded with **31** and **35** were loaded on to dialysis membranes in Franz diffusion cells and photoactivated for 5 minutes to allow conversion of **35a** to **35b** resulting in its release from the micellar environment recorded over 20 minutes of resting time in both dark and visible light conditions. Two parameters were measured simultaneously at various time points in an attempt to correlate the communication seen through **31** with release of **35**. This was achieved by monitoring the amount of **35a** present within the micelles by absorbance at 345 nm. Following removal of the sample for analysis a set period of 20 minutes was observed with the sample subjected to visible irradiation, to ensure that all **35** was in the spiropyran form, **35a**. The results of the depletion in **35a** absorbance can be seen in Figure 3-16a. The simultaneous measurement of bodipy emission (**31**) was collected, following the original 5 minutes UV irradiation, each sample removed for analysis was subjected to 20 minutes visible light before the emission of **31** was recorded, and the decrease in quenching is plotted in Figure 3-16b.

From Figure 3-16, a good correlation is seen between both the fluorescence increase from **31** and the absorbance of **35a**. The largest magnitude of change is observed from the UV stimulation in dark conditions, this is expected as **35b** would favour the more polar environment. Specifically, an 8.4% decrease in **35a** absorbance is observed after 10 minutes, indicating a transfer of **35** across the dialysis membrane. This is indirectly communicated through a 7.0 % increase in the fluorescence emission of **31** (Figure 3-16b). Similarly, a 17.4 % decrease in absorbance of **35a** is seen at 20 minutes compared to 11.6 % increase in fluorescence emission of **31** at the same time point. Visible light conditions led to conversion of **35b** back to **35a** leading to lesser release of only about 7% from micelles which was reflected as approximately 4% increase in fluorescence emission of **31**. However, there was negligible release in the absence of a UV trigger and is suitably revealed as insignificant increase in fluorescence emission of **31**. This close correlation between the FRET communication when compared to the

direct measurement of remaining spiropyran would suggest that there is indeed potential to further develop these smarter DDSs.

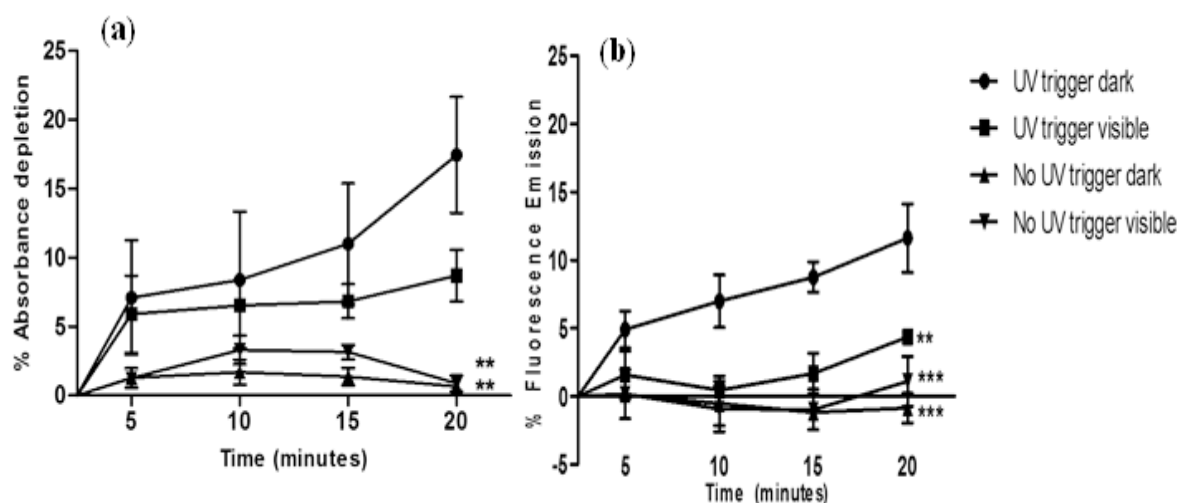


Figure 3-16 (a) In-vitro release of 35a from micelles with and without UV trigger and subsequent resting time in dark and visible light conditions measured by decrease in UV absorbance at 345 nm. (b) Observation of % increase in fluorescence emission of 31 at Ex 503 Em 514 nm measured concomitantly with release of 35a. N=3 represented as average±SEM, ** indicates $p < 0.005$, * indicates $p < 0.0005$.**

3.3 Conclusion

The ability to control drug release at a specific physiological target enables the possibility of an enhanced therapeutic effect with reduced off-target toxic side effects. The discipline of controlled drug release has grown to include most areas of medicine with examples in the literature of targeted drug delivery to the majority of organs within the human body. In addition, a variety of external stimuli used to mediate the drug release process have also been investigated. The number of smart DDSs capable of real time communication with concomitant stimulated drug release is increasing in response to the nanotechnology revolution³⁰². The need for variation between the mechanism of stimulus, as well as the parameters involved in communication is paramount to the success of these advanced materials so to allow these nano-platforms to reach the full echelon of their potential. Recent examples illustrating this diversity can be seen by Huang *et al.*³⁰⁹ whereby they have incorporated the anticancer agent Dox into a supramolecular nanoparticle and also double up its use as

the FRET acceptor to allow self-communicating. Another interesting example is seen by Du *et al.*³¹⁰ and their incorporation of five stimuli responsive moieties on to their NP. Nonetheless, the concurrent real time monitoring of drug release has not been widely studied.

The work presented in this chapter describes a novel micellar drug delivery system that is not only capable of releasing its cargo when stimulated by light but also provides a real time analysis of the amount of cargo remaining. We have designed a photo-activated DDS capable of real time communication using the photochromic properties of spiropyrans and exploiting the differences in physiochemical properties. Controlled drug release from the delivery system was mediated by physicochemical changes of a spiropyran-merocyanine photochromic dyad, while drug quantification was enabled using a Förster Resonance Energy Transfer (FRET) relationship between the photochrome and a co-encapsulated BODIPY fluorophore. The percentage of drug released from the delivery system was significantly greater (24%) when exposed to light irradiation compared to an analogous control maintained in the dark (5%). Furthermore, the fluorescence read-out capability also enabled the drug-release process to be followed in living cells with a significantly reduced fluorescence emission observed for those cells incubated with the delivery system and exposed to light irradiation compared to control cells maintained in the dark. By adopting a prodrug approach, we have developed an ibuprofen-spiropyran analogue, which has displayed significant stimulated release from within a micelle environment. In addition, with the incorporation of a hydrophobic bodipy compound within the micelle hydrophobic core, the FRET communication between the two species present within the micelle has shown significant potential for real time analysis of content. Thus, this smart DDS has the potential to be adapted for a number of different API, by simply linking the API with the spiropyran through an ester or potentially an amide bond, thus increasing application for such nanoplateforms to include a large number of drugs with the only prerequisite being that they contain a suitable reactive functional groups. Combined, these results highlight the utility of this approach to theranostic drug delivery with the potential of light-triggered released together with a fluorescence read-out to enable quantification of the drug release process.

Chapter 4

Multi drug loaded polymersomes for increased efficacy of cancer therapy

4.1 Introduction to cancer chemotherapy

Cancer is one of the leading causes of death and was responsible for nearly 8.8 million deaths in 2015 globally which accounts for 1 in 6 people dying of cancer³¹¹. Cancer is characterised by the uncontrolled proliferation of malfunctioning cells involved in complex interactions with the environment, surrounding healthy tissue and the immune system³¹². There are various ways of treating cancer including surgical removal of the tumour mass, chemotherapy, radiotherapy, hormonal therapy and biological therapy depending on the type of cancer, its size and extent of metastasis and general health of patient³¹³. Chemotherapy with one or more drugs is generally the first line of treatment for patients diagnosed in advanced stages of local and metastatic cancers. The main challenge of chemotherapy is to administer drugs at doses of maximum therapeutic efficiency and reduced toxicity³¹⁴. As well as advances in the chemotherapeutic agents used in chemotherapy, early detection and treatment have benefited cancer patients leading to an increase in the number of cancer survivors³¹⁵. The mechanism of action of many of these anticancer agents such as anthracyclines, antimetabolites, alkylating agents and microtubule disruptors is to destroy any rapidly proliferating cells, although cancer cells are indeed rapidly proliferating, a leading drawback of this type of treatment is due to non-selectivity³¹⁶⁻³¹⁸. These anticancer agents can target healthy cells that divide rapidly such as bone marrow, hair follicles, digestive tract and macrophages causing immunosuppression, rapid hair fall and anaemia. Furthermore these chemotherapeutic agents generally have low solubility and get washed out rapidly from blood circulation. They achieve lesser accumulation in tumour due to multidrug resistance because of the overexpression of P-Glycoprotein, a multidrug resistant protein on the surface of cancerous cells leading to failure of treatment^{319, 320}. Multidrug resistance (MDR) is a major problem in cancer chemotherapy and can occur via various mechanisms. MDR plays a major role in tumour metastasis and relapse accounting for 90% of chemotherapy failures in metastatic cancers³²¹. Tumours are generally a mixed population of malignant cells of which some are drug sensitive and others are drug resistant. Chemotherapeutic drugs kill the sensitive cells but leave behind a good proportion of resistant cells causing the chemotherapy to fail because of the presence

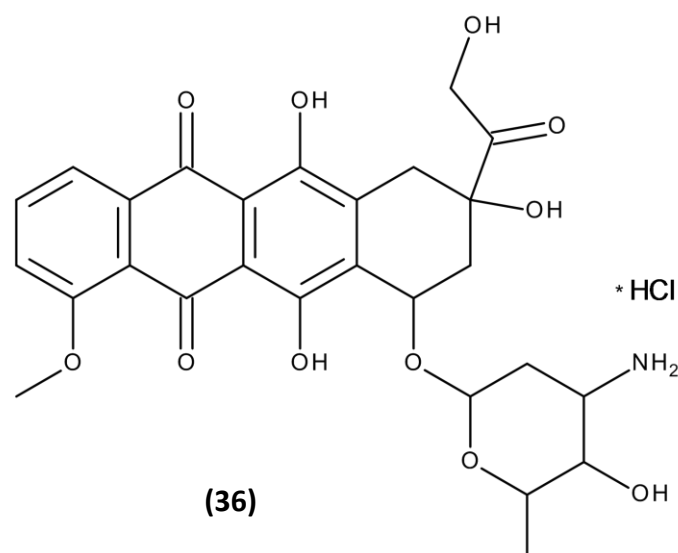
of a large number of drug-resistant cells³²². Other mechanisms of action include increased DNA repair capacity, overexpression of MDR related transporter proteins leading to high drug efflux, reduced drug uptake, activation of detoxification and evasion of apoptosis^{314, 321} leading to gradual decrease in sensitivity to the therapeutic agent and eventual development of MDR. Thus, MDR is multifactorial and can involve various cellular pathways simultaneously in clinical drug resistance. However, knowledge of the particular mechanism of drug resistance can help devise new strategies of cancer treatment³²³.

4.2 Different classes of anticancer agents

Cancer patients are generally treated with either one or a combination of surgery, radiation and chemotherapy regimens. Surgery is often the main line of treatment for early stages whereas chemotherapy with singular or combination drugs is used in later stages of cancer³²⁴. Chemotherapy drugs can be classified by their chemical structure, their mechanism of action and their relation to other drugs. The choice of chemotherapy drug depends on the type of cancer, its size, location, age and health of patient³²⁵.

4.2.1 Anthracycline based antitumour antibiotics

Anthracyclines have shown good efficiency against cancer and are routinely used in the treatment of several types of cancer such as ovarian, breast, lung, thyroid, multiple myelomas, Hodgkin's and non-Hodgkin's lymphomas and soft tissue sarcomas³²⁶. They are highly conjugated rigid structures all containing four six membered rings fused together linearly. They all contain a sugar moiety and are highly oxygenated and contain a net positive charge at physiological pH, Dox (**36**) is a common example of these compounds.

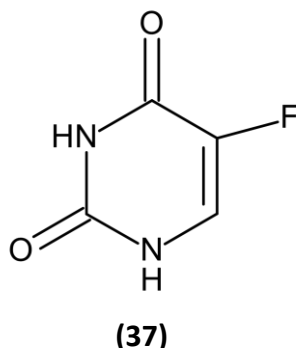


Many mechanisms of action are suggested for the cytotoxic activity of these compounds. Firstly they act by inhibiting the enzyme, topoisomerase II, which is responsible for DNA replication³²⁷. Anthracyclines have also the ability to intercalate between DNA due to the planar lipophilic nature of the cyclic structure and form an adduct independent of topoisomerase II activity leading to further cell death. Finally, it has been shown that anthracyclines can cause oxidative stress and ceramide over production leading to further cytotoxic effects³¹⁶. As these mechanisms of action are not competitive then can act synergistically and it is hypothesised that all these actions make them very effective cytotoxic agents, however, it also increases their non-selectivity and cytotoxicity against healthy cells. Dox was one of the first anthracycline compounds to be described and has a very high cardiotoxicity leading to cardiomyopathy and congestive heart failure which is attributed to the oxidative stress produced due to myocardial production of reactive oxygen and susceptibility of the heart to anthracyclines³²⁸. Other anthracycline compounds include Daunorubicin, Epirubicin and Idarubicin.

4.2.2 Antimetabolites

Antimetabolites such as 5-Fluorouracil (5-FU) (37) is an analogue of Uracil with Fluorine at the C-5 position. Fluoropyrimidines were developed in the 1950's after the observation that uracil, which forms one of the four bases of RNA, was taken up by rat

hepatoma more rapidly than healthy tissues indicating its usefulness for antimetabolite chemotherapy³²⁹.

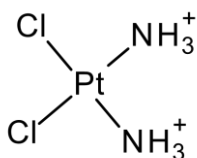


It is frequently used alone or in combination with LV and other anticancer agents for the treatment of a wide range of cancers such as breast cancer, stomach and digestive tract and oesophageal cancers³³⁰⁻³³². Antimetabolites act by inhibiting a compound or enzyme essential for the normal growth of a cell. The cytotoxicity of 5-FU is due to its ability to inhibit the enzyme thymidylate synthase which is the source of synthesis of thymidylate necessary for the replication and repair of DNA. The 5-FU metabolite FdUMP (Fluoro-deoxyuridine monophosphate) binds to thymidylate synthase thereby preventing its binding to the normal metabolite dUMP and thus inhibiting its ability to form thymidylate. Another metabolite of 5-FU, FUTP (fluorouridine triphosphate) incorporates itself into RNA thus disrupting normal RNA functioning and repair and post transcriptional conversion of uridine to pseudouridine thus inducing cell toxicity^{317, 333, 334}. All antimetabolite drugs act at a specific stage of cell cycle and disrupt normal DNA and RNA function. Other antimetabolite agents include methotrexate and gemcitabine.

4.2.3 Alkylating agents

Alkylating agents act by forming covalent bonds with biological molecules such as DNA, RNA and proteins. To induce chemotherapeutic action, they bond with nitrogen at the 7th position of guanine in DNA and also form bonds with other carboxyl, sulfhydryl

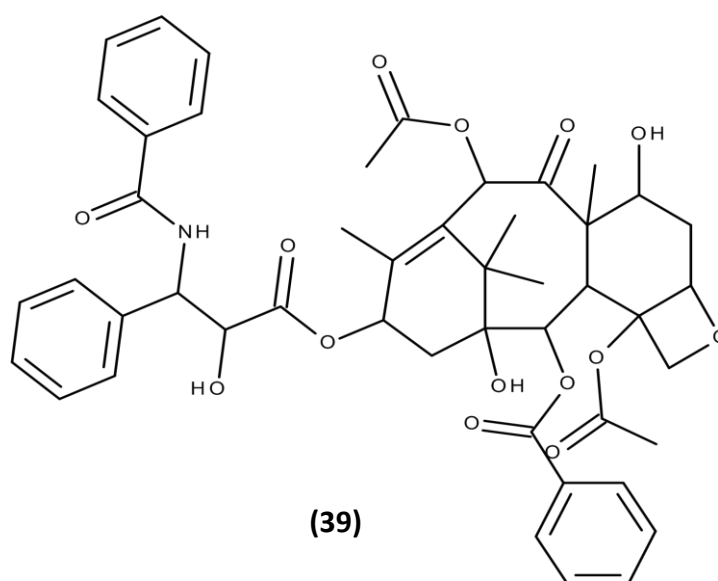
and phosphate groups and are effective at any stage of the cell cycle³³⁵. Different types of alkylating agents include nitrogen mustards such as cyclophosphamide and melphalan, nitrosoureas such as carmustin and streptozosin, aziridines such as mitomycin and platinum derivatives such as cisplatin **(38)**, carboplatin and oxaliplatin^{336, 337}.



(38)

4.2.4 Microtubule disruptors

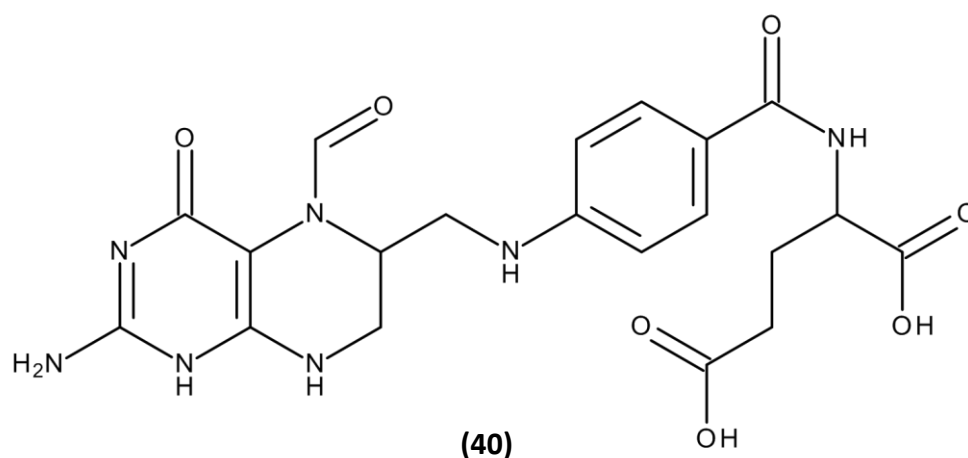
Microtubule disruptors exhibit anticancer activity by disrupting normal polymerisation of microtubules, affecting mitosis leading to inhibition of cell proliferation and thus inducing apoptosis³³⁸. Vinca alkaloids and taxane derivatives such as paclitaxel **(39)** are microtubule inhibitors. Vinca alkaloids prevent the formation of microtubules whereas paclitaxel prevent microtubule disassembly by polymerisation thereby affecting normal cell cycle³¹⁸.



(39)

4.2.5 Nontoxic compounds included within chemotherapeutic regimens

In addition to the cancer reducing compounds included within chemotherapeutic regimes, there are a small amount of other compounds included to either reduce the side effects, such as peripheral neuropathy, hair loss and anaemia, for example the use of multivitamins as neuroprotective agents for taxane induced neuropathy^{339, 340} or enhance the efficacy of the cancer killing drugs, for example leucovorin calcium (LV) **(40)** combined with 5 Fluorouracil.



LV is also known as Folinic acid and is a 5-formyl derivative of tetrahydrofolic acid and converts to folic acid derivatives such as tetrahydrofolate having vitamin activity similar to folic acid. It generally occurs as calcium salt and is used for counteracting the toxic effects of methotrexate and enhance the activity of 5 fluorouracil. LV enhance the inhibition of thymidylase synthetase which is the key mechanism of action of 5-FU metabolite FdUMP. Clinical studies have suggested that LV can significantly enhance the therapeutic efficacy of 5-FU³⁴¹⁻³⁴⁴.

4.3 Multidrug combinations for anticancer therapy

The first combination chemotherapy was introduced towards the end of 1960s with the clinical success of VAMP (Vincristine, amethopterin, 6-mercaptopurine, and prednisone) following the discovery of activity of Vinca Alkaloids by Elle Lily Company in 1963 for the treatment of acute lymphocytic leukemia (L1210) in children^{345, 346}. Since then, many chemotherapeutic drugs showing synergistic action have been used in combination to enhance cytotoxic effects³⁴⁷. Furthermore, combination chemotherapy using multiple anticancer agents injected either simultaneously or sequentially have also proved effective against MDR cancers employing drugs having different molecular pathways or drugs having similar molecular pathways leading to a synergistic or additive action^{348, 349}. For example, Lilenbaum *et al.* compared the efficacy of injecting Paclitaxel alone or in combination with carboplatin in 561 patients with advanced non-small cell lung cancer. The response rate was 17% in patients receiving paclitaxel alone with 2.5 months failure free survival, whereas patients receiving Paclitaxel with Carboplatin had a 30% response rate with 4.6 months failure free survival³⁵⁰. Carrick *et al.* compared single agent vs multiple agent treatment for metastatic breast cancer in 9742 women involving 43 clinical trials. They found that combination therapy showed statistically significant advantage in survival rate, response rates and time to progression than single agent therapy however the women with combination therapy experienced increased toxic effects in terms of alopecia, nausea, vomiting and white cell count. Thus indicating the possibility of sequential treatment with single agents than simultaneous combination therapy³⁵¹. Many combination therapy regimens are used clinically are shown in Table 4-1³⁵².

Table 4-1 Clinically used combination drug regimens

Abbreviation	Composition	Type of cancer
BEAM	Carmustine, Etoposide, Cytarabine, Melphalan	Hodgkin's and non-Hodgkin's lymphoma
BEP	Bleomycin, Etoposide, Cisplatin	Testicular cancer
CMF	Cyclophosphamide, methotrexate, 5-fluorouracil	Breast cancer
CTD	cyclophosphamide, thalidomide, dexamethasone,	Myeloma
CAV	Cyclophosphamide, Doxorubicin, Vincristine	Small cell lung cancer
ECF	Epirubicin, Cisplatin, 5-Fluorouracil	Oesophagus and stomach cancer
FOLFIRINOX	Folinic acid, 5-FU, Irinotecan, Oxaliplatin	Pancreatic cancer
FOLFIRI	Folinic acid, 5-FU, Irinotecan	Bowel cancer
FOLFOX	Folinic acid, 5-FU, Oxaliplatin	Bowel cancer
GemCap	Gemcitabine, Capecitabine.	Pancreatic cancer
TAC	Docetaxel, doxorubicin, cyclophosphamide	Breast cancer

4.4 Nanoparticulate drug delivery for cancer therapy

Nanotechnology provides an alternative delivery mechanism to conventional chemotherapy and offers several approaches to overcome its limitations. Specifically, NPs offer the fundamental advantage of tumour targeting by enhanced accumulation in tumour cells via the EPR effect. This in turn enhances their efficacy and reduces unwanted side effects^{353, 354}. Furthermore, the ability to design NP carrier systems as per their application and their multi-functionality makes them ideal for cancer therapy as active targeting through selective molecular recognition can be achieved. The

surface modifications of NPs can allow them longer circulation times by minimizing uptake from the RES improving their efficacy^{355, 356} and the ability to attached high affinity targeting ligands. NPs can not only carry large therapeutic payloads but can also accommodate multiple drugs with different solubility profiles³⁵⁷. A variety of NPs, made of different materials, such as chitosan²⁴⁵, polycaprolactone¹²⁴, poly (lactic-co-glycolic acid)³⁵⁸, liposomes^{359, 360}, micelles^{361, 362} and dendrimers^{363, 364} are currently being investigated. These NPs involve different mechanisms of action such as active and passive targeting and triggered release.

4.5 Liposomes in multi-drug anticancer therapy

There has been a dramatic rise in the past decade in novel therapies for delivery of therapeutic agents for cancer therapy. The commercialization of Dox liposomes (Doxil®) in 1996 has led to exploration in various areas of cancer chemotherapy involving encapsulation of anticancer drugs in liposomes^{365, 366}. Liposomes have been used as drug delivery vehicles for many anticancer agents such as anthracyclines^{54, 367, 368}, platinum compounds³⁶⁹, antimetabolites³⁷⁰ and Vinca alkaloids³⁷¹⁻³⁷³ aiming to reduce their side effects without affecting their efficacy. Liposomes take advantage of the Enhanced Permeability and Retention (EPR) effects of the tumour vasculature as described in chapter 1^{184, 374}. Co-encapsulation of multiple drugs in liposomes has shown to provide synergistic action increasing their efficacy. For example, Jie Meng *et al.* co-encapsulated resveratrol and paclitaxel in phosphatidylcholine and DSPE-PEG2000 liposomes for MDR reversal in breast cancer cells³⁷⁵. Walls *et al.* co-encapsulated Dox with Listeriolysin O to achieve synergistic effect against ovarian cancer cell line A2780 and Dox resistant ovarian cancer cell line³⁷⁶. Camacho *et al.* encapsulated Dox and 5-FU in zwitterionic and cationic liposomes and evaluated their therapeutic efficacy. They found that the synergistic ratios of the drugs caused up to 90% tumour reduction as compared to free drug solution in 4t1 mammary carcinomas and required doses far below the maximum tolerable doses of individual drugs³⁷⁷. Although there has been much evidence to suggest that liposomes have a great impact in improvement of existing chemotherapeutic treatments for cancer, they still have some problems such as low stability and shelf life and diffusion of drug across the liposomal membrane with time³⁷⁸.

4.6 Polymersomes in multidrug anticancer therapy

The limitations of liposomal delivery systems have led to a shift in focus towards more synthetic alternatives. Discher *et al.* demonstrated in the late 1990s, the ability of diblock copolymers to assemble into bilayer vesicles termed polymersomes^{87, 379}. Polymersomes provide a unique advantage to cancer drug delivery combining the advantages of bilayer forming liposomes and providing more stability to the formulations because of their synthetic nature^{380, 381}. They can be designed to be biodegradable and biocompatible along with the addition of any other desirable properties simply by modifying the core polymer blocks^{175, 382}. The large molecular weights of polymers used for these structures and their versatility in incorporating different functional groups into the polymer backbone gives them attributes which can significantly improve their membrane properties such as permeability, thickness and robustness³⁸³. Similar to liposomes, polymersomes have the ability to encapsulate both hydrophilic and hydrophobic compounds, however owing to the larger size of the hydrophilic cores³⁸⁴ and thicker hydrophobic bilayer (3-5 nm in liposomes and 3-30 nm in polymersomes)¹⁵², the amount of drug that can be incorporated is greater. Polymersomes encapsulating multiple anticancer drugs have been explored recently because of the advantages of multi drug therapy compared to single drug^{385, 386}. Combination anticancer therapy using 5-FU and Dox loaded in NPs such as dendritic nanomicelles³⁸⁷, polymer drug conjugated NPs³⁸⁸ and nanocomplexes³⁸⁹ have revealed their synergistic action against different types of cancer.

Ahmed *et al.* simultaneously encapsulated Dox and paclitaxel in PEG-PLA and PEG-PBD diblock copolymers based polymersomes and observed up to 50% reduction in tumour volume and higher maximum tolerated dose in polymersomes treated groups as compared to free drug solution in human breast xenograft mouse model²¹⁴. Colley *et al.* also coencapsulated Dox and Paclitaxel, however here they included a pH sensitive PMPC-PDPA polymersomes for enhanced anticancer activity against head and neck squamous cancer cells²⁵⁰. Kim *et al.* coencapsulated siRNA with Dox in mPEG-b-PLA block copolymer polymersomes for combination chemotherapy in human gastric cancer cell lines and observed better cytotoxic effects at lower doses³⁹⁰. Thus, polymersomes can prove to be valuable tools for the co-delivery of multi drugs which

is not only effective in treating resistant and recurrent tumours but also improves patient compliance and tolerance. Future designs of multi-modal polymersomes can help extend their applicability to a large variety of drug delivery and imaging applications²².

4.7 Aims of Chapter

In this research work, we report the simultaneous encapsulation of three anticancer agents into random copolymer based polymersomes for enhanced activity against pancreatic cancer. We aim to encapsulate Dox, 5-FU and LV simultaneously in the same polymersome. The presence of three drugs in the same polymersomes has potential for synergistic therapeutic action with enhanced retention in the tumour tissue. The polymersomes will be observed for their anticancer effect in ectopic pancreatic BxPC-3 tumours in mice after intratumoral and intravenous injection. The schematic representation of the drug loaded polymersomes and intended *in-vivo* studies is depicted in Figure 4-1.

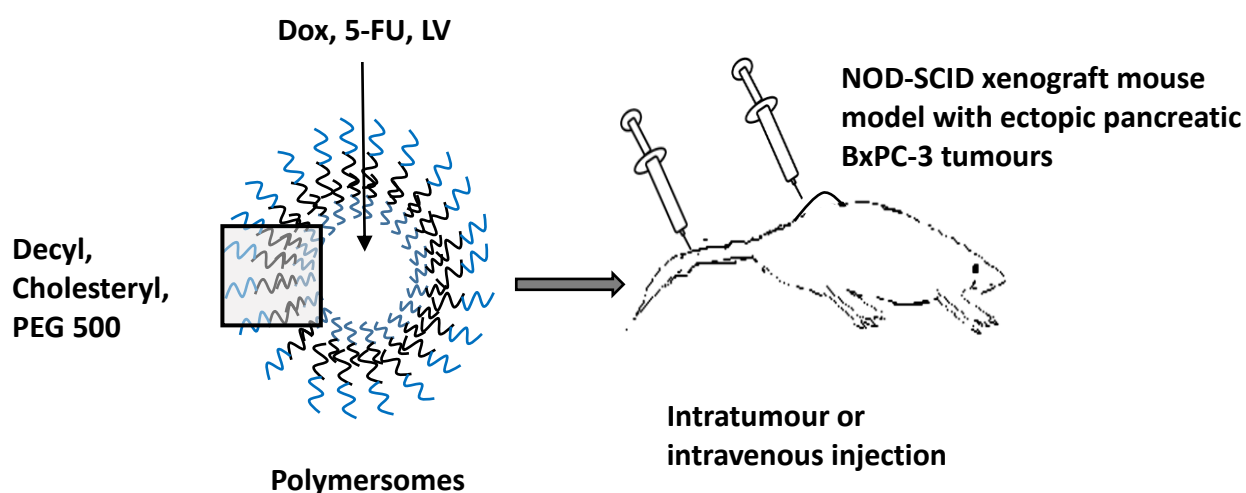


Figure 4-1 Schematic representation of multi drug loaded polymersomes and *in-vivo* mouse model

Thus, the encapsulation of multiple polymersomes and observation of their activity *in-vivo* forms the overall aim of the chapter. The specific objectives are,

1. Preparation of polymersomes loaded with Dox, 5-FU and LV within the same polymersomes and analysing their encapsulation efficiency, particle size, PDI, Zeta potential and *in-vitro* drug release.
2. Cytotoxicity of BxPC-3 cells treated with individual and combination drug solution and their comparison with combination drug loaded and blank polymersomes.
3. Observation of *in-vivo* pharmacokinetics of fluorescently labelled polymersomes in NOD-SCID mice for 24 hours using an *In-vivo* Imaging Systems (IVIS).
4. Observation of anti-tumour activity of combination drugs loaded polymersomes after intra-tumoral injection in mice and comparison with combination free drug solutions and blank polymersomes for a specified time period
5. Observation of anti-tumour activity of combination drugs loaded polymersomes after intravenous injection in mice and comparison with combination free drug solutions for a specified time period.

4.8 Results and Discussion

4.8.1 Preparation and characterisation of polymersomes

The amphiphilic random copolymer used for the preparation of polymersomes was composed of three components, two hydrophobic components comprising of a decyl (C10) chain, and cholesterol as well as a hydrophilic component, poly (ethylene) glycol (PEG) with an average molecular weight of 500Da. The polymerisation was achieved by free radical polymerisation using AICN as the initiator. The molar ratios of each component are detailed in Table 4-2 and the schematic illustration of the amphiphilic copolymer is represented in Figure 4-2. As the polymer formed is a random copolymer the exact positioning of each monomer relative to each other is not guaranteed, however on formation of the polymersome, due to the amphiphilic nature of the components the PEG 500 forms the hydrophilic inner core and outer corona of the polymersome whereas the cholesterol and decyl chain form the hydrophobic bilayer of the polymersomes.

Table 4-2 Ratios of monomers used for the synthesis of amphiphilic copolymer 41

Monomer	MW (Da)	Molar Ratio	% (mol)
PEG methacrylate (27)	500	5	75
Cholesteryl methacrylate (21)	540	0.75	9
Decyl methacrylate (33)	226	2.25	0.11
AICN	244	0.3	4.5

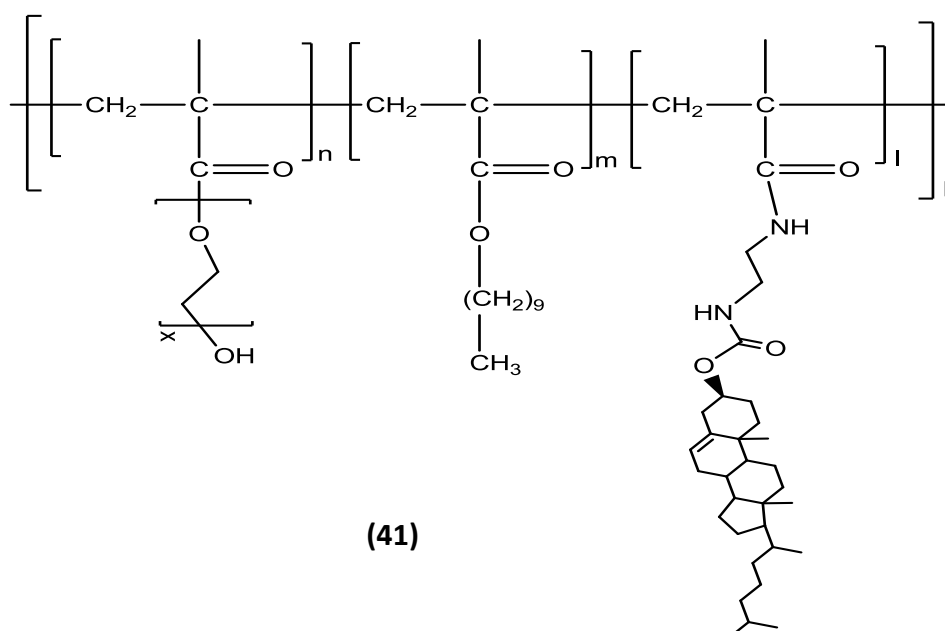


Figure 4-2 Schematic diagram of amphiphilic copolymer 41

Multiple drug loaded polymersomes were prepared by reverse phase evaporation method as discussed in section 6.5.1 with all the three drugs being encapsulated into the aqueous core because of their water-soluble properties. Dox is a red, crystalline solid generally available as a hydrochloride salt which is soluble in water and aqueous alcohols³⁹¹. Dox is administered intravenously at 60-75mg/m² single or divided doses on 2-3 consecutive days every 3 weeks or at 30-60mg/ m² for combination therapy³⁹². 5-FU occurs as a white crystalline powder which is soluble in water³⁹³. For pancreatic cancer, 5-FU is administered in combination with LV as a 400mg/m² bolus dose by IV

injection followed by 2400mg/m² continuous IV infusion over 46 hours at 2 weeks intervals³⁹⁴. LV occurs as a yellow coloured powder which is soluble in water³⁹⁵. It is available in tablet and injection form given as 200mg/m² slow IV injection followed by 5-FU for colorectal cancer³⁹⁶.

Table 4-3 Concentration of compound for *in-vitro* and *in-vivo* studies

Compound	Amount added for <i>in-vitro</i> and cell cytotoxicity studies	Amount added for <i>in-vivo</i> studies
Dox (36)	0.1-0.2mM	5mg/kg
5-FU (37)	4mM	20mg/kg
LV (40)	0.25mM	2.5mg/kg
Polymer (41)	2.5mg/mL	50mg/kg

Table 4-3 displays the concentrations of drugs loaded in polymersomes for *in-vitro* studies and cell toxicity studies. These concentrations were then further optimised for *in-vivo* studies to match the therapeutic concentrations of the drugs. The polymersomes were observed to have similar particle size and PDI across both the concentration ranges. The hydrodynamic size measurement of the combination drugs loaded polymersomes was 132.9±35.5nm with a PDI of 0.4±0.1 indicating particles uniform particles of small size and having zeta potential of 2.7±1.2mV. This small zeta potential is attributed to the neutral charge of the polymer. 5-FU intravenous injections are formulated as alkaline solutions using Sodium Hydroxide, but Dox degrades in alkaline solutions because of its acidic nature. Owing to these physical incompatibilities, 5-FU and Dox solutions are not mixed together³⁹⁷. The simultaneous encapsulation of 5-FU, Dox and LV eliminates their solution incompatibilities and allows their simultaneous administration with enhanced therapeutic effect. The ability to encapsulate multiple drugs into a single nanovehicle highlights the benefit of this platform for drug delivery. The large aqueous core of the polymersomes allows the simultaneous encapsulation of the three drugs with good encapsulation efficiency while still maintaining the small vesicle size and PDI³⁹⁸. The encapsulation efficiency of

the drugs was determined by the centrifugal filtration of polymersomes and analysing the filtrate, as described in detail in section 6.2.9. The encapsulation efficiency of the drugs Dox was $81.5 \pm 5.5\%$, 5-FU was 74.5 ± 20.1 and LV was found to be $72.1 \pm 0.7\%$ in agreement with those reported in literature. Kalra *et al.* evaluated the simultaneous encapsulation of Dox and 5-FU in pegylated cationic liposomes prepared by thin film evaporation method and found that there was more than 90% encapsulation of both drugs and particle size of approximately 200-240nm in the liposomes at various (3,5,10 & 20) molar % drug loaded preparations³⁹⁹. In another example, Chao *et al.* prepared mPEG-b-PCL polymersomes with Dox using thin film hydration method and observed encapsulation efficiency of up to 65% with very small particle sizes of up to 60nm⁴⁰⁰ giving further evidence of the comparability of this method of encapsulation within the polymersome. *In-vitro* release studies were conducted by placing polymersomes in semipermeable dialysis membrane in PBS and stirring at 37°C for fixed intervals of time, the results of which are displayed in Figure 4-3.

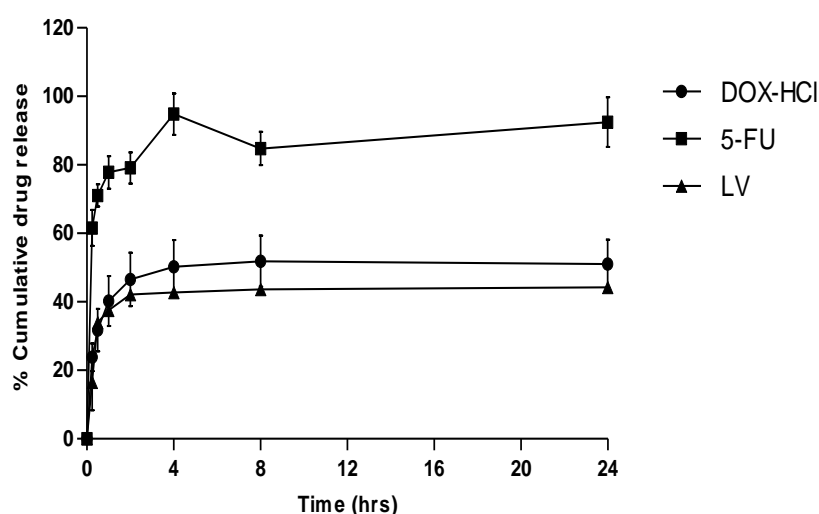


Figure 4-3 In-vitro release profiles of Dox, 5-FU and LV in multi drug loaded polymersomes at 37°C in PBS. N=3 represented as average \pm SEM.

It was found that polymersomes demonstrated a burst effect and had a fast release of drugs with more than $84.7 \pm 4.8\%$ of 5-FU released within 8 hours, whereas $51.8 \pm 7.4\%$ Dox and $43.6 \pm 0.2\%$ LV was released after 8 hours of initiation of study. Almost all of 5-FU $92.4 \pm 7.2\%$ was released after 24 hours however, release of Dox and LV remained

constant at 51.0 ± 7.0 and $44.2 \pm 1.2\%$ respectively after 24 hours indicating no further release. Hence, even though the release of Dox and LV was fast initially, it remained steady to roughly around 50% over 24 hours. Thus, the amphiphilic copolymer polymersomes were small in size with good encapsulation of multiple drugs and capable of immediate release of encapsulated cargo into the surrounding environment.

4.8.2 Cell viability studies

To evaluate the synergistic action of the combination drugs, free solutions of 5-FU, LV and Dox were compared to their combination free solution and combination drugs loaded in polymersomes at concentrations 5-FU (4mM), LV (0.25mM) and Dox (0.1mM) loaded onto BxPC-3 cells as described in section 6.5.2. As seen in Figure 4-4, the viability of individual drug solution treated cells were 91.7 ± 11.0 for Dox, $91.3 \pm 8.6\%$ for 5-FU and $107.7 \pm 7.0\%$ for LV indicating only limited toxicity at the above mentioned concentrations. When the same cells were subjected to the combination solution toxicity was higher with $74.9 \pm 6.6\%$ viable cells, showing a synergistic action with approx. 25% cytotoxicity. The toxicity was greatly enhanced when the same concentrations were combined within polymersomes, they displayed ~65% cell toxicity with only $36.5 \pm 3.6\%$ live cells. The observation of toxicity of blank polymersomes shows that they were biocompatible with 83.50% viable cells after treatment so could not have accounted for this dramatic increase in cytotoxicity. Thus further proving the better uptake and cell death of polymersomes loaded drugs.

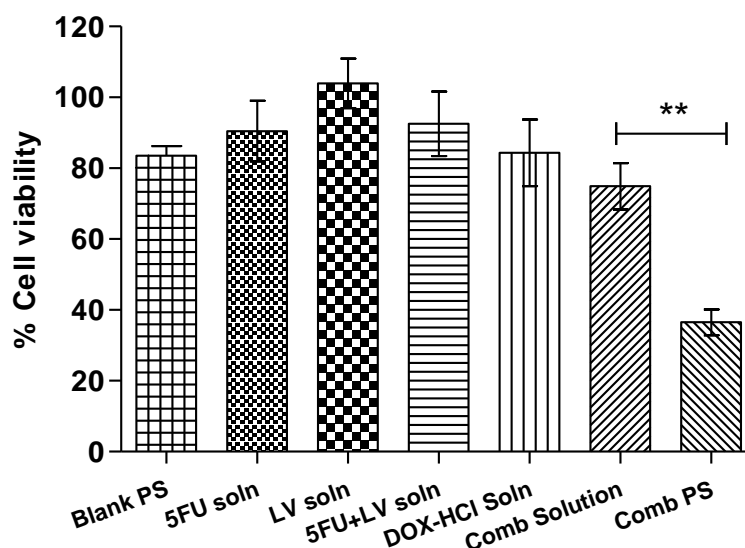


Figure 4-4 Viability of BxPC-3 cells after treatment for 22 hours with 5-FU (4mM), LV (0.25mM), Dox (0.1mM) individual and combination solutions and combination polymersomes at same concentration showing synergistic action. N=3 represented as average \pm SEM. ** indicates $p<0.01$.

In an attempt to further increase the cytotoxicity, the concentration of Dox was doubled to 0.2mM while keeping the other drug and polymersome concentrations the same, the results of which are displayed in Figure 4-5. At this concentration, no synergistic effect was observed for the combined solutions as the free solution of Dox at 0.2mM had similar cell viability to that of the combination solution of Dox with 5-FU and LV. As would be expected the toxicity of both the free Dox and the combination solution was higher with the increased concentration of Dox. The toxicity of combination drug loaded polymersomes with increased Dox (0.2mM) was also enhanced with only $17.0 \pm 1.0\%$ viable cells showing approx. 83% cytotoxicity after 24 hours which is significantly higher than combination free drug solution at the same concentration.

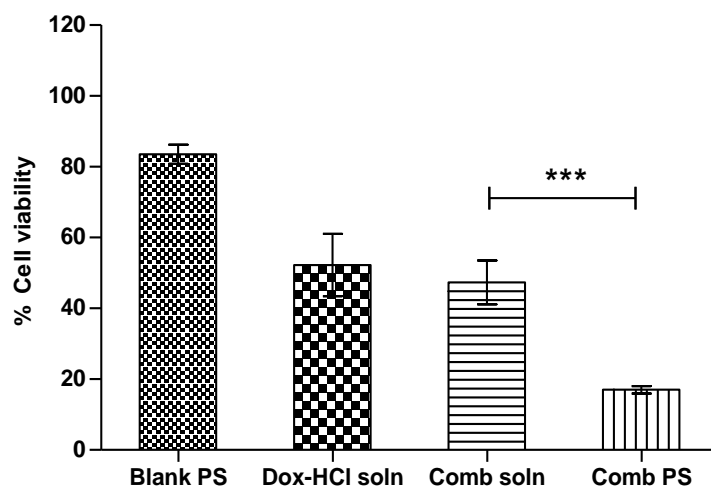


Figure 4-5 Cell viability after treatment with 5-FU (4mM), LV (0.25mM), Dox (0.2mM) combination free solution and polymersomes loaded drugs and individual Dox solution (0.2mM) showing enhanced cytotoxicity. N=3 represented as average \pm SEM. * indicates $p < 0.001$**

4.8.3 *In-vivo* pharmacokinetics of polymersomes

In order to ascertain the behaviour of these polymersomes *in-vivo* we employed polymersomes loaded with Indocyanine green (ICG) (**12**). ICG is a near infrared dye, commonly used for *in-vivo* imaging because of its water solubility, easy loading into NPs, good tissue penetration and reduced light scattering^{401, 402}. Although the method is semi quantitative, it provides the advantage of real time kinetics of polymersomes pathway in the body. Polymersomes loaded with **12** (0.2mg/mL) were injected into the tail vein of mice previously implanted with ectopic BxPC-3 tumour to observe the *in-vivo* kinetics of the polymersomes in real time. As seen from Figure 4-6, the fluorescence after initial injection shows that polymersomes containing the fluorophore **12** were immediately accumulated in the tumour in high amounts. This high accumulation is shown by the bright fluorescence in the tumour area, however some polymersomes also distributed to other parts of the body. The polymersomes in peripheral circulation slowly started to dissipate with a significant amount of polymersomes were retained in the tumour tissue and were seen ever after 22 hours of administration.

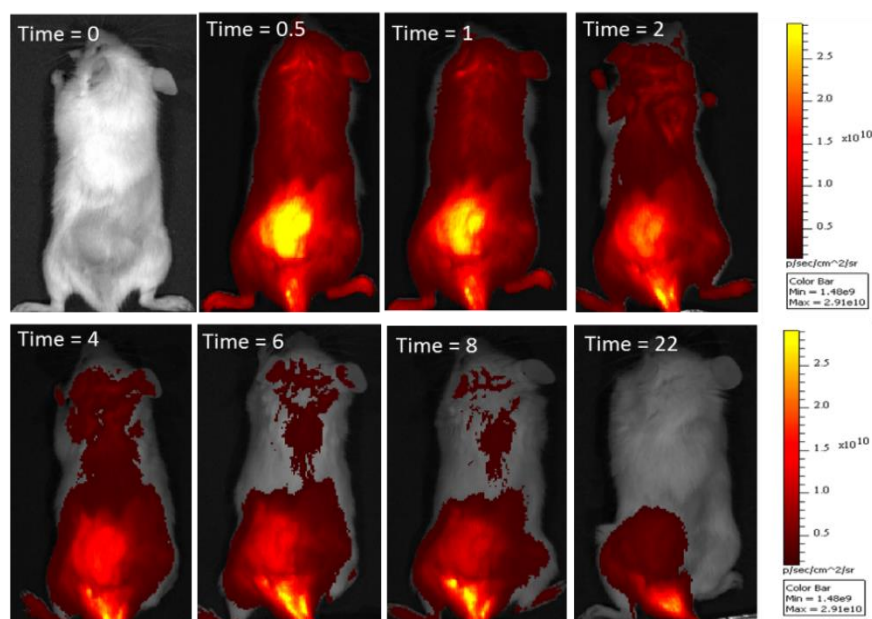


Figure 4-6 In-vivo kinetics of ICG loaded polymersomes at various time intervals showing preferential accumulation in tumour.

The plot of tumour fluorescence expressed as a ratio with respect to the fluorescence of peripheral tissues indicates a 6-fold accumulation of polymersomes in the tumour after 8 hours as compared to systemic circulation which only decreased slightly after 22 hours (Figure 4-7).

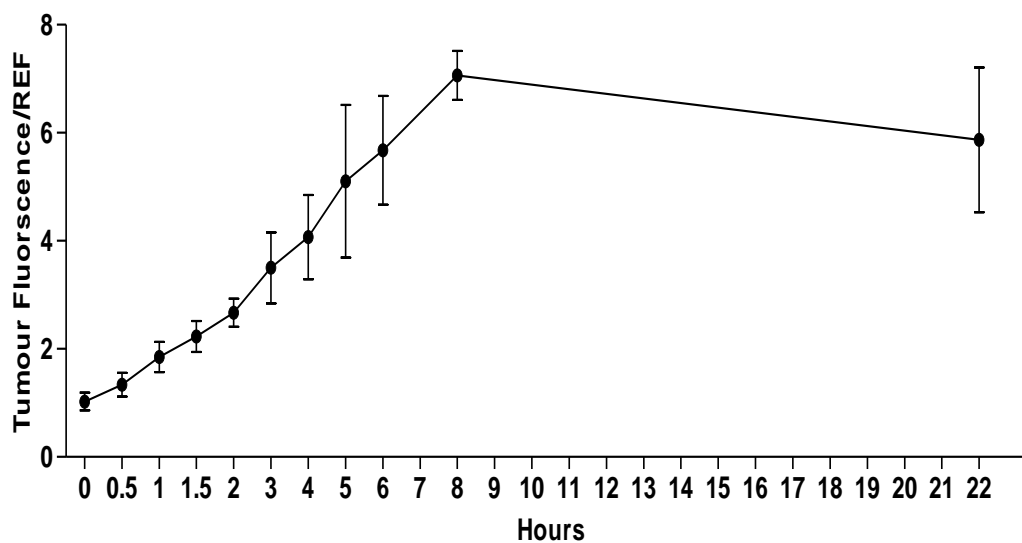


Figure 4-7 Plot of tumour fluorescence with respect to peripheral tissue fluorescence, N=2 represented as average \pm SEM.

This leads to the conclusion that the elimination of polymersomes from the body is slower than the free dye, most likely due to the presence of PEG in the polymer which allows longer circulation times and thus can increase the efficacy of the encapsulated drugs. In order to further confirm the accumulation of polymersomes in tumour and determine their tissue distribution, the mouse was dissected and individual organs were collected for fluorescence observation. Figure 4-8 shows the individual excised organs with the fluorescence emission from each quantified and compared to a blank. It was seen that there was large accumulation of polymersomes in the tumour, however a significant amount was also seen in the liver. This would indicate that polymersomes are mainly accumulated in the liver and tumour. Elimination is mainly through the liver with a small amount being eliminated by the kidneys however no fluorescence was observed in the bladder indicating the possibility of a slow excretion by the kidney. However, Figure 4-9 displays the fluorescence emission seen from the faeces of the mouse before and after injection with polymersome containing **12**, further confirming excretion through the liver.

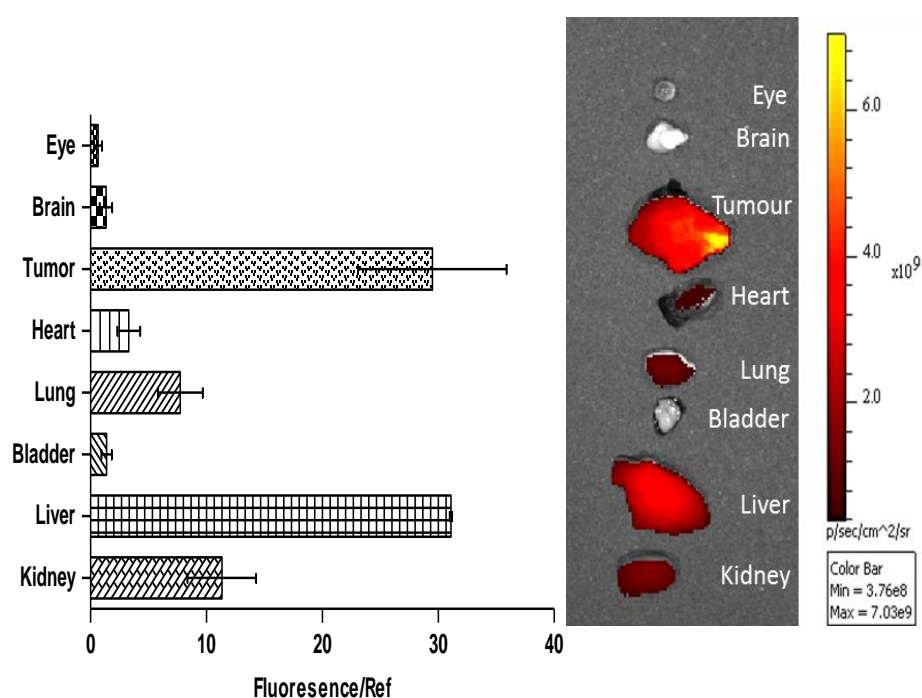


Figure 4-8 Observation of fluorescence in organs obtained from sacrificing the mice after 22 hours pharmacokinetic study. N=2 represented as average \pm SEM.

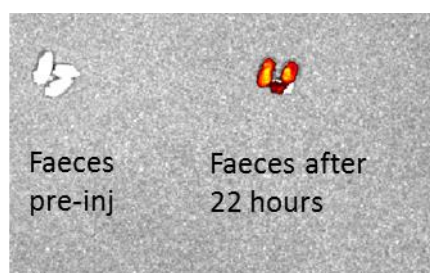


Figure 4-9 Faeces of mouse with fluorescence emission pre injection and 22 hours following injection with polymersome containing 12.

This is in agreement with previous studies carried out by Photos *et al.* and Fei Lu *et al.* They demonstrated that PEG based polymersomes were mainly eliminated by the liver followed by the spleen with a small amount being eliminated by the kidneys^{174, 403}. This observation of tumour accumulation properties of polymersomes provided an insight into their preferential uptake into tumours and formed the basis of further *in-vivo* therapeutic study. In addition, the lack of accumulation in the heart was an encouraging indication for the potential use of NPs with cardio toxic compounds such as Dox.

4.8.4 *In-vivo* toxicity after Intratumoral injection

In the first efficacy study, the formulation was injected by intratumoral injection to eliminate any additional effects of tissue distribution. Intratumoral injection has been shown to improve tumour concentrations and tumour-organ ratios of injected drugs⁴⁰⁴. NOD-SCID mice were implanted with BxPC-3 tumours and allowed to reach an average volume 200-250mm³. Mice were intratumorally injected on Day 0 and Day 5 with combination drug loaded polymersomes, combination solution and compared to mice injected with blank polymersomes and those that received no treatment. Tumour volume was measured every day until the end of treatment at Day 13. Figure 4-10 shows the percent reduction in tumour growth of all the groups. The group treated with blank polymersomes had no effect on the tumour toxicity showing 160.2±21.6% increase in tumour volume from initial and having the same trend as the untreated group whose tumour volume increased by 173.5±42.0% after 13 days.

It was expected that the free drug solutions will provide good reduction in tumour volume since the concentrations of Dox, 5-FU and LV were at therapeutic doses. Indeed, the group treated with combination solution had a significant reduction in tumour growth with an increase of only $59.6 \pm 32.8\%$ tumour volume from the start of the experiment. However the group treated with combination drug loaded polymersomes had a maximum cytotoxic effect on the tumour showing a decrease of $2.3 \pm 20.4\%$ in the tumour volume after 13 days which is significantly higher than the percent increase of free solution and untreated group.

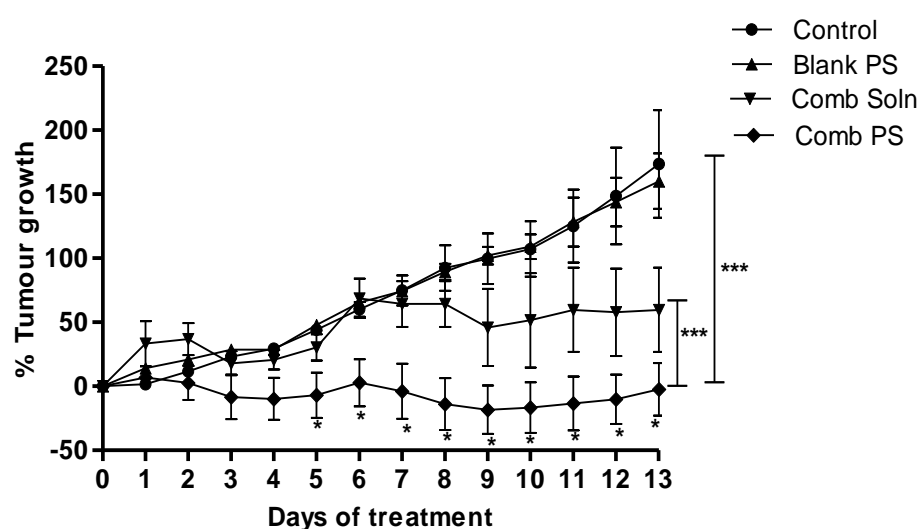


Figure 4-10 Graph of percentage increase in tumour growth after intratumoral injection of combination drugs loaded polymersomes and combination free drugs. N=3 represented as average \pm SEM, * indicates $p < 0.1$, * indicates $p < 0.001$**

It was interesting to note that there was a false increase in tumour volume for 2 days after intratumoral injections on Days 0 and 5 owing to retention in the tumour which slowly dissipated over 2 days as seen by the tumour volumes on Days 1 and 2 and consecutively on Days 6 and 7 of all the treated groups corresponding to treatment days. The false increase in tumour volume for free solution treated group was 30-40% whereas those treated with polymersomes was only 5-10%. This lesser increase in tumour volume can be indicative of better tumour distribution properties of polymersomes due to their nanoparticle size demonstrating EPR effect. The particulate nature of NPs allows them to diffuse through the interstitial space and lymphatic vessels of the tumour leading to homogeneous distribution throughout the

tumour tissue. Whereas intratumoural injection of free unencapsulated drug solution gets absorbed directly into the blood supply of the tumour resulting in non-homogeneous distribution⁴⁰⁵.

Throughout the duration of the study the body weights of the mice were regularly recorded and found to remain steady at $90 \pm 10\%$ throughout the experiment (Figure 4-11) indicating the mice were normal and the injected solutions were solely concentrated in the tumour region without any other systemic toxicity.

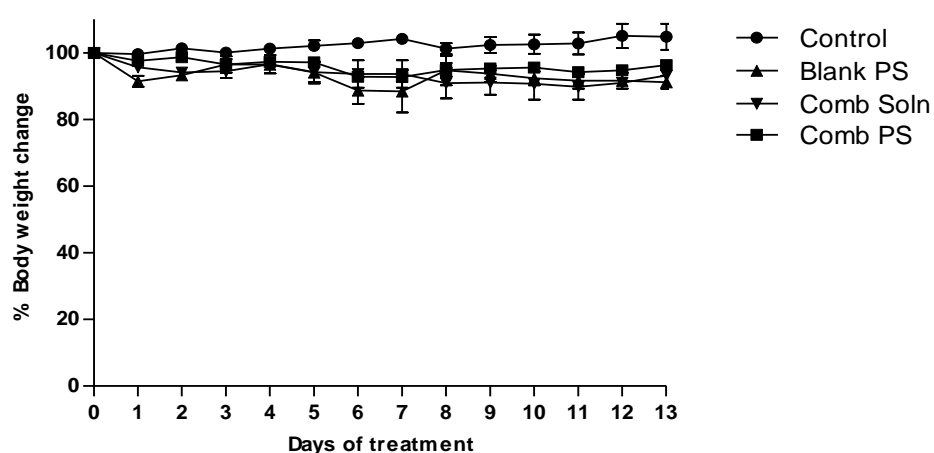


Figure 4-11 Graph showing percentage body weight change after intratumoral injection for each of the four groups over the 13 days duration of experiment.

After the completion of the study, mice were euthanized, their tumours were collected and weighed. Figure 4-12 displays a photo of each group containing both the mouse and the excised tumour. It can be clearly seen that the smallest tumour was excised following polymersomal treatment with the combination drugs, the next most effective treatment was from the free solutions with both the control and the blank polymersomes displaying the largest tumours after 13 days.

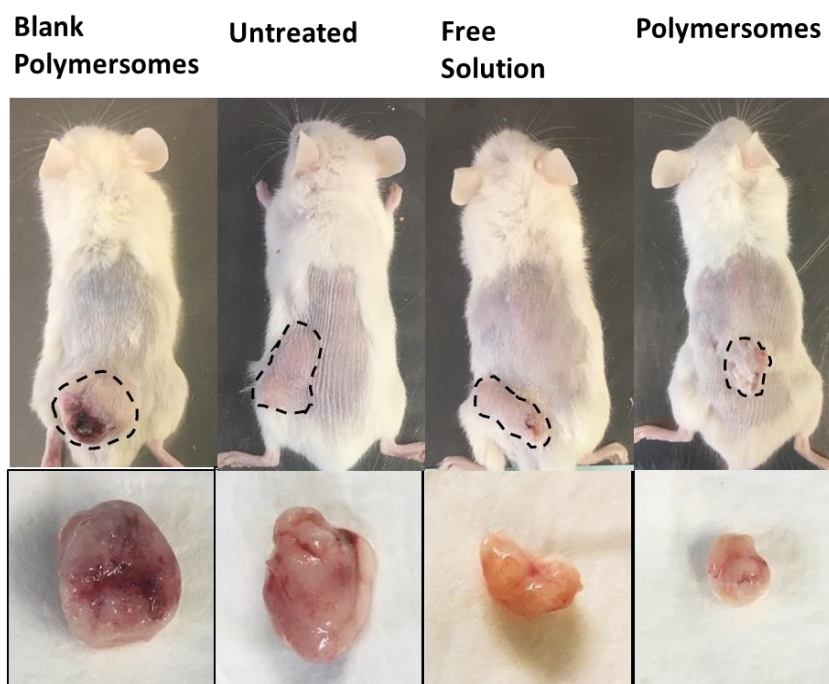


Figure 4-12 Photograph of one mouse from each group before tumour excision with the actual excised tumour below.

The percentage increase in tumour weight was calculated for each mouse with the results of each group displayed in Figure 4-13A. The control and blank polymersomes group show the largest increase in tumour weight of 173.6 ± 42.0 and $160.2 \pm 21.6\%$ increase in tumour weight after 13 days respectively, the combination solution group had $82.3 \pm 29.3\%$ increase from the initiation of treatment with the polymersome containing the three drugs showing a $2.37 \pm 20.4\%$ decrease in tumour weight, illustrating that not only did the combination solution prevent tumour growth, it also showed a slight decrease in tumour size. The calculation of tumour doubling times shows that it took 10.3 ± 1.20 days for the tumour volumes of the control group and 10.0 ± 1.4 days and 6 ± 2.8 days for blank polymersomes and combination solution treated group respectively to increase to double their size from the initial day of treatment (Figure 4-13B), however the rate of tumour growth for the polymersomes group was quite slow and it would take average 67.0 ± 22.0 days for the tumour volume to double in size.

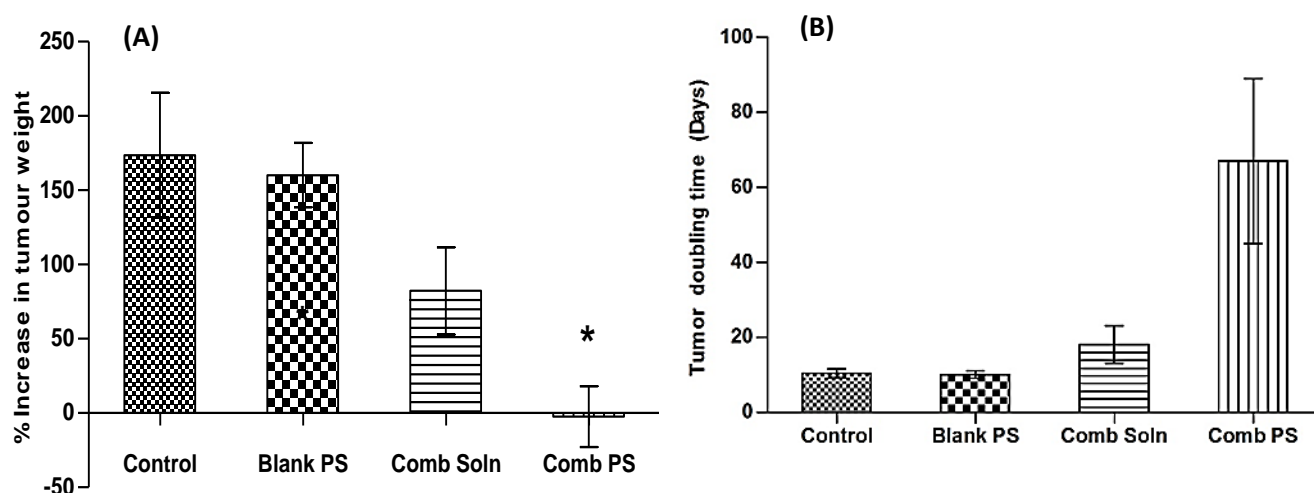


Figure 4-13 (A) Percentage increase in tumour weight after the study. (B) Estimated tumour doubling of different groups after intratumoral injection. N=3 represented as average \pm SEM, * indicates $p<0.1$.

4.8.5 *In-vivo* toxicity after Intravenous injection

The observation of enhanced retention of polymersomes in tumour tissue of **12** loaded polymersomes, provided the basis of the exploration of antitumor activity of multiple drugs loaded polymersomes by intravenous injection. Thus, Intravenous injection of combination drugs in solution and encapsulated in polymersomes formed the next part of the *in-vivo* studies. Similar to intratumoral study, mice with ectopic BxPC-3 tumours were divided randomly into groups receiving intravenous injection of combination drugs solution and other group receiving polymersomes loaded with combination drugs at the same concentration on Day 0 and Day 5 and compared to those that received no treatment. The graph of % tumour growth Figure 4-14 indicates a steady increase in tumour volume throughout the 7 days of treatment with the tumour volume increasing to $74.8\% \pm 11.8\%$ in the control group and an increase of $53.7\pm 11.2\%$ in the combination solution treatment group. Mice treated with combination polymersomes showed least increase in tumour volume with an increase of $40.1\%\pm 10.8\%$ from initial volume.

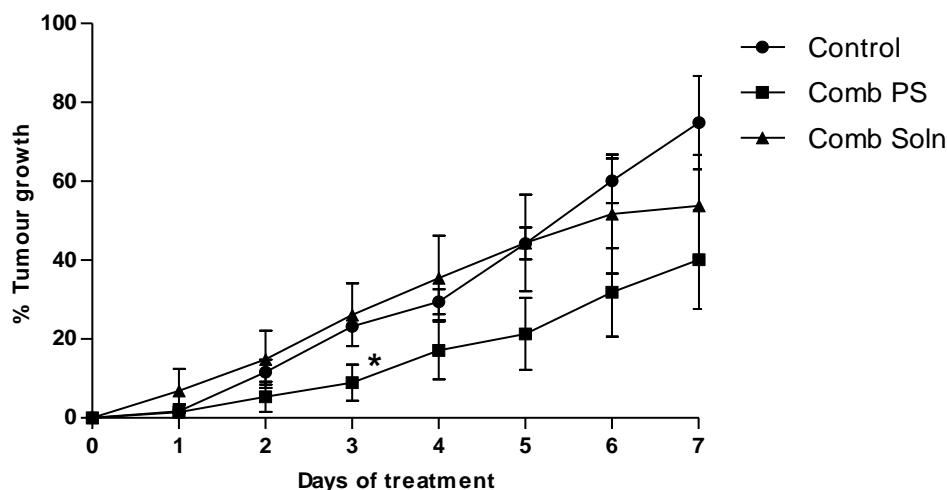


Figure 4-14 Percentage tumour growth of combination drug loaded polymersomes and combination free solution after intravenous injection. N=3 represented as average \pm SEM, * indicates $p<0.1$.

As with the previous study, the body weights of all mice were recorded on a regular basis. There was a drastic effect on the mice body weight as indicated in Figure 4-15. The mice treated with combination free drug solution showed a marked decrease in the body weight from the first day of treatment which potentiated after the second treatment and the weight of mice fell down to 80.0% \pm 4.01% from their initial weight indicating accumulated systemic toxicity and leading to the termination of the study on day 7. The mice were weary, distressed and unable to eat further causing the rapid weight loss. The mice in the untreated and polymersomes treated group were healthy with lesser change in their body weight.

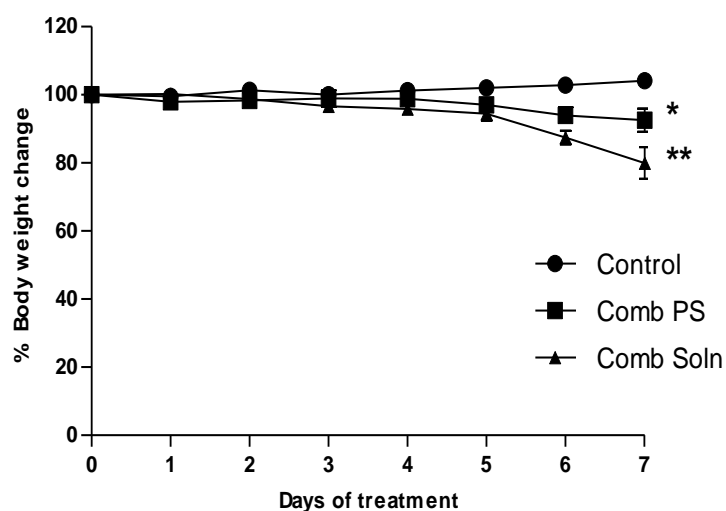


Figure 4-15 Graph showing percentage body weight change after intravenous injection for each of the three groups over the 7 days duration of experiment. N=3 represented as average \pm SEM, * indicates $p<0.1$, ** indicates $p<0.01$.

The rapid weight loss of mice treated with free solution of combination drugs is indicative of acute cardiotoxicity of Dox and toxic effects of combination drug solution at the concentration administered in mice. Dox has been reported to exhibit acute cardiomyopathy which is dose dependant leading to congestive heart failure at higher doses⁴⁰⁶⁻⁴⁰⁸. Other effects of anticancer drugs such as 5-FU and Dox include nausea, vomiting, poor appetite, alopecia and hematopoietic suppression^{409, 410}. Although cardiotoxicity of Dox remains the most feared side effect of chemotherapy, the encapsulation of Dox into liposomes and other NPs has helped reduce its cardiotoxicity, the most common example being the marketed pegylated liposomal Dox, Doxil®⁴¹¹⁻⁴¹³. The encapsulation of the combination drugs into polymersomes at the same concentration produced least toxic side effects in the mice indicating higher maximum tolerated dose.

Following the premature end of the experiment, all the mice were euthanized and their tumours and hearts were excised. Figure 4-16 displays a photograph of one mouse from each group with the corresponding excised tumour.

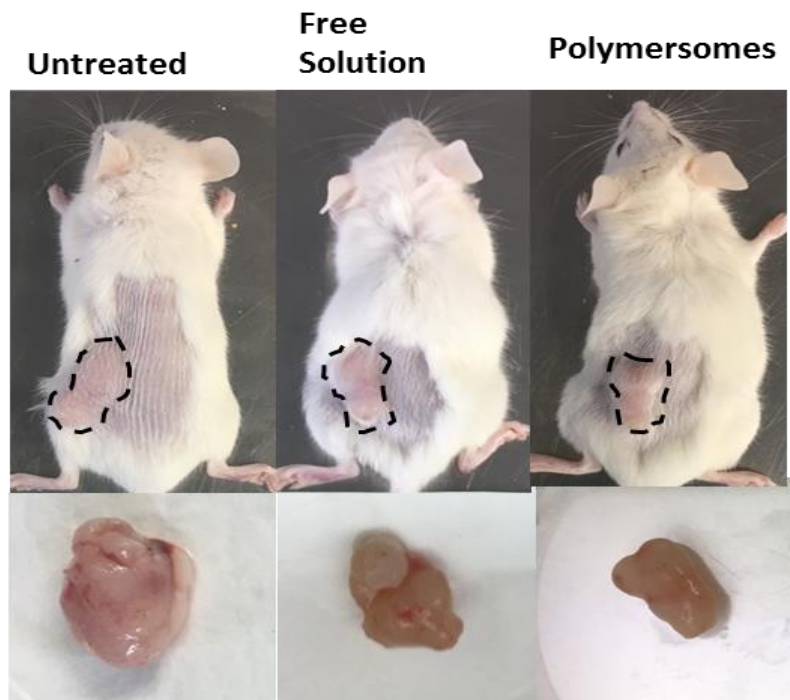


Figure 4-16 Photograph of one mouse from each group before tumour excision with the actual excised tumour below.

It can be seen from Figure 4-16, that the group treated with the combined polymersomal drugs displayed the largest reduction in tumour growth. This has been further quantified in Figure 4-17A which displays the % increase in tumour weight at the end of 7 days. It was found that the tumour weight of mice in the untreated group increased to $92.3 \pm 17.8\%$ of the initial, whereas those in the combination solution and polymersomes treated increased by $53.8 \pm 13.0\%$ and $40.1 \pm 12.5\%$ respectively. Further, the calculation of tumour doubling time indicates that it would take 10.3 ± 1.2 days and 14.7 ± 3.7 days for the untreated group and combination group tumours to double in size, however the polymersomes treated would take longer time of 21.3 ± 7.9 days to double in size (Figure 4-17B).

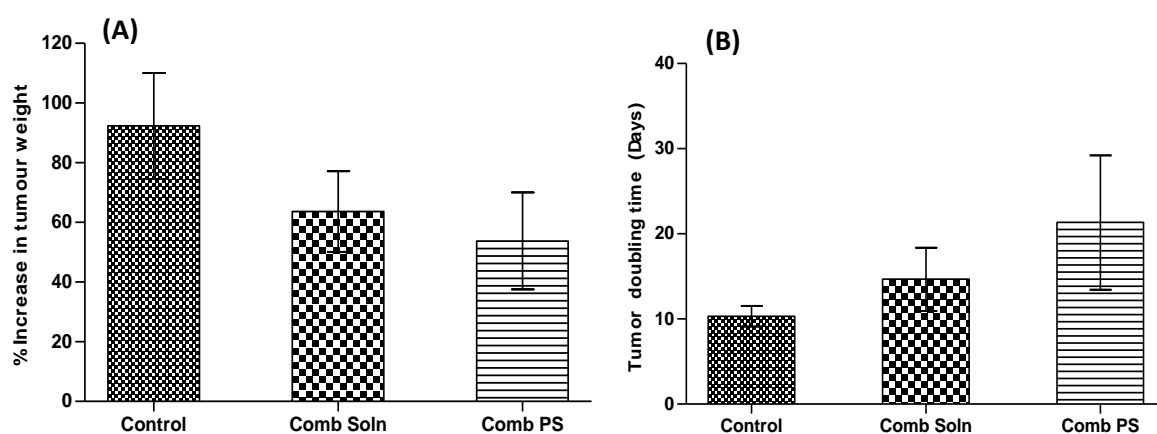


Figure 4-17 (A) Percentage increase in tumour weight after intravenous study. (B) Estimated tumour doubling time of combination polymersomes and combination free drug solutions. $N=3$ represented as average \pm SEM.

Further evaluation of systemic cardiotoxicity was carried out by the observation of the reduction in heart weights after the completion of the study (Figure 4-18). It was found that mice treated with combination solution showed an average heart weight of 0.088 ± 0.02 g which was lower than those of untreated and polymersomes treated groups having heart weights 0.12 ± 0.02 g and 0.10 ± 0.01 g respectively.

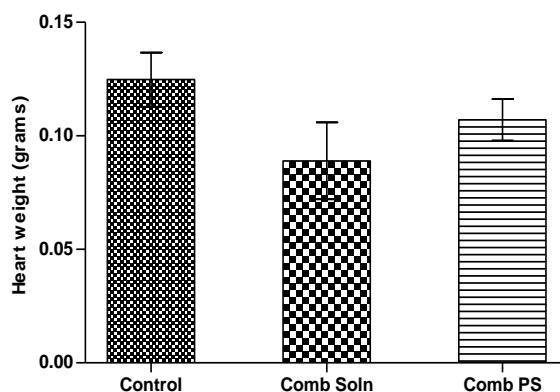


Figure 4-18 Average heart weight of each mouse in the three groups. N=3 represented as average \pm SEM.

Collectively, these observations demonstrate that we have prepared polymersomes having superior tumour toxicity against ectopic BxPC-3 tumours by encapsulation of multiple drugs as compared to combination free drug solutions at the same concentration.

4.9 Conclusion

Polymersomes are versatile drug delivery systems capable of encapsulating large extents of drug solutions proving ideal for multi drug delivery. Cancer chemotherapy using multiple drugs remains the foremost treatment strategy after surgery, for tumours that are hard to remove surgically and for multi drug resistant cancers. Even though liposomes are at the forefront of NP therapy for cancer, the problems associated with them provides the need for exploring other delivery vehicles. In this research work, we have demonstrated excellent anticancer activity of polymersomes made of random copolymers which are facile to synthesize and able to simultaneously encapsulate three drugs namely 5-FU, Dox and LV within the aqueous core at therapeutic concentrations having particle size $\sim 132\text{nm}$ and PDI of ~ 0.43 and good *in-vitro* release within 4 hours. Polymersomes loaded combination drugs have better cell cytotoxicity than corresponding free drug solutions. These polymersomes have shown to largely collect in the tumour tissue with up to 6 fold accumulation in tumour as compared to reference 8 hours after injection and were present in the tumour after 24 hours when observed after intravenous injection of fluorescently labelled

polymersomes. They have shown better efficacy and higher maximum tolerated dose than free combination drug solutions after intratumoral and intravenous administration in mice having ectopic pancreatic BxPC-3 cancer tumours. Intratumorally injected polymersomes exhibited an approximately 2% decrease in tumour volume after 13 days as compared to free drug solutions which showed an approx. 60% increase in tumour volume in the duration of the study. Free drug solutions demonstrated extreme cardiotoxicity and weight loss of the mice whereas no toxicity was observed for polymersome encapsulated drugs. A smaller 40% increase in tumour volume was observed for polymersomes when compared to average 53% increase shown by free solutions after 7 days of treatment. These results further prove the hypothesis that multi drug single carrier systems can provide better tumour cytotoxicity and better tolerance than free drug solutions and polymersomes can be exploited to achieve better efficacy.

Chapter 5

Overall conclusion

5.1 Conclusion

The work presented within this thesis demonstrates the prominence of amphiphilic random copolymers in the formulation of both single layered and bilayered systems for enhanced encapsulation of hydrophilic and hydrophobic molecules. These self-assembling polymeric systems analogous of liposomes, have been employed for various applications ranging from simple drug solubilising agents to multifunctional nanocarriers responsive to various stimuli, discussed in detail in Chapter 1.

In chapter 2, random copolymers having composition similarities to phosphatidylcholine with cholesterol and PEGs 500 and 2000 were designed to mimic structural similarities with conventional PEGylated liposomes. Correspondingly, monomers comprising of cholesteryl, oleic, octadecyl and PEG 500/2000 chains were integrated in specific molar ratios to form random copolymers by the freeze-thaw method using AICN as the free radical initiator. This is the first time that a random copolymer having composition resemblances to liposomes has been reported. Gaitzsch *et al.* discussed the ability of PEG based amphiphilic copolymers to form different types of morphological assemblies such as vesicles and micelles based on the hydrophilic fraction (f) of the fraction and its modulation over time at different temperatures⁴¹⁴. They found an increase in the hydrophobic block created complex aggregates whereas increasing the chain length of the hydrophilic block destabilised the vesicle structure. It was interesting to note that these random copolymers lack the zwitterionic choline head group of phosphatidylcholine²³⁶, rendering them of neutral charge as compared to highly anionic liposomes. The method of preparation played an important role in the size and PDI of these polymersomes with the reverse phase evaporation method providing the lowest particle size with high uniformity as compared to the corresponding liposomes. The percentage encapsulation efficiency was not affected by the method of preparation. Furthermore, the polymersomes were capable of encapsulating various charged fluorescent dyes namely, negatively charged FITC-CM-Dextran, positively charged FITC-DEAE-Dextran and neutral FITC-Dextran and hydrophobic anthracene without significantly affecting the size, encapsulation efficiency and zeta potential. These polymersomes were also found to have a fast *in-vitro* release of encapsulated cargo, hence proving further benefits as a DDS.

Alibolandi *et al.* compared the particle size, encapsulation efficiency and sustained release properties of PEG-PLA copolymers using PEG MW 2000 and 5000, comprising of hydrophilic fraction f value $\sim 25\%$ of the total polymer. Polymersomes were prepared by the thin film hydration method and it was found that polymersomes with PEG 2000 had a particle size of less than 100nm and low PDI⁴¹⁵. Our results indicated particle size of approximately 160nm which was smaller than the corresponding liposomes having particle size approximately 240nm when encapsulating hydrophilic dye.

The polymersomes were taken up by Hela cells mainly by clathrin mediated endocytic pathway and displayed better cellular uptake than liposomes. This is in agreement to research published by Swaminathan *et al.* who studied the effect of chemical inhibition of endocytosis using chlorpromazine on the cellular uptake of amphiphilic random copolymer micelles comprising of a decyl chain and PEG 500 loaded with Bodipy²⁷⁰. They found that after inhibition of endocytosis, the intracellular endocytosis was reduced, further confirming the prominently endocytic uptake mechanism of these polymersomes. The cytotoxicity of these polymersomes when observed in a cervical cancer cell line (HeLa cells), pancreatic cancer cell line (BxPC-3 cells) and non-cancerous cell line (CHO cells) indicated that these amphiphilic copolymers were biocompatible up to 0.25mg/ml concentration after which they significantly reduced the cell viability. However this cytotoxicity can prove advantageous for application in cancer drug delivery where the vehicle can enhance the cytotoxicity of the encapsulated therapeutic compound. A recent example of this kind of cytotoxic enhancement is the formulation of Paclitaxel in cremophore EL vehicle (Taxol®). Cremophore EL itself imparts cytotoxicity to some extent and also enhances the toxicity of the encapsulated paclitaxel through micellar encapsulation⁴¹⁶.

Stability of nanoparticle formulations has been studied extensively throughout the years to establish their efficacy for storage for prolonged periods of time and different temperature conditions. Lipids used for the preparation of liposomes being obtained from natural sources have the tendency for fungal growth over prolonged periods of storage and the susceptibility of lipids to temperature causes particle aggregation and leakage of encapsulated material over time^{266, 281}. Polymersomes loaded with

anthracene were observed to have lesser aggregation and better retention of encapsulated compounds upon storage for 8 weeks at 25°C when compared to liposomes at similar storage and temperature conditions.

The third chapter of this research thesis involved the preparation of a micellar drug delivery systems using amphiphilic copolymers and to employ them for the delivery of dynamic compounds capable of triggered delivery and molecular communication through the FRET mechanism. Micelles prepared from amphiphilic copolymers have been investigated for their potential to simultaneously deliver multiple compounds encapsulated within their core^{212, 213}. They have also been employed as multifunctional nanocarriers for combined delivery of therapeutic agent along with diagnostic/imaging application¹⁹⁷⁻¹⁹⁹. Park *et al.* developed multifunctional stimuli responsive micelles of phenylboronic acid-conjugated pluronic and lactose-modified chitosan Plu-CH, conjugated with spiropyran/boronic acid-conjugated poly(dimethylamino ethyl methacrylate-co-methacrylic acid) (S-PMA) which were responsive to acidic and higher redox environments and encapsulated hydrophobic paclitaxel within their core¹⁹⁶.

For this research, the micelles were made of an amphiphilic random copolymer comprising of a decyl chain attached to PEG 500. These micelles encapsulated the FRET pair compounds comprising of bodipy and either spiropyran alone or spiropyran attached to an API. The triggered ring opening of the hydrophobic spiropyran and its conversion to its hydrophilic merocyanine counterpart has been well established^{93, 305}. Furthermore, merocyanine was utilized to establish a FRET relationship between bodipy, which upon excitation by UV light transfers its energy to merocyanine resulting in a quenching of the bodipy emission. The FRET efficiency between bodipy and merocyanine was observed and it was found that they have optimum FRET efficiency at bodipy: spiropyran molar ratio 1:6. Hence all micelles were prepared encapsulating the compounds at this ratio. It was also established that full conversion of spiropyran to merocyanine took 5 minutes. Additionally, the FRET efficiency between bodipy and merocyanine in HeLa cells in light and dark conditions was determined.

The most interesting observation was the quantification of spiropyran conjugated API release communicated in real time indirectly through bodipy fluorescence. A good correlation between the increase of bodipy fluorescence and the absorbance of spiropyran was observed after subjecting the micelles to UV exposure leading to release of merocyanine from the system. The largest amount of release was observed by UV stimulation in dark conditions since polar merocyanine prefers dark conditions and reverts back to hydrophobic spiropyran in visible light conditions. This release of merocyanine observed by decrease in absorbance was communicated through increase in fluorescence emission of bodipy. The negligible release of merocyanine in the absence of a UV trigger was communicated as insignificant change in bodipy fluorescence thus proving the potential of this super smart drug delivery system. Tang *et al.* demonstrated the efficiency of FRET carbon nanodots (Cdots) coupled systems for real time monitoring of drug release at different pH. They established excellent FRET communication between the PEG and folic acid conjugated Cdots and Dox adsorbed onto the Cdot surface which was regulated by the release of drug molecule from the Cdot surface, further cementing the application of FRET systems for real time monitoring systems of drug delivery⁴¹⁷.

The final part of this research involved application of polymersomes to observe enhanced cytotoxic effects on ectopic pancreatic tumours in mice. Amphiphilic random copolymers containing a decyl chain, cholesterol and PEG500 were prepared as reported by Martin *et al.* to show the highest uptake in HeLa cells¹²⁸. These polymersomes prepared by reverse phase evaporation method encapsulated a combination of anticancer drugs namely Doxorubicin HCl, 5-Fluorouracil and Leucovorin calcium. Multidrug resistance plays an important role in the failure of cancer chemotherapy. The use of combination drugs have proved useful in fighting drug resistance. Polymersomes have been used as vehicles for multi drug anticancer therapy for the encapsulation and delivery of a vast variety of drugs^{214, 250, 390}. The polymersomes indicated good encapsulation efficiency of all the anticancer agents with small and uniform particle size of less than 150nm after drug loading and fast *in-vitro* release. Toxicity measurements in BxPC-3 cells indicated synergistic cytotoxicity of combination drugs encapsulated within the same polymersomes.

The *in-vivo* observation of polymersome toxicity after intratumoral and intravenous injection in pancreatic BxPC-3 ectopic xenograft mouse model form an important part of this chapter. Polymersome pharmacokinetics were first observed by imaging of fluorescently labelled polymersomes after intravenous injection in mice having tumours. Nomikou *et al.* employed ICG loaded PLGA NPs to study the effect of sonodynamic and photodynamic therapy by NIR imaging in ectopic mice RIF-1 tumours. They observed the immediate accumulation of NPs in the tumour region which gradually declined after 6 hours of administration⁴¹⁸. NIR imaging with ICG helped observe the kinetics of the polymersomes and it was found that the accumulation of polymersomes rapidly declined from the peripheral tissue, whereas polymersomes were present in the tumour tissue even after 24 hours of administration. The advantages of injecting anticancer agents in NPs intratumorally has been extensively reviewed by Torchillin⁴⁰⁵ however, intratumoral mode of injection has its own limitations. Intratumoral injection of polymersomes produced better reduction on tumour growth in mice and more stable body weights throughout the experiment duration as compared to free drug solution. Nevertheless, intravenous mode of administration is the most common employed method for the administration of cancer chemotherapeutic drugs³⁹². Additionally, anthracyclines such as Dox, have exhibited dose dependent acute cardiomyopathy. Swain *et al.* retrospectively studied the effect of doxorubicin on congestive heart failure of 630 patients in three different clinical trials⁴⁰⁶. They found that Dox related congestive heart failure occurs at greater frequency and at much lower cumulative dose. Hence observation of multi drug loaded polymersomes by intravenous route formed the second part of the *in-vivo* studies. It was interesting to note that group of mice receiving intravenous free combination drug solutions exhibited peripheral toxicity by displaying a fast reduction in body weights even though they showed significant reduction in tumour volume. However, the group receiving combination drug polymersomes showed no marked change in their body weight and displayed good reduction in tumour volume.

In summary, through this research work we have exhibited the flexibility and versatility of amphiphilic copolymers for different applications. Polymersomes are next generation drug delivery vehicles which are gaining rapid interest in research and

development. Even though polymersomes are different from liposomes, the general aspects of liposome design can be applied to polymersomes to achieve desired functionality. We can easily exercise control over the composition, size, and surface properties of polymersomes depending on their application. We have established the suitability of amphiphilic copolymers for two different types of applications and have confirmed their ability to encapsulate large amounts of drug solutions.

5.2 Challenges and future perspectives

Recent developments in the synthetic methods employed for polymer production have enabled the design of amphiphilic polymers with desirable properties. The numerous applications of these amphiphilic copolymers include the ability to encapsulate different types of drugs as well as being multi-stimuli responsive vesicles capable of performing a wide variety of functions. The future of polymer based drug delivery systems encompasses various fields of therapeutics. Several polymeric systems are in different phases of clinical trials and it won't be long before they will form a significant part of the market of nanoparticulate drug delivery. However biosafety concerns remains a major challenge since these polymeric systems may have to be administered for long durations of time. Hence their long term toxicity and immunogenicity should be of utmost concern especially in the case of systemic administration. The translation of polymeric nanoparticle systems from bench to market is another area in need of a major breakthrough. Most nanoparticle studies are conducted under static conditions at a small scale with limited variability. The adaptation of these systems in complex scenarios at a large scale can truly confirm their potential as advanced therapeutics. Significant efforts for the design of these amphiphilic copolymers and their large scale synthesis and optimization such as assembly line synthesis have to be made. Besides this, there have to be tools for the exact spatial and temporal control of the polymeric units. Nevertheless, polymer drug delivery systems offer exciting new possibilities in the field of advanced drug delivery and it is only a matter of time before they will become indispensable tools in the design of new therapeutic systems.

Chapter 6

Materials and methods

6.1 Materials

Cholesteryl Chloroformate, Ethylene diamine, 1-Octadecanol, (N,N'-Dicyclohexylcarbodiimide) DCC, 4-(Dimethylaminopyridine) DMAP, PEG-methacrylate (Mn 500), PEG-methylmethacrylate (Mn 2000), Methacrylic acid, methoxy PEG (550 & 2000), 1,1'-azobis (cyclohexanecarbonitrile) (AICN), L- α -Phosphatidylcholine from egg yolk, FITC-CM-Dextran 4kDa, FITC-DEAE-Dextran, FITC-Dextran, anthracene, Dialysis membrane (MWCO 14,000), PBS tablets, Fluorescence labelled TLC plates with aluminium backing, Dox, 5 Fluorouracil, Leucovorin Calcium, Indocyanine green were purchased from Sigma chemicals. Dichloromethane (DCM), anhydrous tetrahydrofuran, Chloroform, methanol, Ethanol and Hexane purchased as HPLC grade from Thermofisher Scientific, UK. Oleic acid, CDCl_3 was purchased from TCI, Japan. DMEM, RPMI 1640, Hams F12, Trypsin-EDTA, PenStrep and Foetal bovine serum were sourced from Thermofisher Scientific, UK. Matrigel[®] basement matrix was acquired from Corning Inc. All synthesis were carried out in inert conditions under nitrogen gas unless otherwise stated.

6.2 General methods

6.2.1 Column Chromatography

A glass column sealed at the bottom with cotton wool was utilized for column chromatography. Silica gel was dissolved in mobile phase (chloroform: methanol 18:2) and filled into the column while excessive solvent was removed from the bottom tap to ensure compact packing. About 2cm layer of mobile phase was maintained on top of the column. A fine even layer of sand was added on top of the silica gel packing. Synthesized sample was dissolved in a small amount of mobile phase and added on top of the sand. Roughly 5mL fractions were collected from the bottom of the column while maintaining the mobile phase layer on the top to allow separation of impurities by entrapment into the column. Thin layer chromatography was used to monitor the progress.

6.2.2 Thin layer chromatography (TLC)

Fractions of separated compounds collected during column chromatography were analysed by TLC. This was to ensure acquirement of the right product according to the R_f values and obtain a pure sample with no other trace impurities. Sample solutions in mobile phase were filled in capillary tubes and spotted on fluorescence labelled TLC plates at 1cm distance from the bottom edge. These plates were placed in a TLC chamber filled to 0.5cm with mobile phase and the solvent was allowed to run up to $1/3^{\text{rd}}$ of the plate. The plate was then removed and dried and observed under a hand held UV lamp for the presence of the desired compounds and appropriate level of separation.

6.2.3 Mass spectroscopy (MS)

Molecular weight of all synthesized compounds was determined by mass spectroscopy using Thermo Finnigan LCQ Classic Ion Trap LC-MS. Briefly 1mg mL^{-1} compound was dissolved in methanol and analysed in positive electrospray mode.

6.2.4 Nuclear magnetic resonance (NMR) spectroscopy

^1H NMR spectroscopy was conducted using Varian (500 MHz) NMR spectroscopy by dissolving 5mg mL^{-1} synthesized sample in deuterated chloroform (CDCl_3) in NMR tubes. ^1H NMR Spectra were obtained on Tuneplus Version 1.0 SR1 and analysed on VNMRj 2.2 and Topspin 3.5 pl6 softwares.

6.2.5 Dynamic light scattering (DLS) measurements

Dynamic light Scattering measurements for particle size were conducted by placing diluted 100 μL polymersomes/liposomes in 1mL PBS or undiluted 5mg mL^{-1} polymersomes in disposable cuvettes and analysing using Malvern NanoZS Zetasizer Software V7.03.

6.2.6 Zeta potential measurements

Zeta potential for measurement of surface charge of liposomes and polymersomes was conducted using the Universal Dip cell electrode. Briefly, the electrode was dipped in the liposomes/polymersomes suspension and attached to the Malvern NanoZS Zetasizer and analysed.

6.2.7 Scanning Electron Microscopy (SEM)

Particle morphology was observed using scanning electron microscopy (SEM), nanoparticle suspensions were air dried overnight on aluminium stubs and coated with ultra-thin Gold/Palladium layer at 18mA for 3 minutes using Polaron Equipment Ltd E5100 Sputter coater and observed under FEI Quanta 200 ESEM in high vacuum mode.

6.2.8 Ultraviolet and Fluorescence spectroscopy

Samples for ultraviolet (UV) and fluorescence spectroscopy were placed in glass cuvettes and analysed using Varian Cary Eclipse UV and Fluorescence spectrophotometers at the specific absorbance wavelength for UV and Excitation Emission wavelengths for Fluorescence spectroscopy mentioned in specific sections.

6.2.9 Percentage encapsulation efficiency (% EE)

Encapsulation efficiency of all polymersomes and liposomes loaded with hydrophilic drugs was measured by centrifugal filtration. Polymersomes/liposomes were placed in a dialysis tubing (MWCO 14,000 Da) tied at both ends and placed suspended in a centrifuge tube. These tubes were then centrifuged at 3000rcf at 4°C for 2 hours. Resultant filtrate was collected and measured and analysed for unencapsulated drug. Percentage encapsulation efficiency was calculated using the following formula,

$$\% \text{ Encapsulation efficiency} = \frac{\text{Theoretical drug} - \text{Unencapsulated drug}}{\text{Theoretical Drug}} \times 100$$

Encapsulation efficiency of hydrophobic drugs was analysed by dissolving 100µl Polymersomes/liposomes in appropriate organic solvent such as chloroform/ ethanol to break the nanovesicle assembly and release encapsulated compound and evaluated by UV/ Fluorescence microscopy for direct measuring of encapsulated compound. The percentage encapsulation efficiency was calculated according to the below formula,

$$\% \text{ Encapsulation efficiency} = \frac{\text{Encapsulated drug}}{\text{Theoretical Drug}} \times 100$$

6.2.10 *In-vitro* release studies

In-vitro release studies of polymersomes and liposomes were conducted by placing liposomes/polymersomes in dialysis tubes (MWCO 14,000 Da) tied at both ends and placing them in PBS maintained at 37°C and stirred using a magnetic stirrer. Aliquots were taken out at regular intervals of time and analysed by a relevant analytic method. The amount of sample removed was replaced by fresh PBS to maintain sink conditions.

6.2.11 Maintenance of Cell lines

Three different types of cell lines namely HeLa cells (cervical cancer cell line), BxPC-3 (Human pancreatic cell line) and CHO cells (Non-cancerous Chinese hamster ovarian cell line) were used for various cell culture studies. The types of media and supplements for each cell line are outlined in table 6-1.

Table 6-1 Media composition for cell lines

Cell Line	Medium	FBS (10%)	PenStrep (1%)	NEAA (1%)
Hela	DMEM	√	√	x
BxPC-3	RPMI 1640	√	√	x
CHO	Hams F12	√	x	√

All cells were obtained from in-house frozen cell repository. Briefly, cryovials containing cells were removed either from -80°C storage facility or liquid nitrogen, thawed to 37°C and centrifuged to remove old medium. The resultant pellet was resuspended in fresh media and incubated in HeraCell incubators at 37°C with constant influx of 5% CO₂.

Before each study, cells were confirmed to grow to more than 80% confluence level. After which, supernatant medium from cells was discarded, cells were dislodged using 1x Trypsin-EDTA and incubated at 37°C for 5-7 minutes. After complete detachment from the flask surface, cell were added to centrifuge tubes with fresh media and centrifuged at 1000rpm for 5 minutes. The resultant pellet was resuspended in 5mL

medium and counted using Invitrogen Countess Automated cell counter after staining cells with Trypan blue (1:1 ratio). 100 μ l of 5×10^4 mL⁻¹ were added to 96 well plates and incubated overnight before all treatments. Different treatment conditions and controls are mentioned in relevant sections.

6.2.12 MTT assay for cell viability

3-(4,5-dimethylthiazol-2-yl)-2,5-diphenyltetrazolium bromide (MTT) assay was used for analysing the cell viability after treatment. MTT assay was conducted by first removal of supernatant media from treated cells in 96 well plates. After which 20 μ l of 5mg mL⁻¹ MTT reagent pre-mixed with 100 μ l fresh media was added to the cells and incubated for 3 hours. After which 85 μ l of medium was removed and 50 μ l DMSO was added to the cells and shaken for 5 minutes to ensure complete solubilisation of blue purple formazan taken up by live cells. Absorbance was recorded at 570nm using the Fluostar Omega microplate reader.

6.2.13 Statistical analysis

All data is reported as n=3 unless otherwise stated in figure legends. All values in tables are represented as average \pm SD and all graphs are represented as average \pm SEM. Statistical significance of groups was determined using Two tailed Unpaired Student's t test in Graphpad Prism Version 5.01. * indicates p<0.1, ** indicates p<0.01 and *** indicates p<0.001 level of significance unless otherwise as stated in figure legends.

6.3 Specific methods for Chapter 2

6.3.1 Synthesis of Cholesteryl methacrylate (21)

1.044mL (15.61 moles) of ethylene diamine (**18**) was dissolved in 5mL dry DCM and cooled in ice bath. 0.5007g (1.11 mmoles) cholesteryl chloroformate (**17**) dissolved in 5mL dry DCM was added slowly to the above solution and stirred overnight. Product was washed 3 times with water and brine, traces of water from the organic layer were removed using anhydrous magnesium sulphate and the organic solvent removed to leave cholesteryl ethylene diamine conjugate (**19**). 0.9889g (2.09 mmoles) of the above product was dissolved in 20mL dry DCM with 0.1811gms (2.09 mmoles)

methacrylic Acid (**20**) and 0.0522g (0.20 mmoles) DMAP in a 3 necked round bottom flask in an ice bath. 0.5175g (2.09 mmoles) DCC dissolved in 20 mL DCM was added dropwise and stirred for 24 hours. Product was filtered and purified using column chromatography and characterised by ^1H NMR and mass spectroscopy. ^1H NMR shifts for **21** were ^1H NMR (500 MHz, CDCl_3 , δ ppm): 7.34 (d, 2H), 5.73, 5.34 (s, 2H), 3.44-3.36 (m, 4H), 2.32-1.82 (m, 7H), 0.8575 (m, 9H), 1.82-1.00 (m, 32H).

6.3.2 Synthesis of Oleic methacrylate (**24**)

3.088mL (48.0 moles) ethylene diamine (**18**) was dissolved in 10mL DCM. Separately 2.208 g (7.81 mmoles) of oleic acid (**22**) was dissolved in 5mL DCM with 1.609 (7.81mmoles) DCC and 0.095g (0.78 mmoles) DMAP to which ethylene diamine solution was added slowly and stirred for 48 hrs at 40°C. Product was washed 3 times with brine and dried to obtain oleic acid-ethylene diamine conjugate (**23**). 2.532 g (7.81 mmoles) of the above product was dissolved in 20mL DCM with 0.6729g (7.81mmoles) methacrylic acid (**20**) and 0.09550g (0.78 mmoles) DMAP in ice bath. 1.612g (7.81 mmoles) DCC dissolved in 20 mL DCM solution was added drop wise and stirred for 24 hours. Resultant product was filtered and purified using column chromatography, washed 3 times using 0.1M hydrochloric acid using a separating funnel and dried to obtain the final product which was then characterised as above. The ^1H NMR shifts for **24** were: ^1H NMR (500 MHz, CDCl_3 , δ ppm): 6.08, 5.53 (s, 2H), 4.12 (t, 2H), 1.95 (m, 3H), 1.65 (m, 2H), 1.25 (m, 30H), 0.88 (m, 3H).

6.3.3 Synthesis of Octadecyl methacrylate (**26**)

2.7g (9.98 mmoles) of 1-octadecanol (**25**) was dissolved in 30mL dry DCM with 0.244g (0.002 mmoles) DMAP and 0.86g (0.01 mmoles) methacrylic acid (**20**). 2.06 g (0.01 mmoles) DCC solution was prepared in 20mL dry DCM and added drop wise to this solution and maintained overnight under constant nitrogen gas. The final product was purified and characterised as mentioned in the above procedure. ^1H NMR (500 MHz, CDCl_3 , δ ppm): 5.75 (s, 1H), 5.33 (m, 3H), 3.45 (m, 2H), 3.38 (n, 2H), 2.18 (m, 2H), 1.98 (m, 3H), 1.62 (m, 2H), 1.28 (m, 26H), 0.90 (m, 3H).

6.3.4 Synthesis of Polymers (28)

Cholesteryl methacrylate (**21**), oleic methacrylate (**24**), octadecyl methacrylate (**26**) and PEG methacrylate (Mn 500) (**27**) or PEG methyl ether methacrylate (Mn 2000) (**27**) were taken in a reaction vessel in (1:1:1:1 molar ratio) for P500 and (1:1:1: 0.25) for P2000 in 20mL anhydrous THF with 5mg 1 1'-azobis (cyclohexanecarbonitrile) (AICN), freeze-thawed three times under vacuum using liquid nitrogen and kept at 80°C for 72 hours. Polymer **28** was then precipitated out using hexane and washed 3 times with hexane with centrifugation at 6000 rpm for 5 minutes. The final polymer was obtained as a yellow thick viscous liquid (P500) or white powder (P2000). Characterisation was confirmed by ¹H NMR spectroscopy. The ¹H NMR shifts of each polymer were, Polymer P500: ¹H NMR (500 MHz, CDCl₃, δ ppm): 0.01-2.16 (m, 152H), 3.64 (s, 44H). Polymer P2000: ¹H NMR (500 MHz, CDCl₃, δ ppm): 0.7-2.16 (m, 84H), 3.64 (s, 180H).

6.3.5 Synthesis of CH-mPEG 2000 (30) and CH-mPEG 550 (30) for pegylated liposomes

2g methoxy PEG 2000 (**29**) (0.001 moles) or 0.55g methoxy PEG 550 (**29**) (0.001 moles) and 0.449g (0.001 moles) cholesteryl chloroformate (**17**) were dissolved in THF in an ice bath with a constant influx of nitrogen. Solution was stirred at 45-50°C for 48 hours, dried and washed with hexane to obtain final product. The ¹H NMR shifts of both conjugates were, CH-mPEG 550: ¹H NMR (500 MHz, CDCl₃, δ ppm): 0.01-2.18 (m, 48H), 3.64 (s, 44H). CH-mPEG 2000: ¹H NMR (500 MHz, CDCl₃, δ ppm): 0.7-2.16 (m, 48H), 3.64 (s, 180H).

6.3.6 Measurement of fixed aqueous layer thickness (FALT)

Fixed Aqueous layer thickness (FALT) of polymers was calculated by the zeta potential measured in different concentrations of NaCl, plotted against k giving slope which is fixed aqueous layer thickness in nm. According to Gouy–Chapmann theory,

$$\ln(L) = \ln A - kL,$$

where A is a constant, $k = \sqrt{C}/0.3$ for univalent salts and C is molality of electrolytes⁴¹⁹.

6.3.7 Preparation of liposomes and polymersomes by reverse phase evaporation method

1mL of lipids egg phosphatidylcholine and CH-mPEG 550/2000 (2mg mL⁻¹ **15** and **30** in 9:1 molar ratio) or 0.5mL polymer **28** (2mg mL⁻¹) in chloroform were evaporated in a round bottom flask (RBF) to form a thin film. Anthracene (66μl of 1mg mL⁻¹ in ethanol) was added at chloroform stage. FCD, FDD and F-D (100μl of 2mg mL⁻¹ in PBS) were added to the RBF and evaporated to dryness. 0.5 mL chloroform was added and the solution was sonicated for 15 minutes. 1mL PBS was added to chloroform solution for liposomes or 0.5mL (2mg mL⁻¹) polymer **28** in PBS with 0.5mL plain PBS was added for polymersomes and sonicated for 30 minutes after which chloroform layer was evaporated to form 1mL liposomes/polymersomes. Resultant nanoparticles were sonicated in a bath sonicator for 10 minutes after particle formation.

6.3.8 Preparation of liposomes and polymersomes by emulsion evaporation method (EM-EV)

1mL of lipids (2mg mL⁻¹) (**section 6.3.7**) or 0.5mL polymer **28** (2mg mL⁻¹) in chloroform was mixed with 1mL PBS for liposomes and 0.5mL (2mg mL⁻¹) polymer in PBS with 0.5mL PBS for polymersomes. Anthracene (66μl of 1mg mL⁻¹ in ethanol) was added in chloroform. Hydrophilic dyes (100μl of 2mg mL⁻¹) were added in PBS. Resultant chloroform-PBS mixture was sonicated for 30-40 minutes to form an emulsion. Chloroform layer was evaporated to form nanoparticles instantly and bath sonicated for 10 minutes to form unilamellar particles.

6.3.9 Preparation of liposomes and polymersomes by thin film hydration method (TFH)

1mL of lipids (2mg mL⁻¹) (**as section 6.3.7**) or polymer (**28**) (2mg mL⁻¹) in chloroform was evaporated in a RBF to form a thin film. Anthracene loading (66μl of 1mg mL⁻¹ in ethanol) was added in chloroform and 1mL PBS was added after making the thin film or hydrophilic dyes (100μl of 2mg mL⁻¹ in PBS) were added with 900μl PBS after making the thin film and hydrated by sonication in a water bath for 45-60 minutes.

6.3.10 Characterisation of nanoparticles

Encapsulation efficiency of all dyes was measured as mentioned in Section 6.2.9. Encapsulation efficiency of all dyes was measured by fluorescence spectroscopy. FCD was measured at Ex 490/Em 517 ($y=32.318x$, $R^2 = 0.9982$), FDD was measured at Ex 490/Em 517 ($y = 18.063x$, $R^2 = 0.9997$), F-D was measured at Ex 490/Em 517 ($y=33.788x$, $R^2 = 0.999$). Anthracene concentration was measured at Ex 355/Em 400 ($y = 221.14x$, $R^2 = 0.9987$).

6.3.11 *In-vitro* release studies

Release studies for FCD, FDD and F-D were conducted by tying nanoparticles into a dialysis bag (MWCO 14,000Da) and placing in a vial containing PBS at 37°C with constant stirring. Release of anthracene was determined in Ethanol: PBS 1:1 solution. Aliquots were taken at different intervals of time upto 24 hrs and replaced with fresh media to maintain sink conditions and analysed using fluorescence spectroscopy as stated above.

6.3.12 Cellular uptake

1×10^5 cells mL^{-1} (100 μl) HeLa cells were seeded into 96 well plates and incubated overnight, to which FCD (250 $\mu\text{g mL}^{-1}$) or anthracene (50 $\mu\text{g mL}^{-1}$) liposomes/polymersomes, sterile filtered using 0.45 μm Millex MCE filters were added at a volume of 100 μl in PBS and incubated for 4 hours at 37°C. After incubation cells were washed twice with PBS and measured using Fluostar Omega microplate reader at Ex 480nm/Em 520nm for FCD and Ex 355nm/Em 460nm for anthracene. After fluorescence measurements, protein estimation of cells was done by lysing the cells and adding 25 μl 0.1% Triton-X100 into each well with 15 minutes incubation at 37°C. Protein estimation was done using BCA Protein assay kit after incubation at 37°C for 30 minutes and measuring absorbance at 562nm. Cellular uptake results are reported as fluorescence per mg of protein.

6.3.13 Mechanism of cell uptake by inhibition of endocytosis

For uptake mechanism, HeLa cells were incubated with 100 μl of 30 μM Chlorpromazine Hydrochloride in media for 30 minutes. After which the supernatant medium was

removed and cells were incubated with FCD loaded polymersomes/liposomes for 4 hours as described above. Cells were then washed twice with PBS and analysed for FCD fluorescence as mentioned in Section **6.3.11**.

6.3.14 Observation of cells by Fluorescence microscopy

For fluorescence imaging, HeLa cells were cultured on glass coverslips and allowed to adhere overnight. Cells were treated with liposome/polymersomes suspension having combination of FCD and anthracene at concentrations stated in Section **6.3.11**. and incubated for 4 hours. Coverslips were then washed with water and observed immediately using Nikon Eclipse E400 microscope and analysed using NIS Elements 3.22.01 software.

6.3.15 Stability studies

Nanoparticle suspensions were subjected to stability studies at 5°C (stored in refrigerator) and 25°C (incubator) for 8 weeks. Samples were taken at regular intervals and analysed for encapsulation efficiency and size.

6.4 Specific methods for Chapter 3

6.4.1 Preparation and characterisation of micelles

Micelles were prepared by evaporating the desired amount of polymer **34** in CHCl_3 in a round bottom flask along with **31** and **32** or **35** to form a thin film. The resultant film was hydrated with PBS to form the micelles. Micelles were characterised for particle size, PDI, Zeta potential, Encapsulation efficiency and SEM as mentioned in section **6.2**.

6.4.2 Evaluation of phototransformation 32a to 32b

0.5mL **32** (0.1 mg mL^{-1}) was added to 0.6 mL polymer (**34**) (2.5 mg mL^{-1}) and evaporated into a thin film and hydrated with 3mL PBS to form micelles. These samples were irradiated from a fixed distance of 4 cms at 365 nm (0.4 mW cm^{-2}) with a Mineralight UVGL-25 lamp (UVP 95-0006-03 Model UVL-56 6 Watt). The UV-Vis

spectra was recorded at intervals of 30 seconds for 6.5 minutes until no further increase in absorbance of **32b** (560nm) was observed.

6.4.3 FRET efficiency

Micelles were prepared as described in section **6.4.1.** with 78 μL of **31** (0.08 mg mL^{-1}) and varying volumes of **32** (0.2 mg mL^{-1}) to obtain molar ratios 1: 0.5-10 of **31:32** and hydrated with polymer **34** with 3mL PBS to form micelles. The FRET efficiency was determined by allowing the photo-transformation of **32a** to **32b** while the concentration of **31** remained constant. Fluorescence emission spectra of **31** were recorded (Ex 525nm/Em 545 nm) before and after UV light exposure.

6.4.4 *In-vitro* triggered release using Franz Diffusion cells

Micelles were prepared as above using 0.176 mL of **31** (0.2 mg mL^{-1}) with 0.6 mL of **32** (0.5 mg mL^{-1}) and 2mL polymer **34** (2.5 mg mL^{-1}) and hydrated with 2mL PBS. Release studies were undertaken using Franz diffusion cells through dialysis membrane. 200 μL of the micelle formulation was loaded into the donor compartment while the acceptor chamber comprised of PBS and was maintained at 37°C. The contents of the donor chamber were irradiated with UV light for fixed time periods of 2, 4, 6, 8, 10 and 12 minutes and solutions were analysed using fluorescence spectroscopy at Ex360nm-EM 637nm. Similarly, control studies were conducted in the absence of UV light. For determining stability and reproducibility of the system, micelles containing **31** and **35** were loaded onto Franz diffusion cells and subjected to cycles of 5 minutes UV light and 20 minutes dark conditions during which samples were scanned for fluorescence emission of **31** at Ex 525nm-Em 540nm at 5 minutes intervals for 20 minutes.

6.4.5 Observation of FRET in HeLa cells

100 μL , $5 \times 10^4 \text{ mL}^{-1}$ HeLa cells were seeded in 96 well plates and allowed to adhere overnight. When 60 % confluency was reached, 2 mL micelle solutions were prepared containing either **31** (0.176mL of 0.2 mg mL^{-1}) and **32** (0.6mL of 0.5 mg mL^{-1}) or just **31** (0.176mL of 0.2 mg mL^{-1}). 50 μL of this solution were added to the wells and incubated for 18 hours. The cells were then washed twice with PBS and the fluorescence emission determined using an ELISA plate reader (Ex 485nm and Em 520nm). For confocal microscopy, cells were treated as mentioned above and imaged using a Leica

DMI6000b inverted microscope with a 40x oil immersion lens. All images were analysed using LAS AF v2.3.6 software.

6.4.6 Comparative release study to quantify triggered release by FRET

Release studies were conducted on Franz diffusion cells using dialysis membrane. Briefly micelles loaded with **31** and **35** were loaded into acceptor compartment and the donor compartment was filled with PBS maintained at 37°C. Micelles were irradiated with UV light for 5 minutes after which they were subjected to light and dark conditions for 20 minutes. Samples were taken at 5 minute interval and observed for UV absorbance at 345nm for **35a** and fluorescence emission of **31** following a 20 minute equilibration period in visible light conditions. Similar studies were conducted without UV trigger.

6.5 Specific methods for chapter 4

6.5.1 Preparation and characterisation of polymersomes

0.5mL (5mg mL⁻¹) polymer **41** in chloroform was evaporated in a round bottom flask to form a thin film. 100µl Dox (5mg mL⁻¹ in water), 250µl 5-FU (8mg mL⁻¹ in water) and 50µl LV (5mg mL⁻¹ in water) was added on top of the film and evaporated to form a layer on the polymer film. 1mL Chloroform was added to the round bottom flask and sonicated for 15 minutes, after which 0.5mL Polymer **41** (5mg mL⁻¹) and 0.5mL PBS was added and sonicated again for 30 minutes to form an emulsion. The chloroform layer was evaporated to form polymersomes. Polymersomes were freeze dried and resuspended as per requirement. Resultant polymersomes were characterised using particle size, PDI, zeta potential, encapsulation efficiency and *in-vitro* release studies. Dox was analysed by fluorescence spectroscopy at Ex 485nm/Em 580nm ($y = 91.324x$, $R^2 = 0.9881$), 5FU and LV by UV spectroscopy at absorbance maximum 265nm($y = 0.0581x$, $R^2 = 0.9992$) and 285nm ($y = 0.0543x$, $R^2 = 0.9998$) respectively.

6.5.2 Cell viability studies

BxPC-3 cells were employed to observe cell toxicity of free solutions of individual drugs in solution, combinations loaded in polymersomes and blank polymersomes.

100 μ l, 5×10^5 cells mL^{-1} were seeded in 96 well plates and allowed to adhere overnight after which 100 μ l of test solutions was added to the wells and incubated for 22 hrs. Free solution of individual drugs, combination free solutions or combination drugs encapsulated in polymersomes were loaded on cells at concentrations Dox 0.2mM, 5-FU 4mM, LV 0.25mM, amphiphilic polymer **41** 2.5mg mL^{-1} following sterilization with 0.45 μ Millex MCE syringe filters.

6.5.3 *In-vivo* studies on ectopic xenograft mouse model

Mixed gender NOD-SCID mice (NOD.CB17-Prkdcscid/NCrHsd) having an average weight of 23g, implanted with BxPC-3 tumours were employed for all *in-vivo* studies. BxPC-3 cells (5×10^6 per mouse) were resuspended in RPMI 1640 medium and Matrigel® in 1:1 ratio and implanted ectopically into the rear dorsum of the mouse. Well defined tumours were formed after 2 weeks of implantation and tumour volume was measured regularly using callipers and calculated using the formula $(L \times W \times H)/2$ until the tumour volume reached 200-250mm³ after which animals were employed for *in-vivo* studies. All animals were treated humanely in accordance with UK Animals (Scientific Procedures) Act 1986.

6.5.4 Observation of pharmacokinetics of polymersomes

50 μ l polymersomes loaded with 0.2mg mL^{-1} ICG were injected into the tail vein of mice previously anesthetised with 150 μ l intraperitoneal injection of water for injection: hypnorm: hypnovel (2:1:1,) (VetaPharma Ltd., U.K.). Following administration, animals were placed in Xenogen IVIS® lumina imaging system chamber maintained at 37°C loaded with ICG filter set (Ex 705–780 nm; Em 810–885 nm) in fluorescence mode and images were taken at regular intervals up to 22 hours to observe pharmacokinetics of polymersomes in real time. After 22 hours, mice were euthanized and organs along with tumour were surgically collected and imaged for presence of ICG fluorescence. All data were analysed using Living Image® software version 2.60 and reported as arbitrary fluorescence unit's ratio with respect to background.

6.5.5 *In-vivo* toxicity of polymersomes loaded with combination drugs

After mice reached desired tumour volume, they were segregated into 5 groups- untreated, free solution intratumoral, polymersomes intratumoral, free solution IV and polymersomes IV treated groups. Polymersomes loaded with Dox (5mg/kg), 5-FU (20mg/kg), LV (2.5mg/kg), polymer **41** (50mg/kg) were injected intratumorally and intravenously at 100µl volume on Day 0 and Day 5 of treatment in mice according to their respective groups whereas untreated group received no treatment. Mice in intratumor treatment group received hypnorm/hypnovel intraperitoneal anaesthesia before each treatment. Tumour volume and body weight was measured every day for 13 days after intratumoral injection and 7 days after intravenous injection. Mice were then sacrificed and tumours and hearts were surgically removed for further observations.

Chapter 7

References

1. Yun YH, Lee BK, Park K. Controlled drug delivery: Historical perspective for the next generation. *Journal of Controlled Release* 2015; 219:2-7.
2. Peppas NA. Historical perspective on advanced drug delivery: How engineering design and mathematical modeling helped the field mature. *Advanced Drug Delivery Reviews* 2013; 65:5-9.
3. Lee PI, Li J-. Evolution of oral controlled release dosage forms. In: H. Wen, K. Park, editors. *Oral controlled release formulation design and drug delivery*. Hoboken, NJ.: John Wiley & Sons, Inc.; 2010.
4. Paolino D, Fresta M, Sinha P, Ferrari M. Drug delivery systems. In: John G. Webster, editor. *Encyclopedia of medical devices and instrumentation*. Second ed. John Wiley & Sons, Inc.; 2006.
5. Ye M, Kim K, Park K. Issues in long-term protein delivery using biodegradable microparticles. *Journal of Controlled Release* 2010; 156:241-60.
6. Heinemann L. The failure of exubera: Are we beating a dead horse? *Journal of Diabetes Science and Technology* 2008; 2:518-29.
7. Park K. The controlled drug delivery systems: Past forward and future back. *Journal of Controlled Release* 2014; 190:3-8.
8. Rosen H, Abribat T. The rise and rise of drug delivery. *Nature Reviews Drug Discovery* 2005; 4:381-385.
9. Sudhakar A. History of cancer, ancient and modern treatment methods. *Journal of Cancer Science and Therapy* 2009; 1(2):1-4.
10. Aslan B, Ozpolat B, Sood AK, Lopez-Berestein G. Nanotechnology in cancer therapy. *Journal of Drug Targeting* 2013; 21(10):904-13.
11. Maeda H, Greish K, Fang J. The EPR effect and polymeric drugs: A Paradigm shift for cancer chemotherapy in the 21st century. In: Ronit Satchi-Fainaro, Ruth Duncan, editors. *Polymer therapeutics II*. Berlin, Heidelberg: Springer Berlin Heidelberg; 2006. ID: Maeda2006.
12. Zsigmondy R. "Nobel lecture: Properties of colloids". Nobelprize Org Nobel Media AB 2014.
13. Hulla JE, Sahu SC, Hayes AW. Nanotechnology: History and future. *Human and Experimental Toxicology* 2015; 34(12):1318-21.

14. Krukemeyer MG, Krenn V, Huebner F, Wagner W, Resch R. History and possible uses of nanomedicine based on nanoparticles and nanotechnological progress. *Journal of Nanomedicine and Nanotechnology* 2015; 6:336.
15. Shi J, Votruba AR, Farokhzad OC, Langer R. Nanotechnology in drug delivery and tissue engineering: From discovery to applications. *Nano Letters* 2010; 10(9):3223-30.
16. Qu M, Zeng R, Fang S, Dai Q, Li H, Long J. Liposome-based co-delivery of SiRNA and docetaxel for the synergistic treatment of lung cancer. *Int J Pharm* 2014; 474:112.
17. Torchilin VP. Micellar nanocarriers: Pharmaceutical perspectives. *Pharm Res* 2007; 24:1-16.
18. Yu H, Yan C, Lei X, Qin Z, Yao J. Novel approach to extract thermally stable cellulose nanospheres with high yield. *Materials Letters* 2014; 131:12-5.
19. Musyanovych A, Landfester K. Polymer micro- and nanocapsules as biological carriers with multi functional properties. *Macromolecular Bioscience* 2014; 14:458.
20. Kazi KM, Mandal AS, Biswas N, Guha A, Chatterjee S, Behera M, Kuotsu K. Niosome: A future of targeted drug delivery systems. *Journal of Advanced Pharmaceutical Technology and Reserach* 2010; 4:374.
21. Wang X, Liu G, Hu J, Zhang G, Liu S. Concurrent block copolymer polymersome stabilisation and bilayer permeabilisation by stimuli-regulated 'traceless' crosslinking. *Angewandte Chemie International Edition* 2014; 53:3138.
22. Levine DH, Ghoroghchian PP, Freudenberg J, Zhang G, Therien MJ, Greene MI, Hammer DA, Murali R. Polymersomes: A new multi-functional tool for cancer diagnosis and therapy. *Methods* 2008 09/01; 46(1):25-32.
23. What is nanotechnology and what is nanomedicine? Liverpool, UK: British society for nanomedicine [cited 2017. Available from: <http://www.britishsocietynanomedicine.org/what-is-nanomedicine/>.
24. De Volder, Michael F. L., Tawfick SH, Baughman RH, Hart AJ. Carbon nanotubes: Present and future commercial applications. *Science* 2013 02/01; 339(6119):535.
25. Mody VV, Siwale R, Singh A, Mody HR. Introduction to metallic nanoparticles. *Journal of Pharmacy and Bioallied Sciences* 2010 08/28; 2(4):282-9.
26. Brichkin SB, Razumov VF. Colloidal quantum dots: Synthesis, properties and applications. *Russian Chemical Reviews* 2016; 85(12):1297-312.

27. Bera D, Qian L, Tseng T, Holloway PH. Quantum dots and their multimodal applications: A review. *Materials* 2010; 3(4).
28. Pattni BS, Chupin VV, Torchilin VP. New developments in liposomal drug delivery. *Chemical Reviews* 2015; 115:10938-66.
29. Kamaly N, Yameen B, Wu J, Farokhzad OC. Degradable controlled-release polymers and polymeric nanoparticles: Mechanisms of controlling drug release. *Chem Rev* 2016 02/24; 116(4):2602-63.
30. Branco MC, Schneidera JP. Self-assembling materials for therapeutic delivery. *Acta Biomaterialia* 2009; 5(3):817-31.
31. Koo OM, Rubinstein I, Onyuksel H. Role of nanotechnology in targeted drug delivery and imaging: A concise review. *Nanomedicine: Nanotechnology, Biology, and Medicine* 2005; 1:193-212.
32. Guo P, Coban O, Snead NM, Trebley J, Hoeprich S, Guo S, Shu Y. Engineering RNA for targeted siRNA delivery and medical application. *Adv Drug Deliv Rev* 2010 04/30; 62(6):650-66.
33. Langmuir I. The constitution and fundamental properties of solids and liquids. Part i. solids. *J Am Chem Soc* 1916 11/01; 38(11):2221-95.
34. Bangham AD. Liposomes: The babraham connection. *Chem Phys Lipids* 1993 09/01; 64(1):275-85.
35. Koning GA, Storm G. Targeted drug delivery systems for the intracellular delivery of macromolecular drugs. *Drug Discovery Today* 2003; 8:482-3.
36. Metselaar JM, Storm G. Liposomes in the treatment of inflammatory disorders. *Expert Opinion on Drug Delivery* 2005:465-76.
37. Ding BS, Dziubla T, Shuvaev VV, Muro S, Muzykantov VR. Advanced drug delivery systems that target the vascular endothelium. *Molecular Interventions* 2006; 6:98-112.
38. Hua S, Wu SY. The use of lipid-based nanocarriers for targeted pain therapies. *Frontiers in Pharmacology* 2013; 4:143.
39. Patel HM. Serum opsonins and liposomes - their interaction and opsonophagocytosis. *Critical Reviews in Therapeutic Drug Carrier Systems* 1992;9 :39-90.

40. Marrink SJ, Mark AE. The mechanism of vesicle fusion as revealed by molecular dynamics simulations. *Journal of American Chemical Society* 2003; 125:11144-5.
41. Haluska CK, Riske KA, Marchi-Artzner V, Lehn JM, Lipowsky R, Dimova R. Time scales of membrane fusion revealed by direct imaging of vesicle fusion with high temporal resolution. *Proceedings of the National Academy of Sciences* 2006; 103:15841-6.
42. Blume G, Cevc G. Molecular mechanism of the lipid vesicle longevity in vivo. *Biochimica Et Biophysica Acta* 1993; 1146:157-68.
43. Plotnick AN. Lipid-based formulations of amphotericin B. *Journal of American Veterinary Medical Association* 2000; 216:838-41.
44. Svenson S. Clinical translation of nanomedicines. *Current Opinion in Solid State and Material Science* 2012; 16:287-94.
45. Allen TM, Hansen C, Martin F, Redemann C, Yauyoung A. Liposomes containing synthetic lipid derivatives of poly (ethylene glycol) show prolonged circulation half-lives in vivo. *Biochimica Et Biophysica Acta* 1991; 1066:29-36.
46. Maeda H, Sawa T, Konno T. Mechanism of tumor-targeted delivery of macromolecular drugs, including the EPR effect in solid tumor and clinical overview of the prototype polymeric drug SMANCS. *Journal of Controlled Release* 2001; 74:47-61.
47. Allen C, Dos Santos N, Gallagher R, Chiu GNC, Shu Y, Li WM, Johnstone SA, Janoff AS, Mayer LD, Webb MS, et al. Controlling the physical behavior and biological performance of liposome formulations through use of surface grafted poly (ethylene glycol). *Biosci Rep* 2002 04/01; 22(2):225.
48. Caliceti P, Veronese FM. Pharmacokinetic and biodistribution properties of poly (ethylene glycol)-protein conjugates. *Advanced Drug Delivery Reviews* 2003; 55:1261-77.
49. Allen TM, Cullis PR. Liposomal drug delivery systems: From concept to clinical applications. *Adv Drug Deliv Rev* 2013 1; 65(1):36-48.
50. Gao WW, Hu CMJ, Fang RH, Zhang LF. Liposome-like nanostructures for drug delivery. *Journal of Materials Chemistry B* 2013; 1:6569-85.
51. Batist G, Ramakrishnan G, Rao CS, Chandrasekharan A, Gutheil J, Guthrie T, Shah P, Khojasteh A, Nair MK, Hoelzer K, et al. Reduced cardiotoxicity and preserved antitumor efficacy of liposome-encapsulated doxorubicin and cyclophosphamide compared with conventional doxorubicin and cyclophosphamide in a randomized,

- multicenter trial of metastatic breast cancer. *Journal of Clinical Oncology* 2001; 19:1444-54.
52. Safra T, Muggia F, Jeffers S, Tsao-Wei DD, Groshen S, Lyass O, Henderson R, Berry G, Gabizon A. Pegylated liposomal doxorubicin (doxil): Reduced clinical cardiotoxicity in patients reaching or exceeding cumulative doses of 500 mg/m². *Annals of Oncology* 2000; 11:1029-33.
 53. Yamada A, Taniguchi Y, Kawano K, Honda T, Hattori Y, Maitani Y. Design of folate-linked liposomal doxorubicin to its antitumor effect in mice. *Clin Cancer Res* 2008 12/15; 14(24):8161.
 54. Gabizon A, Horowitz AT, Goren D, Tzemach D, Mandelbaum-Shavit F, Qazen MM, Zalipsky S. Targeting folate receptor with folate linked to extremities of poly(ethylene glycol)-grafted liposomes: in vitro studies. *Bioconjugate Chem* 1999 03/01; 10(2):289-98.
 55. Guo X, Szoka FCJ. Chemical approaches to triggerable lipid vesicles for drug and gene delivery. *Accounts of Chemical Research* 2003; 36(5):335-41.
 56. Jensen SS, Andresen TL, Davidsen J, Høyrup P, Shnyder SD, Bibby MC, Gill JH, Jørgensen K. Secretory phospholipase A2 as a tumorspecific trigger for targeted delivery of a novel class of liposomal prodrug anticancer etherlipids. *Molecular Cancer Therapeutics* 2004; 3(11):1451-8.
 57. Kong G, Braun RD, Dewhirst MW. Hyperthermia enables tumor-specific nanoparticle delivery: Effect of particle size. *Cancer Research* 2000; 60(16):4440-5.
 58. Schroeder A, Honen R, Turjeman K, Gabizon A, Kost J, Barenholz Y. Ultrasound triggered release of cisplatin from liposomes in murine tumours. *Journal of Controlled Release* 2009; 137:63-8.
 59. Evjen TJ, Nilssen EA, Flower RA, Røgnvaldsson S, Brandl M, Fossheim SL. Lipid membrane composition influences drug release from dioleoylphosphatidylethanolamine-based liposomes on exposure to ultrasound. *International Journal of Pharmaceutics* 2011; 406:114-6.
 60. Yavlovich A, Singh A, Blumenthal R, Puri A. A novel class of photo-triggerable liposomes containing DPPC:DC (8,9)PC as vesicles for delivery of doxorubicin to cells. *Biochimica Et Biophysica Acta* 2011; 1808:117-26.
 61. Shum P, Kim J, Thompson DH. Phototriggering of liposomal drug delivery systems. *Advanced Drug Delivery Reviews* 2001; 53:273-84.

62. Yadav AV, Murthy MS, Shete AS, Sfurti S. Stability aspects of liposomes. *Indian Journal of Pharmaceutical Education and Research* 2011; 45(4):402-13.
63. Qin G, Li Z, Xia R, Li F, O'Neill BE, Goodwin JT, Khant HA, Chiu W, Li KC. Partially polymerized liposomes: Stable against leakage yet capable of instantaneous release for remote controlled drug delivery. *Nanotechnology* 2011; 22(15).
64. Barenholz Y. Liposome application: Problems and prospects. *Current Opinion in Colloid & Interface Science* 2001; 6:66-77.
65. Lavik E, Kuehn MH, Kwon YH. Novel drug delivery systems for glaucoma. *Eye* 2011 04/08; 25:578.
66. Pharriss BB, Erickson R, Bashaw J, Hoff S, Place VA, Zaffaroni A. Progestasert: A uterine therapeutic system for long-term contraception: I. philosophy and clinical efficacy. *Fertil Steril* 1974 Nov; 25(11):915-21.
67. Polaneczky M, Slap G, Forke C, Rappaport A, Sondheimer S. The use of levonorgestrel implants (norplant) for contraception in adolescent mothers. *N Engl J Med* 1994 11/03; 331(18):1201-6.
68. Wright JC, Hoffman AS. Historical overview of long acting injections and implants. In: Jeremy C. Wright, Diane J. Burgess, editors. *Long acting injections and implants*. Boston, MA: Springer US; 2012. F: Wright2012.
69. Grund S, Bauer M, Fischer D. Polymers in drug delivery-state of the art and future trends. *Advanced Engineering Materials* 2011; 13(3):B61-87.
70. Yang W, Pierstorff E. Reservoir-based polymer drug delivery systems. *Journal of Laboratory Automation* 2012; 17(1):50-8.
71. da Silva GR, Fialho SL, Siqueira RC, Jorge R, Cunha AD. Implants as drug delivery devices for the treatment of eye diseases. *Brazilian Journal of Pharmaceutical Sciences* 2010; 46(585):595.
72. London NJS, Chiang A, Haller JA. The dexamethasone drug delivery system: Indications and evidence. *Advances in Therapy* 2011; 28:351-66.
73. Rajgor N, Patel M, Bhaskar VH. Implantable drug delivery systems: An overview. *Systematic Reviews in Pharmacy* 2011; 2(2):91-5.
74. Hoare TR, Kohane DS. Hydrogels in drug delivery: Progress and challenges. *Polymer* 2008; 49:1993-2007.

75. Vashist A, Vashist A, Gupta YK, Ahmad S. Recent advances in hydrogel based drug delivery systems for the human body. *Journal of Materials Chemistry B* 2014; 2:147-66.
76. Hoffman AS. Hydrogels for biomedical applications. *Advanced Drug Delivery Reviews* 2002; 54:3-12.
77. Zakir Hossain KM, Patel U, Ahmed I. Development of microspheres for biomedical applications: A review. *Progress in Biomaterials* 2015; 4:1-19.
78. Su CW, Chiang CS, Li WM, Hu SH, Chen. S.Y. Multifunctional nanocarriers for simultaneous encapsulation of hydrophobic and hydrophilic drugs in cancer treatment. *Nanomedicine (London)* 2014; 9(10):1499-515.
79. Mazak K, Noszal B. Drug delivery: A process goverened by species-specific lipophilicities. *European Journal of Pharmaceutical Sciences* 2014; 62:96.
80. Mora-Huertas CE, Fessi H, Elaissari A. Polymer-based nanocapsules for drug delivery. *International Journal of Pharmaceutics* 2010; 385(1-2):113-42.
81. Letchford K, Burt H. A review of the formation and classification of amphiphilic block copolymer nanoparticulate structures: Micelles, nanospheres, nanocapsules and polymersomes. *European Journal of Pharmaceutics and Biopharmaceutics* 2007; 65:259-69.
82. Christian DA, Cai S, Bowen DM, Kim Y, Pajerowski JD, Discher DE. Polymersome carriers: From self-assembly to siRNA and protein therapeutics. *European Journal of Pharmaceutics and Biopharmaceutics* 2009; 71(3):463-74.
83. Anselmo AC, Mitragotri S. Nanoparticles in the clinic. *Bioengineering & Translational Medicine* 2016; 1(1):10-29.
84. Prabhu RH, Patravale VB, Joshi MD. Polymeric nanoparticles for targeted treatment in oncology: Current insights. *International Journal of Nanomedicine* 2015; 10:1001-18.
85. Lombardo D, Kiselev MA, Magazù S, Calandra P. Amphiphiles self-assembly: Basic concepts and future perspectives of supramolecular approaches. *Advances in Condensed Matter Physics* 2015; 2015.
86. Karayianni M, Pispas S. Self-assembly of amphiphilic block copolymers in selective solvents. In: Karel Procházka, editor. *Fluorescence studies of polymer containing systems*. Cham: Springer International Publishing; 2016. ID: Karayianni2016.

87. Discher DE, Eisenberg A. Polymer vesicles. *Science* 2002; 297(5583):967-73.
88. Gaucher G, Dufresne MH, Sant VP, Kang N, Maysinger D, Leroux JC. Block copolymer micelles: Preparation, characterization and application in drug delivery. *Journal of Controlled Release* 2005; 109(1-3):169-88.
89. Fustin CA, Abetz V, Gohy JF. Triblock terpolymer micelles: A personal outlook. *European Physical Journal E: Soft Matter* 2005; 16(3):291-302.
90. Zhang J, Liu K, Müllen K, Yin M. Self-assemblies of amphiphilic homopolymers: Synthesis, morphology studies and biomedical applications. *Chemical Communications* 2015; 51(58):11541-55.
91. Jain JP, Ayen WY, Kumar N. Self assembling polymers as polymersomes for drug delivery. *Current Pharmaceutical Design* 2011; 17:65-79.
92. Wang MJ, Wang H, Chen SC, Chen C, Liu Y. Morphological control of anisotropic self-assemblies from alternating poly (p-dioxanone)-poly (ethylene glycol) multiblock copolymer depending on the combination effect of crystallization and micellization. *Langmuir* 2015; 31(25):6971-80.
93. Yildiz I, Impellizzeri S, Denniz E, McCaughan B, Callan F J, Raymo F. Supramolecular strategies to construct biocompatible and photoswitchable fluorescent assemblies. *J Am Chem Soc* 2011; 133:871-9.
94. Bhattacharya A. Grafting: A versatile means to modify polymers Techniques, factors and applications. *Progress in Polymer Science* 2004; 29(8):767-814.
95. Yang C, Liu SQ, Venkataraman S, Gao SJ, Ke X, Chia XT, Hedrick JL, Yang YY. Structure-directing star-shaped block copolymers: Supramolecular vesicles for the delivery of anticancer drugs. *Journal of Controlled Release* 2015; 208:93-105.
96. Zhang YY, Li Y, Zhou XJ, Zhang XH, Du BY, Fan ZQ. Synthesis of an amphiphilic brush copolymer by a highly efficient 'grafting onto' approach via CO₂ chemistry. *Macromolecular Rapid Communications* 2015; 36(9):852-7.
97. Song D, Lin Y, Gai Y, Colella NS, Li C, Liu XH, Samuel Gido S, Watkins JJ. Controlled supramolecular selfassembly of large nanoparticles in amphiphilic brush block copolymers. *Journal of American Chemical Society* 2015; 137(11):3771-4.
98. Mandal J, Ramakrishnan S. Periodically grafted amphiphilic copolymers: Effects of steric crowding and reversal of amphiphilicity. *Langmuir* 2015; 31(22):6035-44.

99. Huang J, Turner SR. Recent advances in alternating copolymers: The synthesis, modification, and applications of precision polymers. *Polymer* 116 (2017) 572e586 2017; 116:572-86.
100. Kumar N, Ravikumar MNV, Domb AJ. Biodegradable block copolymers. *Advanced Drug Delivery Reviews* 2001; 53:23-44.
101. Hamley IW, editor. *Developments in block copolymer science and technology*. 2004.
102. Falkenhagen J, Much H, Stauf W, Müller A. Characterisation of di- and triblock copolymers using coupled chromatographic methods. *Polymer Preprints (American Chemical Society Division of Polymer Chemistry)* 1999; 40(2).
103. Li L, Raghupathi K, Song C, Prasad P, Thayumanavan S. Self-assembly of random copolymers. *Chem Commun* 2014; 50(88):13417-32.
104. Oda Y, Kanaoka S, Sato T, Aoshima S, Kuroda K. Block versus random amphiphilic copolymers as antibacterial agents. *Biomacromolecules* 2011; 12:3581-91.
105. Matsumoto K, Terashima T, Sugita T, Takenaka M, Sawamoto M. Amphiphilic random copolymers with hydrophobic/hydrogen-bonding urea pendants: Self folding polymers in aqueous and organic media. *Macromolecules* 2016, 49, 7917–7927 2016; 49:7917-27.
106. Sugihara S, Kanaoka S, Aoshima S. Thermosensitive random copolymers of hydrophilic and hydrophobic monomers obtained by living cationic Copolymerization¹. *Macromolecules* 2004; 37:1711-9.
107. Cheng R, Meng F, Deng C, Klok HA, Zhong Z. Dual and multi-stimuli responsive polymeric nanoparticles for programmed site-specific drug delivery. *Biomaterials* 2013 May; 34(14):3647-57.
108. Hong S, Takahashi H, Nadres ET, Mortazavian H, Caputo GA, Younger JG, Kuroda K. A cationic amphiphilic random copolymer with pH-responsive activity against methicillin-resistant staphylococcus aureus. *Plos One* 2017 01/06; 12(1):e0169262.
109. Li S, Chen G, Zhou Z, Li Q. Stimuli-induced multiple dissociation and micellization transitions of random copolymers. *RSC Adv* 2015; 5(81):65847-55.
110. Feng C, Li Y, Yang D, Hu J, Zhang X, Huang X. Well-defined graft copolymers: From controlled synthesis to multipurpose applications. *Chemical Society Reviews* 2011; 40:1282-95.

111. Gao H, Matyjaszewski K. Synthesis of molecular brushes by "Grafting onto" method: A combination of ATRP and click reactions. *J Am Chem Soc* 2007; 129(20):6633-9.
112. Deng Y, Zhang S, Lu G, Huang X. Constructing well-defined star graft copolymers. *Polymer Chemistry* 2013; 4:1289-99.
113. Henze M, Mäde D, Prucker O, Rühle J. "Grafting through": Mechanistic aspects of radical polymerization reactions with surface-attached monomers. *Macromolecules* 2014; 47:2929-37.
114. Hoskins C, Kong Thoo-Lin P, Ping Cheng W. A review on comb-shaped amphiphilic polymers for hydrophobic drug solubilization. *Therapeutic Delivery* 2012; 3(1):59-79.
115. Fan X, Li Z, Loh XJ. Recent development of unimolecular micelles as functional materials and applications. *Polym Chem* 2016; 7(38):5898-919.
116. Palao-Suay R, Gómez-Mascaraquea LG, Aguilera MR, Vázquez-Lasaa B, San Romána J. Self-assembling polymer systems for advanced treatment of cancer and inflammation. *Progress in Polymer Science* 2016; 53:207-48.
117. Kutikov AB, Song J. Biodegradable PEG-based amphiphilic block copolymers for tissue engineering applications. *ACS Biomaterials Science & Engineering* 2015; 1:463-80.
118. Tirelli N, Lutolf MP, Napoli A, Hubbell JA. Poly (ethylene glycol) block copolymers. *Reviews in Molecular Biotechnology* 2002; 90:3-15.
119. Xing G, Lin W, Xiao W, Shaobing Z. Polymer-based drug delivery systems for cancer treatment. *Journal of Polymer Science, Part a: Polymer Chemistry* 2016; 54:3525-50.
120. Gao N, Chen Z, Xiao X, Ruan C, Mei L, Liu Z, Zeng X. Surface modification of paclitaxel-loaded tri-block copolymer PLGA-b-PEG-b-PLGA nanoparticles with protamine for liver cancer therapy. *Journal of Nanoparticle Research* 2015; 14:347.
121. Leiro V, Garcia JP, Moreno P, Spencer AP, Fernandez-Villamarin M, Riguera R, Fernandez-Megia E, Pego AP. Biodegradable PEG–dendritic block copolymers: Synthesis and biofunctionality assessment as vectors of siRNA. *Journal of Materials Chemistry B* 2017; 5:4901-.
122. Quadir MA, Morton SW, Deng ZJ, Shopsowitz KE, Murphy RP, Epps TH, Hammond PT. PEG–Polypeptide block copolymers as pH-responsive endosome- solubilizing drug nanocarriers. *Molecular Pharmaceutics* 2014; 11:2420-30.

123. Laskar P, Saha B, Ghosh SK, Dey J. PEG based random copolymer micelles as drug carriers: The effect of hydrophobe content on drug solubilization and cytotoxicity. *Rsc Advances* 2015; 5:16265-76.
124. Ma Y, Zheng Y, Liu K, Tian G, Tian Y, Xu L, Yan F, Huang L, Mei L. Nanoparticles of poly(lactide-co-glycolide)-d-a-tocopheryl polyethylene glycol 1000 succinate random copolymer for cancer treatment. *Nanoscale Research Letters* 2010; 5:1161-9.
125. Laskar P, Dey J, Ghosh SK. Spontaneously formed redox- and pH-sensitive polymersomes by mPEG based cytocompatible random copolymers. *Journal of Colloid and Interface Science* 2017; 501:22-33.
126. Laskar P, Dey J, Ghosh SK. Evaluation of zwitterionic polymersomes spontaneously formed by pH-sensitive and biocompatible PEG based random copolymers as drug delivery systems. *Colloids and Surfaces B: Biointerfaces* 2016; 139:107-16.
127. Martin C, Dolmazon E, Moylan K, Fowley C, McHale A, Callan J, Callan B. A charge neutral, size tuneable polymersome capable of high biological encapsulation efficiency and cell permeation. *Int J Pharm* 2015; 481:1-8.
128. Martin C, Marino N, Curran C, McHale AP, Callan JF, Callan B. Cholesteryl to improve the cellular uptake of polymersomes within HeLa cells. *Int J Pharm* 2016 09/10; 511(1):570-8.
129. Shao Y, Jia Y, Shi C, Luo J, Zhu XX. Block and random copolymers bearing cholic acid and oligo (ethylene glycol) pendant groups: Aggregation, thermosensitivity, and drug loading. *Biomacromolecules* 2014; 15:1837-44.
130. Cho HY, Srinivasan A, Hong J, Hsu E, Liu S, Shrivats A, Kwak D, Bohaty AK, Paik H, Hollinger JO, et al. Synthesis of biocompatible PEG-based star polymers with cationic and degradable core for siRNA delivery. *Biomacromolecules* 2011; 12:3478-86.
131. Sulistio A, Lowenthal J, Blencowe A, Bongiovanni MN, Ong L, Gras SL, Zhang X, Qiao GG. Folic acid conjugated amino acid-based star polymers for active targeting of cancer cells. *Biomacromolecules* 2011; 12:3469-77.
132. Jukarainen HJ, Clarson SJ, Seppälä JV, Retzinger GS, Ruohonen JK. Block and graft copolymers of poly (ethylene glycol) and poly (dimethylsiloxane) for blood contacting biomedical materials applications. *Silicon* 2012; 4:231-8.
133. Yuan Z, Huang J, Liu J, Cheng S, Zhuo R, Li F. PEG-detachable and acid-labile cross-linked micelles based on orthoester linked graft copolymer for paclitaxel release. *Nanotechnology* 2011; 22:335601.

134. Logie J, Owen SC, McLaughlin CK, Shoichet MS. PEG-graft density controls polymeric nanoparticle micelle stability. *Chemistry of Materials* 2014; 26:2847-55.
135. Maksym P, Neugebauer D. Self-assembling polyether-b-polymethacrylate graft copolymers loaded with indomethacin. *International Journal of Polymeric Materials and Polymeric Biomaterials* 2017 05/03; 66(7):317-25.
136. Masamichi N, Jun A, Teruo O. Polymeric micelles with stimuli-triggering systems for advanced cancer drug targeting. *Journal of Drug Targeting* 2014; 22(7):584-99.
137. Movassaghian S, Merkel OM, Torchilin VP. Applications of polymer micelles for imaging and drug delivery. *WIREs Nanomedicine and Nanobiotechnology* 2015; 7:691-707.
138. Ahmad Z, Shah A, Siddiq M, Kraatz H. Polymeric micelles as drug delivery vehicles. *RSC Advances* 2014; 4:17028-38.
139. Yang L, Wu X, Liu F, Duan Y, Li S. Novel biodegradable polylactide/poly (ethylene glycol) micelles prepared by direct dissolution method for controlled delivery of anticancer drugs. *Pharm Res* 2009 10/01; 26(10):2332-42.
140. Kulthe SS, Choudhari YM, Inamdar NN, Mourya V. Polymeric micelles: Authoritative aspects for drug delivery. *Designed Monomers and Polymers* 2012; 15(5):465-521.
141. Van Butsele K, Sibret P, Fustin CA, Gohy JF, Passirani C, Benoit J-, Jerome R, Jerome C. Synthesis and pH-dependent micellization of diblock copolymer mixtures. *J Colloid Interface Sci* 2009 01/15; 329(2):235-43.
142. Jones M, Leroux J. Polymeric micelles- a new generation of colloidal drug carriers. *European Journal of Pharmaceutics and Biopharmaceutics* 1999; 48:101-11.
143. Ai X, Zhong L, Niu H, He Z. Thin-film hydration preparation method and stability test of DOX-loaded disulfide-linked polyethylene glycol 5000-lysine-di-tocopherol succinate nanomicelles. *Asian Journal of Pharmaceutical Sciences* 2014 10/01; 9(5):244-50.
144. Aliabadi HM, Lavasanifar A. Polymeric micelles for drug delivery. *Expert Opinion on Drug Delivery* 2006; 3(1):139-62.
145. Kedar U, Phutane P, Shidhaye S, Kadam V. Advances in polymeric micelles for drug delivery and tumor targeting. *Nanomedicine: Nanotechnology, Biology, and Medicine* 2010; 6:714-29.
146. Batrakova EV, Bronich TK, Vetro JA, Kabanov AV. Polymer micelles as drug carriers. In: *Nanoparticulates as drug carriers*. 2006.

147. Zhang Y, Huang Y, Li S. Polymeric micelles: Nanocarriers for cancer-targeted drug delivery. *AAPS PharmSciTech* 2014; 15(4):862-71.
148. Wiradharma N, Zhang Y, Venkataraman S, Hedrick JL, Yanga YY. Self-assembled polymer nanostructures for delivery of anticancer therapeutics. *Nano Today* 2009; 4:302-17.
149. Xiao-Bing X, Ziyad B, Ommoleila M, Afsaneh L. Amphiphilic block co-polymers: Preparation and application in nanodrug and gene delivery. *Acta Biomaterialia* 2012; 8:2017-33.
150. Discher DE, Ortiz V, Srinivas G, Klein ML, Kim Y, Christian D, Cai S, Photos P, Ahmed F. Emerging applications of polymersomes in delivery: From molecular dynamics to shrinkage of tumors. *Progress in Polymer Science* 2007 August 1; 32(8-9): 838–857 2007; 32(8-9):838-57.
151. Opsteen JA, Cornelissen, Jeroen J. L. M., van Hest, Jan C. M. Block copolymer vesicles. *Pure and Applied Chemistry* 2004; 76(7-8):1309-19.
152. LoPresti C, Lomas H, Massignani M, Smart T, Battaglia G. Polymersomes: Nature inspired nanometer sized compartments. *Journal of Materials Chemistry* 2009; 19(22):3576-90.
153. Rangelov S, Pispas S, editors. *Polymer and polymer-hybrid nanoparticles*. Boca Raton [etc.]: CRC Press. 2014.
154. Kita-Tokarczyk K, Grumelard J, Haefele T, Meier W. Block copolymer vesicles—using concepts from polymer chemistry to mimic biomembranes. *Polymer* 2005; 46:3540-63.
155. Napoli A, Boerakker MJ, Tirelli N, Nolte RJM, Sommerdijk NAJM, Hubbell JA. Glucose-oxidase based self-destructing polymeric vesicles. *Langmuir* 2004 04/01; 20(9):3487-91.
156. Lee JC, Bermudez H, Discher BM, Sheehan MA, Won Y, Bates FS, Discher DE. Preparation, stability, and in vitro performance of vesicles made with diblock copolymers. *Biotechnology and Bioengineering* 2001; 73(2):135-45.
157. Bucher P, Fischer A, Luisi PL, Oberholzer T, Walde P. Giant vesicles as biochemical compartments: The use of microinjection techniques. *Langmuir* 1998 05/01; 14(10):2712-21.

158. Yildiz ME, Prud'homme RK, Robb I, Adamson DH. Formation and characterization of polymersomes made by a solvent injection method. *Polym Adv Technol* 2007; 18(6):427-32.
159. Kim MR, Cheong IW. Stimuli-triggered formation of polymersomes from W/O/W multiple double emulsion droplets containing poly(styrene)-block-poly(N-isopropylacrylamide-co-spironaphthoxazine methacryloyl). *Langmuir* 2016 09/13; 32(36):9223-8.
160. Liao J, Wang C, Wang Y, Luo F, Qian Z. Recent advances in formation, properties, and applications of polymersomes. *Current Pharmaceutical Design* 2012; 18:3432-41.
161. Oltra NS, Nair P, Discher DE. From stealthy polymersomes and filomicelles to "Self" peptide-nanoparticles for cancer therapy. *Annual Review of Chemical and Biomolecular Engineering* 2014; 5:281-99.
162. Paschalis A. Amphiphilic copolymers and their applications. *Current Opinion in Colloid & Interface Science* 1996; 1:490-201.
163. Sen Gupta A, von Recum HA. Bioconjugation strategies: Lipids, liposomes, polymersomes and microbubbles. In: R. Narain, editor. *Chemistry of bioconjugates: Synthesis, characterization, and biomedical applications*. First ed. John Wiley & Sons, Inc.; 2014.
164. Lu Y, Park K. Polymeric micelles and alternative nanonized delivery vehicles for poorly soluble drugs. *International Journal of Pharmaceutics* 2013; 453(1):198-214.
165. Liversidge GG, Cundy KC. Particle size reduction for improvement of oral bioavailability of hydrophobic drugs: I. absolute oral bioavailability of nanocrystalline danazol in beagle dogs. *Int J Pharm* 1995 10/17; 125(1):91-7.
166. Kawabata Y, Wada K, Nakatani M, Yamada S, Onoue S. Formulation design for poorly water-soluble drugs based on biopharmaceutics classification system: Basic approaches and practical applications. *Int J Pharm* 2011 11/25; 420(1):1-10.
167. Meier MAR, Aerts SNH, Staal BBP, Rasa M, Schubert US. PEO-b-PCL block copolymers: Synthesis, detailed characterization, and selected micellar drug encapsulation behavior. *Macromolecular Rapid Communications* 2005; 26(24):1918-24.
168. Merisko EM, Liversidge GG. Drug nanoparticles: Formulating poorly water-soluble compounds. *Toxicol Pathol* 2008 01/01; 2018/01; 36(1):43-8.

169. Meyer-Losic F, Nicolazzi C, Quinonero J, Ribes F, Michel M, Dubois V, de Coupade C, Boukaissi M, Chene A, Tranchant I, et al. DTS-108, A novel peptidic prodrug of SN38: *in vivo* efficacy and toxicokinetic studies. *Clin Cancer Res* 2008 04/01; 14(7):2145.
170. Matsumura Y, Hamaguchi T, Ura T, Muro K, Yamada Y, Shimada Y, Shirao K, Okusaka T, Ueno H, Ikeda M, et al. Phase I clinical trial and pharmacokinetic evaluation of NK911, a micelle-encapsulated doxorubicin. *British Journal of Cancer* 2004 10/12; 91:1775.
171. Mathot F, des Rieux A, Ari  n A, Schneider Y, Brewster M, Preat V. Transport mechanisms of mmePEG750P(CL-co-TMC) polymeric micelles across the intestinal barrier. *J Controlled Release* 2007 12/20; 124(3):134-43.
172. Muller R, H., Peters K. Nanosuspensions for the formulation of poorly soluble drugs: I. preparation by a size-reduction technique. *Int J Pharm* 1998 01/26; 160(2):229-37.
173. Nagano T, Yasunaga M, Goto K, Kenmotsu H, Koga Y, Kuroda J, Nishimura Y, Sugino T, Nishiwaki Y, Matsumura Y. Synergistic antitumor activity of the SN-38-incorporating polymeric micelles NK012 with S-1 in a mouse model of non-small cell lung cancer. *International Journal of Cancer* 2010; 127(11):2699-706.
174. Photos PJ, Bacakova L, Discher B, Bates FS, Discher DE. Polymer vesicles in vivo: Correlations with PEG molecular weight. *Journal of Controlled Release* 2003; 90:323-34.
175. Liu G, Chen C, Ji J. Biocompatible and biodegradable polymersomes as delivery vehicles in biomedical applications. *Soft Matter*, 2012, 8, 8811–8821 2012; 8:8811-21.
176. Saito N, Okada T, Toba S, Miyamoto S, Takaoka K. New synthetic absorbable polymers as BMP carriers: Plastic properties of poly-D,L-lactic acid-polyethylene glycol block copolymers. *J Biomed Mater Res* 1999; 47(1):104-10.
177. Hu X, Zhang Y, Xie Z, Jing X, Bellotti A, Gu Z. Stimuli-responsive polymersomes for biomedical applications. *Biomacromolecules* 2017; 18(3):649-73.
178. Biswas S, Kumari P, Lakhani PM, Ghosh B. Recent advances in polymeric micelles for anti-cancer drug delivery. *European Journal of Pharmaceutical Sciences* 2016; 83:184-202.
179. Jhaveri AM, Torchilin VP. Multifunctional polymeric micelles for delivery of drugs and siRNA. *Frontiers in Pharmacology* 2014 03/31; 5:77.

180. Fan W, Wang Y, Dai X, Shi L, Mckinley D, Tan C. Reduction-responsive crosslinked micellar nanoassemblies for tumor-targeted drug delivery. *Pharm Res* 2015; 32(4):1325-40.
181. Talelli M, Hennink WE. Thermosensitive polymeric micelles for targeted drug delivery. *Nanomedicine (London)* 2011; 6(7):1245-55.
182. Feng A, Yuan J. Smart nanocontainers: Progress on novel stimuli-responsive polymer vesicles. *Macromol Rapid Commun* 2014; 35(8):767-79.
183. Barhoumi A, Liu Q, Kohane DS. Ultraviolet light-mediated drug delivery: Principles, applications, and challenges. *J Control Release* 2015; 219:31-42.
184. Wang X, Wang Y, Chen Z, Shin D. Advances of cancer therapy by nanotechnology. *Cancer Research and Treatment* 2009; 41(1):1.
185. Cabane E, Malinova V, Meier W. Synthesis of photocleavable amphiphilic block copolymers: Toward the design of photosensitive nanocarriers. *Macromolecular Chemistry and Physics* 2010; 211(17):1847-56.
186. Cabane E, Malinova V, Menon S, Palivan CG, Meier W. Photoresponsive polymersomes as smart, triggerable nanocarriers. *Soft Matter* 2011; 7(19):9167-76.
187. Deng L, Ren J, Li J, Leng J, Qu Y, Lin C, Shi D. Magnetothermally responsive star-block copolymeric micelles for controlled drug delivery and enhanced thermo-chemotherapy. *Nanoscale* 2015; 7(21):9655-63.
188. Hussein GA, Pitt WG. Ultrasonic-activated micellar drug delivery for cancer treatment. *J Pharm Sci* 2009 03/01; 98(3):795-811.
189. Ji G, Yang J, Chen J. Preparation of novel curcumin-loaded multifunctional nanodroplets for combining ultrasonic development and targeted chemotherapy. *Int J Pharm* 2014 05/15; 466(1):314-20.
190. Du L, Jin Y, Zhou W, Zhao J. Ultrasound-triggered drug release and enhanced anticancer effect of doxorubicin-loaded poly(D,L-lactide-co-glycolide)-methoxy-poly(ethylene glycol) nanodroplets. *Ultrasound Med Biol* 2011 08/01; 37(8):1252-8.
191. Nomikou N, Li YS, McHale AP. Ultrasound-enhanced drug dispersion through solid tumours and its possible role in aiding ultrasound-targeted cancer chemotherapy. *Cancer Lett* 2010 02/01; 288(1):94-8.

192. Ghoroghchian PP, Frail PR, Susumu K, Blessington D, Brannan AK, Bates FS, Chance B, Hammer DA, Therien MJ. Near-infrared-emissive polymersomes: Self-assembled soft matter for in vivo optical imaging. *Proc Natl Acad Sci U S A* 2005 02/22; 102(8):2922-7.
193. Torchilin VP. Polymeric contrast agents for medical imaging. *Curr Pharm Biotechnol* 2000 Sep; 1(2):183-215.
194. Nishiyama N, Kataoka K. Current state, achievements, and future prospects of polymeric micelles as nanocarriers for drug and gene delivery. *Pharmacol Ther* 2006; 112(3):630-48.
195. Escobedo JO, Rusin O, Lim S, Strongin RM. NIR dyes for bioimaging applications. *Current Opinion in Chemical Biology* 2010; 14(1):64-70.
196. Lee SY, Lee H, In I, Park SY. pH/redox/photo responsive polymeric micelle via boronate ester and disulfide bonds with spiropyran-based photochromic polymer for cell imaging and anticancer drug delivery. *European Polymer Journal* 2014 08/01; 57:1-10.
197. Vatansever F, Chandran R, Sadasivam M, Chiang LY, Hamblin MR. Multi-functionality in theranostic nanoparticles: Is more always better? *J Nanomed Nanotechnol* 2012 Sep 24; 3(8):10.4172/2157,7439.1000e120.
198. Xiao Y, Hong H, Javadi A, Engle JW, Xu W, Yang Y, Zhang Y, Barnhart TE, Cai W, Gong S. Multifunctional unimolecular micelles for cancer-targeted drug delivery and positron emission tomography imaging. *Biomaterials* 2012 Apr; 33(11):3071-82.
199. Huang C, Neoh KG, Xu L, Kang ET, Chiong E. Polymeric nanoparticles with encapsulated superparamagnetic iron oxide and conjugated cisplatin for potential bladder cancer therapy. *Biomacromolecules* 2012 08/13; 13(8):2513-20.
200. Bae Y, Jang WD, Nishiyama N, Fukushima S, Kataoka K. Multifunctional polymeric micelles with folate-mediated cancer cell targeting and pH-triggered drug releasing properties for active intracellular drug delivery. *Mol Biosyst* 2005 Sep; 1(3):242-50.
201. Duncan R. The dawning era of polymer therapeutics. *Nature Reviews Drug Discovery* 2003 05/01; 2:347.
202. Matsumura Y, Maeda H. A new concept for macromolecular therapeutics in cancer chemotherapy: Mechanism of tumoritropic accumulation of proteins and the antitumor agent smancs. *Cancer Res* 1986; 46(12 Pt 1):6387-92.
203. Stolnik S, Illum L, Davis SS. Long circulating microparticulate drug carriers. *Adv Drug Deliv Rev* 1995 09/01; 16(2):195-214.

204. Seymour LW, Duncan R, Strohalm J, Kopecek J. Effect of molecular weight (mw) of N-(2-hydroxypropyl) methacrylamide copolymers on body distribution and rate of excretion after subcutaneous, intraperitoneal, and intravenous administration to rats. *J Biomed Mater Res* 1987 Nov; 21(11):1341-58.
205. Yuan F, Dellian M, Fukumura D, Leunig M, Berk DA, Torchilin VP, Jain RK. Vascular permeability in a human tumor xenograft: Molecular size dependence and cutoff size. *Cancer Res* 1995 Sep 1; 55(17):3752-6.
206. Simone EA, Dziubla TD, Muzykantov VR. Polymeric carriers: Role of geometry in drug delivery. *Expert Opin Drug Deliv* 2008 Dec; 5(12):1283-300.
207. Geng Y, Dalhaimer P, Cai S, Tsai R, Tewari M, Minko T, Discher DE. Shape effects of filaments versus spherical particles in flow and drug delivery. *Nature Nanotechnology* 2007 03/25; 2:249.
208. Fang J, Nakamura H, Maeda H. The EPR effect: Unique features of tumor blood vessels for drug delivery, factors involved, and limitations and augmentation of the effect. *Adv Drug Deliv Rev* 2011 Mar 18; 63(3):136-51.
209. Ishida O, Maruyama K, Tanahashi H, Iwatsuru M, Sasaki K, Eriguchi M, Yanagie H. Liposomes bearing polyethyleneglycol-coupled transferrin with intracellular targeting property to the solid tumors in vivo. *Pharm Res* 2001 07/01; 18(7):1042-8.
210. Willis M, Forssen E. Ligand-targeted liposomes. *Adv Drug Deliv Rev* 1998; 29(3):249-71.
211. Nobs L, Buchegger F, Gurny R, Allemann E. Current methods for attaching targeting ligands to liposomes and nanoparticles. *J Pharm Sci* 2004 08/01; 93(8):1980-92.
212. Qian X, Long L, Shi Z, Liu C, Qiu M, Sheng J, Pu P, Yuan X, Ren Y, Kang C. Star-branched amphiphilic PLA-b-PDMAEMA copolymers for co-delivery of miR-21 inhibitor and doxorubicin to treat glioma. *Biomaterials* 2014 FEB; 35(7):2322-35.
213. Bian J, Hao Y, He J, Zhang W, Zhang M, Ni P. Synthesis and characterization of a biodegradable ABC triblock terpolymer as co-delivery carrier of doxorubicin and DNA. *J Polym Sci Part A: Polym Chem* 2014 11/01; 52(21):3005-16.
214. Ahmed F, Pakunlu I R, Brannan A, Bates F, Minko T, Discher E D. Biodegradable polymersomes loaded with both paclitaxel and doxorubicin permeate and shrink tumors, inducing apoptosis in proportion to accumulated drug. *J Controlled Release* 2006; 116:150.

215. Iatrou H, Dimas K, Gkikas M, Tsimblouli C, Sofianopoulou S. Polymersomes from polypeptide containing triblock co- and terpolymers for drug delivery against pancreatic cancer: Asymmetry of the external hydrophilic blocks. *Macromol Biosci* 2014 Sep; 14(9):1222-38.
216. Xu W, Ling P, Zhang T. Polymeric micelles, a promising drug delivery system to enhance bioavailability of poorly water-soluble drugs. *Journal of Drug Delivery* 2013; 2013:1-15.
217. Ji W, Wang B, Fan Q, Xu C, He Y, Chen Y. Chemosensitizing indomethacin-conjugated dextran-based micelles for effective delivery of paclitaxel in resistant breast cancer therapy. *Plos One* 2017 12; 7:e0180037.
218. Pei X, Luo F, Zhang J, Chen W, Jiang C, Liu J. Dehydroascorbic acids-modified polymer micelles target cancer cells to enhance anti-tumor efficacy of paclitaxel. *Scientific Reports* 2017; 7(1):975.
219. Jena S, Sangamwar A. Polymeric micelles: A promising tool for tamoxifen delivery in cancer? *Therapeutic Delivery* 2017; 8(3):109-11.
220. Mao J, Li Y, Wu T, Yuan C, Zeng B, Xu Y, Dai L. A simple dual-pH responsive prodrug-based polymeric micelles for drug delivery. *ACS Applied Materials & Interfaces* 2016; 8(27):17109-17.
221. Sawdon A, Peng C. Polymeric micelles for acyclovir drug delivery. *. Colloids and Surfaces B: Biointerfaces* 2014; 122:738-45.
222. Chang S, Chang H, Tong Y, Chen S, Hsiao F, Lu S, Liaw J. Nonionic polymeric micelles for oral gene DeliveryIn vivo. *Human Gene Therapy* 2004; 15(5):481-193.
223. Li C, Li H, Wang Q, Zhou M, Li M, Gong T, Zhang Z, Sun X. pH-sensitive polymeric micelles for targeted delivery to inflamed joints. *Journal of Controlled Release* 2017; 246:133-41.
224. Singh R, James W, Lillard J. Nanoparticle based targeted drug delivery. *Exp Mol Pathol* 2009; 86:215-23.
225. Muller SS, Wurm FR. Nanovesicles as drug delivery vehicles: Liposomes and polymersomes. In: Shiro Kobayashi, Klaus Mullen, editors. *Encyclopedia of polymeric nanomaterials*. Berlin, Heidelberg: Springer Berlin Heidelberg; 2014. ID: Muller2014.

226. Egli S, Nussbaumer M, Balasubramanian V, Chami M, Bruns N, Palivan C, Meier W. Biocompatible functionalization of polymersome surfaces: A new approach to surface immobilization and cell targeting using polymersomes. *Journal of the American Chemical Society* 2011; 133(12):4476-83.
227. Cagdas M, Sezer AD, Bucak S. Liposomes as potential drug carrier systems for drug delivery. In: Ali Demir Sezer, editor. *Application of nanotechnology in drug delivery*. Rijeka: InTech; 2014.
228. Schmitt C, Lippert A, Bonakdar N, Sandoghdar V, Voll L. Compartmentalization and transport in synthetic vesicles. *Frontiers in Bioengineering and Biotechnology* 2016; 4:19.
229. Chandrawati R, Caruso F. Biomimetic liposome and polymersome-based multi compartmentalized assemblies. *Langmuir* 2012 10/02; 2015/01; 28(39):13798-807.
230. Mohammadi M, Ramezani M, Abnous K, Alibolandi M. Biocompatible polymersomes-based cancer theranostics: Towards multifunctional nanomedicine. *International Journal of Pharmaceutics* 2014; 519(1-2):287-303.
231. Ehlerding E, Goel S, Cai W. Cancer theranostics with $^{64}\text{Cu}/^{177}\text{Lu}$ -loaded liposomes. *European Journal of Nuclear Medicine and Molecular Imaging* 2016; 43(5):938-40.
232. Duzgunes N, de Ilarduya C, Simoes S, Zhdanov R, Konopka K, de Lima M. Cationic liposomes for gene delivery: Novel cationic lipids and enhancement by proteins and peptides. *Current Medicinal Chemistry* 2003; 10(14):1213-20.
233. Pangburn T, Georgiou K, Bates F, Kokkoli E. Targeted polymersome delivery of siRNA induces cell death of breast cancer cells dependent upon Orai3 protein expression. *Langmuir* 2012; 28(35):12816-30.
234. Onaca O, Enea R, Hughes D, Meier W. Stimuli-responsive polymersomes as nanocarriers for drug and gene delivery. *Macromolecular Bioscience* 2009; 9(2):129-39.
235. Cell membrane: Structure and physical properties. In: Valerica Raicu, Aurel Popescu, editors. *Integrated molecular and cellular biophysics*. Dordrecht: Springer Netherlands; 2008. ID: Raicu2008.
236. Li J, Wang X, Zhang T, Wang C, Huang Z, Luo X, Deng Y. A review on phospholipids and their main applications in drug delivery systems. *Asian Journal of Pharmaceutical Sciences* 2015; 10(2):81-98.

237. Nguyen T, Nguyen T, Nguyen D. Development and in vitro evaluation of liposomes using soy lecithin to encapsulate paclitaxel. *International Journal of Biomaterials* 2017; 2017:1-7.
238. Yang T, Cui F, Choi M, Lin H, Chung S, Shim C, Kim D. Liposome formulation of paclitaxel with enhanced solubility and stability. *Drug Delivery* 2007; 14(5):301-8.
239. Li Y, Wang J, Gao Y, Zhu J, Wientjes M, Au J. Relationships between liposome properties, cell membrane binding, intracellular processing, and intracellular bioavailability. *The AAPS Journal* 2011; 13(5):585-97.
240. Akbarzadeh A, Rezaei-Sadabady R, Davaran S, Joo SW, Zarghami N, Hanifepour Y, Samiei M, Kouhi M, Nejati-Koshki K. Liposome: Classification, preparation, and applications. *Nanoscale Research Letters* 2013 01/22; 8(1):102-.
241. Klibanov A, Maruyama K, Torchilin V, Huang L. Amphipathic polyethyleneglycols effectively prolong the circulation time of liposomes. *FEBS Letters* 1990; 268(1):235-7.
242. Nag OK, Awasthi V. Surface engineering of liposomes for stealth behavior. *Pharmaceutics* 2013; 5(4):542.
243. Allen TM, Cullis PR. Liposomal drug delivery systems: From concept to clinical applications. *Advanced Drug Delivery Reviews* 2013; 65:36-48.
244. Chang H, Yeh M. Clinical development of liposome-based drugs: Formulation, characterization, and therapeutic efficacy. *International Journal of Nanomedicine* 2011 12/29; 7:49-60.
245. Lee JS, Feijen J. Polymersomes for drug delivery: Design, formation and characterization. *J Controlled Release* 2012 7/20; 161(2):473-83.
246. Laskar P, Dey J, Banik P, Mandal M, Ghosh S. In vitro drug and gene delivery using random cationic copolymers forming stable and pH-sensitive polymersomes. *Macromolecular Bioscience* 2016; 17(4):1600324.
247. Liu F, Kozlovskaya V, Medipelli S, Xue B, Ahmad F, Saeed M, Cropek D, Kharlampieva E. Temperature-sensitive polymersomes for controlled delivery of anticancer drugs. *Chemistry of Materials* 2015; 27(23):7945-56.
248. Kulkarni P, Halder M, You S, Choi Y, Mallik S. Hypoxia-responsive polymersomes for drug delivery to hypoxic pancreatic cancer cells. *Biomacromolecules* 2016; 17(8):2507-13.

249. Nahire R, Haldar M, Paul S, Ambre A, Meghnani V, Layek B, Katti K, Gange K, Singh J, Sarkar K, et al. Multifunctional polymersomes for cytosolic delivery of gemcitabine and doxorubicin to cancer cells. *Biomaterials* 2014; 35(24):6482-97.
250. Colley H, Hearnden V, Avila-Olias M, Cecchin D, Canton I, Madsen J, MacNeil S, Warren N, Hu K, McKeating J, et al. Polymersome-mediated delivery of combination anticancer therapy to head and neck cancer cells: 2D and 3D in vitro evaluation. *Molecular Pharmaceutics* 2014; 11(4):1176-88.
251. Bleul R, Thiermann R, Maskos M. Techniques to control polymersome size. *Macromolecules* 2015; 48(20):7396-409.
252. Discher DE, Ahmed F. Polymersomes. *Annu Rev Biomed Eng* 2006 08/01; 2018/01; 8(1):323-41.
253. Brinkhuis RP, Rutjes, Floris P. J. T., van Hest, Jan C. M. Polymeric vesicles in biomedical applications. *Polymer Chemistry* 2011; 2:1449-62.
254. Dan K, Rajdev P, Deb J, Jana SS, Ghosh S. Remarkably stable amphiphilic random copolymer assemblies: A structure property relationship study. *Journal of Polymer Science Part A: Polymer Chemistry* 2013; 51(22):4932-43.
255. Honglawan A, Ni H, Weissman D, Yang S. Synthesis of random copolymer based pH-responsive nanoparticles as drug carriers for cancer therapeutics. *Polym.Chem.* 2013; 4(13):3667-75.
256. Zhu X, Liu M. Self-assembly and morphology control of newl-glutamic acid-based amphiphilic random copolymers: Giant vesicles, vesicles, spheres, and honeycomb film. *Langmuir* 2011; 27(21):12844-50.
257. Dey S, Dan K, Das M, Saha S, Das P, Ghosh S, Jana S. Amphiphilic random copolymer vesicle induces differentiation of mouse C2C12 myoblasts. *Biomaterials Science* 2013; 1(12):1211-5.
258. Hirai Y, Terashima T, Takenaka M, Sawamoto M. Precision self-assembly of amphiphilic random copolymers into uniform and self-sorting nanocompartments in water. *Macromolecules* 2016; 49(14):5084-91.
259. Guan L, Rizzello L, Battaglia G. Polymersomes and their applications in cancer delivery and therapy. *Nanomedicine* 2015; 10(17):2757-80.
260. Sadzuka Y, Nakade A, Hiram R, Miyagishima A, Nozawa Y, Hirota S, Sonobe T. Effects of mixed polyethyleneglycol modification on fixed aqueous layer thickness and

- antitumor activity of doxorubicin containing liposome. *Int J Pharm* 2002 May 15; 238(1-2):171-80.
261. Elorza B, Elorza M, Frutos G, Chantres J. Characterization of 5-fluorouracil loaded liposomes prepared by reverse-phase evaporation or freezing-thawing extrusion methods: Study of drug release. *Biochim Biophys Acta* 1993; 1153(2):135-142.
 262. Patil YP, Jadhav S. Novel methods for liposome preparation. *Chem Phys Lipids* 2014 01/01; 177:8-18.
 263. Cortesi R. Preparation of liposomes by reverse-phase evaporation using alternative organic solvents. *J Microencapsul* 1999 01/01; 16(2):251-6.
 264. Sardan M, Kilinc M, Genc R, Tekinay A, Guler M. (2013). Cell penetrating peptide amphiphile integrated liposomal systems for enhanced delivery of anticancer drugs to tumor cells. , 166, p.269. *Faraday Discussions* 2013; 166:269-83.
 265. Colletier JP, Chaize B, Winterhalter M, Fournier D. Protein encapsulation in liposomes: Efficiency depends on interactions between protein and phospholipid bilayer. *BMC Biotechnol* 2002 May 10; 2:9.
 266. Thompson A, Couchoud A, Singh H. Comparison of hydrophobic and hydrophilic encapsulation using liposomes prepared from milk fat globule-derived phospholipids and soya phospholipids. *Dairy Science and Technology* 2009; 89(1):99-113.
 267. Hillaireau H, Couvreur P. Nanocarriers' entry into the cell: Relevance to drug delivery. *Cellular and Molecular Life Sciences* 2009; 66(17):2873-96.
 268. Sams S, Sheikh T, Haddadi A. Effects of size and surface charge of polymeric nanoparticles on in vitro and in vivo applications. *Journal of Biomaterials and Nanobiotechnology* 2016; 7:91-108.
 269. Vercauteren D, Vandenbroucke R, Jones A, Rejman J, Demeester J, De Smedt S, Sanders N, Braeckmans K. The use of inhibitors to study endocytic pathways of gene carriers: Optimization and pitfalls. *Molecular Therapy* 2010; 18(3):561-9.
 270. Swaminathan S, Fowley C, McCaughan B, Cusido J, Callan J, Raymo F. Intracellular guest exchange between dynamic supramolecular hosts. *Journal of the American Chemical Society* 2014; 136(22):7907-13.
 271. Immordino ML, Dosio F, Cattell L. Stealth liposomes: Review of the basic science, rationale, and clinical applications, existing and potential. *International Journal of Nanomedicine* 2006 09; 1(3):297-315.

272. Liu H, Doane T, Cheng Y, Lu F, Srinivasan S, Zhu J, Burda C. Control of surface ligand density on PEGylated gold nanoparticles for optimized cancer cell uptake. *Particle & Particle Systems Characterization* 2014; 32(2):197-204.
273. Pelaz B, del Pino P, Maffre P, Hartmann R, Gallego M, Rivera-Fernández S, de la Fuente J, Nienhaus G, Parak W. Surface functionalization of nanoparticles with polyethylene glycol: Effects on protein adsorption and cellular uptake. *ACS Nano* 2015; 9(7):6996-7008.
274. Pozzi D, Colapicchioni V, Caracciolo G, Piovesana S, Capriotti A, Palchetti S, De Grossi S, Riccioli A, Amenitsch H, Laganà A. Effect of polyethyleneglycol (PEG) chain length on the bio–nano-interactions between PEGylated lipid nanoparticles and biological fluids: From nanostructure to uptake in cancer cells. *Nanoscale* 2014; 6(5):2782-92.
275. Miller C, Bondurant B, McLean S, McGovern K, O'Brien D. Liposome–Cell interactions in vitro: Effect of liposome surface charge on the binding and endocytosis of conventional and sterically stabilized liposomes. *Biochemistry* 1998; 37(37):12875-83.
276. Marqués-Gallego P, de Kroon A. Ligation strategies for targeting liposomal nanocarriers. *BioMed Research International* 2014; 2014:1-12.
277. van den Hoven J, Nemes R, Metselaar J, Nuijen B, Beijnen J, Storm G, Szebeni J. Complement activation by PEGylated liposomes containing prednisolone. *European Journal of Pharmaceutical Sciences* 2013; 49(2):265-71.
278. Zhang Q, Lu L, Zhang L, Shi K, Cun X, Yang Y, Liu Y, Gao H, He Q. Dual-functionalized liposomal delivery system for solid tumors based on RGD and a pH-responsive antimicrobial peptide. *Scientific Reports* 2016; 6(1):19800.
279. Ahmed F, Discher D. Self-porating polymersomes of PEG–PLA and PEG–PCL: Hydrolysis-triggered controlled release vesicles. *Journal of Controlled Release* 2004; 96(1):37-53.
280. Chiang W, Huang W, Chang C, Shen M, Shih Z, Huang Y, Lin S, Chiu H. Functionalized polymersomes with outlayered polyelectrolyte gels for potential tumor-targeted delivery of multimodal therapies and MR imaging. *Journal of Controlled Release* 2013; 168(3):280-8.
281. Muppidi K, Pumerantz AS, Wang J, Betageri G. Development and stability studies of novel liposomal vancomycin formulations. *ISRN Pharmaceutics* 2012; 2012:8.
282. Hruby M, Filippov K S, Stepanek P. Smart polymers in drug delivery systems on crossroads: Which way deserves following? *European Polymer Journal* 2015; 65:82-97.

283. Brun-Graeppi AKAS, Richard C, Bessodes M, Scherman D, Merten O. Cell microcarriers and microcapsules of stimuli-responsive polymers. *J Controlled Release* 2011 2/10; 149(3):209-24.
284. Ashley CE, Carnes EC, Phillips GK, Padilla D, Durfee PN, Brown PA, Hanna TN, Liu J, Phillips B, Carter MB, et al. The targeted delivery of multicomponent cargos to cancer cells by nanoporous particle-supported lipid bilayers. *Nat Mater* 2011; 10(5):389-97.
285. Zayats M, Kanwar M, Ostermeier M, Searson P. Tuning protein recognition at the molecular level. *Macromolecules* 2011; 44:3966-72.
286. Ramasamy T, Ruttala HB, Gupta B, Poudel BK, Choi HG, Yong CS, Kim JO. Smart chemistry-based nanosized drug delivery systems for systemic applications: A comprehensive review. *J Control Release* 2017 Jul 28; 258:226-53.
287. Furgeson D, Dreher M, Chilkoti A. Structural optimisation of a 'smart' doxorubicin-polypeptide conjugate for thermally targeted delivery of solid tumors. *J Controlled Release* 2006; 110:362-9.
288. Hruby M, Konak C, Ulbrich K. Polymeric micellar pH-sensitive drug delivery system for doxorubicin. *J Controlled Release* 2005; 103:137-48.
289. Banerjee S, Chen D. A multifunctional magnetic nanocarrier bearing fluorescent dye for targeted drug delivery by enhanced two photon triggered release. *Nanotechnology* 2009; 20:185103-12.
290. Murdan S. Electro responsive drug delivery from hydrogels. *J Controlled Release* 2003; 92:1-17.
291. Nomikou N, Arthur C, Sterrett C, McCaughan B, Callan JF, McHale AP. Ultrasound enhanced photoactivation of indocyanine green in vitro and in vivo - implications for targeted cancer therapy. *Chem.Med.Chem.* 2012; 7:1465-71.
292. Glangchi L, Caldorera-Moore M, Shi L, Roy K. Nanoimprint lithography based fabrication of shape specific enzymatically-triggered smart nanoparticles. *J Controlled Release* 2008; 125:263-72.
293. McCoy C, Rooney C, Edwards C, Jones D, Gorman S. Light-triggered molecule-scale drug dosing devices. *J Am Chem Soc* 2007; 129:9572-3.
294. D'Souza S. A review of in vitro drug release test methods for nano-sized dosage forms. *Advances in Pharmaceutics* 2014; 2014:12.

295. Xing Q, Li N, Chen D, Sha W, Jiao Y, Qi X, Xu Q, Lu J. Light-responsive amphiphilic copolymer coated nanoparticles as nanocarriers and real-time monitors for controlled drug release. *Journal of Materials Chemistry B* 2014; 2:1182-9.
296. Li X, Hao N, Chen H, Xu J. Tumor-marker-mediated 'on-demand' drug release and real time monitoring system based on multifunctional mesoporous silica nanoparticles. *Anal Chem* 2014; 86:10239-45.
297. Lai J, Shah P B, Garfunkel E, Lee K. Versatile fluorescence resonance energy transfer based mesoporous silica nanoparticles for real-time monitoring of drug release. *ACS Nano* 2013; 7:2741-50.
298. Cardullo RA. Principles of non-radiative FRET: The spectroscopic ruler. *Microscopy and Analysis (UK)* 2002; 88:19-21.
299. Linlin M, Fan Y, Jie Z. Application of fluorescence resonance energy transfer in protein. *J Mol Struct* 2014; 1077:87-100.
300. Day RN, Davidson MW. Fluorescent proteins for FRET microscopy: Monitoring protein interactions in living cells. *Bioessays* 2012; 34(5):341-50.
301. Honey J, Rijo J, Anju A, Anoop K. Smart polymers for the controlled delivery of drugs - a concise overview. *Acta Pharmaceutica Sinica B* 2014; 4:120-7.
302. Karimi M, Sahandi Zangabad P, Baghaee-Ravari S, Ghazadeh M, Mirshekari H, Hamblin MR. Smart nanostructures for cargo delivery: Uncaging and activating by light. *J Am Chem Soc* 2017 04/05; 139(13):4584-610.
303. Swaminathan S. Photoresponsive polymer nanocarriers with multifunctional cargo. *Chem Soc Rev* 2014; 43:4167-78.
304. Lukyanov B, Lukyanova M. Syropyrans: Synthesis, properties and application. *Chem.Heterocycl.Comp* 2005; 41:281-311.
305. Zhou Q, Zhu Y, Sheng P, Wu Z, Cai Q. A highly selective and reversible fluorescent Cu²⁺ and S²⁻ probe under physiological conditions in live cells. *RSC Advances* 2014; 4(87):46951-4.
306. Balter M, Hammarson M, Remon P, Li S, Gale N, Brown T, Andreasson J. Reversible energy transfer switching on a DNA scaffold. *J Am Chem Soc* 2015; 137:2444-7.
307. Loudet A, Burgess K. BODIPY dyes and their derivatives: Syntheses and spectroscopic properties. *Chem Rev* 2007 11/01; 107(11):4891-932.

308. Tomasulo M, Deniz E, Alvarado RJ, Raymo FM. Photoswitchable fluorescent assemblies based on hydrophilic BODIPY-Spiropyran conjugates. *J Phys Chem C* 2008 05/01; 112(21):8038-45.
309. Yu G, Zhao R, Wu D, Zhang F, Shao L, Zhou J, Yang J, Tang G, Chen X, Huang F. Pillar[5]arene-based amphiphilic supramolecular brush copolymers: Fabrication, controllable self-assembly and application in self-imaging targeted drug delivery. *Polym.Chem.* 2016; 7(40):6178-88.
310. Jiang L, Huang X, Chen D, Yan H, Li X, Du X. Supramolecular vesicles coassembled from disulfide-linked benzimidazolium amphiphiles and carboxylate-substituted pillar[6]arenes that are responsive to five stimuli. *Angew Chem Int Ed Engl* 2017 Mar 1; 56(10):2655-9.
311. World Health Organisation. Cancer fact sheet. February 2017.
312. Reichert JM, Wenger JB. Development trends for new cancer therapeutics and vaccines. *Drug Discov Today* 2008 Jan; 13(1-2):30-7.
313. Treatment for cancer London: Cancer Research UK; c2017 [cited 2017]. Available from: <http://www.cancerresearchuk.org/about-cancer/cancer-in-general/treatment>.
314. Gillet J, Gottesman MM. Mechanisms of multidrug resistance in cancer. In: Jun Zhou, editor. Multi-drug resistance in cancer. Totowa, NJ: Humana Press; 2010. ID: Gillet2010.
315. Miller K, Siegel R, Lin C, Mariotto A, Kramer J, Rowland J, Stein K, Alteri R, Jemal A. Cancer treatment and survivorship statistics, 2016. *CA: A Cancer Journal for Clinicians* 2016; 66(4):271-89.
316. Yang F, Teves SS, Kemp CJ, Henikoff S. Doxorubicin, DNA torsion, and chromatin dynamics. *Biochim Biophys Acta* 2014; 1845(1):84-9.
317. Noordhuis P, Holwerda U, Van der Wilt C, Van Groenigen C, Smid K, Meijer S, Pinedo H, Peters G. 5-fluorouracil incorporation into RNA and DNA in relation to thymidylate synthase inhibition of human colorectal cancers. *Annals of Oncology* 2004; 15(7):1025-32.
318. Amin A, Gali-Muhtasib H, Ocker M, Schneider-Stock R. Overview of major classes of plant-derived anticancer drugs. *Int J Biomed Sci* 2009 Mar; 5(1):1-11.
319. Sutradhar K, Amin M. Nanotechnology in cancer drug delivery and selective targeting. *ISRN Nanotechnology* 2014; 2014:1-12.

320. Misra R, Acharya S, Sahoo SK. Cancer nanotechnology: Application of nanotechnology in cancer therapy. *Drug Discov Today* 2010 Oct; 15(19-20):842-50.
321. Zhang M, Liu E, Cui Y, Huang Y. Nanotechnology-based combination therapy for overcoming multidrug-resistant cancer. *Cancer Biology and Medicine* 2017; 14(3):212-27.
322. Persidis A. Cancer multidrug resistance. *Nat Biotechnol* 1999 Jan; 17(1):94-5.
323. Filipits M. Mechanisms of cancer: Multidrug resistance. *Drug Discovery Today: Disease Mechanisms* 2004 11/01; 1(2):229-34.
324. Luo D, Carter K, Miranda D, Lovell J. Chemophototherapy: An emerging treatment option for solid tumors. *Advanced Science* 2017; 4(1):1600106.
325. Making treatment decisions USA: American Chemical Society; c2015 [cited 2017]. Available from: <https://www.cancer.org/treatment/understanding-your-diagnosis/after-diagnosis/making-treatment-decisions.html>.
326. Thorn C, Oshiro C, Marsh S, Hernandez-Boussard T, McLeod H, Klein T, Altman R. Doxorubicin pathways: Pharmacodynamics and adverse effects. *Pharmacogenetics and Genomics* 2011; 21(7):440-6.
327. Minotti G, Menna P, Salvatorelli E, Cairo G, Gianni L. Anthracyclines: Molecular advances and pharmacologic developments in antitumor activity and cardiotoxicity. *Pharmacological Reviews* 2004; 56(2):185-229.
328. Cheung-Ong K, Giaever G, Nislow C. DNA-damaging agents in cancer chemotherapy: Serendipity and chemical biology. *Chemistry & Biology* 2013; 20(5):648-59.
329. Longley D, Harkin D, Johnston P. 5-fluorouracil: Mechanisms of action and clinical strategies. *Nature Reviews Cancer* 2003; 3(5):330-8.
330. Moran RG, Keyomarsi K. Biochemical rationale for the synergism of 5-fluorouracil and folinic acid. *NCI Monogr* 1987; (5)(5):159-63.
331. Scholnik AP, Arnold DJ, Walker WS, Schwenke P, Suhrland LG, Balcueva EP, Dimitrov NV. High-dose folinic acid and 5-fluorouracil in the treatment of advanced colon cancer. *Am J Clin Oncol* 1988 Oct; 11(5):558-63.
332. Prete SP, Turriziani M, Massara MC, De Rossi A, Correale P, De Vecchis L, Torino F, Bonmassar L, Aquino A. Combined effects of 5-fluorouracil, folinic acid and oxaliplatin on the expression of carcinoembryonic antigen in human colon cancer cells:

- Pharmacological basis to develop an active antitumor immunochemotherapy. *Journal of Experimental & Clinical Cancer Research* 2008; 27(1):5.
333. Zhang N, Yin Y, Xu S, Chen W. 5-fluorouracil: Mechanisms of resistance and reversal strategies. *Molecules* 2008; 13(8):1551-69.
 334. Thorn C, Marsh S, Carrillo M, McLeod H, Klein T, Altman R. PharmGKB summary: Fluoropyrimidine pathways. *Pharmacogenetics and Genomics* 2011; 21(4):237-42.
 335. Malhotra V, Perry MC. Classical chemotherapy: Mechanisms, toxicities and the therapeutic window. *Cancer Biology & Therapy* 2003; 2:1-3.
 336. Siddik ZH. Mechanisms of action of cancer chemotherapeutic agents: DNA-interactive alkylating agents and antitumour platinum-based drugs. 2005.
 337. Kondo N, Takahashi A, Ono K, Ohnishi T. DNA damage induced by alkylating agents and repair pathways. *Journal of Nucleic Acids* 2010; 2010:1-7.
 338. Yue Q, Liu X, Guo D. Microtubule-binding natural products for cancer therapy. *Planta Medica* 2010; 76(11):1037-43.
 339. Rivera E, Cianfrocca M. Overview of neuropathy associated with taxanes for the treatment of metastatic breast cancer. *Cancer Chemotherapy and Pharmacology* 2015; 75(4):659-70.
 340. De Iuliis F, Taglieri L, Salerno G, Lanza R, Scarpa S. Taxane induced neuropathy in patients affected by breast cancer: Literature review. *Critical Reviews in Oncology/Hematology* 2015; 96(1):34-45.
 341. Rustum YM. Biochemical rationale for the 5-fluorouracil leucovorin combination and update of clinical experience. *J Chemother* 1990 Feb; 2 Suppl 1:5-11.
 342. Boarman DM, Baram J, Allegra CJ. Mechanism of leucovorin reversal of methotrexate cytotoxicity in human MCF-7 breast cancer cells. *Biochem Pharmacol* 1990 Dec 15; 40(12):2651-60.
 343. DeLap RJ. The effect of leucovorin on the therapeutic index of fluorouracil in cancer patients. *Yale J Biol Med* 1988 Jan-Feb; 61(1):23-34.
 344. Arkenau HT, , Bermann A, , Rettig K, , Strohmeyer G, , Porschen R, , 5-fluorouracil plus leucovorin is an effective adjuvant chemotherapy in curatively resected stage III colon cancer: Long-term follow-up results of the adjCCA-01 trial. *Annals of Oncology* 2003; 14(3):395-9.

345. DeVita V, Chu E. A history of cancer chemotherapy. *Cancer Research* 2008; 68(21):8643-53.
346. Morrison W. Cancer chemotherapy: An annotated history. *Journal of Veterinary Internal Medicine* 2010; 24(6):1249-62.
347. Damon L, Cadman E. Advances in rational combination chemotherapy. *Cancer Investigation* 1986; 4(5):421-44.
348. Hu C, Aryal S, Zhang L. Nanoparticle-assisted combination therapies for effective cancer treatment. *Therapeutic Delivery* 2010; 1(2):323-34.
349. Gadde S. Multi-drug delivery nanocarriers for combination therapy. *MedChemComm* 2015;6(11):1916-29.
350. Lilenbaum R, Herndon J, List M, Desch C, Watson D, Miller A, Graziano S, Perry M, Saville W, Chahinian P, et al. Single-agent versus combination chemotherapy in advanced Non-Small-cell lung cancer: The cancer and leukemia group B (study 9730). *Journal of Clinical Oncology* 2005; 23(1):190-6.
351. Carrick S, Parker S, Thornton C, Gherzi D, Simes J, Wilcken N. (2009). Single agent versus combination chemotherapy for metastatic breast cancer. *Cochrane Database of Systematic Reviews* 2009(3).
352. Chemotherapy drugs and combination regimens UK [cited 2017]. Available from: <https://www.macmillan.org.uk/information-and-support/treating/chemotherapy/drugs-and-combination-regimens>.
353. Gmeiner W, Ghosh S. Nanotechnology for cancer treatment. *Nanotechnology Reviews* 2014; 3(2):111-22.
354. Piktel E, Niemirowicz K, Wątek M, Wollny T, Deptuła P, Bucki R. Recent insights in nanotechnology-based drugs and formulations designed for effective anti-cancer therapy. *Journal of Nanobiotechnology* 2016; 14(1).
355. Xin Y, Yin M, Zhao L, Meng F, Luo L. Recent progress on nanoparticle-based drug delivery systems for cancer therapy. *Cancer Biology & Medicine* 2017; 14(3):228.
356. Nie S. Understanding and overcoming major barriers in cancer nanomedicine. *Nanomedicine (London)* 2010 Jun; 5(4):523-8.
357. Cancer nanotechnology. . In: S. Grobmyer, B. Moudgil, editors. New York: Humana Press.; 2010. .

358. Ni M, Xiong M, Zhang X, Cai G, Chen H, Zeng Q, Yu Z. Poly(lactic-co-glycolic acid) nanoparticles conjugated with CD133 aptamers for targeted salinomycin delivery to CD133(+) osteosarcoma cancer stem cells. *International Journal of Nanomedicine* 2015 03/31; 10:2537-54.
359. Medina O, Zhu Y, Kairemo K. Targeted liposomal drug delivery in cancer. *Current Pharmaceutical Design* 2004; 10(24):2981-9.
360. Deshpande P, Biswas S, Torchilin V. Current trends in the use of liposomes for tumor targeting. *Nanomedicine* 2013; 8(9):1509-28.
361. Cho H, Lai T, Tomoda K, Kwon G. Polymeric micelles for multi-drug delivery in cancer. *AAPS PharmSciTech* 2014; 16(1):10-20.
362. Shin D, Tam Y, Kwon G. Polymeric micelle nanocarriers in cancer research. *Frontiers of Chemical Science and Engineering* 2016; 10(3):348-59.
363. Madaan K, Kumar S, Poonia N, Lather V, Pandita D. Dendrimers in drug delivery and targeting: Drug-dendrimer interactions and toxicity issues. *Journal of Pharmacy & Bioallied Sciences* 2013 11/14; 6(3):139-50.
364. Somani S, Dufès C. Applications of dendrimers for brain delivery and cancer therapy. *Nanomedicine* 2014; 9(15):2403-14.
365. Lopes S, Giuberti C, Rocha T, Ferreira D, Leite E, Oliveira M. Liposomes as carriers of anticancer drugs. In: L. Rangel, editor. *Cancer treatment - conventional and innovative approaches*. InTech; 2013.
366. Yingchoncharoen P, Kalinowski D, Richardson D. Lipid-based drug delivery systems in cancer therapy: What is available and what is yet to come. *Pharmacological Reviews* 2016; 68(3):701-87.
367. Rivera E. Liposomal anthracyclines in metastatic breast cancer: Clinical update. *The Oncologist* 2003; 8(90002):3-9.
368. Krown SE, Northfelt DW, Osoba D, Stewart JS. Use of liposomal anthracyclines in kaposi's sarcoma. *Semin Oncol* 2004 Dec; 31(6 Suppl 13):36-52.
369. Hang Z, Cooper M, Ziora Z. Platinum-based anticancer drugs encapsulated liposome and polymeric micelle formulation in clinical trials. *Biochemical Compounds* 2016; 4(1):1.

370. Jin Y, Li J, Rong LF, Lu XW, Huang Y, Xu SY. Pharmacokinetics and tissue distribution of 5-fluorouracil encapsulated by galactosylceramide liposomes in mice. *Acta Pharmacol Sin* 2005 Feb; 26(2):250-6.
371. Zhigaltsev IV, Maurer N, Akhong QF, Leone R, Leng E, Wang J, Semple SC, Cullis PR. Liposome-encapsulated vincristine, vinblastine and vinorelbine: A comparative study of drug loading and retention. *J Control Release* 2005 May 5; 104(1):103-11.
372. Lee C, Huang Y, Yang C, Huang K. Drug delivery systems and combination therapy by using vinca alkaloids. *Current Topics in Medicinal Chemistry* 2014 12/20; 15(15):1491-500.
373. Hofheinz R, Gnad-Vogt S, Beyer U, Hochhaus A. Liposomal encapsulated anti-cancer drugs. *Anti-Cancer Drugs* 2005; 16(7):691-707.
374. Huwyler J, Drewe J, Krähenbühl S. Tumor targeting using liposomal antineoplastic drugs. *International Journal of Nanomedicine* 2008; 3(1):21-9.
375. Meng J, Guo F, Xu H, Liang W, Wang C, Yang X. Combination therapy using co-encapsulated resveratrol and paclitaxel in liposomes for drug resistance reversal in breast cancer cells in vivo. *Scientific Reports* 2016; 6(1):22390.
376. Walls Z, Gong H, Wilson R. Liposomal coencapsulation of doxorubicin with listeriolysin O increases potency via subcellular targeting. *Molecular Pharmaceutics* 2016; 13(3):1185-90.
377. Camacho K, Menegatti S, Vogus D, Pusuluri A, Fuchs Z, Jarvis M, Zakrewsky M, Evans M, Chen R, Mitragotri S. DAFODIL: A novel liposome-encapsulated synergistic combination of doxorubicin and 5FU for low dose chemotherapy. *Journal of Controlled Release* 2016; 229:154-62.
378. Massing U, Fuxius S. Liposomal formulations of anticancer drugs: Selectivity and effectiveness. *Drug Resistance Updates* 2000 06/01; 3(3):171-7.
379. Discher M B, Won Y, Ege S D, Lee C. M. J, Bates S F, Discher E D, Hammer A D. Polymersomes: Tough vesicles made from diblock copolymers. *Science* 1999; 284:1143.
380. Poschenrieder S, Schiebel S, Castiglione K. Polymersomes for biotechnological applications: Large-scale production of nano-scale vesicles. *Engineering in Life Sciences* 2017; 17(1):58-70.

381. Johnston AH, Dalton PD, Newman TA. Polymersomes, smaller than you think: Ferrocene as a TEM probe to determine core structure. *Journal of Nanoparticle Research* 2010 08/01; 12(6):1997-2001.
382. Rikken R, Engelkamp H, Nolte R, Maan J, van Hest J, Wilson D, Christianen P. Shaping polymersomes into predictable morphologies via out-of-equilibrium self-assembly. *Nature Communications* 2016; 7:12606.
383. Le Meins JF, Schatz C, Lecommandoux S, Sandre O. Hybrid polymer/lipid vesicles: State of the art and future perspectives. *Materials Today* 2013; 16(10):397-402.
384. Peyret A, Ibarboure E, Pippa N, Lecommandoux S. Liposomes in polymersomes: Multicompartment system with temperature-triggered release. *Langmuir* 2017; 33(28):7079-85.
385. Callari M, Wong S, Lu H, Aldrich-Wright J, de Souza P, Stenzel M. Drug induced self-assembly of triblock copolymers into polymersomes for the synergistic dual-drug delivery of platinum drugs and paclitaxel. *Polymer Chemistry* 2017; 8(40):6289-99.
386. Zhu D, Wu S, Hu C, Chen Z, Wang H, Fan F, Qin Y, Wang C, Sun H, Leng X, et al. Folate-targeted polymersomes loaded with both paclitaxel and doxorubicin for the combination chemotherapy of hepatocellular carcinoma. *Acta Biomaterialia* 2017; 58:399-412.
387. Han R, Sun Y, Kang C, Sun H, Wei W. Amphiphilic dendritic nanomicelle-mediated co-delivery of 5-fluorouracil and doxorubicin for enhanced therapeutic efficacy. *Journal of Drug Targeting* 2016; 25(2):140-8.
388. Yang Q, Yang Y, Li L, Sun W, Zhu X, Huang Y. Polymeric nanomedicine for tumor-targeted combination therapy to elicit synergistic genotoxicity against prostate cancer. *ACS Applied Materials & Interfaces* 2015; 7(12):6661-73.
389. Di Martino A, Kucharczyk P, Capakova Z, Humpolicek P, Sedlarik V. Chitosan-based nanocomplexes for simultaneous loading, burst reduction and controlled release of doxorubicin and 5-fluorouracil. *International Journal of Biological Macromolecules* 2017; 102:613-24.
390. Kim H, Kim E, An Y, Choi J, Jang E, Choi E, Kukreja A, Kim M, Kang B, Kim D, et al. A biodegradable polymersome containing bcl-xL siRNA and doxorubicin as a dual delivery vehicle for a synergistic anticancer effect. *Macromolecular Bioscience* 2013; 13(6):745-54.

391. PubChem Compound Database; CID=443939 [Internet]: National Center for Biotechnology Information. [cited Jan. 14, 2018]. Available from: <https://pubchem.ncbi.nlm.nih.gov/compound/443939>.
392. [cited 2017]. Available from: <https://www.mims.co.uk/drugs/cancer/antineoplastics/doxorubicin>.
393. PubChem Compound Database; CID=3385 [Internet]: National Center for Biotechnology Information [cited Jan. 14, 2018]. Available from: <https://pubchem.ncbi.nlm.nih.gov/compound/3385>.
394. [cited 2017] . Available from: <https://www.drugs.com/dosage/fluorouracil.html>.
395. PubChem Compound Database; CID=15150 [Internet]: National Center for Biotechnology Information [cited Jan. 14, 2018]. Available from: <https://pubchem.ncbi.nlm.nih.gov/compound/15150>.
396. [cited 2017]. Available from: <https://www.drugs.com/dosage/leucovorin.html>.
397. Fluorouracil 25 mg/ml Injection: Hospira UK Limited; c2017 [cited 2017]. Available from: <https://www.medicines.org.uk/emc/product/3790>.
398. Griepenburg J, Sood N, Vargo K, Williams D, Rawson J, Therien M, Hammer D, Dmochowski I. Caging metal ions with visible light-responsive nanopolymersomes. *Langmuir* 2015; 31(2):799-807.
399. Kalra A, Campbell R. Development of 5-FU and doxorubicin-loaded cationic liposomes against human pancreatic cancer: Implications for tumor vascular targeting. *Pharmaceutical Research* 2006; 23(12):2809-17.
400. Chao Y, Liang Y, Fang G, Haibing He H, Yao Q, Xu H, Chen Y, Tang X. Biodegradable polymersomes as nanocarriers for doxorubicin hydrochloride: Enhanced cytotoxicity in MCF-7/ADR cells and prolonged blood circulation. *Pharmaceutical Research* 2017; 34(3):610-8.
401. Zheng C, Zheng M, Gong P, Jia D, Zhang P, Shi B, Sheng Z, Ma Y, Cai L. Indocyanine green-loaded biodegradable tumor targeting nanoprobe for in vitro and in vivo imaging. *Biomaterials* 2012; 33(22):5603-9.
402. Sheng Z, Hu D, Xue M, He M, Gong P, Cai L. Indocyanine green nanoparticles for theranostic applications. *Nano-Micro Letters* 2013; 5(3):145-50.

403. Lu F, Pang Z, Zhao J, Jin K, Li H, Pang Q, Zhang L, Pang Z. Angiopep-2-conjugated poly (ethylene glycol)-co-poly(ϵ -caprolactone) polymersomes for dual-targeting drug delivery to glioma in rats. *International Journal of Nanomedicine* 2017; 12:2117-27.
404. Lammers T, Peschke P, Kühnlein R, Subr V, Ulbrich K, Huber P, Hennink W, Storm G. Effect of intratumoral injection on the biodistribution, the therapeutic potential of HPMA copolymer-based drug delivery systems. *Neoplasia* 2006; 8(10):788-95.
405. Torchilin VP. Nanoparticulates as drug carriers. Imperial College Press; 2006.
406. Swain S, Whaley F, Ewer M. Congestive heart failure in patients treated with doxorubicin. *Cancer* 2003; 97(11):2869-79.
407. Volkova M, Russell R. Anthracycline cardiotoxicity: Prevalence, pathogenesis and treatment. *Current Cardiology Reviews* 2012; 7(4):214-20.
408. De Angelis A, Urbanek K, Cappetta D, Piegari E, Ciuffreda L, Rivellino A, Russo R, Esposito G, Rossi F, Berrino L. Doxorubicin cardiotoxicity and target cells: A broader perspective. *Cardio-Oncology* 2016; 2(1).
409. Thomas S, Grami Z, Mehta S, Patel K. Adverse effects of 5-fluorouracil: Focus on rare side effects. *Cancer Cell & Microenvironment* 2016; 3:e1266.
410. Octavia Y, Tocchetti C, Gabrielson K, Janssens S, Crijns H, Moens A. Doxorubicin-induced cardiomyopathy: From molecular mechanisms to therapeutic strategies. *Journal of Molecular and Cellular Cardiology* 2012; 52(6):1213-25.
411. Lyass O, Uziely B, Ben-Yosef R, Tzemach D, Heshing N, Lotem M, Brufman G, Gabizon A. Correlation of toxicity with pharmacokinetics of pegylated liposomal doxorubicin (doxil) in metastatic breast carcinoma. *Cancer* 2000; 89(5):1037-47.
412. Rafiyath S, Rasul M, Lee B, Wei G, Lamba G, Liu D. Comparison of safety and toxicity of liposomal doxorubicin vs. conventional anthracyclines: A meta-analysis. *Experimental Hematology & Oncology* 2012; 1(1):10.
413. Gonzalez-Fajardo L, Mahajan L, Ndaya D, Hargrove D, Manautou J, Liang B, Chen M, Kasi R, Lu X. Reduced in vivo toxicity of doxorubicin by encapsulation in cholesterol-containing self-assembled nanoparticles. *Pharmacological Research* 2016; 107:93-101.
414. Gaitzsch J, Messenger L, Morecroft E, Meier W. Vesicles in multiple shapes: Fine-tuning polymersomes' shape and stability by setting membrane hydrophobicity. *Polymers* 2017; 9(10):483.

415. Alibolandi M, Sadeghi F, Sazmand SH, Shahrokhi SM, Seifi M, Hadizadeh F. Synthesis and self-assembly of biodegradable polyethylene glycol-poly (lactic acid) diblock copolymers as polymersomes for preparation of sustained release system of doxorubicin. *International Journal of Pharmaceutical Investigation* 2015; 5(3):134-41.
416. Gelderblom H, Verweij J, Nooter K, Sparreboom A. Cremophor EL: The drawbacks and advantages of vehicle selection for drug formulation. *Eur J Cancer* 2001 Sep; 37(13):1590-8.
417. Tang J, Kong B, Wu H, Xu M, Wang Y, Wang Y, Zhao D, Zheng G. Carbon nanodots featuring efficient FRET for real-time monitoring of drug delivery and two-photon imaging. *Adv Mater* 2013; 25(45):6569-74.
418. Nomikou N, Curtis K, McEwan C, O'Hagan BMG, Callan B, Callan JF, McHale AP. A versatile, stimulus-responsive nanoparticle-based platform for use in both sonodynamic and photodynamic cancer therapy. *Acta Biomater* 2017 Feb; 49:414-21.
419. Shimada K, Miyagishima A, Sadzuka Y, Nozawa Y, Mochizuki Y, Ohshima H, Hirota S. Determination of the thickness of the fixed aqueous layer around polyethyleneglycol-coated liposomes. *J Drug Target* 1995 01/01; 2015/06; 3(4):283-9.

Appendix 1

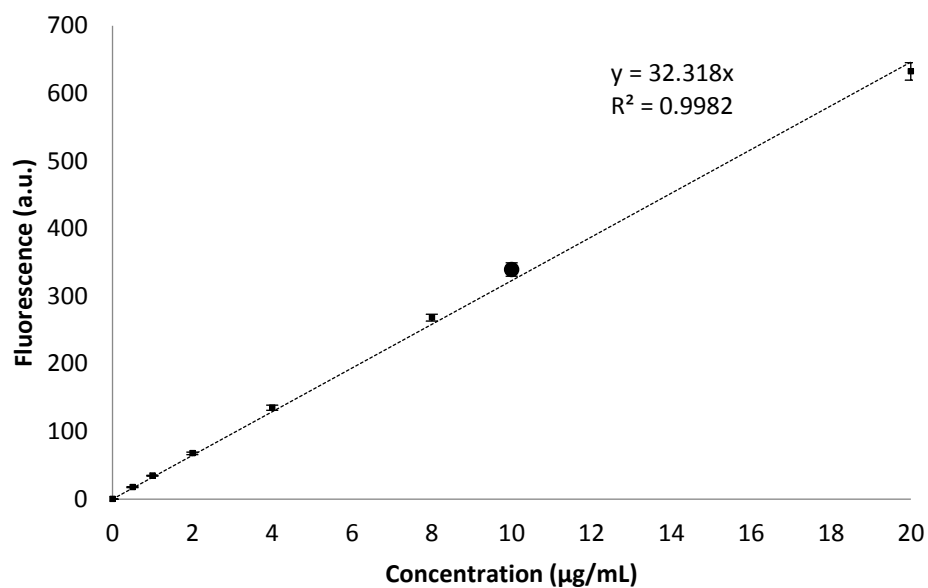


Figure 8-1 Standard Calibration curve of FITC-CM-Dextran (FCD) by fluorescence spectroscopy at Ex 490nm Em 517nm.

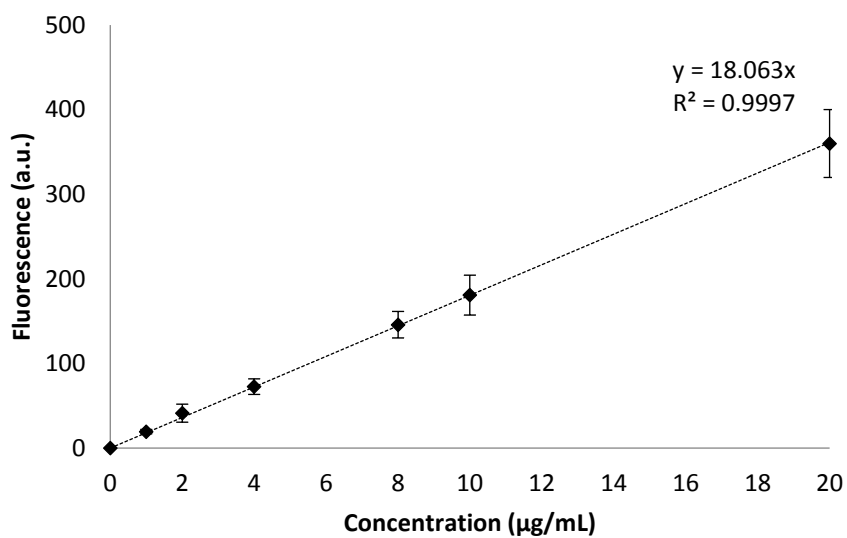


Figure 8-2 Standard Calibration curve of FITC-DEAE-Dextran (FDD) by fluorescence spectroscopy at Ex 490nm Em 517nm.

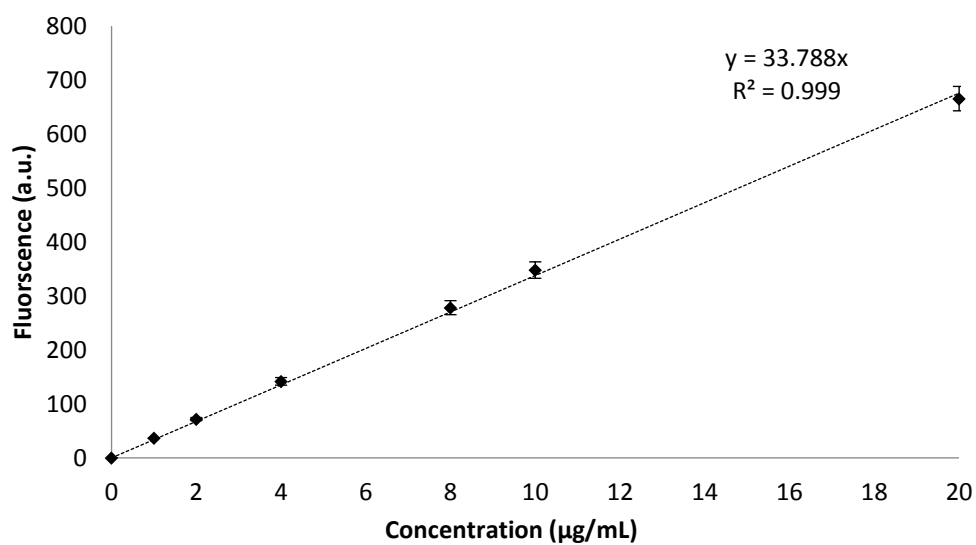


Figure 8-3 Standard Calibration curve of FITC-Dextran (F-D) by fluorescence spectroscopy at Ex 490nm Em 517nm.

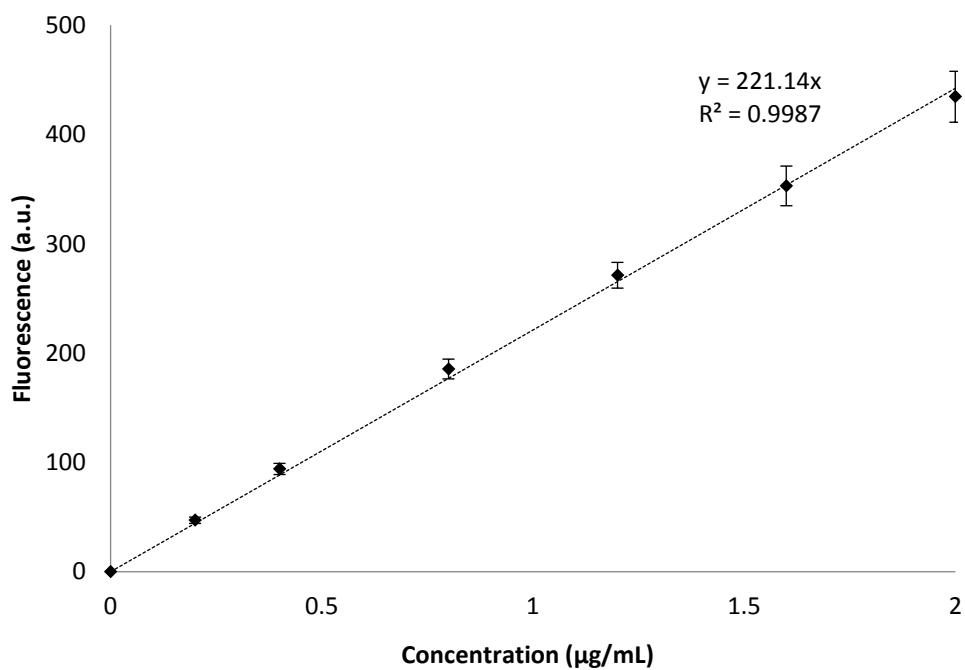


Figure 8-4 Standard calibration curve of anthracene by fluorescence spectroscopy at Ex 355nm Em 400nm

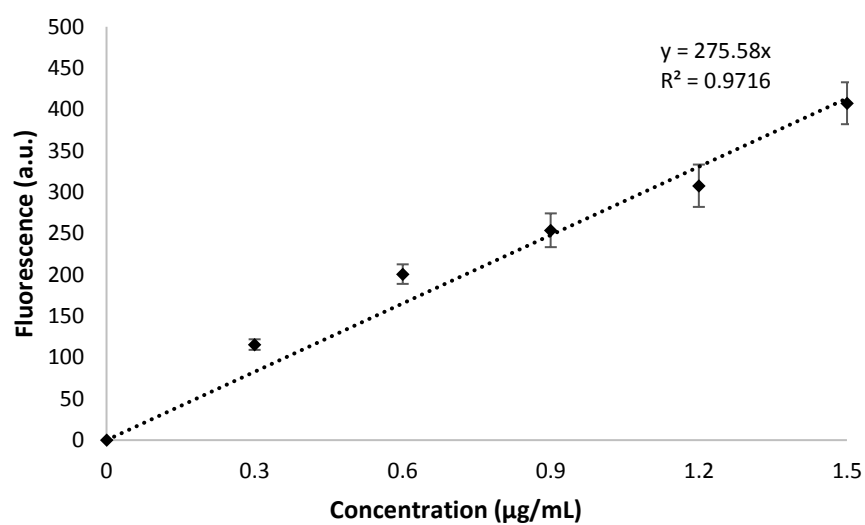


Figure 8-5 Standard Calibration curve of merocyanine using fluorescence spectroscopy at Ex 360nm Em 637 nm

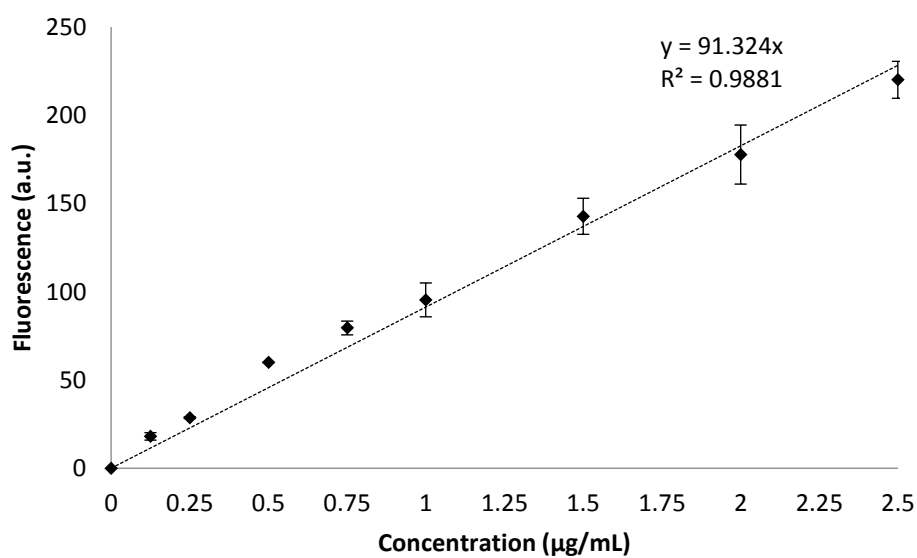


Figure 8-6 Standard Calibration curve of Dox by fluorescence spectroscopy at Ex 485nm Em 580nm

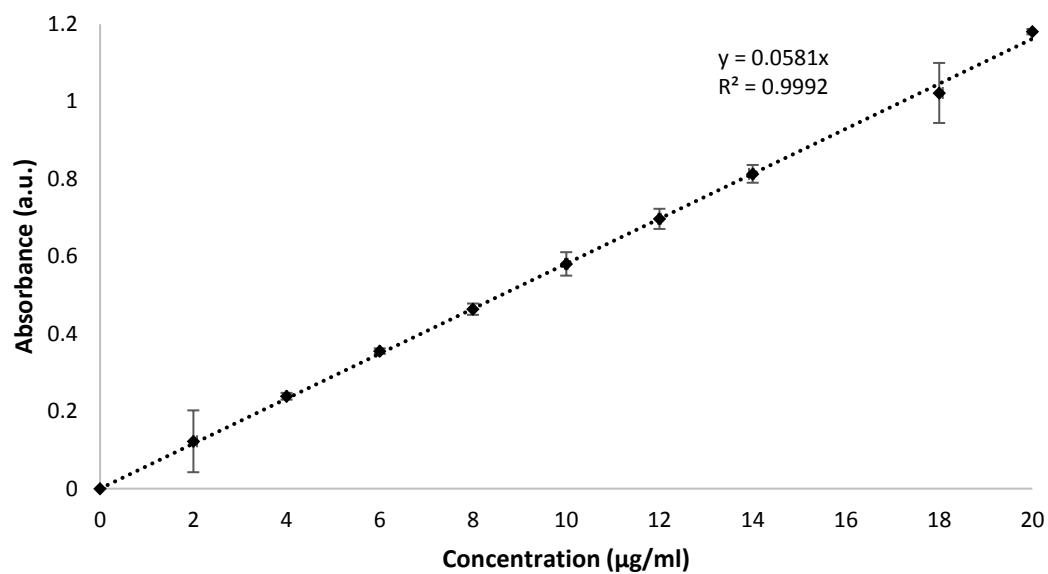


Figure 8-7 Standard Calibration curve of 5- fluorouracil by UV spectroscopy at absorbance maximum 265nm

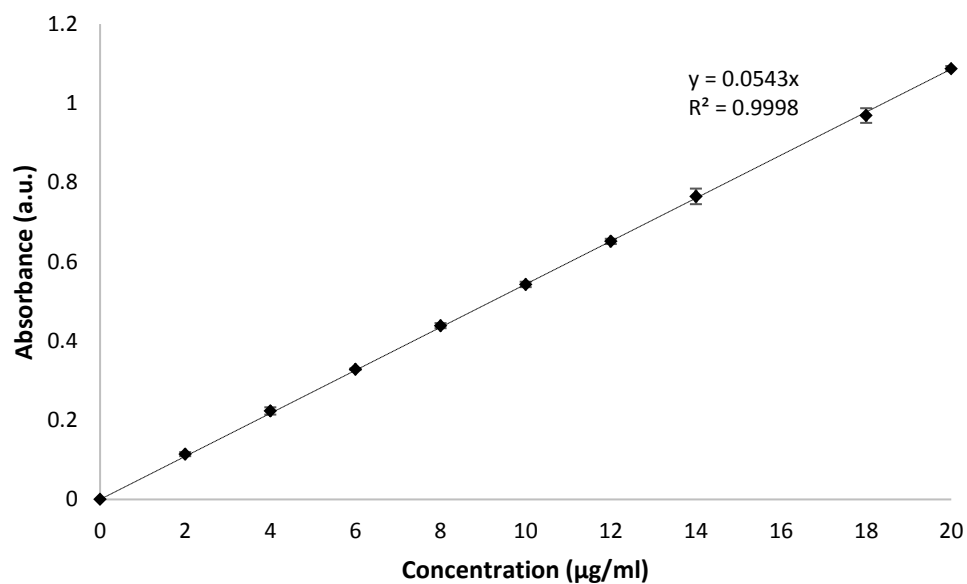


Figure 8-8 Standard Calibration curve of LV by UV spectroscopy at absorbance maximum 285nm

Appendix 2



The integration of triggered drug delivery with real time quantification using FRET; creating a super ‘smart’ drug delivery system

Noorjahan Aibani^a, Paola Fontoura da Costa^a, Jodie Masterson^a, Nino Marino^a,
Francisco M. Raymo^b, John Callan^a, Bridgeen Callan^{a,*}

^a School of Pharmacy and Pharmaceutical Sciences, University of Ulster, Coleraine, BT52 1SA, Northern Ireland, United Kingdom

^b Laboratory for Molecular Photonics, Department of Chemistry, University of Miami, 1301 Memorial Drive, Coral Gables, FL, United States

ARTICLE INFO

Keywords:

Real-time analysis
Photo-transformation
FRET
Hydrophobic drug delivery
Micelles
Stimuli responsive

ABSTRACT

The ability to control drug release at a specific physiological target enables the possibility of an enhanced therapeutic effect with reduced off-target toxic side effects. The discipline of controlled drug release has grown to include most areas of medicine with examples in the literature of targeted drug delivery to the majority of organs within the human body. In addition, a variety of external stimuli used to mediate the drug release process have also been investigated. Nonetheless, the concurrent real time monitoring of drug release has not been widely studied. In this manuscript, we present a novel micellar drug delivery system that is not only capable of releasing its cargo when stimulated by light but also provides a real time analysis of the amount of cargo remaining. Controlled drug release from the delivery system was mediated by physicochemical changes of a spiropyran-merocyanine photochromic dyad, while drug quantification was enabled using a Förster Resonance Energy Transfer (FRET) relationship between the photochrome and a co-encapsulated BODIPY fluorophore. The percentage of drug released from the delivery system was significantly greater (24%) when exposed to light irradiation compared to an analogous control maintained in the dark (5%). Furthermore, the fluorescence read-out capability also enabled the drug-release process to be followed in living cells with a significantly reduced fluorescence emission observed for those cells incubated with the delivery system and exposed to light irradiation compared to control cells maintained in the dark. Combined, these results highlight the utility of this approach to theranostic drug delivery with the potential of light-triggered released together with a fluorescence read-out to enable quantification of the drug release process.

1. Introduction

In order for a drug to produce a therapeutic effect, it must not only reach the site of action but also have the correct physicochemical properties to allow it to be absorbed at an appropriate concentration. In the past few decades, smart drug delivery systems (DDS) have evolved to deliver an appropriate dose to meet the patients needs [1]. Delivering the drug at a controlled rate, triggered drug release and targeted drug delivery are some methods that have been extensively investigated. Some examples of such systems include the development of bio-pharmaceutical systems capable of interacting with intracellular components that respond as a direct result to environmental stimuli [2] and nanoparticles that specifically bind to tumour cells using receptor targeted systems [3,4]. Among these, triggered release plays a substantial role on controlling timing and location of drug release, since it can be induced by several external stimuli acting on the intracellular vehicles

response [5]. Examples of stimuli used to facilitate drug release are temperature [6], pH [7], magnetic field [8], electric field [9], ultrasound [10], enzymatic activity [11] and light [12].

Light responsive drug release is an attractive mechanism because of the ability to control the spatial and temporal triggering of the release process [13]. Numerous examples of photochromic materials capable of transforming under the influence of activating radiation have been explored over recent years [14]. However, the photo activating ability of Spiropyran compounds was recognised as early as the 1920s [15]. Spiropyran can undergo a reversible response to light and chemical stimulations. The closed ring stable state of Spiropyran (a) can be converted to its open form, Merocyanine (b), when irradiated with UV light, which is converted back into its original state when irradiated with visible light (Fig. 1).

This simple photochromic transformation has found many applications ranging from molecular sensors [16] to DNA-based logic

* Corresponding author.

E-mail address: b.callan@ulster.ac.uk (B. Callan).

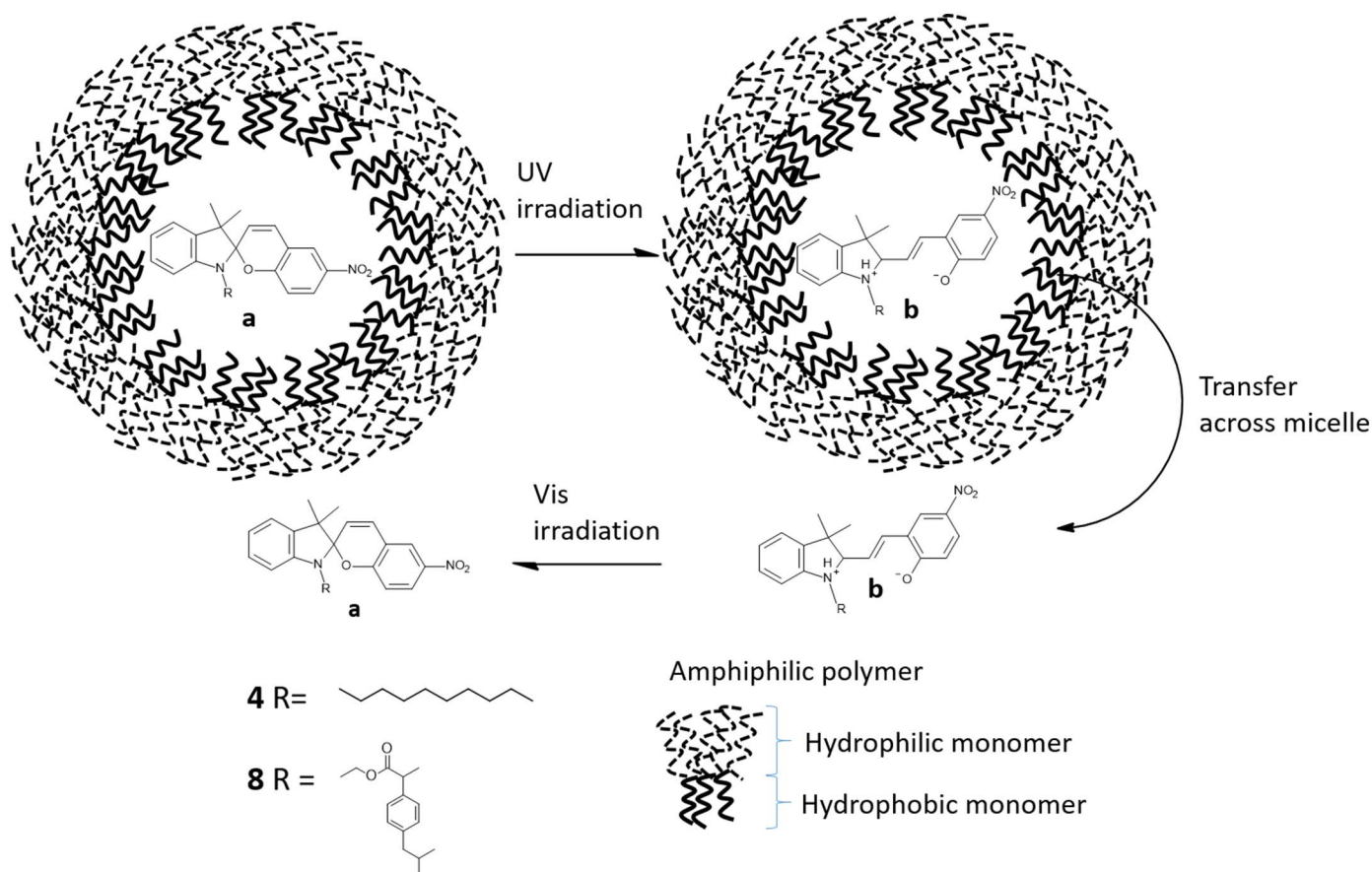


Fig. 1. Illustration of the phototransformation of spiropyran (a) to its merocyanine (b) counterpart and subsequent movement within the micellar environment before transformation back under visible irradiation.

operations [17] and bioimaging [18]. Here, we exploit differences in the hydrophobic/hydrophilic balance between the two isomers to mediate drug release from a micellar based delivery system. The spiropyran form, with its hydrophobic four-ring system preferentially favours a non-polar environment whereas its open ring zwitterionic merocyanine counterpart prefers a more hydrophilic environment.

In addition to the triggered delivery mechanism there are also a number of considerations to make when selecting the type of DDS. More than 40% of newly discovered drugs have little or no aqueous solubility (as determined by the Biopharmaceutical Classification System): 90% of drugs approved since 1995 have poor aqueous solubility, poor permeability or both [19]. The delivery of hydrophobic drugs can be achieved in a number of ways. For example, a pro drug of the active compound may be prepared to catabolize to the original drug. Alternatively, a specific functional group can be altered to create a synthetic analogue with more appropriate hydrophilicity, or the compound may be formulated in such a way as to enable delivery by enteric coating for oral delivery or by an alternative method such as rectal or intravenous administration. All of these approaches have proven successful in delivering hydrophobic compounds. However, these approaches can often lead to enhanced first pass effects and thus the requirement for higher dosage or enhanced expense or, depending on the dosage form, poor patient compliance.

An alternative and successful method for the delivery of hydrophobic drugs is the use of polymeric drug delivery systems. These DDSs can be formulated as, micelles [20], liposomes [21], nanofibers [22], dendrimers [23], colloids [24] or carbon nanotubes [25] with the majority of them falling into the category of nanoparticle drug delivery vehicles. It has been suggested that the polymeric nano carriers can become concentrated preferentially in tumors, inflammatory sites, and

at antigen sampling sites by virtue of the enhanced permeability and retention (EPR) effect of the vasculature [26]. Once accumulated at the site, these polymeric drug delivery vehicles can act as a drug depot, providing a source of API to be released as and when required. This leads to enhanced bioavailability, sustained/controlled release and decreased toxicity caused by potential burst release of the API. There are numerous examples where polymeric compounds are shown to enhance drug delivery [27]. Among these systems Polyethylene glycol (PEG) is frequently used as a polymeric component. We have previously developed a PEG-micellar DDS and determined the size of our PEG copolymers to have an average hydrodynamic diameter of 26 nm [18]. As a direct result of their size, these micelles can navigate through the endothelium in inflammatory sites, epithelium tumors or penetrate micro capillaries, allowing for uptake by a variety of cell types. We have previously shown these micelles to efficiently cross the cell membrane of Chinese hamster ovarian cells and distribute themselves in the cytosol.

Finally, the ability to quantitatively monitor the amount of drug release, from a DDS in real time using a simple but effective approach is an essential companion in the advance towards second-generation health care. To this end, there have been a number of examples where mesoporous silica nanoparticles (MSN) have been used as a cage for drug delivery with the drug co-incorporated alongside a photochromic compound [28], an oligonucleotide containing a recognition element [29] or a redox active FRET pair [30] so that the system operates like a molecular valve. In each case, the drug was prevented from exiting the pores of the NP due to the large bulky groups surrounding the MSN. On application of external stimuli, the outer layer (valve) was disrupted and the inner cargo released from the MSN. In addition to the triggered release, a Förster Resonance Energy Transfer (FRET) mechanism was

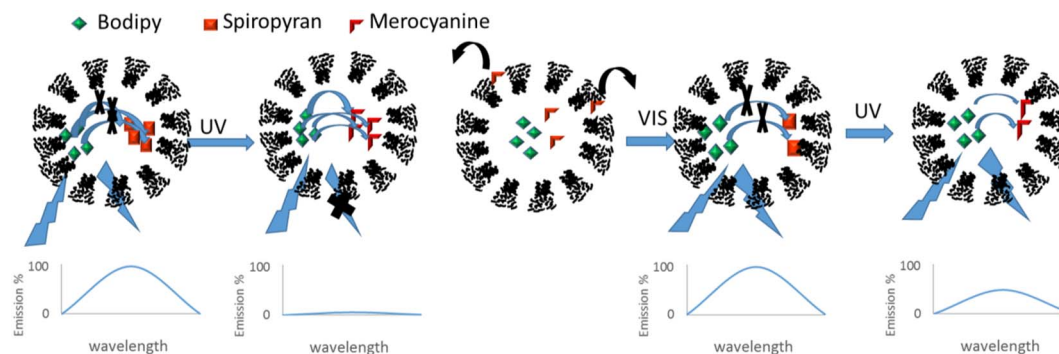


Fig. 2. Schematic representation of the UV triggered release caused by the photoisomerism of Spiropyran to the zwitterionic Merocyanine transcending the amphiphilic micelle and concomitant quantification using FRET with the simulated emission of the Bodipy donor moiety.

utilised to enable real time monitoring of drug release.

In this manuscript, an alternative approach has been developed that combines a triggered release of hydrophobic drugs encapsulated within a polymeric micellar drug delivery system with real time analysis through molecular communication. This was achieved using a FRET mechanism whereby a FRET pair was contained within the hydrophobic interior of a self-forming amphiphilic micelle. Upon application of an external UV light trigger, one of the FRET pair, a Spiropyran moiety, undergoes a photo transformation to the more hydrophilic merocyanine isomer and transcends the micellar membrane into the aqueous external environment. The other half of the FRET pair, a hydrophobic bodipy fluorochrome, remains within the non-polar environment of the micelle. Thus, release of the merocyanine isomer from the micelle modulates the donor-acceptor energy transfer process enabling the release process to be followed by fluorescence spectroscopy, illustrated in Fig. 2. A decrease in the quenching ability of the merocyanine for the bodipy emission is observed relative to the amount of merocyanine remaining within the micellar structure.

Indeed, the scope of this approach can be further extended by conjugating an Active Pharmaceutical Ingredient (API) onto the Spiropyran isomer enabling its release to be controlled and monitored in real time. To illustrate this, we have attached ibuprofen to spiropyran using an ester linkage, determined the release of this conjugated ibuprofen-spiropyran compound from the micelle upon UV light irradiation and compared these results to the release of unmodified spiropyran from the micelle.

2. Materials and methods

2.1. Materials

All reagents and solvents were purchased from Sigma-Aldrich and used without further purification. 2,3,3-trimethylindolenine 98%, 1-bromodecane 98%, 2-hydroxy-5-nitrobenzaldehyde 98%, Piperidine $\geq 99.5\%$, 2-bromoethanol 95%, Potassium Hydroxide 85% KOH Basis, Triethylamine $\geq 99\%$, Boron Trifluoride $\geq 99.5\%$, Trifluoroacetic Acid 99%, 2,3-Dichloro-5,6-dicyano-*p*-benzoquinone 98%, 4-Formylbenzoic acid 97%, 2,4-Dimethylpyrrole 97%, Phosphate Buffered Saline Tablets, Dialysis tubing cellulose membrane flat width 10 mm, Ibuprofen, 4-(dimethylamino)pyridine, *N,N'*-Dicyclohexylcarbodiimide, Chloroform, Acetonitrile, Ethanol, Dichloromethane, Diethyl Ether, Hexane, Ethyl Acetate, Tetrahydrofuran.

2.2. Synthesis of compounds

The synthesis of hydrophobic spiropyran 1'-decyl-3',3'-dimethyl-6-nitro-spiro[chromene-2,2'-indol-1-ium] (HSP) (4) has been previously described [18].

2.2.1. Synthesis of (10-(4-(decylcarbamoyl)phenyl)-5,5-difluoro-1,3,7,9-tetramethyl-5H-dipyrrolo[1,2-c:2',1'-f] [1-3]diazaborinin-4-ium-5-uide) (3)

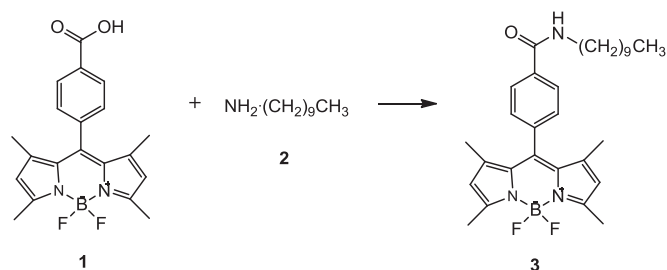
Compound 3 was synthesized following a two-step procedure as detailed below.

Step 1: Synthesis of (10-(4-carboxyphenyl)-5,5-difluoro-1,3,7,9-tetramethyl-5H-dipyrrolo[1,2-c:2',1'-f] [1-3]diazaborinin-4-ium-5-uide) (1) (S1).

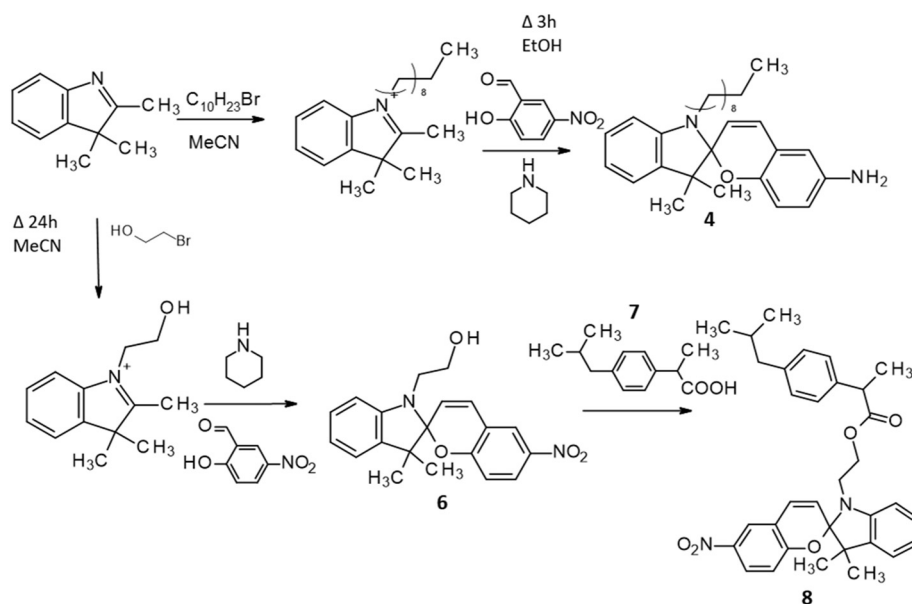
To a solution of 4-formylbenzoic acid (0.5 g, 3.3 mmol) and 2, 4-dimethylpyrrole (0.69 g, 7.3 mmol) in THF (90 mL) was added several drops of trifluoroacetic acid. The mixture was stirred at ambient temperature overnight, then a solution of 2,3-dichloro-5,6-dicyano-*p*-benzoquinone (0.75 g, 3.3 mmol) in THF (120 mL) was added. The mixture was stirred continuously for another 4 h. After the addition of triethylamine (18 mL, 0.13 mol), $\text{BF}_3\cdot\text{OEt}_2$ (18 mL, 0.15 mol) was added dropwise to the mixture, which was cooled in an ice-water bath. The mixture was kept stirring at ambient temperature overnight, then filtered through a celite pad. The residue was washed with CH_2Cl_2 (ca. 50 mL), then the combined filtrate was rotary evaporated to dryness. The residue was redissolved in CH_2Cl_2 (100 mL) and the solution was washed with 5% aqueous NaHCO_3 solution (100 mL) followed with water (100 mL \times 2). The organic portion was dried over anhydrous MgSO_4 , then evaporated in vacuo. The crude product was purified by silica gel column chromatography using $\text{CH}_2\text{Cl}_2/\text{MeOH}$ 99/1 as the eluent to give 1 as a red solid (0.615 g, 51%) (S2).

Step 2: Synthesis of compound 3 (Scheme 1).

A mixture of 1 (127 mg, 0.34 mmol), dodecylamine 2 (45 mg, 0.28 mmol), EDC (110 mg, 0.57 mmol), and DMAP (7 mg, 0.056 mmol) was dissolved in 20 mL of CH_2Cl_2 . After stirring at 27 °C for 1 h in the dark the solvent was removed under vacuum. The obtained crude product was purified by column chromatography (hexane/EtOAc 1:1) to give 160 mg of 3 as an orange oil (yield 91%). ^1H NMR (CDCl_3 , 500 MHz): δ = 7.91 (d, J = 8 Hz, 2H), 7.39 (d, J = 8 Hz, 2H), 6.18 (br s, 1H), 5.98 (s, 2H), 3.49 (t, J = 6 Hz, 2H), 2.55 (s, 6H), 1.65 (m, 2H), 1.4–1.2 (m, 14H), 1.35 (s, 6H), 0.87 (t, J = 6.5 Hz, 3H); ESIMS: m/z 506 $[\text{M} - 1]^-$.



Scheme 1. Amidation of Bodipy compound 1 to increase the hydrophobicity of compound 3.



Scheme 2. Synthesis of Spiropyran compounds hydrophobic spiropyran (HSP) (4) and Ibuprofen spiropyran (IBSP) (8).

2.2.2. Synthesis of Spiropyran compound 2-(3',3'-dimethyl-6-nitro-spiro[chromene-2,2'-indol-1-ium]-1'-yl)ethyl 2-(4-isobutylphenyl)propanoate (8)

The synthesis of compound 8 (SP-IB) was a two-step process. The intermediate compound 2-(3',3'-dimethyl-6-nitro-spiro[chromene-2,2'-indol-1-yl)ethanol (6) was prepared following a literature procedure [31] (S3). The SP-IB was synthesized by a modified method from Baumann et al. [32]. Synthesis of SP-IB 8 is detailed in Scheme 2. A mixture of 6 (100 mg, 0.28 mmol), Ibuprofen 7 (70 mg, 0.34 mmol), EDC (108 mg, 0.56 mmol), and DMAP (7 mg, 0.056 mmol) was dissolved in 20 mL of CH_2Cl_2 . After stirring at room temperature for 1 h in dark, the purple solution becomes colorless and solvent was removed under vacuum. The obtained crude product was purified by column chromatography (hexane/EtOAc 4:1) to give 145 mg of 8 as a green oil (yield 94%). 1H NMR ($CDCl_3$, 500 MHz): δ = 7.99–7.94 (m, 2H), 7.18 (t, J = 7.0 Hz, 1H), 7.14–7.12 (m, 2H), 7.07–7.06 (m, 3H), 6.89 (t, J = 7.0 Hz, 1H), 6.79–6.66 (m, 2H), 6.26 (d, J = 6.5 Hz, 1H), 5.62 (t, J = 11.0 Hz, 1H), 4.22 (m, 2H), 3.63 (m, 1H), 3.45–3.31 (m, 2H), 2.44 (t, J = 6.0 Hz, 2H), 1.83 (m, 1H), 1.45 (dd, J = 21.0 Hz, J = 7.0 Hz, 3H), 1.23 (s, 3H), 1.06 (d, J = 22.0 Hz, 3H), 0.90 (d, J = 6.5 Hz, 6H); ESIMS: m/z 541 [M + H] +.

2.3. Preparation and characterisation of micelles

The synthesis of the random co-polymer has been extensively described previously by the authors as both a hydrophobic [18] and hydrophilic [33] drug carrier and was prepared without further modification. It was comprised of two monomers (polyethylene glycol (PEG) (Mn 500) and a decyl chain (C10)) both containing a methacrylate functional group and polymerized using a free radical initiator in a 5:3 M ratio of PEG:C10 (scheme displayed in S5). The polymer has previously been determined to be biocompatible with negligible toxicity at the concentrations used. Micelles were prepared by evaporating the desired amount of polymer in $CHCl_3$ in a round bottom flask along with 3 and 4 or 8 to form a thin film. The resultant film was hydrated with PBS to form the micelles. Micelle size, polydispersity index and zeta potential was analysed by dynamic light scattering using a Malvern Nano-ZS Zeta sizer. Particle morphology was observed by scanning electron microscopy (SEM) at high vacuum mode using FEI Quanta ESEM. A particle suspension was air dried for 24 h on stainless steel stubs and further coated with ultra-thin Gold/Palladium layer at 18 mA for 3 min using Polaron Equipment Ltd. E5100 Sputter coater and

observed.

2.4. Evaluation of phototransformation of 4a to 4b

0.5 mL 4a (0.1 mg mL^{-1}) was added to 0.6 mL polymer (2.5 mg mL^{-1}) and evaporated into a thin film and hydrated with 3 mL PBS to form micelles. These samples were irradiated from a fixed distance of 4 cm at 365 nm (0.4 mW cm^{-2}) with a Mineralight UVGL-25 lamp (UVP 95-0006-03 Model UVL-56 6 W). The UV–Vis spectra was recorded using a Varian Cary Eclipse UV spectrophotometer at intervals of 30 s for 6.5 min until no further increase in absorbance of 4b (560 nm) was observed.

2.5. FRET efficiency

Micelles were prepared as described in Section 2.3 with 78 μL of 3 (0.08 mg mL^{-1}) and varying volumes of 4 (0.2 mg mL^{-1}) to obtain molar ratios 1: 0.5–10 of 3:4 and hydrated with 3 mL PBS to form micelles. The FRET efficiency was determined by allowing the phototransformation of 4a to 4b while the concentration of 3 remained constant. Fluorescence emission spectra of 3 were recorded (Ex 525 nm Em 545 nm) before and after UV light exposure using a Varian Cary Eclipse Fluorescence spectrophotometer.

2.6. In vitro triggered release

Micelles were prepared as above using 0.176 mL of 3 (0.2 mg mL^{-1}) with 0.6 mL of 4 (0.5 mg mL^{-1}) and 2 mL polymer (2.5 mg mL^{-1}) and hydrated with 2 mL PBS. Release studies were undertaken using Franz diffusion cells and dialysis membrane (MWCO 14,000). 200 μL of the micelle formulation was loaded into donor compartment while the acceptor chamber comprised of PBS and maintained at 37 °C. The contents of the donor chamber were irradiated with UV light for fixed time periods of 2, 4, 6, 8, 10 and 12 min and solutions were analysed using fluorescence spectroscopy at Ex360 nm–Em 637 nm. Similarly, control studies were conducted in the absence of UV light. For determining stability and reproducibility of the system, micelles containing 3 and 8 were loaded onto Franz diffusion cells and subjected to cycles of 5 min UV light and 20 min dark conditions during which samples were scanned for fluorescence emission of 3 at Ex 525 nm–Em 540 nm at 5 min intervals for 20 min.

2.7. Observation of FRET in HeLa cells

HeLa cells were incubated in modified DMEM with 10% FBS and 1% Pen/strep in 96 well plates at a cell density of 5×10^3 cells in each well and allowed to adhere overnight. When 60% confluency was reached, 2 mL micelle solutions were prepared containing either **3** (0.176 mL of 0.2 mg mL^{-1}) and **4** (0.6 mL of 0.5 mg mL^{-1}) or just **3** (0.6 mL of 0.5 mg mL^{-1}). 50 μL of this solution were added to the wells and incubated for 18 h. The cells were then washed twice with PBS and the fluorescence emission determined using an ELISA plate reader (Ex 485 nm and Em 520 nm). For confocal microscopy, cells were treated as mentioned above and imaged using a Leica DMI6000b inverted microscope with a $40\times$ oil immersion lens. All images were analysed using LAS AF v2.3.6 software.

2.8. Comparative release study to quantify triggered release by FRET

Release studies were conducted on Franz diffusion cells using dialysis membrane. Briefly micelles loaded with **3** and **8** were loaded into acceptor compartment and the donor compartment was filled with PBS maintained at 37°C . Micelles were irradiated with UV light for 5 min after which they were subjected to light and dark conditions for 20 min. Samples were taken at 5 min interval and observed for UV absorbance at 345 nm for **8a** and fluorescence emission of **3** following a 20 min equilibration period in visible light conditions. Similar studies were conducted without UV trigger.

3. Results and discussion

3.1. Synthesis of compounds

The synthesis of compound **1** was achieved by the synthetic procedure outlined in Scheme S1 (Supporting information). Successful product formation was confirmed by mass spectroscopy and ^1H NMR spectroscopy. Compound **3** was synthesized to increase the hydrophobicity of the FRET donor and hence ensure continued encapsulation within the micelle. Synthesis was achieved by a modification of a previous procedure [18] with characterisation detailed in Section 2.2.1. Compound **4** was synthesized as described in Scheme 2 and again successful product formation was confirmed by ^1H NMR and mass spectroscopy. Compound **8** is a novel compound and was formed by an esterification between **6** and **7** in a 1:1 stoichiometry with a yield of 94%. Successful product formation was again confirmed by ^1H NMR and mass spectroscopy, as detailed in Section 2.2.2.

3.2. Preparation and characterisation of micelles

DLS measurements of micelles loaded with **3** and **4** indicate an average particle size of $27.5 \pm 0.98 \text{ nm}$ with PDI 0.416 ± 0.009 and surface charge of -1.67 ± 0.73 as determined by zeta potential measurements. These observations were in agreement with those observed previously by Yildiz et al. using the same polymeric micelle with encapsulated cargo [18]. However when **4** was replaced by **8**, the micelle size increased to $45.93 \pm 2.72 \text{ nm}$ and PDI was 0.346 ± 0.04 with -2.05 ± 0.61 zeta potential. This slight increase in micelle size may be attributed to the greater rigidity of **8** causing a larger hydrophobic internal core within the micelle. There was no major change in the PDI and zeta potential values for micelles following encapsulation with regards to content indicating successful incorporation of **8** inside the micelle. Fig. 3a shows a representative particle size distribution graph for micelles loaded with **3** and **4**, while a scanning electron microscopic image of micelles loaded with **3** and **8** (Fig. 3b) show well-formed particles with spherical morphology.

3.3. Quantification of photo physical transformation of **4a** to **4b**

For efficient FRET to occur between a donor-acceptor pair two main criteria must be met. First, the donor and acceptor molecules must be in close proximity to each other and secondly, the emission spectrum of the donor must overlap effectively with the absorption spectrum of the acceptor. In the context of the micellar delivery system described above, as both the donor and acceptor are originally confined within the micelle, a nanoscale distance between the two molecules can be guaranteed [34]. In terms of spectral overlap, the absorbance spectrum of **4a** encapsulated within the micelle was determined to have a maximum absorbance centered at 360 nm. Upon activation by UV light, **4a** undergoes a ring opening of the spiro carbon to its corresponding merocyanine, **4b** (Fig. 1). The merocyanine is zwitterionic, and therefore more hydrophilic. It has also an elongated area of conjugation and therefore induces a significant bathochromic shift to a new absorbance maximum at 550 nm which coincides with the emission wavelength of **3** (Fig. 4) when excited at 525 nm.

This spectral cohesion of absorbance and emission of **4b** and **3** is imperative for energy transfer from **3** (the fluorescent donor) and **4b** (the photochromic acceptor). Nevertheless, the time required for conversion of **4a** to **4b** can significantly affect the energy transfer from **3** to **4b**. Hence we irradiated **4a** with UV light and monitored the UV-Vis spectrum at increments of 30 s in aqueous medium and found that it required 5 min irradiation for complete conversion from **4a** to **4b** as shown in Fig. 5.

After 5 min, the absorption reached a plateau beyond which there was no increase in the absorption intensity. However complete conversion of **4a** to **4b** took 12 min in DMF medium which can be explained by the polar nature of **4b** enabling faster conversion in aqueous medium (S4). The polar nature of **4b** is fundamental to encourage its release from within the micelle to the surrounding polar aqueous environment, enabling a triggered release of micellar content.

3.4. FRET efficiency between **3** and **4b**

In order to identify the ratio of **3** to **4b** which allows maximum energy transfer between the fluorophore and photochrome, the two compounds were encapsulated into the micelles at different molar ratios and the observed decrease in fluorescence emission of **3** following irradiation with UV light for 5 min to facilitate the conversion of **4a** to **4b**. Fig. 6 shows the emission profile of **3** at varying ratios of **4b**. As expected, the emission of **3** was highest when there was no **4b** present in the micelle (spectrum a). As the concentration of **4a** in the micelles increased, more **4a** was converted to **4b** upon irradiation with UV light and quenched the emission of **3** at 540 nm proportionately (spectra b–h). In addition, emission from **4b** at 637 nm was observed to increase upon increasing **4a** concentration indicating a successful energy transfer between **3** and **4b**. However, the plot of percentage depletion in fluorescence emission of **3** (Fig. 6 insert) shows that a plateau was reached after a ratio 1:6 of **3:4b** suggesting a saturation concentration was reached with no more **3** available for energy transfer. This suggests that the optimal FRET molar ratio between donor and acceptor to allow for quantitative analysis is 1:6. This is reflective of the difference in extinction coefficient between our donor and acceptor moieties. This was the ratio chosen for all subsequent studies.

3.5. In vitro triggered release

UV light acts as a trigger for photoinduced transformation of **4a** which is hydrophobic with a closed ring system to an open ring **4b** which is polar in nature with higher solubility in aqueous medium. The hydrodynamic properties of micelles allow **4b** to easily come out of the system permitting release of encapsulated cargo. Continuous photo-activation of **4a** within the micelle lead up to 24% release of **4b** into the surrounding environment within 12 min which was significantly higher

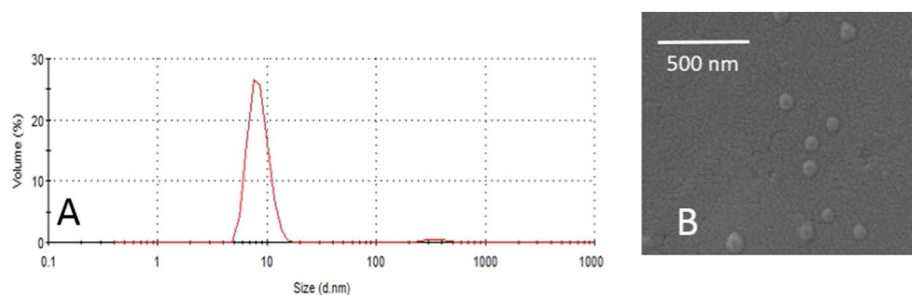


Fig. 3. A. Dynamic light scattering displaying the hydrodynamic radius of micelles. B. SEM image of micelles.

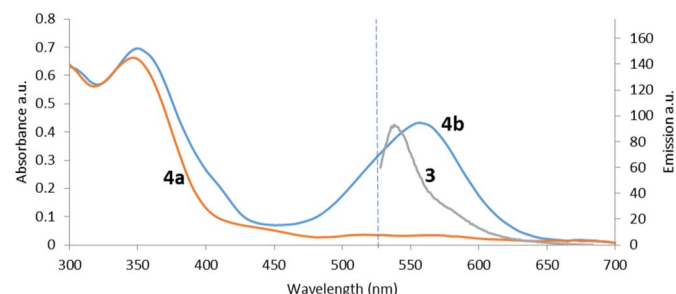


Fig. 4. Absorbance spectra of 4a and following photoconversion to 4b with the emission spectra of 3 with Ex 525 nm.

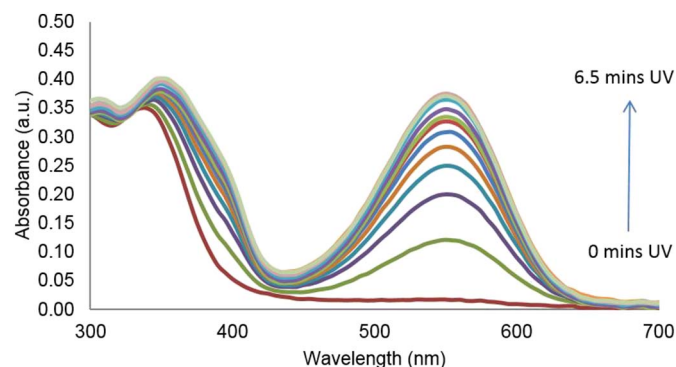


Fig. 5. Absorbance spectra of 4b at λ_{max} 550 nm increasing with increasing exposure to UV light of 365 nm. Spectra displayed following exposure to 0, 0.5, 1.0, 1.5, 2, 2.5, 3, 3.5, 4, 4.5, 5, 5.5, 6 and 6.5 min UV light at 465 nm from a fixed distance.

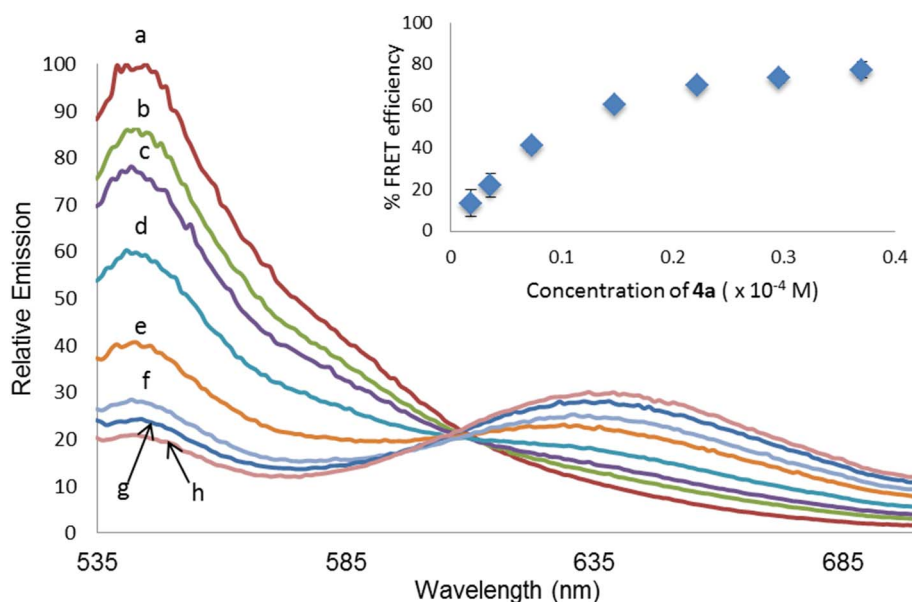


Fig. 6. Fluorescence emission of 3 following exposure to varying molar ratios of 4a and photoconversion to 4b. a: no UV exposure and b-h: solutions were exposed to 5 mins UV light at 365 nm from a fixed distance and molar ratios of compounds bodipy 3: merocyanine 4b 1:0.5; 1:1; 1:2; 1:4; 1:6; 1:8 and 1:10 consecutively. Insert: FRET efficiency of 3 and 4 following exposure to 5 mins UV light at 365 nm from a fixed distance. Concentration of 3 remains constant at 3.64 μM . Percentage efficiency was determined by the relation depletion in the emission of 1 at 545 nm, $n = 3$.

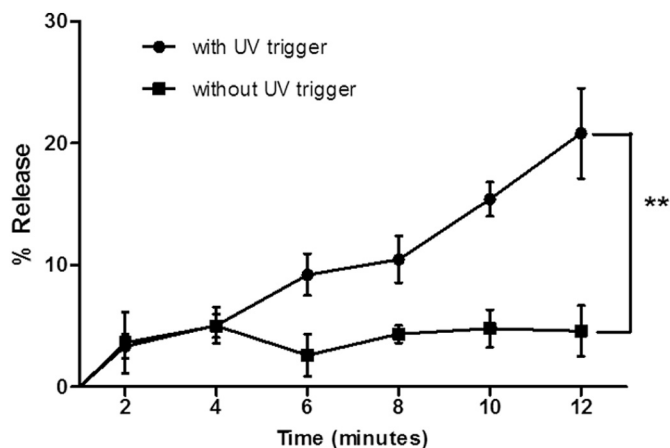


Fig. 7. In-vitro triggered release of 4b from micelles after continuous activation with UV light for 12 min and no UV activation. ** indicates $p < 0.005$.

than the 5% release in the absence of photoactivation as seen in Fig. 7. This design of a triggered fast release system is essential for successful release of drugs attached to 4 for therapeutic applications.

3.6. Reproducibility of system

The integration of photoswitchable assemblies with fluorophores capable of resonance energy transfer allows the formation of a system which has the ability to switch on and off on demand. Fig. 8 shows the fluorescence emission of 3 in the presence of 8 and subsequent photochromic switching between the spiropyran form (8a) to its merocyanine

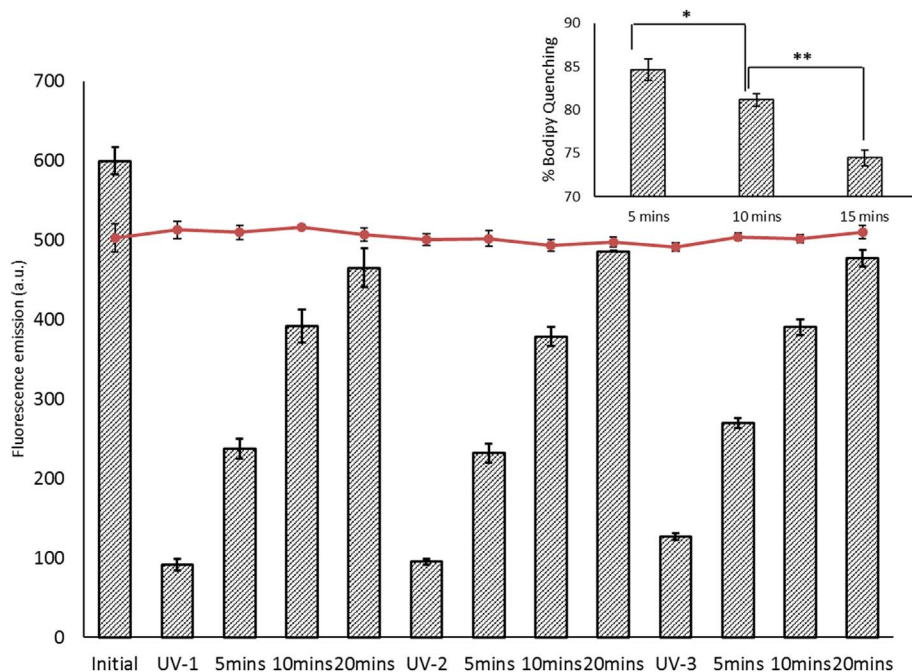


Fig. 8. Bar chart: Fluorescence emission of **3** within micelles loaded with **8a** following cycles of UV exposure (365 nm, 5 mins) leading to conversion of **8a** to **8b** and subsequent resting time in dark conditions permitting reversion of **8b** back to **8a**. Line graph: control with micelles containing only **3**. Insert: % quenching of **3** following UV irradiation. ** indicates $p < 0.005$.

counterpart (**8b**) indicating the reproducibility of the system.

Compound **8** was created as a prodrug, to contain an API (Ibuprofen) covalently linked to the photochromic spiropyran moiety. Once released from the internal core of the micelle it is anticipated that it would be subjected to hydrolysis via esterase's enzymes and hence release the API. When there was no **8b** present in the system (in the absence of UV light), there was a significantly high emission of **3**. This emission was quenched upon photoactivation of **8a** to **8b** as the absorption signature of **8b** overlaps with emission signature of **3**. As **8b** slowly reverted back to **8a** owing to its reversibility in heat and visible light conditions, the emission of **3** slowly increased. The hydrophilic nature of **8b** encourages it to transcend the hydrophobic internal core of the micellar system into the wider aqueous environment. Although the system was kept in the dark, there were three cycles of 5 minute irradiation, allowing for significant movement outside the micelle. This movement was observed as a decrease in the quenching efficiency of **3** upon subsequent photoactivation cycles (Fig. 8 insert) as less **8b** was present within nanoscale distance for FRET to successfully take place between the two molecules in each subsequent excitation. This decrease in the quenching of emission of **3** is of similar magnitude to the % release of internalised compound **4**, observed in Fig. 7, with 19% release after 10 min of **8** when compared to the 15% release of **4** after 10 min displayed in Fig. 7. The increase in release is attributed to the time lapse between UV stimulation and subsequent photoconversion allowing for more hydrophobic **8b** to leave the micelle. It is seen from Fig. 8 that a further fluorescence quenching of 74.4% is recorded after 15 min UV irradiation and would suggest that 25.6% of **8** has been released. A similar effect was seen in light conditions, but the % of quenching of **3** was slightly less, due to the faster photoconversion back to the original more hydrophobic spiropyran moiety (**8a**), ensuring that less compound was released and hence more available for the subsequent energy transfer to the donor (S6). Micelles loaded with only **3** did not show any changes in fluorescence emission after photoactivation and after subsequent resting periods, in addition there was limited photobleaching of **3** after UV irradiation.

3.7. Observation of FRET in HeLa cells

Encapsulation of cargo within micelles enables them to be transported across the cell membrane leading to better cellular uptake owing

to their biocompatibility and size. In order to determine the feasibility of communication and triggered release from within the micelles, we incubated HeLa cells with micelles loaded with **3** and **4a** and enabled the photoconversion of **4a** to **4b** present within the cells to confirm FRET communication between **3** and **4b**. As seen in Fig. 9, fluorescence emission of **3** fluctuated drastically according to status of **4b** present within the cells, as a direct result of molecular communication between them. The ability of **4b** to switch back to **4a** in the presence of visible light broke the communication between **3** and **4b** allowing the emission of **3** to be observed. These results in HeLa cells support our previous observations in vitro conditions in Section 3.6. It can be seen that immediately following 5 min UV irradiation there is a 82.5% quench in the fluorescence emission of **3**, attributed to the energy transfer to the acceptor moiety, **4b**. Upon subsequent photoactivation cycles of **4b** there was significantly less quenching of the emission from our donor compound **3** (75.3% and 64.2% respectively). This can be attributed to the more polar **4b** form leaving the micelle DDS (24.7% and 35.8% released after 10 and 15 min irradiation).

As expected the emission of **3** lapsed back faster in visible light conditions compared with dark conditions (S7), further confirming that the photoconversion of **4b** to **4a** is faster in the presence of visible light and is indirectly communicated in the form of higher emission of **3**. Additionally, the quenching effect after subsequent UV irradiation cycles in the dark was similar to that seen in light conditions. Similarly, observations of cells by confocal microscopy indicated significant reduction in fluorescence emission of **3** on photoactivation of **4b** confirming its presence within cells (Fig. 10).

3.8. Real time quantification of encapsulated cargo

The photoswitchable nature of **8** and its molecular communication with **3** can prove beneficial in real time quantification of release of encapsulated materials from within the micellar environment. To quantify this occurrence, micelles loaded with **3** and **8** were loaded on to dialysis membranes in Franz diffusion cells and photoactivated for 5 min to allow conversion of **8a** to **8b** resulting in its release from the micellar environment recorded over 20 min of resting time in both dark and visible light conditions. Two parameters were measured simultaneously at various time points in an attempt to correlate the communication seen through **3** with release of **8**. This was achieved by

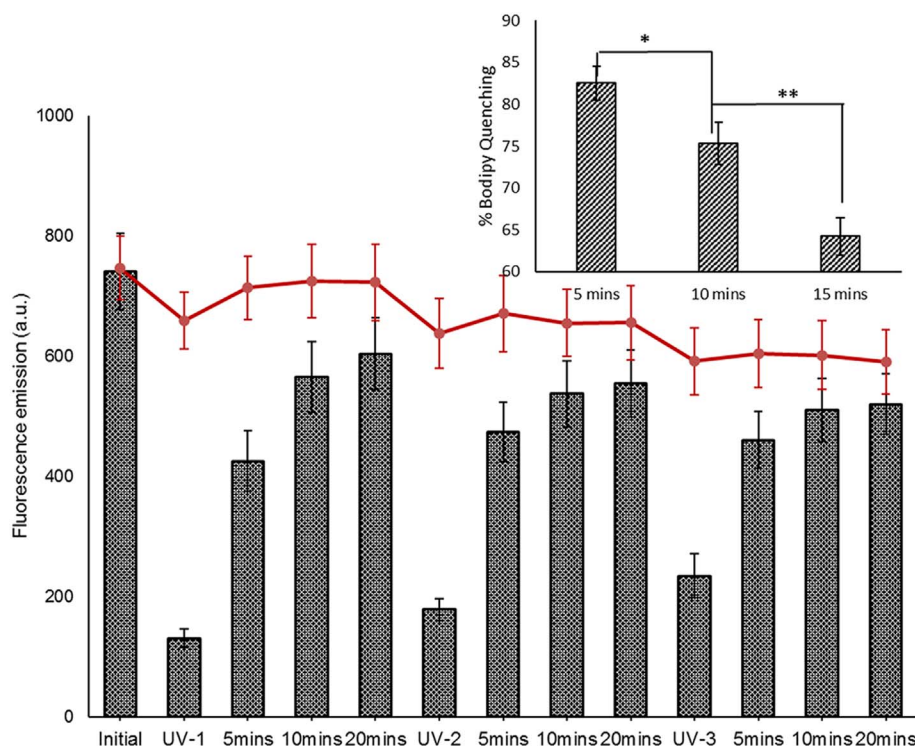


Fig. 9. Bar chart: Fluorescence emission of **3** in HeLa cells incubated overnight with micelles loaded with **3** and **4a** and following cycles of UV exposure (365 nm, 5 min) leading to conversion of **4a** to **4b** and subsequent resting time in visible light conditions permitting reversion of **4b** back to **4a**. Line graph: control using micelles containing **3** only. **Insert:** % quenching of **3** following UV irradiation. ** indicates $p < 0.005$, * indicates $p < 0.05$.

monitoring the amount of **8a** present within the micelles by absorbance at 345 nm. Following removal of the sample for analysis a set period of 20 min was observed with the sample subjected to visible irradiation, to ensure that all **8** was in the spiropyran form, **8a**. The results of the depletion in **8a** absorbance can be seen in Fig. 11a. The simultaneous measurement of bodipy emission (**3**) was collected, following the original 5 mins UV irradiation, each sample removed for analysis was subjected to 20 min visible light before the emission of **3** was recorded, the decrease in quenching is plotted in Fig. 11b. From Fig. 11 a good correlation is seen between both the fluorescence increase from **3** and the absorbance of **8a**. The largest magnitude of change is observed from the UV stimulation in dark conditions, this is expected as **8b** would favour the more polar environment. Specifically, a 8.4% decrease in **8a** absorbance is observed after 10 min, indicating a transfer of **8** across the dialysis membrane. This is indirectly communicated through a 7.0% increase in the fluorescence emission of **3** (Fig. 11b). Similarly a 17.4% decrease in absorbance of **8a** is seen at 20 min compared to 11.6% increase in fluorescence emission of **3** at the same time point. Visible light conditions led to conversion of **8b** back to **8a** leading to lesser release of only about 7% from micelles which was reflected as approximately 4% increase in fluorescence emission of **3**. However there was negligible release in the absence of a UV trigger and is suitably revealed as insignificant increase in fluorescence emission of **3**. This close correlation between the FRET communication when compared to the direct measurement of remaining spiropyran would suggest that there is indeed potential to further develop these smarter DDSs.

4. Conclusion

The number of smart DDSs capable of real time communication with concomitant stimulated drug release is increasing in response to the nanotechnology revolution [35]. The need for variation between the mechanism of stimulus, as well as the parameter involved in communication is paramount to the success of these advanced materials so to allow these nano-platforms to reach the full echelon of their potential. Recent examples illustrating this diversity can be seen by Huang et al. [36], whereby they have incorporated the anticancer agent doxorubicin into a supramolecular nanoparticle and also double up its use as the FRET acceptor to allow self-communicating. Another interesting example is seen by Du et al. [37] and their incorporation of five stimuli responsive moieties on to their NP.

We have designed a photo-activated DDS capable of real time communication using the photochromic properties of spiropyrans and exploiting the differences in physiochemical properties. By adopting a prodrug approach, we have developed an ibuprofen-spiropyran analogue, which has displayed significant stimulated release from within a micelle environment. In addition, with the incorporation of a hydrophobic bodipy compound within the micelle hydrophobic core, we have created a FRET communication between the two species present within the micelle that has shown significant potential for real time analysis of content. In vitro analysis has confirmed this system remains intact within HeLa cells. This smart DDS has the potential to be adapted for a number of different API, by simply linking the API with the spiropyran

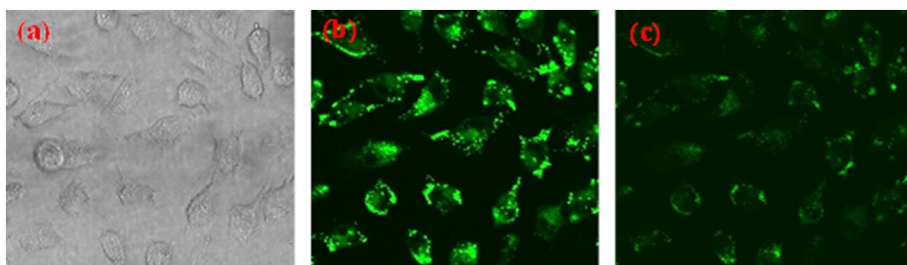


Fig. 10. Confocal microscopic images of HeLa cells incubated with micelles loaded with **3** and **4a** showing (a) Clear field (b) Fluorescence emission of **3** (Ex 514 nm, Em 520–590 nm) before UV exposure (c) Fluorescence emission of **3** after UV exposure (365 nm, 5 min).

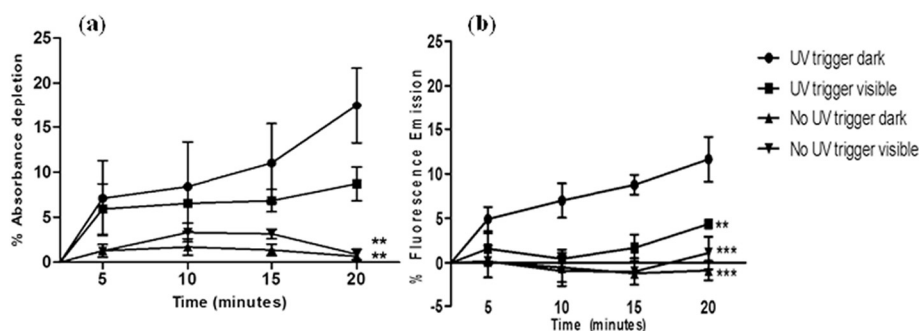


Fig. 11. (a) In vitro release of 8a from micelles with and without UV trigger and subsequent resting time in dark and visible light conditions measured by decrease in UV absorbance at 345 nm. (b) Observation of % increase in fluorescence emission of 3 at Ex 503 Em 514 nm measured concomitantly with release of 8a. ** indicates $p < 0.005$, *** indicates $p < 0.0005$.

through an ester or potentially an amide bond, thus increasing application for such nanoplatforms to include a large number of drugs with the only prerequisite being that they contain a suitable reactive functional groups.

Supplementary data to this article can be found online at <http://dx.doi.org/10.1016/j.jconrel.2017.08.013>.

Acknowledgements

This work was funded by the University of Ulster.

References

- [1] M. Hruby, S.K. Filippov, P. Stepanek, Smart polymers in drug delivery systems on crossroads: which way deserves following? *Eur. Polym. J.* 65 (2015) 82–97.
- [2] A. Brun-Graeppe, C. Richard, M. Bessodes, D. Scherman, O. Merten, Cell microcarriers and microcapsules of stimuli-responsive polymers, *J. Control. Release* 149 (2011) 209–224.
- [3] C. Ashley, E. Carnes, G. Philips, D. Padilla, P. Durfee, P. Brown, T. Hanna, J. Lui, B. Phillips, M. Carter, N. Carroll, X. Jiang, D. Dunphy, C. Willman, D. Petsev, D. Evans, A. Parikh, B. Chacherian, W. Wharton, D. Peabody, C. Brinker, The targeted delivery of multicomponent cargos to cancer cells by nanoporous particle-supported lipid bilayers, *Nat. Mater.* 10 (2011) 389–394.
- [4] M. Zayats, M. Kanwar, M. Ostermeier, P. Seanson, Tuning protein recognition at the molecular level, *Macromolecules* 44 (2011) 3966–3972.
- [5] T. Ramasamy, H.B. Ruttala, B.G. Kanu, B.K. Poudel, H.-G. Choi, C.S. Yong, J.O. Kim, Smart chemistry based nanosized drug delivery systems for systemic applications: a comprehensive review, *J. Control. Release* 258 (2017) 226–253.
- [6] D. Furgeson, M. Dreher, A. Chilkoti, Structural optimisation of a 'smart' doxorubicin-polypeptide conjugate for thermally targeted delivery of solid tumors, *J. Control. Release* 110 (2006) 362–369.
- [7] M. Hruby, C. Konak, K. Ulbrich, Polymeric micellar pH-sensitive drug delivery system for doxorubicin, *J. Control. Release* 103 (2005) 137–148.
- [8] S. Banerjee, D. Chen, A multifunctional magnetic nanocarrier bearing fluorescent dye for targeted drug delivery by enhanced two photon triggered release, *Nanotechnology* 20 (2009) 185103–185112.
- [9] S. Murdan, Electro responsive drug delivery from hydrogels, *J. Control. Release* 92 (2003) 1–17.
- [10] N. Nomikou, C. Arthur, C. Sterrett, B. McCaughan, J.F. Callan, A.P. McHale, Ultrasound enhanced photoactivation of indocyanine green in-vitro and in-vivo - implications for targeted cancer therapy, *ChemMedChem* 7 (2012) 1465–1471.
- [11] L. Glangchi, M. Caldorera-Moore, L. Shi, K. Roy, Nanoimprint lithography based fabrication of shape specific enzymatically-triggered smart nanoparticles, *J. Control. Release* 125 (2008) 263–272.
- [12] C. McCoy, C. Rooney, C. Edwards, D. Jones, S. Gorman, Light-triggered molecule-scale drug dosing devices, *J. Am. Chem. Soc.* 129 (2007) 9572–9573.
- [13] J. Honey, J. Rijo, A. Anju, K. Anoop, Smart polymers for the controlled delivery of drugs - a concise overview, *Acta Pharm. Sin. B* 4 (2014) 120–127.
- [14] S. Swaminathan, Photoresponsive polymer nanocarriers with multifunctional cargo, *Chem. Soc. Rev.* 43 (2014) 4167–4178.
- [15] B. Lukyanov, M. Lukyanova, Syroprans: synthesis, properties and application, *Chem. Heterocycl. Compd* 41 (2005) 281–311.
- [16] Q. Zhou, Y. Zhu, P. Sheng, Z. Wu, Q. Cai, A highly selective and reversible fluorescent Cu²⁺ and S²⁻ probe under physiological conditions in live cells, *RSC Adv.* 4 (2014) 46951–46954.
- [17] M. Balter, M. Hammarson, P. Remon, S. Li, N. Gale, T. Brown, J. Andreasson, Reversible energy transfer switching on a DNA scaffold, *J. Am. Chem. Soc.* 137 (2015) 2444–2447.
- [18] I. Yildiz, S. Impellizzeri, E. Denniz, B. McCaughan, J.F. Callan, F. Raymo, Supramolecular strategies to construct biocompatible and photoswitchable fluorescent assemblies, *J. Am. Chem. Soc.* 133 (2011) 871–879.
- [19] F. Khan, R. Katara, S. Remteke, Enhancement of bioavailability of cefpodoxime proxetil using different polymeric microparticles, *APPS Pharm. Sci. Tech.* 11 (2010) 1368–1372.
- [20] M. Talelli, M. Barz, C. Rijcken, F. Kiessling, W. Hennink, T. Lammers, Core-cross-linked polymeric micelles: principles, preparation, biomedical applications and clinical translation, *Nano Today* 10 (2015) 93–117.
- [21] G. Kohli, H. Kierstead, J. Venditto, L. Walsh, C. Szoka, Designer lipids for drug delivery: from heads to tails, *J. Control. Release* 190 (2014) 274–287.
- [22] H. Kapahi, Implication of nanofibers in oral drug delivery, *Curr. Pharm. Des.* 21 (2015) 2021–2036.
- [23] Y. Yang, J. Bugno, S. Hong, Nanoscale polymeric penetration enhancers in topical drug delivery, *Polym. Chem.* (9) (2013) 2651–2657.
- [24] S. Hocine, Thermoresponsive self-assembled polymer colloids in water, *Soft Matter* 9 (2013) 5839–5861.
- [25] A. Di Crescenzo, V. Etter, A. Fontana, Non-covalent and reversible functionalization of carbon nanotubes, *Beilstein J. Nanotechnol.* 5 (2014) 1675–1690.
- [26] R. Singh, W. James, J. Lillard, Nanoparticle based targeted drug delivery, *Exp. Mol. Pathol.* 86 (2009) 215–223.
- [27] K. Miyata, R. Christie, K. Kataoka, Polymeric micelles for nano-scale drug delivery, *React. Funct. Polym.* 71 (2011) 227–234.
- [28] Q. Xing, N. Li, D. Chen, W. Sha, Y. Jiao, X. Qi, Q. Xu, J. Lu, Light-responsive amphiphilic copolymer coated nanoparticles as nanocarriers and real-time monitors for controlled drug release, *J. Mater. Chem. B* 2 (2014) 1182–1189.
- [29] X. Li, N. Hao, H. Chen, J. Xu, Tumor-marker-mediated 'on-demand' drug release and real time monitoring system based on multifunctional mesoporous silica nanoparticles, *Anal. Chem.* 86 (2014) 10239–10245.
- [30] J. Lai, B. Shah, E. Garfunkel, K. Lee, Versatile fluorescence resonance energy transfer based mesoporous silica nanoparticles for real-time monitoring of drug release, *ACS Nano* 7 (2013) 2741–2750.
- [31] F.M. Raymo, S. Giordani, Signal processing at the molecular level, *J. Am. Chem. Soc.* 123 (2001) 4651–4652.
- [32] L. Baumann, K. Scholler, D. de Courten, D. Marti, M. Frenz, M. Wolf, R.M. Rossi, L.J. Scherer, Development of light-responsive porous polycarbonate membranes for controlled caffeine delivery, *RSC Adv.* 3 (2013) 23317–23326.
- [33] C. Martin, E. Dolmazon, K. Moylan, C. Fowley, A. McHale, J. Callan, B. Callan, A charge neutral, size tuneable polymersome capable of high biological encapsulation efficiency and cell permeation, *Int. J. Pharm.* 481 (2015) 1–8.
- [34] M. Linlin, Y. Fan, Z. Jie, Application of fluorescence resonance energy transfer in protein studies, *J. Mol. Struct.* 1077 (2014) 87–100.
- [35] M. Karimi, P.S. Zangabad, S. Baghaee-Ravari, M. Ghazadeh, H. Mirshekari, M.R. Hamblin, Smart nanostructures for cargo delivery: uncaging and activating by light, *J. Am. Chem. Soc.* 139 (2017) 4584–4610.
- [36] G. Yu, R. Zhao, D. Wu, F. Zhang, L. Shao, J. Zhou, J. Yang, G. Tang, X. Chen, F. Huang, Pillar[5]arene-based amphiphilic supramolecular brush copolymer: fabrication, controllable self-assembly and application in self-imaging targeted drug delivery, *Polym. Chem.* (40) (2016) 6178–6188.
- [37] L. Jiang, X. Huang, D. Chen, H. Yan, X. Li, X. Du, Supramolecular vesicles coassembled from disulphide linked benzimidazolium amphiphiles and carboxylate substituted pillar[6]arenes that are responsive to five stimuli, *Angew. Chem. Int. Ed.* 56 (2017) 2655–2659.

Appendix 3

Recent advances in amphiphilic polymers for simultaneous delivery of hydrophobic and hydrophilic drugs

Nanomedicine has evolved with the use of biological compounds such as proteins, peptides and DNA. These hydrophilic and often highly charged compounds require a delivery system to allow effective transport and release at the site of action. These new biological therapeutics have not replaced the more traditional smaller molecule, but instead are working synergistically to the benefit of the end user. To that end, drug delivery systems are now required to encapsulate both larger hydrophilic compounds as well as the smaller and generally more hydrophobic compound. This review highlights the emerging role in drug delivery of amphiphilic polymers that by their very nature can associate with compounds of differing physicochemical properties, in particular the role of micelles, polymersomes and nanocapsules.

Submitted: 1 September 2015; Accepted: 26 October 2015; Published online: 10 December 2015

The requirement for delivering hydrophilic drugs has significantly increased in the past decade as medicine has evolved from the 'one size fits all' approach to drug development with thanks in part to the Human Genome Project (HGP) [1]. Since the completion of this landmark discovery there has been a pervasive increase and exploration of personalized medicine. The therapeutic use of siRNAs, proteins and enzymes has allowed for a revolution in healthcare regimes [2]. In order to reach its full potential, it is essential that such therapeutics can be delivered to their required site of action. The size and hydrophilic nature of these compounds, combined with the fact they are often highly charged, presents a significant challenge from a formulation perspective. One successful method of delivering these types of compounds to their target cells is through the use of liposomes. Since the late nineteenth/early twentieth century scientists have appreciated that the cellular membrane consists of a lipid bilayer [3] and as such, most nonpolar compounds can readily pass through this membrane to the interior of the cell. The translation of this mech-

anism for drug delivery purposes occurred in 1965 when Bangham [4] coined the term 'liposomes' with a description of self-forming lipid vehicles capable of encapsulating compounds for cellular transport. By mimicking the lipid bilayer, these vehicles, together with their content, could transcend the structurally similar cell membrane and enter the interior of the cell. These self-assembling drug delivery systems (DDS) expanded from lipids to include both natural and synthetic polymers with the only prerequisite for successful formation being the presence of both hydrophobic and hydrophilic units.

The use of biopharmaceuticals have not replaced traditional small molecule drugs; indeed, when prescribed together they often display a synergistic benefit to the patient. The advances in such combination therapies has led to the requirement of drug delivery systems to expand so that both hydrophobic and hydrophilic drugs can be delivered in the same vehicle simultaneously [5]. This can present a significant challenge as the physicochemical properties of these two classes of compounds are quite literally 'polar opposites'.

Chloe Martin¹, Noorjahan Aibani¹, John F Callan¹ & Bridgeen Callan^{*1}

¹School of Pharmacy & Pharmaceutical Sciences, University of Ulster, Coleraine, BT52 1SA, Northern Ireland, UK

*Author for correspondence:

Tel.: +44 28 701 23510

b.callan@ulster.ac.uk

**FUTURE
SCIENCE** part of

fsg

Key terms

Amphiphilic polymer: Co-polymers possessing both a hydrophobic and hydrophilic subunit.

Polymeric micelle: Self-assembling nanoparticles comprised of amphiphilic polymers with a hydrophobic core and hydrophilic corona.

Polymersome: Self-assembling nanoparticles comprised of amphiphilic polymers with a hydrophilic cavity, a hydrophobic interdigitated membrane and an outer hydrophilic corona.

Nanocapsule: Nano-sized self-assembling structures containing an amphiphilic polymeric wall surrounding a hydrophobic or oil core.

Hydrophilic compounds: Compounds belonging to Biopharmaceutics Classification System (BCS) class III, with high water solubility but low cell permeability. These compounds tend to be larger and often charged.

Hydrophobic compounds: Compounds belonging to BCS class II drug substances, with low water solubility and high cell permeability.

Simultaneous drug delivery: The incorporation of both a hydrophobic and hydrophilic drug into the same vehicle and subsequent drug delivery.

The development of drug delivery systems formed from amphiphilic building blocks has obvious benefits when considering the delivery of compounds with distinctly different physical properties. These amphiphiles can self-assemble in solution to form particles with both hydrophilic and hydrophobic regions that are capable of delivering a wide range of both polar and nonpolar compounds [6]. Often these particles have diameters in the nanometer range and provide improved stability for their cargo, have good biocompatibility with tissues and cells and due to their subcellular size display a relatively high intracellular uptake [7]. It has been established that nanocarriers can become concentrated preferentially in tumors, inflammatory sites and at antigen sampling sites by virtue of the enhanced permeability and retention (EPR) effect of the vasculature. Once accumulated at the site, these nanoparticles can act as a drug depot, providing a source of API to be released as and when required. This leads to enhanced bioavailability, a more sustained/controlled release and reduced toxicity that can be caused by a 'burst release' of the API. Current nanoparticulate drug delivery systems being investigated include liposomes [8], micelles [9], nanospheres [10], nanocapsules [11], niosomes [12] and polymersomes [13,14] among others. Central to the development of these delivery systems is the flexibility offered by using polymers as the building block. In particular, amphiphilic co-polymers [15], that are formed from covalently linked polymer chains in blocks of two or more [16], have demonstrated significant potential for the delivery of both large highly charged biological compounds as well as the more conventional small molecule and typically hydrophobic drug compounds. This article reviews the role

amphiphilic polymers have played in creating such multifunctional delivery systems and in particular the recent developments in polymeric micelles, polymersomes and nanocapsules.

Amphiphilic polymers

Many examples can be found in the literature where amphiphilic polymers have been used for drug delivery applications [17]. Such polymers have the ability to form a variety of assemblies depending on both the number of monomers used in the polymer synthesis and the particular polymerization process chosen for their assembly [17,18]. The most common number of monomers used for the preparation of amphiphilic polymers is two, hence the term co-polymer [18], three monomers polymerized are known as ter-polymers [19], while one amphiphilic monomer can also create an amphiphilic homopolymer [20]. There are a vast number of hydrophobic and hydrophilic monomers used in the creation of amphiphilic polymers with some of the more common examples listed in Table 1. Co-polymers can form conformations with alternating [21], random [22], graft [23], star [24] or brush [25,26] type structures (Figure 1), with the particular type created dependent upon the method of polymerization chosen. The simplest and most widely used of these structures is the random co-polymer, however these can be difficult to control in terms of reproducibility and so it is not surprising that the brush copolymer and more recently the periodically grafted copolymers (PGCP) [27], which are a nonionic version of the ionenes, have generated significant interest. Once the polymer has been synthesized, it can then be assembled into a supramolecular drug delivery system, using a number of different techniques, such as the one step solvent evaporation (simple emulsion evaporation [SEE]) method. In this procedure, the polymer is dissolved in an organic solvent and the drug added to the polymer solution. This solution is then combined with an aqueous phase to create an emulsion after which the organic solvent is removed, usually by heat or continuous stirring [28]. Although this method is the most common method used for NP preparation, it can be difficult to scale up for industrial applications and hence the use of supercritical fluid technologies is also being investigated [29] among others [30]. This review will focus primarily on examples where amphiphilic polymers have been used to form polymeric micelles, polymersomes and nanocapsules, as drug delivery vehicles, with a focus on block co-polymers. There is a high degree of diversity within these formations depending upon both the polymer used and the method of formation. Figure 2 illustrates a common formation of each of the DDSs to be discussed.

Polymeric micelles

Polymeric micelles have been extensively studied due to their simple structure, ease of production and capabilities of encapsulating and delivering hydrophobic drugs in their water insoluble core while their surrounding hydrophilic surface enables the vehicle itself to be stored and administered in aqueous solution [31]. Polymeric micelles are formed by the self-assembly of amphiphilic polymers to form a hydrophobic core and hydrophilic outer layer (corona) as shown in Figure 2. They are typically very small in size (usually >100 nm) and enable protection of their cargo by limiting opsonin adsorption, which contributes toward a longer blood circulation time and better blood stability [32]. They have gained considerable interest in recent years because of their applicability to cancer therapy and their ability to incorporate a range of drugs with different physicochemical properties. The hydrophobic core of micelles allows enhanced solubilization of hydrophobic drugs while the outer surface can be modified to attach specific ligands such as RNAs, DNAs and also other anticancer drugs [33] allowing for the simultaneous delivery of both hydrophobic and hydrophilic compounds.

There are many interesting examples of where amphiphilic polymer micelles have been used for the simultaneous delivery of both hydrophobic and hydrophilic drugs [34]. The most common approach is where the nonpolar core is used to encapsulate the hydrophobic drug while a charged outer corona (usually positively charged) is used to electrostatically interact with the biological component. Both Qian *et al.* and Bian *et al.* have successfully encapsulated doxorubicin in the core of the micelle and conjugated micro-RNA and green fluorescence labeled DNA [35,36] to the corona. Qian *et al.* used amphiphilic star branched copolymers using polylactic acid (PLA) and polydimethylaminoethyl methacrylate (PDMAEMA) while Bian *et al.* used poly(ethylene phosphate)-block-poly(ϵ -caprolactone)-block-poly[2-(dimethylamino)ethyl methacrylate] (PEEP-b-PCL-b-PDMAEMA). The PLA and PCL chains formed the hydrophobic core whereas the PDMAEMA forms the positively charged outer corona to which the RNA/DNA was attached by electrostatic interactions. Another cationic monomer that has been used successfully to interact with miRNA is tetra-ethylene-pentamine (TEPA). Kumar *et al.* [37] created a co-polymer using TEPA, PEG, poly(2-methyl-2-carboxyl-proylenecarbonate) (PCC) and a decyl chain (DC) to treat pancreatic ductal adenocarcinoma with a hydrophobic hedgehog (Hh) inhibitor encapsulated within the center of the micelle and the tumor suppressant *miR-let7b* electrostatically attached to the surface, both compounds

were effectively delivered using the NP. Another polymer used to form of cationic polymeric micelles is branched polyethylenimine (PEI), in particular low molecular weight (LMW) PEI as it has reduced toxicity when compared to its higher molecular weight counterpart [38]. Gaspar *et al.* have incorporated PEI into a triblock copolymer to create a polymeric micelle capable of delivering minicircle DNA (mcDNA) [39]. These promising therapeutics are a class of nonviral gene expression vectors that present excellent characteristics for future use in cancer therapy. Gaspar *et al.* combined the mcDNA delivery with hydrophobic DOX, which caused the zeta potential of the cationic micelle to reduce from +42.3 mV without the mcDNA to +21.9 mV after complexation. Mittal *et al.* [40] have also used cationic polymers to electrostatically bind with siRNA, however, instead of encapsulating a hydrophobic drug within the polymeric micelle, they chose to deliver the antimetabolite gemcitabine for the enhanced treatment of pancreatic cancer. Gemcitabine is a highly water soluble structure that if given orally suffers extensive first pass metabolism to inactive compounds. Its anticancer activity works by inducing S-phase arrest and inhibiting DNA synthesis. In this example, the authors conjugated the primary amine of gemcitabine onto the polymer backbone through amidation, which was released upon hydrolysis *in vivo*. They concluded that their cationic polymeric micelle achieved an 8–12% w/w gemcitabine loading and successfully transfected and reversed chemo-resistance, invasion and metastasis in gemcitabine-resistant pancreatic cancer cells [40].

The alternative mechanism to utilizing a cationic corona is to create an anionic micelle. There are numerous examples within the literature whereby an anionic corona has been created thus attracting positively charged hydrophilic compounds for complexation. One of the most common drugs to be electrostatically attached to the corona is doxorubicin. As a chemotherapy agent DOX works by binding to DNA and inhibiting nucleic acid synthesis [41]. It can be combined with alternative chemotherapeutic agents that have different mechanisms of action, such as paclitaxel and curcumin. In the examples discussed above where DOX was the hydrophobic drug encapsulated within the micelle, it was in its free base state and therefore possesses limited solubility. However, when the primary amine becomes protonated it is both positively charged and water soluble which is why DOX is generally administered as its HCL salt form (DOX-HCl). Sun *et al.* [42] have developed a micelle capable of encapsulating curcumin within the micelle and subsequently binding DOX-HCl using a biodegradable poly(ethylene glycol)-poly(3-caprolactone) (mPEG–

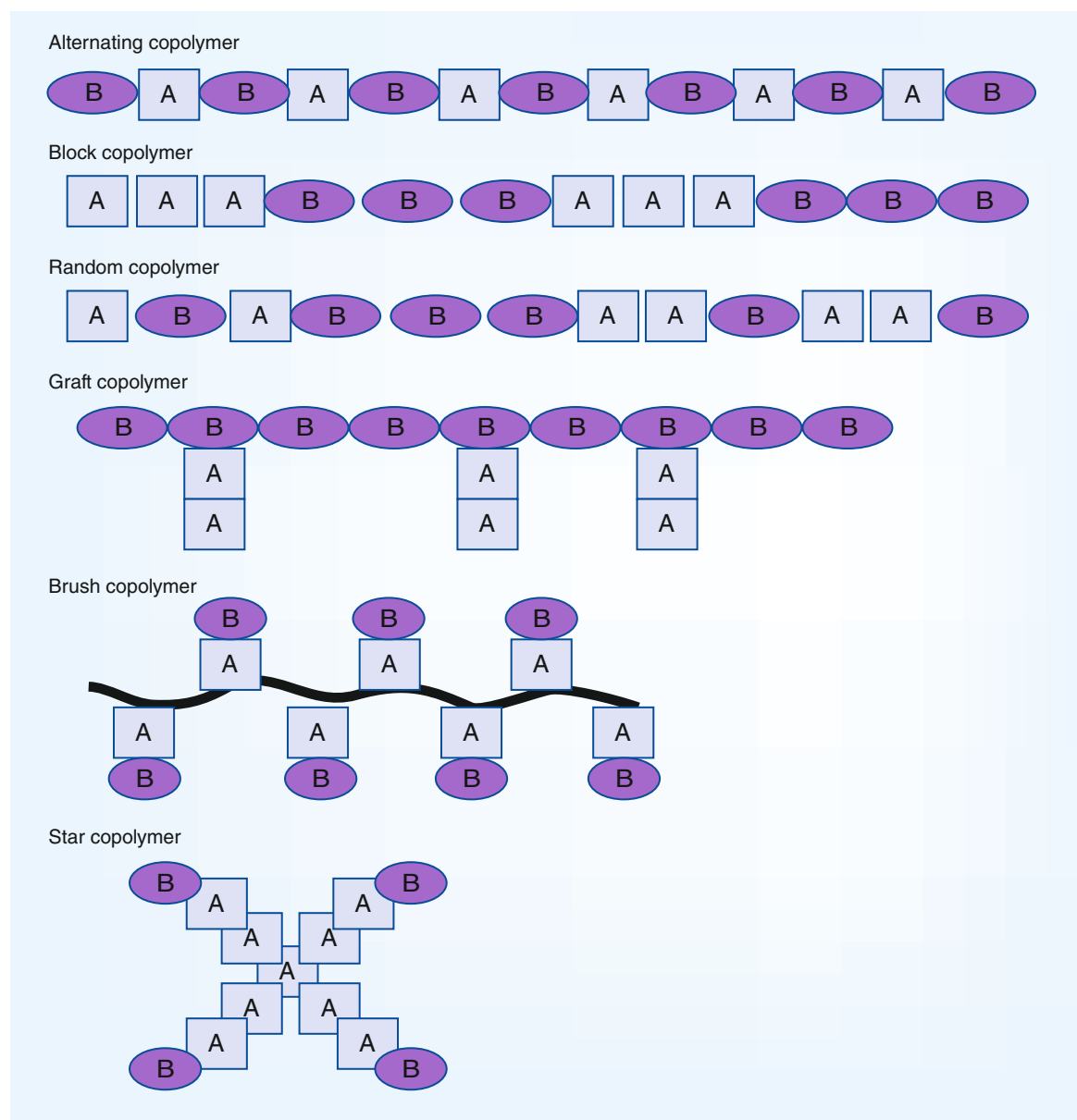


Figure 1. Different forms of copolymers that can be created from monomers (A and B) using different polymerization techniques.

PCL) co-polymer. The resultant micelles were very small having a hydrodynamic radius of 25.3 ± 0.2 nm with a polydispersity index (PDI) of 0.065 ± 0.011 and good encapsulation efficiency of $96.8 \pm 0.30\%$ and $99.3 \pm 0.47\%$ and drug loading of $4.85 \pm 0.01\%$ and $4.97 \pm 0.02\%$, for DOX and curcumin, respectively. The exact mechanism of DOX-HCl association is unclear, so it was presumed that hydrogen bonding must play a significant role as DOX has 12 hydrogen bond acceptors and six donors per molecule. Perhaps electrostatic interactions of the positive DOX are also involved, however the zeta potential for this micelle was not quoted. Lv *et al.* have also chosen DOX-HCl

as the hydrophilic drug to deliver using polymeric micelles. They utilized micelles prepared from the negatively charged poly (glutamic acid) to electrostatically bond to DOX-HCl with paclitaxel (PTX) encapsulated within the core for synergistic anticancer activity [43]. Li *et al.* also describe DOX-HCl and PTX encapsulation using the polymer methoxy-poly(ethylene glycol)-b-poly(L-glutamic acid) (mPEG-b-PLG) [44]. In this example paclitaxel was covalently bonded to micelle via an ester bond while DOX-HCl attached using electrostatic and hydrophobic interactions. This system displayed increased release at both pH 6.8 and 5.4 indicative of the pH found in tumor interstitial

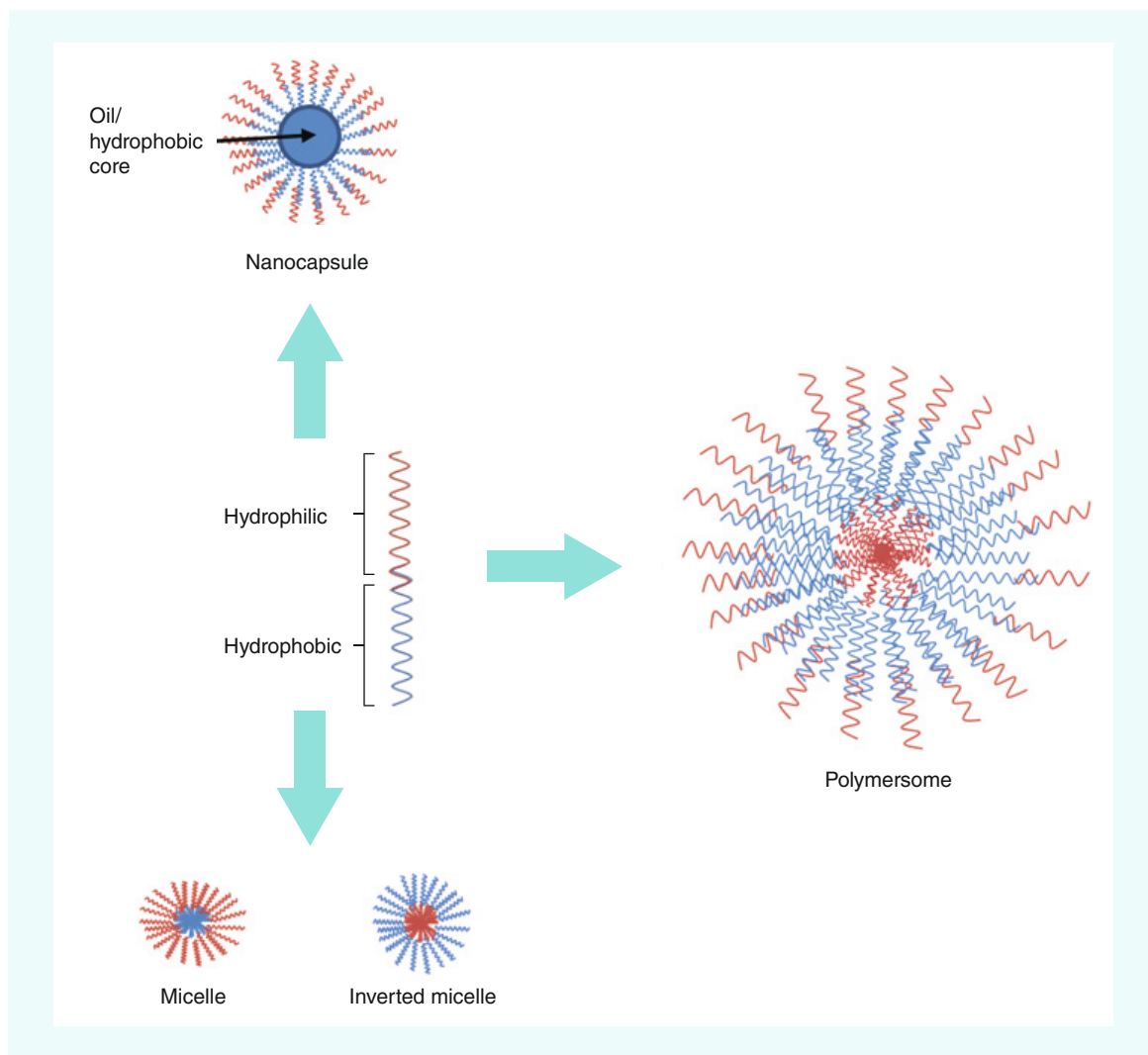


Figure 2. Simplified illustration of some types of nanoparticle that can form from amphiphilic polymers.

fluid and endosomes respectively as well as enhanced accumulation at tumor sites due to the EPR effect illustrating its potential for tumor delivery. When tested in human cancer cells (A549 and MCF-7) a synergistic effect was observed when both PTX and DOX were administered together while in vivo a 95.5% tumor suppression rate was observed which was significantly better than micelles containing free DIX (59.7%) or PTX (67.7%) showing its potential as a dual drug delivery system.

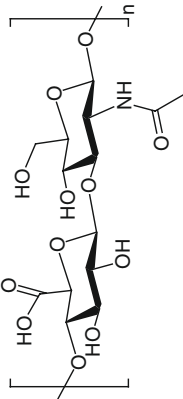
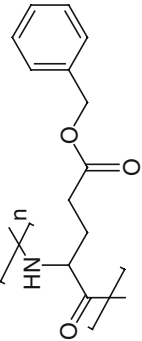
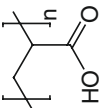
Tain *et al.* [45] have taken an interesting approach to dual drug delivery using micelles for the simultaneous delivery of two hydrophobic drugs. They prepared an amphiphilic PEGylated rapamycin micelle to solubilize the hydrophobic drug rapamycin and use the PEG-rapamycin to further encapsulate another chemotherapeutic agent, in this case PTX. PEG-succinic acid (SA) was used to conjugate with the alcohol groups on

the rapamycin, creating a PEG-SA-rapamycin amphiphilic polymer which self-assembled and encapsulated PTX. The zeta potential of the overall system was -11 mV and the novel nanomedicine offered a 20-fold improved potency over free PTX against a model multidrug resistant human breast cancer cell again reiterating the benefits of a synergistic approach.

The third and final option for the delivery of both hydrophobic and hydrophilic drugs by polymeric micelles is by the creation of neutral NPs. There are fewer examples of this type of micelle than either the cationic or the anionic forms; however the neutral nature of the micelle will be beneficial when it comes to cell retention as it has been shown that the RES uptake of particles cannot be avoided if their zeta potential values are above -5 mV [46]. In these examples the amphiphilic polymers have the capability of encapsulating hydrophobic drugs and

Hydrophilic			Hydrophobic		
Name	Abbrev.	Structure	Name	Abbrev.	Structure
Polyethylene glycol	PEG, sometimes referred to as PEO (polyethylene oxide)		Poly(lactic acid)	PLA, sometimes referred to as PDLLA to denote a racemic stereochemistry	
Polyethylenimine	PEI		Poly caprolactone	PCI	
Poly (2-dimethyl-aminoethyl methacrylate)	PDMAEMA		Poly (2-ethyl-2-oxazoline)	PEOz	
Poly (ethylene ethyl phosphate)	PEEP		Poly L-Lysine	PLL	
Tetra ethylene pentamine	TEPA		Poly(2-methyl-2-carboxy-propylene carbonate)	PCC, referred to as many different abbreviations including PMC and PC	
Poly (ethyl glycinate methacrylamide),	PEGMA		Poly(propylene glycol) or poly propylene oxide	PPO	
Poly (allyl glycidyl ether)	PAGE		Poly (styrene)	PS	

Table 1. Structural representation of some of the more commonly used polymers (cont.).

Hydrophilic			Hydrophobic		
Name	Abbrev.	Structure	Name	Abbrev.	Structure
Hyaluronic acid	HYA		Poly (benzyl glutamate)	PBLG	
Poly (acrylic acid)	PAA				

further provide cross linking or conjugation of the micelles with another more hydrophilic drug. One such example of this was seen with the platinum-based anticancer drug, cisplatin. Scarano *et al.* used a polycaprolactone-based amphiphilic copolymer to encapsulate curcumin and crosslinked the resultant micelles with cis,cis,trans-diaminedichloro disuccinatoplatinum (IV) (Pt IV(COOH)₂) derived from oxoplatin [47]. The resulting cross linked micelles had a very small size of about 38 nm explained by the loss of surface charge and possible contraction of micelles during cross linking. The resultant incorporation of both drugs in the same micelle provided a very high synergistic effect with the curcumin and platinum complex providing enhanced cytotoxicity. Another example using cisplatin was described by Li *et al.* [48] where the free carboxylic acid groups on the side chain of the polymer were cross linked with the cisplatin. As observed by Scarano *et al.*, there was a significant reduction in the hydrodynamic radius of the micelle from 42 to 17 nm attributed to the cross linking within the micelle. Similarly, a synergistic effect was again observed when the combination therapy was used. A further interesting example of a neutral delivery system was described by Noh *et al.* [49]. They used two separate micelles, and brought them together through electrostatic interactions to form a single delivery system; a multi-prodrug nanocarrier (MPDNC). They achieved this by conjugating the hydrophilic drug gemcitabine (GEM) onto one polymer and the hydrophobic paclitaxel (PTX) onto another. To facilitate interaction between the two polymers a cationic charge was included within the hydrophobic carrier and an anionic charge on the hydrophilic carrier, thus ensuring the facile creation of a nanoparticle through electrostatic interactions between the two polymers and an overall net neutral species.

All of the examples described above have used either encapsulation (dominated by hydrophobic interactions) or chemical conjugation to incorporate the hydrophobic drug compound within the micelle. The effect of each approach on the release kinetics of the drug has been explored by Li *et al.* [50]. They investigated PTX release from amphiphilic micelles where the drug was either encapsulated with or chemically attached to the micelle. They concluded that at physiological pH (7.4) the encapsulated micelle resulted in a cumulative release of 16.3% after 48 h compared to only 1.8% release for the covalently attached counterpart. However, in acidic solution where hydrolysis can facilitate release of the PTX an improved 25% cumulative release was observed. The overall zeta potential of this system was quoted as

Table 2. Recent examples of simultaneous delivery of hydrophobic and hydrophilic compounds in polymeric micelles and the polymers used in their preparation.

Hydrophobic		Hydrophilic		Copolymer	Zeta (mV)	PEG	Ref.
Monomer	Drug	Monomer	Drug				
PLA	DOX	PDMAEMA	mi-RNA	Star	+10 to +27	x	[35]
PCL	DOX	PDMAEMA/ PEEP	GFP-DNA	Triblock terpolymer	+18	x	[36]
PCC/DC	GDC-0449	TEPA	miR-let7b	Copolymer with pendant chains	+5	√	[37]
PCC/DC	————	TEPA	siRNA Gem	Copolymer with pendant chains	+15	√	[40]
PEO ₂ / PLA	DOX	PEI	mcDNA	Triblock copolymer	+22	x	[39]
OA	PTX	PEI	siRNA	Graft copolymer	+14	x	[51]
PCHLG	Docetaxel	PEI	pDNA	Trilock copolymer	+33	x	[52]
PLL	Docetaxel	PEG	siRNA	Triblock copolymer	+20	√	[53]
PCL	curcumin	PEG	DOX-HCl	Copolymer	N/Q	√	[42]
PLL/DOCA	PTX	PLG	DOX-HCl	Triblock copolymer	-18	√	[43]
rapamycin	PTX	PEG-SA	None	Copolymer	-11	√	[45]
PLG-PTX	PTX	PEG	DOX-HCL	Triblock copolymer	-7	√	[44]
MPA/PLA	PTX	PEG/PAGE	Cisplatin	Block copolymer	N/EQ	√	[48]
PCL	Curcumin	PEGMEA/ PABPA	Oxoplatin	Triblock copolymer	N/EQ	√	[47]

N/Q: Not quoted; N/EQ: Not expected or quoted.

-11 mV, which can be attributed to the folic acid used as a cell targeting moiety.

Table 2 provides a summary of some current polymeric micelles reported for the delivery of both hydrophobic and hydrophilic drugs.

Polymersomes

Polymersomes are polymeric capsules with an interdigitated membrane comprised of synthetic amphiphilic block copolymers, Figure 2. Their macromolecular structure is similar to that of the liposome in that they are both composed of a bilayer of amphiphiles enclosing an aqueous compartment [54]. However, the difference between these two vehicles is that most liposomes are naturally occurring phospholipids and as such have both a strong negative charge and lower molecular weight than the synthetic polymeric alternatives. This enhanced ability to specifically tailor polymersome formulation methods, physicochemical properties, release mechanisms and even targeting chemistries make polymersomes an ideal platform for the encapsulation of a broad range of therapeutic molecules [16]. They can load hydrophilic, hydrophobic or amphiphilic compounds allowing them to be exceptional in delivering bioactive molecules and combined loading of multiple drugs for synergistic therapy [55]. With the ability to

tailor the properties of each polymer block as well as altering the hydrophilic to hydrophobic ratio a range of properties can be specifically tuned including size [56], encapsulation efficiency, pharmacokinetics including release rates, degradability and cellular entry as well as highly stable membranes avoiding drug leakage [57].

Another advantage of polymersomes is the ability to attach targeting moieties onto their surface to target receptors on cell membranes leading to site-specific delivery and so a more targeted release of payload. Targeting complexes such as RGD-containing peptides, folic acid and carbohydrates have been used to recognize specific cancer cells [58,59]. It is not surprising therefore that one of the major avenues of research into polymersomes is focussed on cancer therapies. Interestingly carbohydrates are known to be involved in many biomolecular recognition events such as cell adhesion and growth regulation; extracellular recognition as well as cancer cell metastasis and inflammation [59]. In a study by Das *et al.* [58] a glycopeptide-based polymer glycopeptide-b-poly(propylene oxide) (GP-PPO) was used to form polymersomes to encapsulate both hydrophilic and hydrophobic dyes calcein and rhodamine B octadecyl ester percholate (RBOE), respectively. Upon encapsulation of both complexes using the co-assembly method the hydrodynamic radius of the polymersomes

increased and encapsulation efficiencies (EE) were found to be on average 6.3% calcein and 23% RBOE. Although these EEs are relatively low it is important to note that a higher percentage of the hydrophobic agent has been encapsulated into the bilayer itself than the hydrophilic drug into the inner aqueous compartment. A similar observation was also reported by Xu *et al.* [60] who compared the uptake of DOX-HCl with its free base DOX using PEP polymersomes. The maximum encapsulation of hydrophilic DOX HCl was found to be 16.3% compared to a maximum 90% for DOX. These lower drug encapsulation efficiencies for the inner compartment of the polymersome could be due to the method of preparation of the nanoparticles, with the outer bilayer being more easily accessed than the inner cavity.

With drug resistance and toxicity a major limiting factor in cancer chemotherapy the idea of a combined treatment allowing the simultaneous delivery of multi anticancer drugs and or genetic components could overcome these issues as well as improve the pharmacokinetics of treatments for patient. Using the biodegradable amphiphilic copolymer mPEG-b-PLA to encapsulate small interfering RNA (siRNA) against the anti-apoptotic gene *Bcl-xL* and widely used DOX, Hyun-Ouk *et al.* [61] reported a marked increase in the cell death of two gastric cancer cell lines MKN-45 and MKN-28 with the administration of these co-loaded polymersomes, compared with free doxorubicin, *Bcl-xL*-specific siRNA loaded Lipofectamine with doxorubicin as well as doxorubicin polymersomes. Release profiles for the co-loaded polymersomes at pH 5.5 and 7.4 showed an initial burst release which was reflected in the results of the MTT study which show more than a 50% decrease in cell viability after 24 h and a plateau of less than 30% viable cells reached after 48 h. This was compared with free doxorubicin, *Bcl-xL*-specific siRNA loaded Lipofectamine with doxorubicin as well as doxorubicin polymersomes which all displayed a much lower cellular toxicity after 72 h of 60–70%.

The combination of the DOX-HCL and PTX has been found to be highly effective in the treatment of advanced breast cancer, however when administered alone or together without the aid of a nano-carrier, the severe dose-dependent side effects such as cardiotoxicity, neutropenia and neuropathy along with multidrug resistance limit its use in the clinic [43]. This has led to extensive research into drug delivery systems for co-delivery of anticancer drugs. Table 1 displays some recent examples of where both these drugs have been combined within a polymeric micelle delivery system. However, unlike micelles, polymersomes do not require either chemical conjugation or electrostatic

interactions to combine both of these compounds, as they contain both hydrophilic and hydrophobic compartments. There are a few examples where these same drugs have been combined within a polymersome [57]. Iatrou *et al.* [62] have investigated two different polymersomes for the independent delivery of DOX and PTX, comparing a tri block co-polymer with a ter-polymer. They concluded that both forms of polymer were capable of encapsulating both drugs, but did not allude to whether the possibility of simultaneous delivery was to be investigated in the future but did anticipate the incorporation of genes with either of the anticancer drugs. Colley *et al.* reported the pH-sensitive poly2-(methacryloyloxy)ethyl phosphorylcholine (PMPC)-poly 2-(diisopropylamino)ethyl methacrylate (PDPA) polymersome for both the combined and independent delivery of DOX and PTX [63]. They recorded combined encapsulation efficiencies (%) of 42.7 ± 10.2 and 37.1 ± 13.5 for PTX and DOX respectively with a hydrodynamic radius of 224.5 ± 43.5 nm, which is better than some independent therapies. They conclude that the polymersomal combination of PTX and DOX in an *in vitro* tumor model displayed significantly less cell survival than any of the controls experiments.

As well as the research into polymersomes as dual drug delivery systems for cancer chemotherapy, they have more recently been investigated for a novel bacterial sensing application which allows the differentiation between a serious pathogenic infection and a minor inflammatory response; in certain cases like bandage covered burn wounds, symptoms are often similar including elevated temperature and a decline in wound condition [64]. Haas *et al.* [65] described a hyaluronidase responsive amphiphilic block copolymer which specifically targets the common *Staphylococcus aureus* bacterium. Over 90% of strains of this bacteria secrete hyaluronidase and is known to be produced by *Clostridium* and *Streptococcus* spp, so by incorporating the naturally produced, biocompatible, polysaccharide hyaluronic acid (HYA) into the polymer, Haas *et al.* have shown that in the presence of bacteria secreting this enzyme the polymersome itself was degraded. Enzymatic degradation begins slowly with only minimal reduction in size from 100 nm after 10 min, however this lull is followed by a fast decrease, with degradation ceasing after 30 min with vesicles reducing in size to on average 30 nm. This 70% reduction in size of the polymersomes due to the enzymatic breakdown of its structure was then harnessed to allow the encapsulation of specific antimicrobials. This allows the system to not only recognize the bacterial infection but also release appropriate therapeutics, as well as reporter dye molecules, at the correct sites to treat it.

Dual delivery of silver nanoparticles with the hydrophilic antibiotic ampicillin using polymersomes have also recently been investigated by Geilich *et al.* [66] who found the co-administration led to synergistic activity against the gram-negative genetically modified antibiotic-resistant *Escherichia coli* (*E. coli*) inhibiting or delaying its growth. Gram-negative bacteria are particularly problematic in relation to antibiotic resistance due to their outer selectively permeable lipopolysaccharide membrane, the presence of efflux pumps and the production of hydrolyzing β -lactamase. The co-delivery of reactive silver nanoparticles known to disrupt and indent the bacteria cell wall leading to increased permeability as well as possible reactive oxygen species (ROS) release and ampicillin in a 1:0.64 ratio led to complete growth inhibition in the resistant strain. Additionally, in the absence of silver nanoparticles no bacteriostatic effect was observed at any ampicillin concentration (free and polymersome loaded) suggesting its therapeutic efficacy is potentiated by the presence of the metal nanoparticles.

Table 3 summarizes recent examples where polymersomes have been used to deliver both hydrophobic and

hydrophilic drugs as well as some interesting examples of single drug delivery.

Nanocapsules

One further nanoparticulate delivery system derived from amphiphilic polymers and discussed within this review is that of nanocapsules. These are nano-sized structures containing an amphiphilic polymeric wall surrounding a hydrophobic or oil core (Figure 2). These vesicles are generally larger than micelles, typically ranging between 40 and 240 nm. They are commonly formed by an emulsification method [71] or the interfacial polymer deposition method [72]. There are a number of recent examples in the literature where nanocapsules have been used to deliver insoluble drugs such as naturally occurring compounds from plants such as polyphenols and carotenoids. These compounds have gained increased interest due to their therapeutic potential [73,74–75] as antioxidants. Free radicals leading to oxidative stress are known to be a major cause of many disease states including degenerative and inflammatory conditions such as cancer, cardiovascular disease, diabetes, rheumatoid arthritis and age-related macular degeneration (AMD) [72,75].

Table 3. Recent examples of simultaneous delivery of hydrophobic and hydrophilic compounds in polymersomes and the polymers used in the preparation.

Hydrophobic		Hydrophilic		Copolymer	Zeta (mV)	PEG	Ref.
Monomer	Drug	Monomer	Drug				
EAB	DOX	PEG	DOX-HCL	Graft copolymer	N/EQ	√	[60]
PPO	RBOE	GP	Calcein	Copolymer	N/EQ	x	[58]
PCHLG	———	PEI + OA	pDNA	Brush copolymer	N/EQ	x	[67]
PCL	Nile red	HYA	Calcein/gentamicin/carboxy fluorescein	Copolymer	N/EQ	x	[65]
PLA	DOX	PEG	siRNA	Copolymer	N/EQ	√	[61]
PBLG	PTX	PLL	DOX-HCl	Triblock copolymer	+ 45.3 - +48.2	x	[62]
PBLG/PEO	PTX	PLL	DOX-HCl	Terpolymer	+3.2 - + 5.4	x	[62]
PNIPAM	DOX	amilFP497	PE545 (protein)	Bioconjugate	N/EQ	x	[68]
PLA/DAC	———	PEG	Hb	Graft co-polymer	N/EQ	√	[69]
PDLLA	Ag NPs	PEG	Ampicillin	Copolymer	0.3	√	[66]
PDPA	PTX	PMPC	DOX-HCl	Copolymer	N/EQ	x	[63]
PLA	DOX	PEG	Herceptin®	Triblock copolymer	+27	√	[59]
PLA	Atorvastatin	PEG	Lisinopril	Tri block copolymer	-13	√	[70]

N/EQ: Not expected or quoted.

Curcumin, resveratrol and lutein have all shown antioxidant, anti-inflammatory and chemotherapeutic properties through their interactions with various molecular and cellular targets and most importantly their ability to neutralize harmful free radicals, however they display reduced bioavailability due to poor water solubility, rapid systemic clearance, inadequate tissue absorption and degradation at physiological pH. Nanocapsules have been studied in order to increase the water solubility of these compounds and subsequently increase their bioavailability enabling them to achieve their true therapeutic potential [74,75–76]. The nanocapsule can encapsulate these compounds within the hydrophobic protective inner core.

Nanocapsules derived from amphiphilic polymers that are capable of delivering two drugs with opposing solubility have not been widely studied. This is due to the oily core acting as the hydrophobic compartment while the hydrophilic polymers role is to impart polarity into the vehicle. There has been a significant amount of research into the different oils that can be included within the center of these capsules and the synergistic co-encapsulation of hydrophobic drugs within. One example is the co-encapsulation of curcumin and resveratrol in lipid-core nanocapsules (LNC) by Friedrich *et al.* [73] and Coradini *et al.* [72] for the treatment of topical skin conditions and rheumatoid arthritis, respectively. They demonstrate that co-encapsulation of the polyphenols showed the most pronounced beneficial effect when compared with individually loaded nanoparticles or the free drugs in solution. In a similar study using curcumin encapsulated in oil core nanocapsules (NC) for colon cancer treatment *in vivo* [77], it was discovered that altering the oil material in which the core was derived has a direct effect on size, zeta potential and encapsulation efficiency. Klippstein *et al.* looked at NCs derived from a PLGA-PEG conjugate (PLGA-NH-PEG-NH-DTPA) with central cavities composed of either castor oil, soybean oil or miglyol 812 oil [77]. Nanocapsules with castor oil cores were found to be optimal

as they showed the smallest size $150.5 \text{ nm} \pm 4.7$ and the highest encapsulation and loading efficiencies of $92.3 \pm 1.6\%$ and $18.4 \pm 0.3\%$ respectively as well as proving the most stable over a 28-day period with no significant changes in size. Miglyol 812 oil had the second highest encapsulation efficiency of $88 \pm 0.4\%$ and size of $205.5 \text{ nm} \pm 5.3$ with soybean oil having the largest size ($235.4 \text{ nm} \pm 9.6$), lowest encapsulation efficiency (68.9 ± 2.9) and zeta potential (-45.3 mV) of all three. Castor oil possesses the highest viscosity, surface tension and solubility of curcumin of all three oils and this is reflected in the characterization of the nanocapsules.

There is however a small number of reports highlighting the simultaneous delivery of hydrophobic and hydrophilic drugs (Table 4), such as the example presented by Chen *et al.* [78]. Similar to the mechanism adopted with polymeric micelles, they have used positively charged tertiary amine functionalized PLA as their hydrophilic monomer and allyl functionalized PLA as the hydrophobic counterpart creating a brush co-polymer. This positively charged nanocapsule can then electrostatically bind to negatively charged species, in this case siRNA with the hydrophobic DOX encapsulated within the core. Using confocal microscopy they successfully visualized both DOX and fluorescently labeled IL-8 siRNA in the same PC3 cells delivered using their nanocapsule.

Another example of simultaneous drug delivery is that by Hu *et al.* [81]. They have incorporated an additional triggered release into their nanocapsule. The release of drugs from nanocapsules has been shown to be slow, in particular for systems where a ‘stealth’ property has been added by incorporation or adsorption of PEG or heparin onto the surface of the capsule [76,82]. The ability to actively control release of the payload by application of an external stimulus also has its advantages. A recent study by Hu *et al.* [83] showed that the encapsulation of magnetic nanoparticles (MNPs) into the hydrophobic compartment of the capsules enabled a triggered release effect when

Table 4. Recent examples of simultaneous delivery of hydrophobic and hydrophilic compounds in nanocapsules and the polymers used in their preparation.

Hydrophobic		Hydrophilic		Copolymer	Zeta (mV)	PEG	Ref.
Monomer	Drug	Monomer	Drug				
Allyl-PLA	DOX	Tert amine-PLA	siRNA	Brush copolymer	+45	x	[78]
PtBA	DOX	PEG	Folate	Brush copolymer	N/Q	√	[79]
PCL	—	PEO	Rhodamine-dextran	Star copolymer	-16.3	√	[80]
PS	Magnetic NPs	PAA	FITC-DNA	Copolymer	N/Q	x	[81]

N/Q: Not quoted.

a magnetic field was subsequently applied. Amphiphilic polymer PS₁₆-PAA₁₀ used to produce nanocapsules through a simple scalable double emulsion method demonstrated that the release of hydrophilic FITC-labeled plasmid DNA and the hydrophobic dye pyrene could be increased by applying a high frequency magnetic field (HFMF) when co-encapsulated with MNPs. Release studies revealed FITC-pDNA showed only 10–25% release after 10 days with pyrene less than 5% over the same time period; when HFMF was applied at different pulsed field strengths both showed initial burst release after 5 min with a total of 80% FITC-pDNA and 10% pyrene released after only 25 min at the highest field strength of 2.0 kA/m. Although the hydrophobic drug release rate overall was lower with and without the presence of a magnetic field the quantity released for pDNA and pyrene seems to be field strength dependent as the stronger the magnetic field resulted in more drug being released.

The use of nanocapsules for simultaneous delivery of hydrophobic and hydrophilic drugs is still relatively new and with the efforts being made to develop new and advanced methods of preparation such as the melt dispersion technique described by Govender *et al.* [83] or the use of organometallic coordination polymers to allow capsules to release cargo without themselves being damaged [84], these initiatives will allow for a rapid expansion in this particular field of drug delivery. Table 4 displays some recent examples of dual drug delivery using nanocapsules.

Triggered drug release

One of the fundamental problems associated with this area of drug delivery is that of drug release. The ability to only deliver the active component at the required site of action is the gold standard when considering therapeutic drug delivery. There have been significant advances made in the quest to deliver this ‘second generation health care’ such as the development of biopharmaceutical systems capable of interacting with intracellular components that respond as a direct result to environmental stimuli [85], lipid functionalized nanoparticles that specifically bind to tumor cells [86] and receptor targeted systems [87]. The use of stimulated release is also becoming more prevalent with amphiphilic polymers and indeed in many reported examples have used external environmental changes to trigger the drug release, such as pH [73,79,88] redox [51,59,89, heat [59,68,90] and enzymes [59,65] among others [46,59].

Conclusion

This particular field of research, although having rapidly expanded in the past few decades, has still

much to offer. The types of nanospheres available for assembly and encapsulation have increased to include more complex internal and surface structures such as those described by Sommerdijk *et al.* with their biocontinuous polymer nanospheres (BPNs) [91] whereby the amphiphilic block copolymers are formed with a biocontinuous internal structure. This is achieved by the twisted hydrophobic phase intertwining with the hydrated hydrophilic moiety and could potentially allow for the simultaneous controlled release of both hydrophobic and hydrophilic compounds. In addition to the changing morphologies, we are also developing a deeper understanding into the materials being used and how they can be manipulated for the benefit of therapeutics. Such examples are displayed by Swaminathan *et al.* [92] who have described the phenomenon of intercellular guest exchange using the Forster Resonance Energy Transfer (FRET) process. They describe two separate micelles showing intercellular exchange of their hydrophobic cargo and this mechanism could potentially be further exploited for dual drug delivery. Another notable example has been the advances made to overcome the more complicated delivery routes such as using polymersomes as delivery systems to cross the blood–brain barrier (BBB) [93] and the use of nanocapsules in nose to brain drug delivery [94], as delivery across the BBB remains a major obstacle in the development of drugs targeted to the brain. One further example of the versatility of these compounds is presented by Wong *et al.* [68]. They have created a bio-conjugated thermoresponsive polymersome capable of encapsulating DOX and light harvesting proteins. However, a special feature of this work is the ability to clearly visualize where in the polymersome the cargo is situated so enhancing further our understanding of these systems.

In conclusion, there has been much progress made over the past decade in the development of delivery systems based on amphiphilic polymers for dual drug delivery applications. However, examples of where such systems have been used in the clinic are limited, with most trails to date focussing on the delivery of paclitaxel [95–97]. There is still much work to be done, in particular to improve the encapsulation and subsequent release of hydrophilic compounds. Nonetheless, few other drug delivery systems can rival the versatility offered by micelles, polymersomes and nanocapsules prepared from amphiphilic polymers when it comes to exploiting these nanoparticles for simultaneous drug delivery. This is a relatively new area of research and no doubt more interesting examples will emerge in the coming years and we look forward to reporting on these in due course.

Future perspective

As the use of multidrug therapies continues to show improved efficacies, the role of drug delivery systems capable of transporting these combined therapies increases. This review discusses some of the most recent examples using amphiphilic polymers. A number of the DDSs discussed have patents associated with them [98,99–106] suggesting that translation into the clinic may be on the horizon. As a note of caution however, the fundamental and major limitation of this particular area of research is cost. Without a financial incentive the use of concomitant delivery of such drugs will remain the biggest rival to these advanced systems,

and so the use of cheaper materials with facile scale ups and enhanced encapsulation capacities will be the future focus for such research.

Financial & competing interests disclosure

The authors have no relevant affiliations or financial involvement with any organization or entity with a financial interest in or financial conflict with the subject matter or materials discussed in the manuscript. This includes employment, consultancies, honoraria, stock ownership or options, expert testimony, grants or patents received or pending, or royalties.

No writing assistance was utilized in the production of this manuscript.

Executive summary

Amphiphilic polymers

- Amphiphilic polymers contain both a region of hydrophobicity and hydrophilicity.
- Depending on both number and type of monomers chosen as well as the method of polymerization they can be formed into a variety of different structures.
- Examples in the random, block and alternating copolymers as well as draft, star and brush-type polymers.
- These macromolecules have unique properties that they bestow on the final formulation, insuring that they can self-assemble into a large variety of nanoparticles utilized in drug delivery systems.

Micelles

- Self-assembling structure prepared from amphiphilic polymers and containing a hydrophobic core and a hydrophilic corona.
- Dual drug delivery is achieved by either electrostatically or covalently attaching hydrophilic compounds to the surface with hydrophobic compounds encapsulated within.

Polymersomes

- Self-assembling structure prepared from amphiphilic polymers with a hydrophilic cavity, a hydrophobic interdigitated membrane and an outer hydrophilic corona.
- The nature of these structures render them suitable for dual drug delivery with encapsulation of hydrophilic compounds within the central cavity and hydrophobic compounds dispersed within the hydrophobic membrane.

Nanocapsules

- Self-assembling containing an oily core surrounded by an amphiphilic polymer wall.
- Less commonly used for dual drug delivery than either the micelle or polymersome.
- Dual drug delivery has been achieved by electrostatically attaching a hydrophilic drug to the surface with the hydrophobic drug within the core.

Triggered drug release

- The use of an external or internal stimulant to trigger drug release at a particular time/region.
- Stimulated release is also becoming more prevalent with amphiphilic polymers.
- Examples can be found using pH, redox, heat and enzymes to trigger drug release.

References

- 1 Lander ES, Linton LM, Birren B *et al.* Initial sequencing and analysis of the human genome. *Nature* 409(6822), 860–921 (2001).
- 2 Guo P, Coban O, Snead NM *et al.* Engineering RNA for targeted siRNA delivery and medical application. *Adv. Drug Deliv. Rev.* 62(6), 650–666 (2010).
- 3 Langmuir I. The constitution and fundamental properties of solids and liquids. II. Liquids. 1. *J. Am. Chem. Soc.* 39(9), 1848–1906 (1917).
- 4 Bangham A. Liposomes – the Babraham connection. *Chem. Phys. Lipids* 64(1–3), 275–285 (1993).
- 5 Su C-W, Chiang C-S, Li W-M, Hu S-H, Chen S-Y. Multifunctional nanocarriers for simultaneous encapsulation of hydrophobic and hydrophilic drugs in cancer treatment. *Nanomedicine (Lond.)* 9(10), 1499–1515 (2014).
- 6 Mazák K, Noszá B. Drug delivery: a process governed by species-specific lipophilicities. *Eur. J. Pharm. Sci.* 62, 96–104 (2014).
- 7 Mora-Huertas CE, Fessi H, Elaissari A. Polymer-based nanocapsules for drug delivery. *Int. J. Pharm.* 385(1–2), 113–142 (2010).
- 8 Qu M-H, Zeng R-F, Fang S, Dai Q-S, Li H-P, Long J-T. Liposome-based co-delivery of siRNA and docetaxel for the synergistic treatment of lung cancer. *Int. J. Pharm.* 474(1–2), 112–122 (2014).

- 9 Torchilin VP. Micellar nanocarriers: pharmaceutical perspectives. *Pharm. Res.* 24(1), 1–16 (2007).
- 10 Yu H, Yan C, Lei X, Qin Z, Yao J. Novel approach to extract thermally stable cellulose nanospheres with high yield. *Mater. Lett.* 131, 12–15 (2014).
- 11 Musyanovych A, Landfester K. Polymer micro- and nanocapsules as biological carriers with multifunctional properties. *Macromol. Biosci.* 14(4), 458–477 (2014).
- 12 Kazi KM, Mandal AS, Biswas N *et al.* Niosome: a future of targeted drug delivery systems. *J. Adv. Pharm. Technol. Res.* 1(4), 374–380 (2010).
- 13 Wang X, Liu G, Hu J, Zhang G, Liu S. Concurrent block copolymer polymersome stabilization and bilayer permeabilization by stimuli-regulated ‘traceless’ crosslinking. *Angew. Chem. Int. Ed. Engl.* 53(12), 3138–3142 (2014).
- 14 Levine DH, Ghoroghchian PP, Freudenberg J *et al.* Polymersomes: a new multi-functional tool for cancer diagnosis and therapy. *Methods* 46(1), 25–32 (2008).
- 15 Letchford K, Burt H. A review of the formation and classification of amphiphilic block copolymer nanoparticulate structures: micelles, nanospheres, nanocapsules and polymersomes. *Eur. J. Pharm. Biopharm.* 65(3), 259–269 (2007).
- 16 Christian DA, Cai S, Bowen DM, Kim Y, Pajeroski JD, Discher DE. Polymersome carriers: from self-assembly to siRNA and protein therapeutics. *Eur. J. Pharm. Biopharm.* 71(3), 463–474 (2009).
- 17 Discher DE, Eisenberg A. Polymer vesicles. *Science* 297(5583), 967–73 (2002).
- 18 Gaucher G, Dufresne M-H, Sant VP, Kang N, Maysinger D, Leroux J-C. Block copolymer micelles: preparation, characterization and application in drug delivery. *J. Control. Release* 109(1–3), 169–188 (2005).
- 19 Fustin CA, Abetz V, Gohy JF. Triblock terpolymer micelles: a personal outlook. *Eur. Phys. J. E. Soft Matter.* 16(3), 291–302 (2005).
- 20 Zhang J, Liu K, Müllen K, Yin M. Self-assemblies of amphiphilic homopolymers: synthesis, morphology studies and biomedical applications. *Chem. Commun. (Camb.)* 51(58), 11541–11555 (2015).
- 21 Wang M-J, Wang H, Chen S-C, Chen C, Liu Y. Morphological control of anisotropic self-assemblies from alternating poly(p-dioxanone)-poly(ethylene glycol) multiblock copolymer depending on the combination effect of crystallization and micellization. *Langmuir.* 31(25), 6971–6980 (2015).
- 22 Yildiz I, Impellizzeri S, Deniz E, McCaughan B, Callan JF, Raymo FM. Supramolecular strategies to construct biocompatible and photoswitchable fluorescent assemblies. *J. Am. Chem. Soc.* 133(4), 871–879 (2011).
- 23 Bhattacharya A. Grafting: a versatile means to modify polymers Techniques, factors and applications. *Prog. Polym. Sci.* 29(8), 767–814 (2004).
- 24 Yang C, Liu SQ, Venkataraman S *et al.* Structure-directing star-shaped block copolymers: supramolecular vesicles for the delivery of anticancer drugs. *J. Control. Release* 208, 93–105 (2015).
- 25 Zhang Y-Y, Li Y, Zhou X-J, Zhang X-H, Du B-Y, Fan Z-Q. Synthesis of an amphiphilic brush copolymer by a highly efficient ‘grafting onto’ approach via CO₂ chemistry. *Macromol. Rapid Commun.* 36(9), 852–857 (2015).
- 26 Song D-P, Lin Y, Gai Y *et al.* Controlled supramolecular self-assembly of large nanoparticles in amphiphilic brush block copolymers. *J. Am. Chem. Soc.* 137(11), 3771–3774 (2015).
- 27 Mandal J, Ramakrishnan S. Periodically grafted amphiphilic copolymers: effects of steric crowding and reversal of amphiphilicity. *Langmuir* 31(22), 6035–6044 (2015).
- 28 Yoneki N, Takami T, Ito T *et al.* One-pot facile preparation of PEG-modified PLGA nanoparticles: effects of PEG and PLGA on release properties of the particles. *Colloids Surfaces A Physicochem. Eng. Asp.* 469, 66–72 (2015).
- 29 Miladi K, Ibraheem D, Iqbal M, Sfar S, Fessi H, Elaissari A. Particles from preformed polymers as carriers for drug delivery. *EXCLI J.* 13, 28–57 (2014).
- 30 Soppimath KS, Aminabhavi TM, Kulkarni AR, Rudzinski WE. Biodegradable polymeric nanoparticles as drug delivery devices. *J. Control. Release.* 70(1–2), 1–20 (2001).
- 31 Kataoka K, Harada A, Nagasaki Y. Block copolymer micelles for drug delivery: design, characterization and biological significance. *Adv. Drug Deliv. Rev.* 47(1), 113–131 (2001).
- 32 Lu Y, Park K. Polymeric micelles and alternative nanonized delivery vehicles for poorly soluble drugs. *Int. J. Pharm.* 453(1), 198–214 (2013).
- 33 Li J, Wang Y, Zhu Y, Oupický D. Recent advances in delivery of drug-nucleic acid combinations for cancer treatment. *J. Control. Release* 172(2), 589–600 (2013).
- 34 Jhaveri AM, Torchilin VP. Multifunctional polymeric micelles for delivery of drugs and siRNA. *Front. Pharmacol.* 5, 77 (2014).
- 35 Qian X, Long L, Shi Z *et al.* Star-branched amphiphilic PLA-b-PDMAEMA copolymers for co-delivery of miR-21 inhibitor and doxorubicin to treat glioma. *Biomaterials* 35(7), 2322–2335 (2014).
- 36 Bian J, Hao Y, He J, Zhang W, Zhang M, Ni P. Synthesis and characterization of a biodegradable ABC triblock terpolymer as co-delivery carrier of doxorubicin and DNA. *J. Polym. Sci. Part A Polym. Chem.* 52(21), 3005–3016 (2014).
- 37 Kumar V, Mondal G, Slavik P, Rachagani S, Batra SK, Mahato RI. Codelivery of small molecule hedgehog inhibitor and miRNA for treating pancreatic cancer. *Mol. Pharm.* 12(4), 1289–1298 (2015).
- 38 Wang C, Li M, Yang T *et al.* A self-assembled system for tumor-targeted co-delivery of drug and gene. *Mater. Sci. Eng. C. Mater. Biol. Appl.* 56, 280–285 (2015).
- 39 Gaspar VM, Gonçalves C, de Melo-Diogo D *et al.* Poly(2-ethyl-2-oxazoline)-PLA-g-PEI amphiphilic triblock micelles for co-delivery of minicircle DNA and chemotherapeutics. *J. Control. Release* 189, 90–104 (2014).
- 40 Mittal A, Chitkara D, Behrman SW, Mahato RI. Efficacy of gemcitabine conjugated and miRNA-205 complexed micelles for treatment of advanced pancreatic cancer. *Biomaterials* 35(25), 7077–7087 (2014).
- 41 Wang H, Zhao Y, Wu Y *et al.* Enhanced anti-tumor efficacy by co-delivery of doxorubicin and paclitaxel with

- amphiphilic methoxy PEG-PLGA copolymer nanoparticles. *Biomaterials* 32(32), 8281–8290 (2011).
- 42 Sun L, Deng X, Yang X *et al.* Co-delivery of doxorubicin and curcumin by polymeric micelles for improving antitumor efficacy on breast carcinoma. *RSC Adv.* 4(87), 46737–46750 (2014).
 - 43 Lv S, Tang Z, Li M *et al.* Co-delivery of doxorubicin and paclitaxel by PEG-polypeptide nanovehicle for the treatment of non-small cell lung cancer. *Biomaterials* 35(23), 6118–6129 (2014).
 - 44 Li Q, Lv S, Tang Z *et al.* A co-delivery system based on paclitaxel grafted mPEG-b-PLG loaded with doxorubicin: preparation, in vitro and in vivo evaluation. *Int. J. Pharm.* 471(1–2), 412–420 (2014).
 - 45 Tian W, Liu J, Guo Y, Shen Y, Zhou D, Guo S. Self-assembled micelles of amphiphilic PEGylated rapamycin for loading paclitaxel and resisting multidrug resistant cancer cells†Electronic supplementary information (ESI) available: chemicals and reagents, detailed experimental procedures for materials s. *J. Mater. Chem. B. Mater. Biol. Med.* 3(7), 1204–1207 (2015).
 - 46 Duong HHP, Yung L-YL. Synergistic co-delivery of doxorubicin and paclitaxel using multi-functional micelles for cancer treatment. *Int. J. Pharm.* 454(1), 486–495 (2013).
 - 47 Scarano W, de Souza P, Stenzel MH. Dual-drug delivery of curcumin and platinum drugs in polymeric micelles enhances the synergistic effects: a double act for the treatment of multidrug-resistant cancer. *Biomater. Sci.* 3(1), 163–174 (2015).
 - 48 Li J, Li Z, Li M, Zhang H, Xie Z. Synergistic effect and drug-resistance relief of paclitaxel and cisplatin caused by Co-delivery using polymeric micelles. *J. Appl. Polym. Sci.* 132(6) 41440–41449(2015).
 - 49 Noh I, Kim H-O, Choi J *et al.* Co-delivery of paclitaxel and gemcitabine via CD44-targeting nanocarriers as a prodrug with synergistic antitumor activity against human biliary cancer. *Biomaterials* 53, 763–774 (2015).
 - 50 Li M, Liu Y, Feng L, Liu F, Zhang L, Zhang N. Polymeric complex micelles with double drug-loading strategies for folate-mediated paclitaxel delivery. *Colloids Surf. B. Biointerfaces* 131, 191–201 (2015).
 - 51 Yin T, Wang L, Yin L, Zhou J, Huo M. Co-delivery of hydrophobic paclitaxel and hydrophilic AURKA specific siRNA by redox-sensitive micelles for effective treatment of breast cancer. *Biomaterials* 61, 10–25 (2015).
 - 52 Zhang J, Fang D, Ma Q *et al.* Dual-functional PEI-poly(γ -cholesterol-1-glutamate) copolymer for drug/gene co-delivery. *Macromol. Chem. Phys.* 215(2), 163–170 (2014).
 - 53 Zheng C, Zheng M, Gong P *et al.* Polypeptide cationic micelles mediated co-delivery of docetaxel and siRNA for synergistic tumor therapy. *Biomaterials* 34(13), 3431–3438 (2013).
 - 54 Discher BM, Won YY, Ege DS *et al.* Polymersomes: tough vesicles made from diblock copolymers. *Science* 284(5417), 1143–1146 (1999).
 - 55 Discher DE, Ortiz V, Srinivas G *et al.* Emerging applications of polymersomes in delivery: from molecular dynamics to shrinkage of tumors. *Prog. Polym. Sci.* 32(8–9), 838–857 (2007).
 - 56 Martin C, Dolmazon E, Moylan K *et al.* A charge neutral, size tuneable polymersome capable of high biological encapsulation efficiency and cell permeation. *Int. J. Pharm.* 481(1–2), 1–8 (2015).
 - 57 Ahmed F, Pakunlu RI, Brannan A, Bates F, Minko T, Discher DE. Biodegradable polymersomes loaded with both paclitaxel and doxorubicin permeate and shrink tumors, inducing apoptosis in proportion to accumulated drug. *J. Control. Release* 116(2), 150–158 (2006).
 - 58 Das S, Sharma DK, Chakrabarty S, Chowdhury A, Sen Gupta S. Bioactive polymersomes self-assembled from amphiphilic PPO-glycopolypeptides: synthesis, characterization, and dual-dye encapsulation. *Langmuir* 31(11), 3402–3412 (2015).
 - 59 Lale S V, Kumar A, Prasad S, Bharti AC, Koul V. Folic acid and trastuzumab functionalized redox responsive polymersomes for intracellular doxorubicin delivery in breast cancer. *Biomacromolecules.* 16(6), 1736–1752 (2015).
 - 60 Xu J, Zhao Q, Jin Y, Qiu L. High loading of hydrophilic/hydrophobic doxorubicin into polyphosphazene polymersome for breast cancer therapy. *Nanomedicine.* 10(2), 349–358 (2014).
 - 61 Kim H-O, Kim E, An Y *et al.* A biodegradable polymersome containing Bcl-xL siRNA and doxorubicin as a dual delivery vehicle for a synergistic anticancer effect. *Macromol. Biosci.* 13(6), 745–754 (2013).
 - 62 Iatrou H, Dimas K, Gkikas M, Tsimblouli C, Sofianopoulou S. Polymersomes from polypeptide containing triblock Co- and terpolymers for drug delivery against pancreatic cancer: asymmetry of the external hydrophilic blocks. *Macromol. Biosci.* 14(9), 1222–1238 (2014).
 - 63 Colley HE, Hearnden V, Avila-Olias M *et al.* Polymersome-mediated delivery of combination anticancer therapy to head and neck cancer cells: 2D and 3D *in vitro* evaluation. *Mol. Pharm.* 11(4), 1176–1188 (2014).
 - 64 Baier G, Cavallaro A, Vasilev K, Mailänder V, Musyanovych A, Landfester K. Enzyme responsive hyaluronic acid nanocapsules containing polyhexanide and their exposure to bacteria to prevent infection. *Biomacromolecules.* 14(4), 1103–1112 (2013).
 - 65 Haas S, Hain N, Raoufi M *et al.* Enzyme degradable polymersomes from hyaluronic acid-block-poly(ϵ -caprolactone) copolymers for the detection of enzymes of pathogenic bacteria. *Biomacromolecules.* 16(3), 832–841 (2015).
 - 66 Geilich BM, van de Ven AL, Singleton GL, Sepúlveda LJ, Sridhar S, Webster TJ. Silver nanoparticle-embedded polymersome nanocarriers for the treatment of antibiotic-resistant infections. *Nanoscale* 7(8), 3511–3519 (2015).
 - 67 Huang Z, Teng W, Liu L, Wang L, Wang Q, Dong Y. Efficient cytosolic delivery mediated by polymersomes facilely prepared from a degradable, amphiphilic, and amphoteric copolymer. *Nanotechnology* 24(26), 265104 (2013).
 - 68 Wong CK, Laos AJ, Soeriyadi AH *et al.* Polymersomes prepared from thermoresponsive fluorescent protein-polymer

- bioconjugates: capture of and report on drug and protein payloads. *Angew. Chem. Int. Ed. Engl.* [Internet]. 54(18), 5317–5322 (2015). Available from: <http://www.ncbi.nlm.nih.gov/pubmed/25736460>.
- 69 Wang Y, Yan L, Li B *et al.* Protein-resistant biodegradable amphiphilic graft copolymer vesicles as protein carriers. *Macromol. Biosci.* 15(9), 1304–1313 (2015).
 - 70 Danafar H, Rostamizadeh K, Davaran S, Hamidi M. PLA-PEG-PLA copolymer-based polymersomes as nanocarriers for delivery of hydrophilic and hydrophobic drugs: preparation and evaluation with atorvastatin and lisinopril. *Drug Dev. Ind. Pharm.* 40(10), 1411–1420 (2014).
 - 71 Landfester K. Miniemulsion polymerization and the structure of polymer and hybrid nanoparticles. *Angew. Chemie Int. Ed.* 48(25), 4488–4507 (2009).
 - 72 Coradini K, Friedrich RB, Fonseca FN *et al.* A novel approach to arthritis treatment based on resveratrol and curcumin co-encapsulated in lipid-core nanocapsules: *in vivo* studies. *Eur. J. Pharm. Sci.* 78, 163–170 (2015).
 - 73 Friedrich RB, Kann B, Coradini K, Offerhaus HL, Beck RCR, Windbergs M. Skin penetration behavior of lipid-core nanocapsules for simultaneous delivery of resveratrol and curcumin. *Eur. J. Pharm. Sci.* 78, 204–213 (2015).
 - 74 Gressler LT, Oliveira CB, Coradini K *et al.* Trypanocidal activity of free and nanoencapsulated curcumin on *Trypanosoma evansi*. *Parasitology* 142(3), 439–448 (2015).
 - 75 Arunkumar R, Prashanth KVH, Manabe Y *et al.* Biodegradable poly (lactic-co-glycolic acid)-polyethylene glycol nanocapsules: an efficient carrier for improved solubility, bioavailability, and anticancer property of lutein. *J. Pharm. Sci.* 104(6), 2085–2093 (2015).
 - 76 Wadhwa J, Asthana A, Gupta S, Shilkari Asthana G, Singh R. Development and optimization of polymeric self-emulsifying nanocapsules for localized drug delivery: design of experiment approach. *Scientific World J.* 2014 516069 (2014).
 - 77 Klippstein R, Wang JT-W, El-Gogary RI *et al.* Passively targeted curcumin-loaded pegylated plga nanocapsules for colon cancer therapy *in vivo*. *Small.* 11(36), 4704–4722 (2015).
 - 78 Chen C-K, Law W-C, Aalinker R *et al.* Biodegradable cationic polymeric nanocapsules for overcoming multidrug resistance and enabling drug-gene co-delivery to cancer cells. *Nanoscale* 6(3), 1567–1572 (2014).
 - 79 Tian K, Zeng J, Zhao X, Liu L, Jia X, Liu P. Synthesis of multi-functional nanocapsules via interfacial AGET ATRP in miniemulsion for tumor micro-environment responsive drug delivery. *Colloids Surf. B. Biointerfaces.* 134, 188–195 (2015).
 - 80 Maglio G, Nicodemi F, Conte C, *et al.* Nanocapsules based on linear and Y-shaped 3-miktoarm star-block PEO-PCL copolymers as sustained delivery system for hydrophilic molecules. *Biomacromolecules* 12(12), 4221–4229 (2011).
 - 81 Hu S-H, Chen S-Y, Gao X. Multifunctional nanocapsules for simultaneous encapsulation of hydrophilic and hydrophobic compounds and on-demand release. *ACS Nano.* 6(3), 2558–2565 (2012).
 - 82 Baier G, Winzen S, Messerschmidt C *et al.* Heparin-based nanocapsules as potential drug delivery systems. *Macromol. Biosci.* 15(6), 765–776 (2015).
 - 83 Govender T, Choonara Y, Kumar P *et al.* A Novel melt-dispersion technique for simplistic preparation of chlorpromazine-loaded polycaprolactone nanocapsules. *Polymers (Basel).* 7(6), 1145–1176 (2015).
 - 84 Liang G, Ni H, Bao S *et al.* Amphiphilic nanocapsules entangled with organometallic coordination polymers for controlled cargo release. *Langmuir* 30(21), 6294–6301 (2014).
 - 85 Brun-Graepi AKAS, Richard C, Bessodes M, Scherman D, Merten O-W. Cell microcarriers and microcapsules of stimuli-responsive polymers. *J. Control. Release* 149(3), 209–224 (2011).
 - 86 Ashley CE, Carnes EC, Phillips GK *et al.* The targeted delivery of multicomponent cargos to cancer cells by nanoporous particle-supported lipid bilayers. *Nat. Mater.* 10(5), 389–397 (2011).
 - 87 Zayats M, Kanwar M, Ostermeier M, Searson PC. Molecular imprinting of maltose binding protein: tuning protein recognition at the molecular level. *Macromolecules* 44(10), 3966–3972 (2011).
 - 88 Chen W, Meng F, Cheng R, Zhong Z. pH-Sensitive degradable polymersomes for triggered release of anticancer drugs: a comparative study with micelles. *J. Control. Release.* 142(1), 40–46 (2010).
 - 89 Jia L, Cui D, Bignon J *et al.* Reduction-responsive cholesterol-based block copolymer vesicles for drug delivery. *Biomacromolecules* 15(6), 2206–2217 (2014).
 - 90 Chang C, Dan H, Zhang L-P *et al.* Fabrication of thermoresponsive, core-crosslinked micelles based on poly[N -isopropyl acrylamide- co -3-(trimethoxysilyl) propylmethacrylate] - b -poly{ N -[3-(dimethylamino) propyl]methacrylamide} for the codelivery of doxorubicin and nucleic acid. *J. Appl. Polym. Sci.* 132(15), 41752–41762 (2015).
 - 91 McKenzie BE, Friedrich H, Wirix MJM *et al.* Controlling internal pore sizes in bicontinuous polymeric nanospheres. *Angew. Chem. Int. Ed. Engl.* 54(8), 2457–2461 (2015).
 - 92 Swaminathan S, Fowley C, McCaughan B, Cusido J, Callan JF, Raymo FM. Intracellular guest exchange between dynamic supramolecular hosts. *J. Am. Chem. Soc.* 136(22), 7907–7913 (2014).
 - 93 Dieu L-H, Wu D, Palivan CG, Balasubramanian V, Huwyler J. Polymersomes conjugated to 83-14 monoclonal antibodies: *in vitro* targeting of brain capillary endothelial cells. *Eur. J. Pharm. Biopharm. Off. J. Arbeitsgemeinschaft für Pharm. Verfahrenstechnik e.V.* 88(2), 316–324 (2014).
 - 94 Fonseca FN, Betti AH, Carvalho FC *et al.* Mucoadhesive amphiphilic methacrylic copolymer-functionalized poly(ϵ -caprolactone) nanocapsules for nose-to-brain delivery of olanzapine. *J. Biomed. Nanotechnol.* 11(8), 1472–1481 (2015).
 - 95 Lee J-L, Ahn J-H, Park SH *et al.* Phase II study of a cremophor-free, polymeric micelle formulation of paclitaxel for patients with advanced urothelial cancer previously treated with gemcitabine and platinum. *Invest. New Drugs.* 30(5), 1984–1990 (2012).

- 96 Ahn HK, Jung M, Sym SJ *et al.* A phase II trial of Cremophor EL-free paclitaxel (Genexol-PM) and gemcitabine in patients with advanced non-small cell lung cancer. *Cancer Chemother. Pharmacol.* 74(2), 277–282 (2014).
- 97 Saif MW, Podoltsev NA, Rubin MS *et al.* Phase II clinical trial of paclitaxel loaded polymeric micelle in patients with advanced pancreatic cancer. *Cancer Invest.* 28(2), 186–194 (2010).
- 98 Pacific Corporation: US6569528 (2003).
- 99 Regents of the University of Minnesota, MN, USA, US7217427 (2007).
- 100 Labopharm Inc. US7108655 (2006).
- 101 The trustees of the University of Pennsylvania: US20100098773 (2010).
- 102 Torchilin Vladimir P, Lukyanov Anatoly N, Zhonggao Gao: US20060216342 (2006).
- 103 Koninklijke Philips Electronics NV: WO2009072079 (2009).
- 104 Vindico Nanobio Technology Inc: EP-2661275-A2 (2013).
- 105 The Regents of The University of Michigan: US20150051534 (2015).
- 106 Shi Yang: CN104193925A (2014).

